University of Maribor Press

ISSN 1854-0171

ACTA GEOTECHNICA SLOVENICA

2021/1
VOL. 18

ISSN: 1854-0171

ACTA GEOTECHNICA SLOVENICA

Ustanovitelji | Founders

Univerza v Mariboru, Fakulteta za gradbeništvo, prometno inženirstvo in arhitekturo
University of Maribor, Faculty of Civil Engineering, Transportation Engineering and Architecture

Univerza v Ljubljani, Fakulteta za gradbeništvo in geodezijo
University of Ljubljana, Faculty of Civil and Geodetic Engineering

Univerza v Ljubljani, Naravoslovnotehniška fakulteta
University of Ljubljana, Faculty of Natural Sciences and Engineering

Slovensko geotehniško društvo
Slovenian Geotechnical Society

Društvo za podzemne in geotehniške konstrukcije
Society for Underground and Geotechnical Constructions

Izdajatelj | Publisher

Univerza v Mariboru, Fakulteta za gradbeništvo, prometno inženirstvo in arhitekturo
Faculty of Civil Engineering, Transportation Engineering and Architecture

Odgovorni urednik | Editor–in–Chief

Borut Macuh — University of Maribor

Tehnična urednica | Technical Editor

Tamara Bračko — University of Maribor

Uredniki | Co–Editors

Jakob Likar	Geoportal d.o.o.
Janko Logar	University of Ljubljana
Primož Jelušič	University of Maribor
Stanislav Škrabl	University of Maribor
Goran Vižintin	University of Ljubljana
Bojan Žlender	University of Maribor

Posvetovalni uredniki | Advisory Editors

Heinz Brandl	Vienna University of Technology
Chandrakant. S. Desai	University of Arizona
Bojan Majes	University of Ljubljana
Pedro Seco e Pinto	National Laboratory of Civil Eng.

Lektor | Proof–Reader

Paul McGuiness

Naklada | Circulation

200 izvodov - issues

Cena | Price

25 EUR/letnik - 25 EUR/vol.; (50 EUR for institutions/za institucije)

Tisk | Print

Tiskarna Saje

Revija redno izhaja dvakrat letno. Članki v reviji so recenzirani s strani priznanih mednarodnih strokovnjakov. Baze podatkov v katerih je revija indeksirana: SCIE - Science Citation Index Expanded, JCR – Journal Citation Reports / Science Edition, ICONDA - The international Construction database, GeoRef. Izid publikacije je finančno podprla Javna agencija za raziskovalno dejavnost Republike Slovenije iz naslova razpisa za sofinanciranje domačih periodičnih publikacij.

Založnik | Published by

Univerzitetna založba Univerze v Mariboru
Slomškov trg 15, 2000 Maribor, Slovenija
e-pošta: zalozba@um.si, http://press.um.si/, http://journals.um.si/

University of Maribor Press
Slomškov trg 15, 2000 Maribor, Slovenia
e-mail: zalozba@um.si, http://press.um.si/, http://journals.um.si/

Naslov uredništva | Address

ACTA GEOTECHNICA SLOVENICA
Univerza v Mariboru, Fakulteta za gradbeništvo, prometno inženirstvo in arhitekturo
Smetanova ulica 17, 2000 Maribor, Slovenija
Telefon / Telephone: +386 (0)2 22 94 300
Faks / Fax: +386 (0)2 25 24 179
E-pošta / E-mail: ags@um.si

Spletni naslov | web Address

http://www.fg.uni-mb.si/journal-ags/

The journal is published twice a year. Papers are peer reviewed by renowned international experts. Indexation data bases of the journal: SCIE - Science Citation Index Expanded, JCR – Journal Citation Reports / Science Edition, ICONDA- The international Construction database, GeoRef. The publication was financially supported by Slovenian Research Agency according to the Tender for co-financing of domestic periodicals.

A FRAMEWORK FOR THE USE OF RELIABILITY METHODS IN DEEP URBAN EXCAVATIONS ANALYSIS

OKVIR ZA UPORABO METOD ZANESLJIVOSTI PRI ANALIZAH GLOBOKIH IZKOPOV V URBANIH OKOLJIH

Arefeh Arabaninezhad
University of Tehran,
Department of civil engineering
Enghelab Ave, Tehran, Iran
E-mail: arefeh.arbani@ut.ac.ir

Ali Fakher *(corresponding author)*
University of Tehran,
Department of civil engineering
Enghelab Ave, Tehran, Iran
E-mail: afakher@ut.ac.ir

DOI https://doi.org/10.18690/actageotechslov.18.1.2-14.2021

Keywords

deep excavation, random set finite element method, reliability analysis, system performance; uncertainty

Ključne besede

globoki izkop, metoda naključnih nizov s končnimi elementi, analiza zanesljivosti, zmogljivost sistema, nezanesljivost

Abstract

Deep excavations in urban areas impose deformation to adjacent structures; hence the reliability of deformation analysis for the real deep excavation projects is very important to be assessed. In this study a framework is presented for the use of reliability methods in deformation analysis of deep urban excavations. The suggested framework is applied for 5 real deep excavation projects implemented during last 10 years. All studied cases were recognized as projects of high importance in urban areas, and were monitored during the excavation process. A non-probabilistic reliability analysis procedure, Random set method, in combination with finite element numerical modeling is applied to obtain the probability of unsatisfactory performance for each case. The reliability analysis results are confirmed by field observations and measurements. Typical results for the probability of analytical deformations exceeding the acceptable values along with the site observations and measured displacements for 5 real deep excavation projects show that the reliability analysis could be a beneficial tool for designer. It is concluded that applying the suggested framework in the design stage of deep excavation projects may lead to design more appropriate systems compared to common deterministic design methods.

Izvleček

Izvedbe globokih izkopov v urbanih območjih povzročajo deformacije na sosednjih konstrukcijah; zato je zelo pomembna ocena zanesljivosti analize deformacij za dejanske projekte globokih izkopov. V tej študiji je predstavljen okvir za uporabo metod zanesljivosti pri analizi deformacij globokih izkopov v urbanih okoljih. Predlagani okvir je bil uporabljenih za pet dejanskih projektov globokih izkopov, izvedenih v zadnjih 10 letih. Vsi preučeni primeri so bili prepoznani kot projekti velikega pomena v urbanih območjih in so bili spremljani med izvedbo izkopov. Za verjetnostno analizo uspešnosti izvedbe izkopov se za vsak od primerov ni uporabil postopek verjetnostne analize zanesljivosti, temveč metoda naključnih nizov v kombinaciji z numeričnim modeliranjem končnih elementov. Rezultate analize zanesljivosti potrjujejo terenska opazovanja in meritve. Tipični rezultati verjetnosti analitičnih deformacij, ki presegajo sprejemljive vrednosti, skupaj z opazovanji na lokaciji in izmerjenimi premiki za pet dejanskih projektov globokih izkopov kažejo, da bi bila analiza zanesljivosti lahko koristno orodje za projektante. Ugotovljeno je bilo, da uporaba predlaganega okvira v fazi načrtovanja projektov globokih izkopov lahko privede do zasnove ustreznejših sistemov v primerjavi s splošnimi metodami deterministčnega načrtovanja.

1 INTRODUCTION

As a result of the extensive development of urban areas, deep excavation design has become an increasingly pursued issue in engineering analyses in recent years. Because of the great effects of deep excavation-induced ground movements on the nearby structures, the assessment of the effects of deep excavations on ground movements has been the subject of interest of several studies [1-6]. Ignoring the deformation caused by excavating process in the design stage can cause significant damage to adjacent structures and utilities. Excessive movements can occur without a failure mechanism occurring [7], hence it should be considered in the design stage as long as the failure control. In other words, both the serviceability and ultimate limit state of the system should be evaluated in-order to design sufficient support plan for a deep excavation wall. Structure failure events pose a significant threat not only to human life but also to the environment and in general to economic development. Sources of ground movement are lateral displacement of excavation wall and displacement due to support system installation [8]. Hence, in the presented study the horizontal displacement of the excavation top point (as a significant system response affecting the nearby facilities) is considered as the main system response to be controlled.

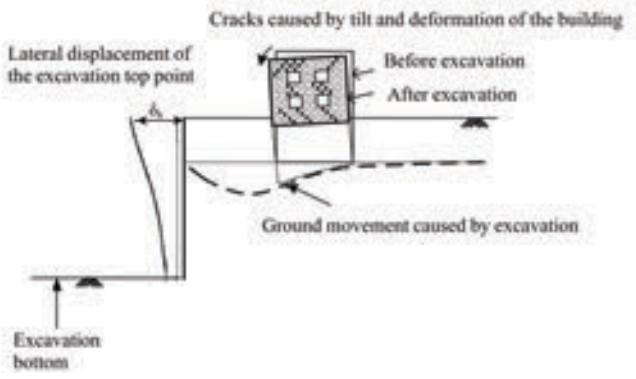

Figure 1. Schematic figure for effects of deep excavation on ground movement and adjacent buildings.

The uncertainty caused by soil and rock properties such as cohesion and elastic modulus poses a major challenge in geotechnical problems. Soils are variable, whether such variability is recognized in design or not. Addressing uncertainty does not increase the level of safety, but allows a more rational design as the engineer can calibrate the decisions on a desired or required performance level of a structure [9]. Reliability analysis methods represent the most important aspect of performance, namely the probability of unsatisfactory performance of a system. Using deterministic methods, excavations are designed based on the stability safety factor, deformation of excavation walls and adjacent buildings, ignoring the existing uncertainties in soil properties. The main advantage of reliability analysis over deterministic methods in terms of safety lies in the fact that, the designer is able to provide more complete and realistic information regarding the level of safety of design.

In recent years, the technology for implementing deep excavations in Iran has improved considerably. Using simple reliability analysis methods is encouraged in the design stage of the projects in order to propose optimum support system plans. In this study a framework is represented for the use of reliability methods in deep urban excavations analysis. Due to the great effect of deformation induced by deep urban excavations on the nearby facilities, the framework is based on controlling the horizontal displacement of the excavation top point as the main system response. The Random Set Method (RS) is selected for performing reliability analysis and a finite element software was used to model the deep excavations. The main reason to choose RS method is that it works well with the limited soil data available in real deep excavation projects and it takes the soil input variables in the form of intervals.

Being able to select and communicate the level of performance and reduce undesired conservatism, in turn, is beneficial in the economic sense [9]. It also reduces the risk of incorrect decisions due to unintentionally optimistic modeling [10]. In order to estimate the probability of unsatisfactory performance of the system, a threshold value is considered for horizontal displacement of the excavation top point as a target value and the probability of having displacement more than this value is compared to the acceptable probability of excessive deformation.

The presented framework is based on applying the previously published research findings. The Innovation is (I) to combine these methods in order to present a simple and practical framework and (II) applying it for 5 important deep excavation projects implemented during the last 10 years. The results were compared to the site measurements and field observations on the problems encountered in reality. The selected cases have been implemented in Tehran during 2010 to 2018. The support system plans for all cases were implemented based on deterministic analysis methods and no reliability analysis had been performed at the design stage. All studied cases were recognized as projects of high importance in urban areas, and were therefore monitored during the excavation process.

2 THE METHODOLOGY OF PRESENTED FRAMEWORK

The steps to implement the presented framework for reliability analysis of deep excavations in urban areas are summarized below:

[Step 1]: Performing the reliability analysis for the selected deep excavation projects.

[Step 2]: Selecting the target value for horizontal displacement of the excavation top point (as the main system response) and the acceptable probability of excessive deformation.

[Step 3]: Comparing the probability of excessive deformation to the acceptable value and evaluating the performance of proposed support system to find out whether any revision is required or not.

3 USED RELIABILITY ANALYSIS METHOD

Although various mathematical methods have been proposed and investigated for reliability analysis [11-23], applying these methods to geotechnical problems presents certain difficulties. It highlights the importance of proposing methods that draw on limited input data which are available in real geotechnical project such as deep excavations in order to represent an appropriate estimate from the system performance. Accordingly, the random set method benefiting a simple mathematical framework for reliability analysis has been selected for the presented study.

The random set theory was first proposed by Kendall [24], and consequently developed by different researchers. This method consists of a mathematical model that can deal with the system uncertainties when the exact input variable values are not available. Since 2000, the random set method has been applied to a certain extent in geotechnical studies, and has mostly been used in tunnel studies. Peschl [25] and Schweiger and Peschl [26] combined the random set theory with the finite element method, developing the random set finite element method (RS-FEM) and investigated its applicability to slope stability analysis. Nasekhian [27] conducted a tunnel project case study to investigate the advantages and disadvantages of RS-FEM for reliability analysis. Shen and Abbas [28] applied random set method in combination with distinct element method to investigate the reliability of rock slopes. Ghaziyan-Arabi & Fakher [29] and Arabaninezhad & Fakher [30] examined the use of the random set method in the finite element analysis of deep excavations; however, only one case study in Tehran was considered in each study, which was not sufficient for a practical conclusion. Momeni et al. [31] evaluated the random set method for reliability analysis of deep excavations using Monte Carlo technique.

3.1 Concept of Random Set Method

The random set theory provides a general framework for dealing with set-based information and discrete probability distributions [26].

Assume that X is a non-empty set containing all possible values of a variable x. Dubois and Prade [32] defined a random set on X as a pair $(\Im, m)$, where $\Im = \{A_i: i = 1,...,n\}$ and m is a mapping, $\Im \rightarrow [0,1]$, so that $m(\phi) = 0$ and

$$\sum_{A \in \Im} m(A) = 1 \qquad (1)$$

In the above, $\Im$ is known as the support of the random set, the sets A_i are the focal elements, and m is known as the basic probability assignment. Each set contains certain possible values for the variable x, and $m(A)$ can be viewed as the probability that A is the range of x. Because of the imprecision of this formulation, it is not possible to calculate the precise probability of a generic $x \in X$ or generic subset $E \in X$, but only the lower and upper bounds of this probability.

With numerical modeling based on the finite element method (FEM), it is possible to obtain more than one system response without making any changes to the model. Therefore, the random set in combination with the FEM will be a sufficient reliability analysis method.

Assume that function $f(A_i)$ represents a numerical model in the RS-FEM framework. The number of system input variables is N and n information sources are available. Hence, n^N FE runs are required to consider all possible combinations of input variables based on the input sources of information. Because only extreme values of input random sets are considered, 2^N FE runs are also required to perform interval analysis.

The number of all calculations n_c required to determine the bounds of the system response are:

$$n_c = 2^N \prod_{i=1}^{N} n_i \qquad (2)$$

Assuming that input variables $(A_1, \ldots, A_n)$ are stochastically independent, the joint probability for the system response focal element obtained from each deterministic FE calculation is equal to the product of probability assignment m for each input focal element as:

$$m(A_1 \times ... \times A_N) = \prod_{i=1}^{n} m_i(A_i) \qquad (3)$$

3.2 Radom Set Finite Element Method

With numerical modeling based on the finite element method, it is possible to obtain more than one system response without making any changes to the model. Therefore, in this study, reliability analysis is accomplished by using the random set in combination with the finite element method.

The steps to implement random set reliability analysis in combination with numerical modeling are summarized below:

[Step 1]: Define the geometry of the system, prepare the finite element model and select the appropriate constitutive model for material.

[Step 2]: Provide available sources of information to define different input random sets for the basic system variables. In the case that two sources of information are available, the probability of each basic variable can be set to 0.5. In this way, almost all sources of uncertainties are taken into consideration in the modeling procedure. [31]

[Step 3]: Consider spatial variability in order to reduce uncertainty over the input random sets.

[Step 4]: Determine the most influential input variables using sensitivity analysis to reduce the number of required FE runs.

[Step 5]: Generate all possible combinations of input variables for the FEM and calculate the relevant probability share for each individual run. Each combination (set) is keyed into a finite element model, the model is run and the desired output is recorded. This process is repeated n_c times (Eq. 2) and the model outputs are recorded. The probability share assigned to the model output for each combination is calculated from multiplying the probability of each basic variable (Eq. 3).

[Step 6]: Perform FE calculations and represent the main system responses in terms of the lower and upper bounds of discrete cumulative probability functions (CDF). The resulting CDF are fitted using a best-fit method (Easyfit software [34] in this study) to achieve a continuous distribution function.

[Step 7]: Define suitable performance functions which can be evaluated using the reliability analysis results (bounds on continuous distribution functions of the system response) to obtain a range for the probability of failure or unsatisfactory performance. In this study an acceptable value is defined for horizontal displacement of the excavation top point as a target value and the probability of having displacement more than this value which indicates the probability of unsatisfactory performance of the system can be determined.

4 SELECTED PROJECTS SPECIFICATION

In-order to assess the presented framework for reliability analysis of deep excavation projects, a number of monitored case studies must be undertaken. Tall buildings are common in northern Tehran. In order to supply sufficient space for parking, multi-story basements are constructed for these buildings; thus major deep excavation projects are performed to construct the basements. The routine depth of a deep excavation is 20 to 40 m. The soil layers generally consist of fill materials near the ground surface (1.5 to 3 m in depth), with clayey gravel and clayey sand being mostly frequently observed in succession. In order to consider the mentioned specifications of general deep excavations in Tehran, five excavation walls from 3 important monitored projects were selected as summarized in Table 1. The excavation areas of the selected projects are large and the inclination of the ground surface causes different excavation depths at different parts of the same project.

Table 1. General specifications of selected projects.

Project	Excavation depth (m)	Fill material depth (m)	Excavation area (m^2)	Support system	Main type of soil layers	Number of walls investigated
South Atlas Plaza, Commercial center	23 and 25	3	32000	nail-anchor combination	clayey gravel and clayey sand	2
Shiraz Street, Golestan Administrative-commercial building	34 and 36.5	1.5	8500	nail-anchor combination	clayey gravel and stiff clay	2
North Atlas, Hotel	36.5	1.5	16000	nail-anchor combination	clayey gravel and clayey sand	1

(a) First project site (including case studies nos. 1 & 2.)

(b) Second project site (including case studies nos. 3 & 4.)

(c) Third project site (including case study no. 5.)

Figure 2. Aerial view of intended deep excavation projects locations.

Fig. 2 shows the excavation location and neighboring facilities, including buildings and roads for intended excavation projects. In the first project, as illustrated in Fig. 2(a), two walls were selected for the study because of the differences in horizontal displacements and surcharges. It should be noted that, according to the monitoring reports, several small cracks were observed on the ground surface near wall 2. The second excavation project (Fig. 2(b)) was launched in 2012. As activities proceeded, several cracks were observed around the northern part of the excavation, leading to anxiety in residents of nearby buildings; thus, excavation activities were suspended for a period in order to revise the stabilization plan. The soil profile that appeared during the excavation process indicated that the primary geotechnical investigations were not consistent with real soil conditions. Several residential buildings exist adjacent to the street located on the north side of the project, and according to the monitoring reports, the majority of horizontal displacements occurred in the northwestern part of the excavation; hence, reliability analysis is performed for walls nos.3 and 4 located in this region. The third excavation project is located in the northern half of the first deep excavation project site as illustrated in Fig. 2(c). This project was being carried out in order to construct a hotel, and during the excavation process, a building located in the southern half of the current excavation was being built.

The excavation support system implemented for all projects was a nail-anchor combination. Support systems were designed by geotechnical engineers applying deterministic methods. In the presented study the effect of uncertainty in soil properties on reliability of deep excavations has been taken into account applying RS-FEM. The support system is considered to be equal in all finite element runs performed for reliability analysis of each intended wall. Hence for the sake of brevity the details of support systems are not explained in detail.

5 IMPLEMENTATION OF RS-FEM

Numerical modeling was done using finite element software [35]. Fig. 3 plots the system model cross-section for intended walls.

For each soil variable, according to the geotechnical reports and engineering judgment, along with expert knowledge, two ranges with a weight of 0.5 each are suggested.

In order to consider the spatial variations in soil parameters, the primary values of the variables are modified slightly, using a variance reduction technique. In this study, the method proposed by Schweiger and Peschl [26] is applied. For the purpose of brevity, details of this method are not presented here and can be found in other studies [26, 31].

The modified upper and lower bounds of the suggested ranges, and the reference values for each soil variable, are represented in Tables 2-5.

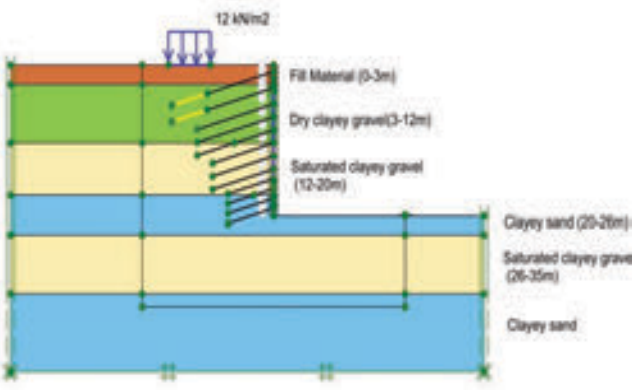

(a) Case study 1

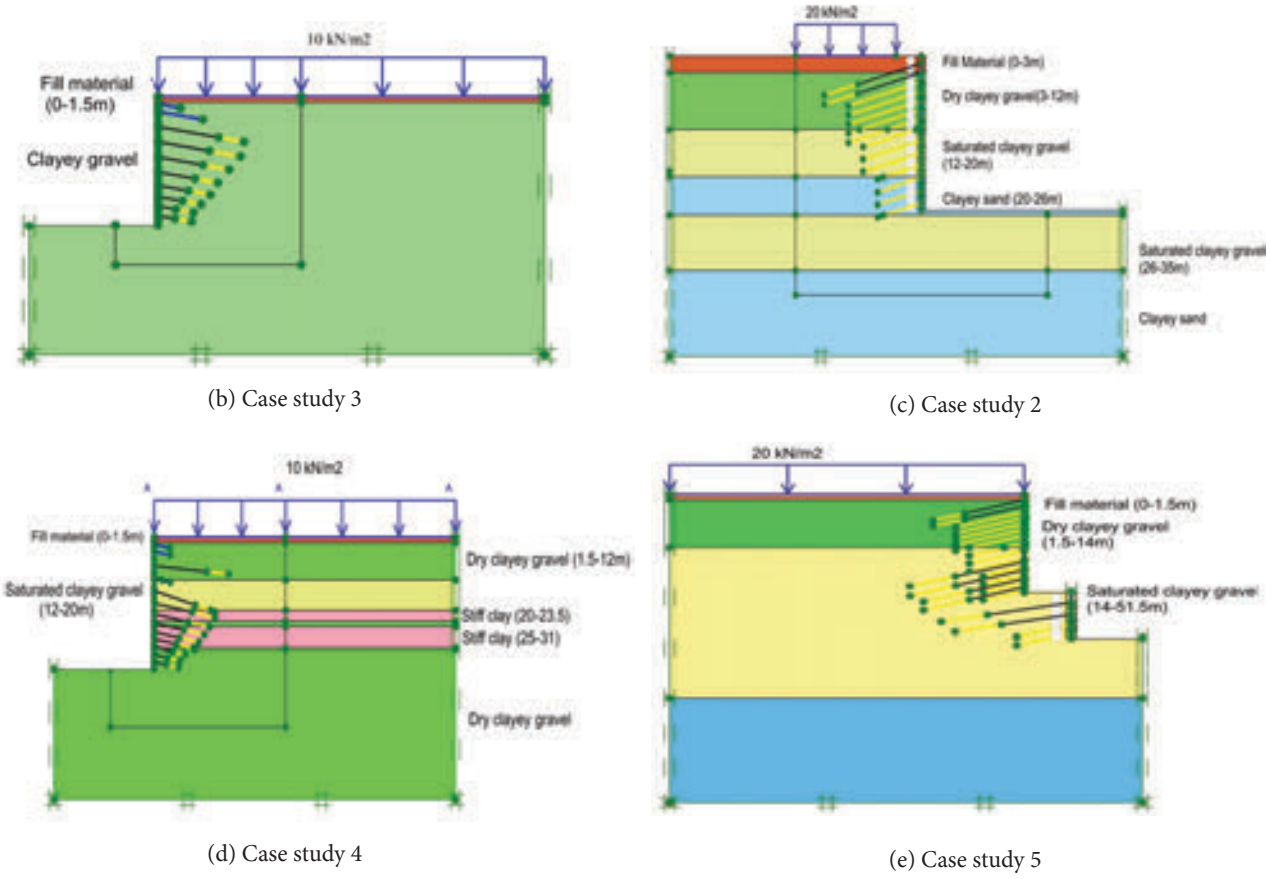

(b) Case study 3

(c) Case study 2

(d) Case study 4

(e) Case study 5

Figure 3. Cross section of the system for investigated case studies.

Table 2. The ranges of random sets and reference values for soil variables considering spatial variation (case studies 1, 2).

Layer		Cohesion c (kN/m^2)		Friction angle φ (°)		Elastic modulus E_{ref}^{50} (MN/m^2)	
		Range of sets	Ref	Range of sets	Ref	Range of sets	Ref
Fill Material	Set 1	6.93-13.21	9.65	29.29-33.29	31	26.43-46.43	35
	Set 2	6.07-11.79		28.71-32.71		23.57-43.57	
Clayey gravel (dry)	Set 1	72.86-102.86	85	38.57-43.29	40.36	83.57-103.57	95
	Set 2	67.14-97.14		37.43-42.71		86.43-106.43	
Clayey gravel (saturated)	Set 1	62.86-92.86	75	31.29-35.29	33	92.86-126.43	106.79
	Set 2	57.14-87.14		30.71-34.71		87.14-123.57	
Clayey sand	Set 1	46.43-66.43	55	29.93-33.93	31	66.43-86.43	71.79
	Set 2	43.57-63.57		29.07-33.07		57.14-83.57	

Table 3. The ranges of random sets and reference values for soil variables considering spatial variation (case study 3)

Layer		Cohesion c (kN/m^2)		Friction angle φ (°)		Elastic modulus E_{ref}^{50} (MN/m^2)	
		Range of sets	Ref	Range of sets	Ref	Range of sets	Ref
Fill Material	Set 1	5.75-13.13	9.81	26.75-30.75	29	10.75-14.75	13
	Set 2	6.25-13.87		27.25-31.25		11.25-15.25	
Clayey gravel	Set 1	53.77-73.77	65	32.75-36.75	35	33.77-67.55	53.11
	Set 2	56.23-76.23		33.25-37.25		36.23-72.45	

Table 4. The ranges of random sets and reference values for soil variables considering spatial variation (case study 4).

Layer		Cohesion c (kN/m^2)		Friction angle φ (°)		Elastic modulus E_{ref}^{50} (MN/m^2)	
		Range of sets	Ref	Range of sets	Ref	Range of sets	Ref
Fill Material	Set 1	5.77-13.15	9.81	26.77-30.77	29	10.77-14.77	13
	Set 2	6.23-13.85		27.23-31.23		11.23-15.23	
Clayey gravel (dry)	Set 1	33.83-67.66	53.09	32.77-36.77	35	33.83-67.66	53.09
	Set 2	36.17-72.34		33.23-37.23		36.17-72.34	
Clayey gravel (saturated)	Set 1	13.83-33.83	25	32.77-36.77	35	33.83-67.66	53.09
	Set 2	16.17-36.17		33.23-37.23		36.17-72.34	
Stiff Clay	Set 1	75.74-107.66	94.04	8.77-12.77	11	16.91-33.83	26.54
	Set 2	79.26-112.34		9.23-13.23		18.09-36.17	

Table 5. The ranges of random sets and reference values for soil variables considering spatial variation (case study 5).

Layer		Cohesion c (kN/m^2)		Friction angle φ (°)		Elastic modulus E_{ref}^{50} (MN/m^2)	
		Range of sets	Ref	Range of sets	Ref	Range of sets	Ref
Fill Material	Set 1	3.75-8.75	6.5	30.75-34.75	33	6.89-16.89	12.5
	Set 2	4.25-9.25		31.25-35.25		8.11-18.11	
Clayey gravel (dry)	Set 1	48.77-66.89	58.44	32.75-36.75	35	11.89-26.89	20
	Set 2	51.23-68.11		33.25-37.25		13.11-28.11	
Clayey gravel (saturated)	Set 1	38.77-60.66	51.56	32.75-36.75	35	65.66-88.77	78.45
	Set 2	41.23-64.34		33.25-37.25		69.34-91.23	

Sensitivity analysis is carried out to identify which variables exert the most influence on the system response, and subsequently reduces the number of required finite element runs. In this study, the method provided by the U.S. Environmental Protection Agency (EPA) [36] generalized and made compatible with the random set approach by Peschl [25], is used.

Table 6. The most influential input variables based on sensitivity analysis

Case study no.	Number of basic variables	Basic variables
1, 2	4	1. Cohesion of fill material. 2. Elastic modulus of fill material 3. Cohesion of clayey sand. 4. Elastic modulus of the saturated clayey gravel layers
3	3	1. Cohesion of clayey gravel 2. Friction angle of clayey gravel 3. Elastic modulus of clayey grave
4	4	1. Cohesion of of dry clayey gravel. 2. Elastic modulus of dry/saturated clayey gravel. 3. Elastic modulus of stiff clay.
5	4	1. Cohesion of saturated clayey gravel. 2. Friction angle of saturated clayey gravel. 3. Elastic modulus of saturated clayey gravel. 4. Elastic modulus of dry clayey gravel.

According to the sensitivity analysis conducted based on the horizontal displacement of the excavation top point, the variables listed in Table. 6 were selected as the most influential ones for each case study.

In order to establish belief and plausibility functions (for example, upper and lower bounds) for a specific system response obtained from finite element calculations; the probability box (p-box) of model output has been constructed. A p-box is a pair of cumulative probability distribution functions (CDFs) that represents the imprecise probability distribution of a random variable [37]. The discrete cumulative probability functions are fitted by means of best-fit methods; to obtain a continuous distribution function matched with each of the upper and lower bounds of the reliability analysis results.

5.1 Acceptable value for horizontal displacement of the excavation top point

Considering an acceptable (Threshold) value for horizontal displacement of the excavation top point for each

Table 7. The acceptable value for horizontal displacement of the deep excavations top point.

Case study NO.	Excavation depth (m)	Neighboring situation	Acceptable δ_{max}/H (%)	Threshold value considered for horizontal displacement of the excavation top point (mm)
1	23	No important facility and building	0.5	100
2	25		0.5	100
3	36.5	Several residential buildings	0.2	65
4	34		0.2	65
5	36.5	No important infrastructure and facilities within a distance of 2*H* from the excavation	0.5	150

case study, one can estimate the probability of unsatisfactory performance of the system. The acceptable displacement depends on national codes and engineering judgment to some extent [38].

Depending on project constraints, requirements with respect to control of wall and ground movements will vary. Estimates of wall and ground movements are typically made using semi-empirical relationships developed from past performance data. According to federal highway administration manual [39] the maximum horizontal deformation, δ_{max}, for anchored walls constructed in sands and stiff clays average approximately 0.002*H* with a maximum of approximately 0.005*H* where *H* is the height of the wall. Navy design manual DM 7.2 [40] suggests that walls in sands and silts might displace laterally up to 0.002*H*. This value for stiff and soft clay was recommended to be 0.005*H* and 0.002*H*, respectively. PSCG [41], based on the importance of utilities adjacent to excavation, set some criteria for excavation protection levels in Shanghai, China. According to these criteria, δ_{max} should be less than 0.003*H* in the case that important infrastructure or facilities exist within a distance of 1-2*H* from the excavation. If no important infrastructure and facilities exist within a distance of 2*H* from the excavation, then δ_{max} should not exceed 0.007*H*.

According to the above-mentioned references the acceptable value of horizontal displacement for the intended deep excavation walls are presented in Table 7.

6 ACCEPTABLE PROBABILITY OF EXCESSIVE DEFORMATION

As mentioned earlier, excessive movements can occur without a failure mechanism occurring [7], and should be considered in the design stage as long as the failure control. It is worth mentioning that the probability of excessive deformation for a deep excavation is different from probability of ultimate failure or collapse. In order to decide whether the determined values for aforementioned probabilities are acceptable, a target value should be considered for each one. The acceptable range for the probability of failure reported in many researches is from 10-6 to 10-4 [42-45]. The acceptable probability of excessive deformation (APED) is certainly higher than these values because of the catastrophic consequences of deep excavation collapse compared to excessive deformation which might cause serviceability failure. In this study the value of 0.1 is considered for APED as proposed by Momeni et al. [38].

7 RESULTS

Figures 4 to 8 represent the reliability analysis results in comparison with the acceptable horizontal displacement value and in-situ measurements for the excavation top point in all studied cases. Such figures could be used as a tool for engineers to discuss on reliability of the system and improve the decision making procedure in order to represent proper support system plans.

7.1 Comparison and discussion for case study 1

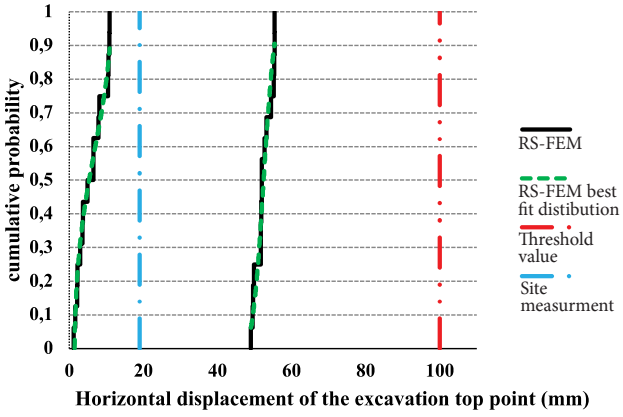

Figure 4. Reliability analysis results compared to threshold value and in-situ measurements for case study 1.

Fig. 4 shows that:

- The site measurement values (19 mm) fall within the upper and lower bounds. This observation is indicative of the appropriateness of the soil variable input values and shows the validity of the selected reliability method in estimating the deformation of system for case study 1.
- Even in the most unfavorable circumstances (upper bound), the horizontal displacement of the excavation top point does not exceed 57 mm, which is considerably less than the threshold value (100 mm); hence, it can be concluded that the support system implemented for the investigated wall was designed conservatively during the deterministic design stage.

7.2 Comparison and discussion for case study 2

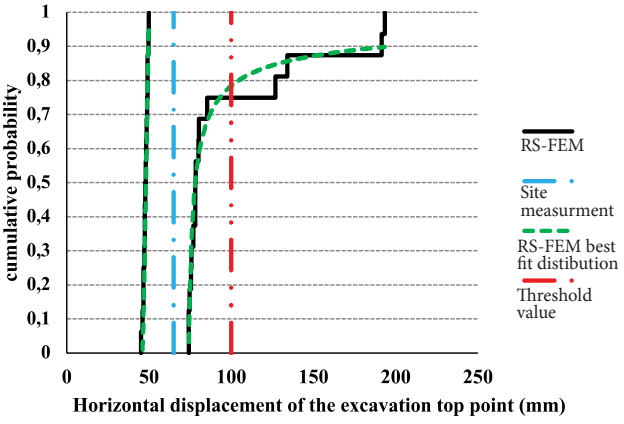

Figure 5. Reliability analysis results compared to threshold value and in-situ measurements for case study 2.

Fig. 5 shows that:

- The site measurement value of the horizontal displacement at the end of the excavation process is equal to 65 mm, which falls within the lower and upper bounds of the results.
- Under the least favorable circumstances (upper bound), the probability that the horizontal displacement of the excavation top point will exceed the threshold value is equal to 0.22 which is more than the APED value of 0.1. This result is in line with the small cracks observed on the ground surface near the excavation.

The walls investigated in case studies nos. 1 and 2 are designed by the same designers, based on identical safety factors and displacement criteria for the deterministic approach. However, according to the field observations, the probabilities of unsatisfactory performance of these two walls were different. This issue is in line with the reliability analysis results and may indicate the applicability of non-deterministic methods to predicting deep excavation system performance compared to the common deterministic methods.

7.3 Comparison and discussion for case study 3

As mentioned in Section 4, due to incorrect investigation of soil conditions considered during the deterministic design stage, the horizontal displacement calculated by means of numerical modeling was less than the threshold value. This inaccuracy led to the proposal of an inappropriate support system and subsequently the appearance of large cracks around the project location during excavation.

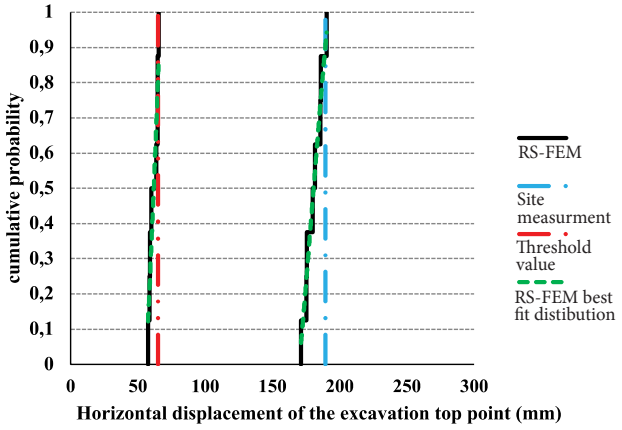

Figure 6. Reliability analysis results compared to threshold value and in-situ measurements for case study 3.

Fig. 6 shows that:

- The site measurement value is 189.5 mm, which exceeds the threshold value (65 mm). This indicates that the implemented support system, designed based on the deterministic approach, was not safe.
- The site measurement data is not placed within the range between the lower and upper bound of reliability analysis results. This is because of the significant differences between the geotechnical site investigation data and actual condition of the soil layers. However, the horizontal displacement threshold value falls within the upper and lower bounds, and is very close to the lower bound of the reliability analysis results. The threshold value position may be considered as a warning of the possibility of inappropriate system performance; hence, even in such

circumstances, the non-deterministic approaches may provide more reliable results than deterministic analysis methods.
- According to the lower bound of the results, the probability of the horizontal displacement being more than the threshold value (65 mm) is approximately 0.2. However, when considering the upper bound of the reliability analysis results, the probability of displacements being more than the threshold value is equal to 1. This demonstrates the large difference between the lower and upper bounds of the reliability analysis results, and may serve as a significant warning to the designer regarding the input data and considered support system.

7.4 Comparison and discussion for case study 4

Fig. 7 shows that:

- Although the geotechnical site investigation was not implemented correctly and did not represent the actual soil conditions, the field measurement of the horizontal displacement (152 mm) falls within the lower and upper bounds of the reliability analysis results.

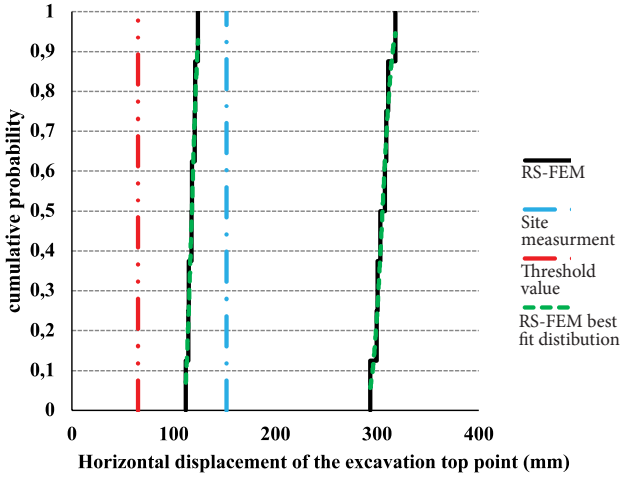

Figure 7. Reliability analysis results compared to threshold value and in-situ measurements for case study 4.

- The site measurement value (152 mm) exceeds the horizontal displacement threshold value (65 mm). As per the conclusion for the third case study, incorrect investigation of the soil condition resulted in the proposal of an inappropriate support system, and consequently, large cracks appeared around the project location during excavation activities.
- The probability of excessive deformation for both the upper and lower bounds of the results are equal to 1 and more than the APED; hence, in case study 4, the reliability analysis results demonstrates the inappropriateness of the support system, which was not recognized during the deterministic design stage.

7.5 Comparison and discussion for case study 5

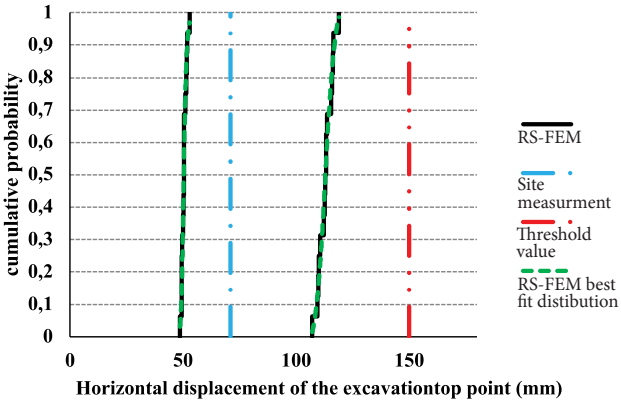

Figure 8. Reliability analysis results compared to threshold value and in-situ measurements for case study 5.

Fig. 8 shows that:

- The site measurement value (71mm) falls within the upper and lower bounds of the reliability analysis results.
- The threshold value is greater than the values of the upper and lower bounds of the reliability analysis results; hence, the reliability analysis results demonstrate that even in the least favorable circumstances (upper bound), the probability of inappropriate system performance is zero.

8 OVERALL DISCUSSION ON PROBABILITY OF UNSATISFACTORY PERFORMANCE OF STUDIED CASES

The threshold values for horizontal displacement of the excavation top point for case studies 1 to 5 are displayed in Table 8, along with the reliability analysis results, in order to evaluate the performance of the studied cases.

The conclusions drawn from the data presented in Table 8 are:

For case studies 1 and 5, which encountered no problems in practice, the probability of unsatisfactory system performance for both the lower and upper bounds of results is equal to zero. The reliability of the system in case study 2 is worse than those of nos. 1 and 5, as

Table 8. Probability of unsatisfactory performance for all case studies.

Case study NO. and related fig.	Field observation		Threshold horizontal displacement (mm)	Probability of unsatisfactory performance	
	Measured horizontal displacement (mm)	Observed cracks		Considering lower bound	Considering upper bound
NO.1, Fig.4	19	None	100	0	0
NO.2, Fig.5	65	Small	100	0	0.22 > (APED = 0.1)
NO.3, Fig.6	189.5	Large	65	0.2 > (APED = 0.1)	1 > (APED = 0.1)
NO.4, Fig.7	152	Large	65	1 > (APED = 0.1)	1 > (APED = 0.1)
NO.5, Fig.8	71	None	150	0	0

small cracks were observed on the ground surface near the excavation. According to the upper bound of the results for case study 2, the probability of the horizontal displacement exceeding the threshold value is equal to 0.22 which exceeds the APED of 0.1 and is in line with the field observations. The system performance for case studies 3 and 4 become significantly worse. For case study 3, in which excavation activities were suspended because of large cracks being observed around the excavation, the lower bound of the results was very close to the threshold value, and when the upper bound of results are considered, the probability of unsatisfactory system performance is equal to 1. For case study 4, in which excavation activities were suspended as in case 3, even in the most favorable circumstances (lower bound of results) the probability of unsatisfactory support system performance is equal to 1 and exceeds the acceptable value of 0.1. Hence, the reliability analysis results and actual field observations are in good agreement for all of the studied cases.

9 CONCLUSION

In this paper the performance of 5 real deep excavation projects were evaluated by a suggested framework and the following conclusions were drawn.

- When applying deterministic analysis methods, inaccurate site investigations may lead to the design of unsafe support systems for deep excavation. However, when using the reliability analysis method, the large difference between the upper and lower bounds of the results (as concluded for case studies 3 and 4) could be considered as a warning to evaluate the geotechnical site investigation process and revise the support system plan for deep excavation. This would prevent problems that may occur as a result of improper system design.
- When a system is designed very conservatively, the reliability analysis results could reveal it. For example in the case studies 1 and 5, the probability of unsatisfactory performance of system is equal to zero according to both lower and upper bounds of the results. This observation is indicative of the conservative design of the system in the deterministic design stage. Applying reliability analysis method for such cases may lead to optimize the plan.
- The results of reliability analysis could be used to predict unsatisfactory performance of deep excavation systems. For the five studied cases, wherever large cracks were observed on the ground surface near the deep excavation (case studies 3 and 4), in the least favorable circumstances, the probability of unsatisfactory system performance was equal to 1 which was more than the APED of 0.1. For the cases that encountered no problems in reality (1 and 5), the probability of unsatisfactory system performance was equal to zero according to both lower and upper bounds of the results. For the situation in which small cracks were observed on the ground surface near the excavation (case study 2), in the least favorable circumstances the probability of unsatisfactory system performance was equal to 0.22 and more than 0.1.

The suggested framework was applied for 5 real deep excavation projects implemented during the last 10 years. The combination of field observations and site measurements with the probability of unsatisfactory performance determined using reliability analysis, and the APED showed that the presented framework is an applicable tool to help the designer improve the decision making procedure and represent more proper support system plans compared to deterministic analysis methods.

REFERENCES

[1] El Sawwaf M, Nazir AK. The effect of deep excavation-induced lateral soil movements on the behavior of strip footing supported on reinforced sand. Journal of Advanced Research. 2012;3(4):337-44.

[2] Peck, R.B. (1969) Deep Excavation and Tunneling in Soft Ground. State of the Art Report. 7th

International Conference on Soil Mechanics and Foundation Engineering, Mexico City, 225-290.
[3] Clough GW, O'Rourke TD. Closure to "Construction Induced Movements of Insitu Walls" by G. W. Clough and Thomas D. O'Rourke (June 18–21, 1990, No. 25). Journal of Geotechnical Engineering. 1992;118(4):665-6.
[4] Boscardin Marco D, Cording Edward J. Building Response to Excavation-Induced Settlement. Journal of Geotechnical Engineering. 1989;115(1):1-21.
[5] Burland JB, Wroth CP, Establishment BR. Settlement of Buildings and Associated Damage: Building Research Establishment; 1975.
[6] Dalgic KD, Hendriks MAN, Ilki A. Building response to tunnelling- and excavation-induced ground movements: using transfer functions to review the limiting tensile strain method. Structure and Infrastructure Engineering. 2018;14(6):766-79.
[7] Marr WA, Hawkes M. Displacement-Based Design for Deep Excavations, Earth Retention Conference 3. p. 82-100, 2010.
[8] Zumrawi M, El-Amin A. Importance of Deep Excavation Support and Its Influence on Adjacent Buildings2016.
[9] Uzielli M, Lacasse S, Nadim F, Phoon K-K. Soil variability analysis for geotechnical practice. 2nd International Workshop on Characterisation and Engineering Properties of Natural Soils. 2006;3:1653-752.
[10] Beer M, Zhang Y, Quek ST, Phoon KK. Reliability analysis with scarce information: Comparing alternative approaches in a geotechnical engineering context. Structural Safety. 2013;41(Supplement C):1-10.
[11] Christian, JT., CC, Ladd, GB, Baecher, "Reliability applied to slope stability analysis", Geotechnical Engineering, 1994: 120(12), 2180.
[12] Kaymaz I. Application of kriging method to structural reliability problems. Structural Safety. 2005;27(2):133-
[13] Kyung Park J, Tanner Blackburn J, Gardoni P. Reliability assessment of excavation systems considering both stability and serviceability performance. Georisk: Assessment and Management of Risk for Engineered Systems and Geohazards. 2007;1(3):123-41.
[14] Muhanna RL, Zhang H, Mullen RL. Interval Finite Elements as a Basis for Generalized Models of Uncertainty in Engineering Mechanics. Reliable Computing. 2007;13(2):173-94.
[15] Nadim F. Tools and Strategies for Dealing with Uncertainty in Geotechnics. In: Griffiths DV, Fenton GA, editors. Probabilistic Methods in Geotechnical Engineering. Vienna: Springer Vienna; 2007. p. 71-95.
[16] Pula W, Bauer J. Application of the response surface method. In: Griffiths DV, Fenton GA, editors. Probabilistic Methods in Geotechnical Engineering. Vienna: Springer Vienna; 2007. p. 147-68.
[17] Zhang J, Zhang LM, Tang WH. Bayesian Framework for Characterizing Geotechnical Model Uncertainty. Journal of Geotechnical and Geoenvironmental Engineering. 2009;135(7):932-40.
[18] Suchomel R, Mašı´n D. Comparison of different probabilistic methods for predicting stability of a slope in spatially variable c–φ soil. Computers and Geotechnics. 2010;37(1):132-40.
[19] Beer M, Zhang Y, Quek ST, Phoon KK. Reliability analysis with scarce information: Comparing alternative approaches in a geotechnical engineering context. Structural Safety. 2013;41(Supplement C):1-10.
[20] Javankhoshdel S, Luo N, Bathurst RJ. Probabilistic analysis of simple slopes with cohesive soil strength using RLEM and RFEM. Georisk: Assessment and Management of Risk for Engineered Systems and Geohazards. 2017;11(3):231-46.
[21] Goswami S, Ghosh S, Chakraborty S. Reliability analysis of structures by iterative improved response surface method. Structural Safety. 2016;60(Supplement C):56-66.
[22] Marrapu, B.M., Ravi, S.Jakka "Assessment of slope stability using multiple regression analysis", Geomechanics and Engineering, 2017: 13(2), 237-254.
[23] Zhao, L., Xia, P., Li, L., Zhang, Y., Cheng, X, "Stability analysis of homogeneous slopes with benches", Geomechanics and Engineering, 2017; 13(3), 517-533.
[24] Kendall, D.G. (1974), Foundations Of A Theory Of Random Sets, In: Harding, E.F., Kendall, D.G., (eds.) Stochastic Geometry, Wiley, New York, U.S.
[25] Peschl, GM. (2004), "Reliability analyses in geotechnics with the random set finite element method", Ph.D. Dissertation, Graz University of Technology, Graz.
[26] Schweiger, HF., G.M, Peschl. (2005), "Reliability analysis in geotechnics with the random set finite element method", Computers and Geotechnics, 32(6), 422-435.
[27] Nasekhian, A., H.F, Schweiger. (2011), "Random set finite element method application to tunnelling", International Journal of Reliability and Safety, 5(3-4), 299-319.
[28] Shen, H., S.M, Abbas. (2013), "Rock slope reliability analysis based on distinct element method and random set theory", International Journal of Rock

Mechanics and Mining Sciences, 61, 15-22.
[29] Ghazian Arabi, M., A, Fakher. (2016), "Reliability analysis in Iran-Zamin excavation by application of Random Set Finite Element Method", Proceedings of the 4th International Reliability Engineering Conference, Tabriz, Iran, May.
[30] Arabani A, Fakher A. Application of non-probabilistic Random set theory in reliability analysis of excavations. In: The 4th International Reliability Engineering Conference. Sahand University of Technology, Tabriz, Iran; 2016.
[31] Momeni E, Poormoosavian M, Mahdiyar A, Fakher A. Evaluating random set technique for reliability analysis of deep urban excavation using Monte Carlo simulation. Computers and Geotechnics. 2018;100:203-15.
[32] Dubois, D., H, Prade. (1991), "Random sets and fuzzy interval analysis", Fuzzy Sets and Systems, 42(1), 87-101.
[33] Tonon, F., A, Bernardini., A, Mammino. (2000), "Determination of parameters range in rock engineering by means of random set theory", Reliability Engineering & System Safety. 70(3), 241-261.
[34] Schittkowski K. EASY-FIT User Guide. Germany: Department of Mathematics, University of Bayreuth; 2008.
[35] Brinkgreve RBJ. PLAXIS, Finite element code for soil and rock analyses. Users manual. Rotterdam: Balkema, 2007.
[36] USEPA T. Total risk integrated methodology status report. US Environmental Protection Agency Office of Air Quality Planning and Standards: Research Triangle Park; 1999.
[37] Nasekhian, A. (2011), "Application of non-probabilistic and probabilistic concepts in Finite Element analysis of tunneling", Ph.D. Dissertation, Graz University of Technology, Graz.
[38] Momeni E, Poor moosavian S, Fakher A. Acceptable probability of excessive deformation for deep urban excavations. In: Proceeding of the 70th Canadian geotechnical conference, Ottawa, Ontario, Canada; 2017.
[39] Sabatini P.J., Pass D.G., Bachus R.C. Geotechnical Engineering Circular No. 4, Ground Anchors and Anchored Systems, FHWA Publication No.FHWA-IF-99-015, Technical Manual, 1999; 281.
[40] Navy, U. S. 1982. Foundations and earth structures, NAVFAC design manual. DM-7.2.
[41] PSCG (2000). Specification for Excavation in Shanghai Metro Construction, Professional Standards Compilation Group, Shanghai, China.
[42] Smith GN. A suggested method of reliability analysis for earth retaining structures; 1986.
[43] Santamarina J, Altschaeffl A, Chameau J. Reliability of slopes: incorporating qualitative information (abridgment). Transport Res Rec; 19921343).
[44] Risks R. Protecting people. Health and safety executive; 2001.
[45] Anon A. New focus on landslide risk management. The earthmover & Civil Contractor; 2000.

DIAMETRIC SPLITTING TESTS ON UNSATURATED EXPANSIVE SOIL WITH DIFFERENT DRY DENSITIES BASED ON PARTICLE IMAGE VELOCIMETRY TECHNIQUE

DIAMETRALNI CEPITVENI PREIZKUSI NA NENASIČENI EKSPANZIVNI ZEMLJINI Z RAZLIČNO SUHO GOSTOTO NA OSNOVI OPTIČNE METODE PIV

Junran Zhang *(corresponding author)*
North China university of water resources and electric powery,
Henan province key laboratory of geomechanics and structural engineering
Zhengzhou, Henan 450046, China
E-mail: zhangjunran@ncwu.edu.cn

Lijin Wang
North China university of water resources and electric powery,
Henan province key laboratory of geomechanics and structural engineering
Zhengzhou, Henan 450046, China
E-mail: 201300804@stu.ncwu.edu.cn

Tong Jiang
North China university of water resources and electric powery,
Henan province key laboratory of geomechanics and structural engineering
Zhengzhou, Henan 450046, China
E-mail: jiangtong@ncwu.edu.cn

Miao Ren
North China university of water resources and electric powery,
Henan province key laboratory of geomechanics and structural engineering
Zhengzhou, Henan 450046, China
E-mail: renmiao@ncwu.edu.cn

Min Wei
North China university of water resources and electric powery,
Henan province key laboratory of geomechanics and structural engineering
Zhengzhou, Henan 450046, China
E-mail: 190620115@qq.com

DOI https://doi.org/10.18690/actageotechslov.18.1.15-27.2021

Keywords

diametric splitting, tensile strength, unsaturated expansive soil, particle image velocimetry

Ključne besede

diametrična cepitev, natezna trdnost, nenasičena ekspanzivna zemljina, optična metoda delec-slika-meritev hitrosti (PIV)

Abstract

There is a close relationship between tensile strength of soil and crack development, but the tensile stress-strain in full failure process is rarely studied because challenges exist in accurately measuring shear strain using traditional methods. In this paper, we employed a newly developed diametric splitting testing apparatus and particle image velocimetry (PIV) system to study the tensile strength of compacted unsaturated expansive soil with different water contents and initial dry densities. Soil water characteristic curves of compacted expansive soil with different initial dry densities were determined using the filter paper method. Test results show that the tensile strength increases first and then decreases with increasing water content,

Izvleček

Med natezno trdnostjo zemljin in nastankom razpok obstaja tesna povezava, vendar se odnos med nateznimi napetostmi in specifičnimi deformacijami v celotnem procesu porušitve redko preučujejo, ker obstajajo dvomi v natančnost merjenja strižnih specifičnih deformacij s tradicionalnimi metodami. V tem prispevku smo uporabili novo razvito diametralno cepilno preskusno napravo in optično metodo delec-slika-meritev hitrosti (PIV) za preučevanje natezne trdnosti trdne, nenasičene, ekspanzivne zemljine z različno vlažnostjo in začetno suho gostoto. Krivulje zemljina-voda za trdne ekspanzivne zemljine z različnimi začetnimi suhimi gostotami so bile določene z metodo filtrirnega papirja. Rezultati preizkusov kažejo, da se nate-

and there is a critical water content for the peak load vs. water content curve. The diametric splitting test process can be divided into four stages on the basis of the plotted load-displacement curves: a stress contact adjustment stage (I); stress approximately linear increasing stage (II); tensile failure stage (III); and residual stage (IV). Under the same water content, the angle between the major directions of the displacement vector and the major crack decreases with increasing the dry density, especially when the fissure appears. Using the particle image velocimetry technique, the displacement and strain during the test process recorded is helpful for better understanding the soil failure mechanism.

zna trdnost najprej poveča in nato zmanjša z naraščanjem vlažnosti, za krivuljo največja obtežba-vlažnost pa obstaja kritična vlažnost. Na podlagi izrisanih krivulj obtežba--premik lahko postopek preizkusa diametralne cepitve razdelimo na štiri stopnje: (I) stopnja vzpostavitve stika napetosti; (II) stopnja približno linearno naraščajoče napetosti; (III) stopnja natezne porušitve; in (IV) rezidualna stopnja. Pri enaki vlažnosti se kot med glavnimi smermi vektorja premika in glavno razpoko zmanjšuje z naraščajočo suho gostoto, zlasti ko se pojavi razpoka. Uporaba optične metode PIV je koristna, ker nam posneti premiki in specifične deformacije med preizkusnim postopkom omogočajo boljše razumevanje mehanizma porušitve zemljine.

1 INTRODUCTION

Tensile strength is an important soil-strength parameter to describe the soil's resistance to loading, and is considerably smaller than other aspects of soil strength [47]. Expansive soil is a typical special soil, which has the characteristics of expansion, contraction, fissuring, and over-consolidation, owing to its hydrophilic minerals, such as montmorillonite. Expansive soils are particularly sensitive to climate changes. As shown in Ng et al. [25], the hydro-mechanical behavior of expansive soils was significantly affected by climate changes, which can lead to a severe disaster for geotechnical engineering. Desiccation cracking is a common phenomenon during the drying and wetting cycles for expansive soils that occur in various geotechnical engineering projects, such as dams, slopes and embankments [5], [35], [38]. Previous studies have shown that the cracks change remarkably through the hydro-mechanical behavior of soils [41]. Cracks in the soils lead to a sharp increase in the permeability coefficient. At the same time, the existence of cracks will aggravate the corrosion of soils and leads to an increase in the probability of geological disaster [33], [36].

Extreme drought has occurred in recent years, with increasing frequency and soil desiccation cracking [42], [34], [14]. Desiccation cracking occurs when the tensile stress in the soil exceeds a certain limit (i.e., tensile strength) [23]. Determination of the soil-cracking mechanism and improving the safety of geotechnical structures are therefore of great significance to comprehensively understand the tensile strength of special soils, especially for expansive soil.

The testing methods for measuring soil's tensile strength include direct and indirect methods. The indirect tensile-test methods include the split tensile test, the beam bending test and the axial fracturing test [7], [37], [12], [18], [24], [22], [6]. The above methods are suitable for rock and concrete. For soft soils, some coefficients are necessary [7] to correct the test results.

Most previous studies used a linear variable differential transducer (LVDT) to measure the deformation of the specimens with regard to the tensile strain. The LVDT method is suitable for uniform soils. The development of image-processing techniques in recent decades has significantly improved strain measurements. The displacement and strain on the specimen's surface can be tracking in a full process by using the particle-image-velocimetry (PIV) and digital-image-correlation (DIC) techniques [46], [11], [1]. The PIV technique has the advantages of non-contact and high resolution, and it has been widely applied in geotechnical engineering [45], [5], [19], [31], [44], [43], [49]. These studies reported that desiccation crack sites can be reliably predicted on the basis of the surface strain field.

Many researches have focused on the tensile strength of unsaturated soil (e.g., [20], [21], [13], [4], [38], [40], [17], [47], [8], in which most studies are mainly focused on the tensile strength. However, the tensile stress-strain in a full-failure process is rarely studied, and because of that there are challenges in accurately measuring the shear strain using traditional methods. Moreover, the influence of the initial dry density and the water content on the tensile stress of expansive soil during the tensile-test process and the failure mechanism remain unclear. It needs further study [16].

In order to study the tensile stress-strain in the full-failure process of expansive soil systematically, we have designed a new diametric splitting test with a PIV system. The DIC and PIV techniques were employed to obtain the strain field. A series of diametric splitting tests were conducted on compacted, unsaturated, expansive soil specimens with different water contents

of 10–22 % and initial dry densities of 1.35–1.65 Mg/m^3. The test results are analyzed and discussed in the following, together with the PIV images.

2 MATERIAL AND METHODS

2.1 Testing apparatus

The diametric splitting testing apparatus with the PIV system is shown in Figure 1. The diametric splitting testing apparatus consists of three systems: the loading test system, the data collection system, and the PIV system. During the test, the three systems were synchronized. The loading system used in the tests is the CMT4000 electronic universal testing machine developed by the American Meester Company. This instrument includes the loading equipment and the data-acquisition system and can automatically control the constant-velocity displacement rate. The load is applied using the strain control type with the compression rate ranging from 0 to 10 mm per minute. The speed selected in this study is 1.4 mm per minute. The data of the load is monitored using a load cell with a maximum range of 160 N, and a working resolution of 0.001 N. During the test, the displacement and load measurements are carried out simultaneously. The displacement is monitored by a LVDT with a maximum range of 100 mm and a working resolution of 0.001 mm.

A high-speed CCD camera with high sensitivity and image quality was vertically mounted above the specimen and manually focused on the specimen's surface. Seven pictures were taken per second to record the deformation in the full process. Davis8.3 software was then used to obtain the required images and specific locations were selected and analyzed using PIVview2C and Tecplot10 instruments. The size range of the specimens photographed in the tests is about 38.5 × 38.5 cm^2. The initial specimen size used in the tests is d_0 = 6.18 cm and h_0 = 2 cm.

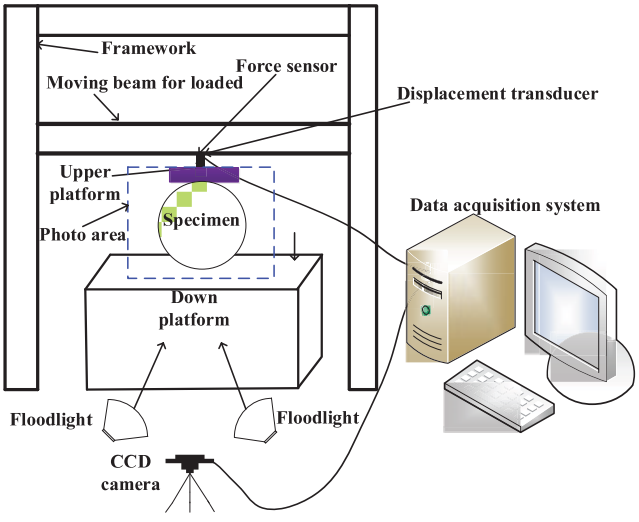

Figure 1. Schematic diagram of testing apparatus.

2.2 Soil sample

The expansive soil was collected from Nanyang City, Henan Province, China, and is similar to that used in Zhang et al. [48] but from a different location. The expansive soil has a liquid limit of 52.7 % and a plasticity index of 29 %. Other physical property indexes, such as specific gravity, liquid limit, plastic limit, optimum water content, maximum dry density, and free swelling ratio, are listed in Table 1.

Fig. 2 shows the grading curve determined by the hydrometer analyses. The soil is composed of 21.1 % clay fraction (<2 μm). According to the USCS soil classification, the expansive soil from the Nanyang site is CL.

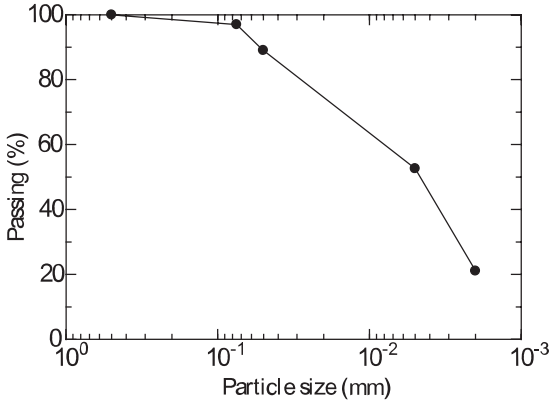

Figure 2. Grading curve of the expansive soil.

2.3 Sample preparation

The dried and pressed sample first passed through a 2-mm sieve. Then the sample was mixed with distilled water. Seven groups of samples were prepared with water contents of 10 %, 12 %, 14 %, 16 %, 18 %, 20 %, and 22 %. The soil samples were stored in an airtight container for 96 hours to distribute the water evenly. The required quantity of samples was then put into a mold

Table 1. Property indexes of expansive soil.

Specific gravity G_s	Liquid limit w_L (%)	Plastic limit w_P (%)	Plasticity index I_p (%)	Maximum dry density $\delta_{d,max}$ (Mg/m^3)	Optimum water content w_{opt} (%)	Free swelling ratio (%)	Unified Soil Classification System
2.73	52.7	23.7	29	1.68	18.9	49	CL

and compacted to different initial dry densities of 1.35, 1.50, or 1.65 Mg/m^3. The specimen-preparation method is different from that of specimens undergoing drying from saturated specimens to specimens with different water contents [48]. It is known that in the drying process, the dry density of expansive soil will increase, and resulting in an increase in strength.

2.4 Test procedure

The diametric splitting tests were performed at a constant speed. The speed is 0.14 mm/min in the vertical direction. The tensile load and displacement were monitored during the testing. For each test group, two parallel specimens were prepared to check the procedural reproducibility.

2.5 Image processing

Surface deformation was monitored during the tests using the PIV system with images taken at 7-s intervals. After the tests, the images were changed to grayscale images and the study area with 60 × 60 mm^2 around the specimen (as shown in Figure 1) was selected and imported into the programs PIVview2C and Tecplot10 for the image analyses. Deformation information at different stages was obtained by comparing the images with the reference images taken prior to the tests. The length and orientation of the vectors representing the deformation are shown in the displacement vector field.

2.6 Soil-water characteristic curve test

The specimen-preparation method used in the soil-water characteristic curve test is the same as that used in the diametric splitting test. The suction was measured at different compaction water contents (6–22 %) of specimens with dry densities of 1.35, 1.50, and 1.65 Mg/m^3 using the filter-paper method. Circular quantitative filter paper Whatman No. 42 was used for the filter paper method and the expression for determining the matrix suction from Leong et al. [15] is formulated as follows:

$$\log s = 2.909 - 0.0229 w_f \quad (w_f \geq 47) \qquad (1)$$

$$\log s = 4.945 - 0.0673 w_f \quad (w_f > 47) \qquad (2)$$

In the above formula, s is the matrix suction, and w_f is the water content of the filter paper.

Before the tests, the filter paper was kept in an oven at 105°C for more than 16 h to ensure dryness and then put in a dryer for cooling and storage. The soil specimen and filter paper contacted together and were put into a sealed box, which was held at constant temperature (20±2 °C) and humidity for two weeks. After that the papers were quickly, carefully, and individually removed using forceps. The weight of the filter paper was measured with a balance having 0.0001-g precision and the water content of the filter paper was measured. The weight of the soil specimen was also measured. The matrix suction was calculated according to Eq. (1) or (2) and the soil-water characteristic curve (SWCC) was determined. More details about the suction measurement procedures can be found in Leong et al. [15].

3 RESULTS AND DISCUSSION

3.1 Soil-water characteristic curve of expansive soil

The results of the soil-water characteristic curves (SWCCs) tests for the expansive soil with different initial dry densities are shown in Fig. 3. The water content (w) and degree of saturation (S_r) both decrease with increasing suction. The relationships w-s and S_r-s are shown in Fig. 3a and Fig. 3b, respectively. The SWCCs move left and down with increasing initial dry density when the suction is less than 5000 kPa, as shown in Fig. 3a. The influence of the initial dry density on the soil-water characteristic curve is very obvious, especially for low suction, i.e., the water content decreases with increasing dry density under the same suction. When the suction is greater than 5000 kPa, the dry density's influence on the SWCCs is not apparent. A similar test result for SWCCs was found by Romeroe and Vanat [27] and Gao et al.

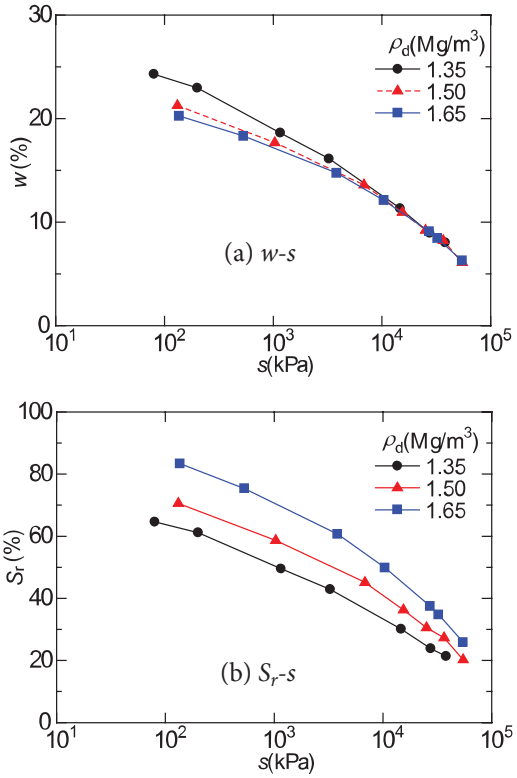

Figure 3. Soil-water characteristic curves of expansive soil.

[9]. In terms of the saturation degree, the SWCC curves move right and upwards with increasing dry density, as shown in Fig. 3b. The influence of the initial dry density on the soil-water characteristic curve is very obvious in the full suction range, the degree of saturation decreases with decreasing initial dry density under the same suction conditions, which is similar to that reported by Sun et al. [28], [29] and Sun and Sun [30].

3.2 Influence of initial dry density on the stress and strain behavior

The Influence of the initial dry density on the relationship between the load and the displacement of specimens with different water contents is shown in Fig. 4. For the plastic soil, the relationship between the load

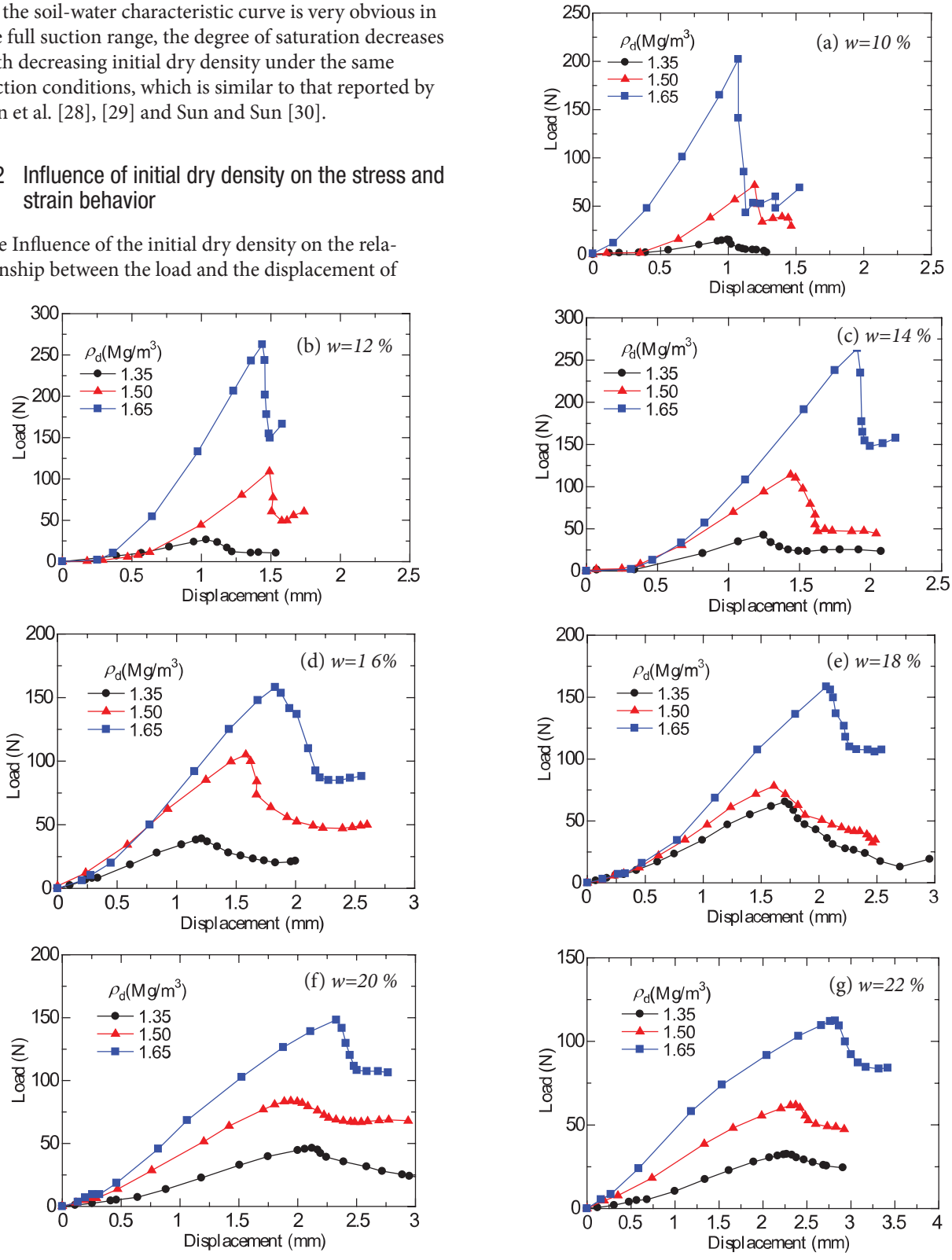

Figure 4. Influence of initial dry density on the relationship between load and displacement.

and the displacement in the splitting tests appears as a double-peak phenomenon. However, the soil underwent substantial plastic deformation in the second peak stage, which indicates that the stage poses little significance for studying the tensile strength. We therefore focus mainly on the curves in the first peak stage.

The results in Fig. 4 also show that the influence of the initial dry density on the tensile strength is very obvious. Under the same water-content conditions, the peak load increases with increasing initial dry density. As shown in Fig. 4a, when the water content is 10 %, the average peak load increases by 322.1 % and 1065.7 % as the dry density increases from 1.35 to 1.50 and from 1.35 to 1.65 Mg/m^3, respectively. A similar test result was found by Blazejczak et al. [3]. This is because the specimen with a higher initial dry density has more contacts between the soil particles, and the number of water bridges increased, which leads to a higher peak load. The test results are more obvious, especially for expansive soil with a low water content.

The average increases of the peak load as the initial dry density increases from 1.35 to 1.50 Mg/m^3 and to 1.65 Mg/m^3 are shown in Figure 5. The average increase of the peak load decreases with increasing water content. Above, a similar test result was obtained by Li et al. [16].

3.3 Influence of water content on tensile stress-strain behavior

The influence of the initial water content on the relationship between the load and the displacement at different initial dry densities is shown in Fig. 6, which shows that the peak load first increases and then decreases with an increasing water content. The displacement where the relationship curve between the load and stress reaches the first peak value essentially increases with the water content. When the initial dry density is 1.35 Mg/m^3, the peak value increases in the water content range from about 10 % to 18 %, and decreases from 18 % to 22 %. However, when the initial dry density is 1.50 and 1.65 Mg/m^3, the peak value increases in the water content range from 10 % to 14 % and decreases from 14 % to 22 %. In addition, part of the slope of the curve that reaches the first peak value is larger with lower water content, which indicates that the brittleness is more apparent for compacted expansive soil with a low water content.

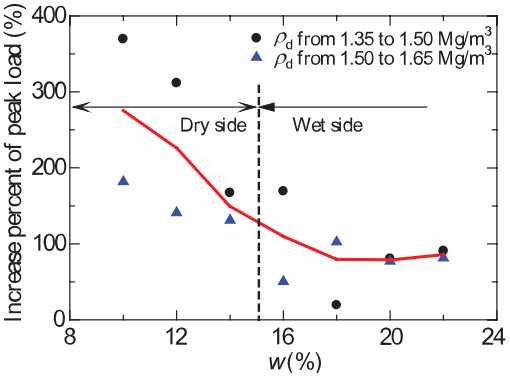

Figure 5. Average increase of peak load at different water contents with increasing initial dry density from 1.35 to 1.50 Mg/m^3 and from 1.50 to 1.65 Mg/m^3.

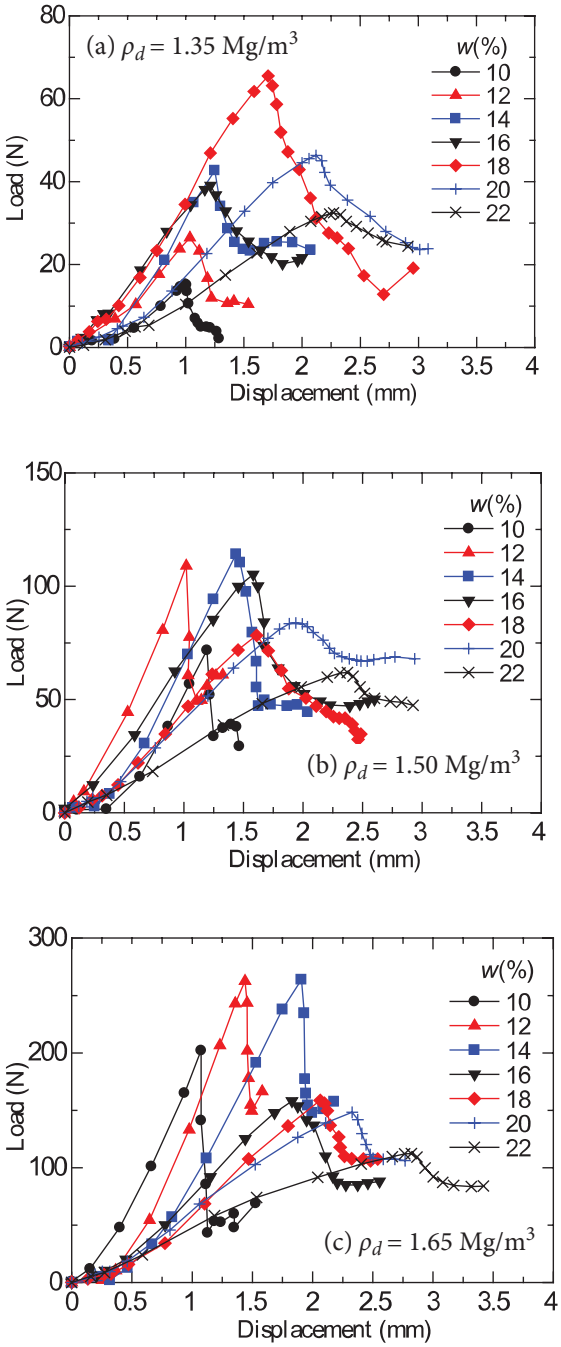

Figure 6. Effect of water content on the relationship between load and displacement.

There is a close functional relationship between the tensile strength and the suction for unsaturated soils [20], [32], [40]. As soils are subjected to drying conditions and the suction increases during the drying [50], which increases the tensile strength [39]. The peak-load characteristic curves (PLCCs) are shown in Fig. 7, which are according to relationship between the load and displacement in Fig. 6. And the soil-water characteristic curves (i.e., SWCCs) are also presented in Fig. 7.

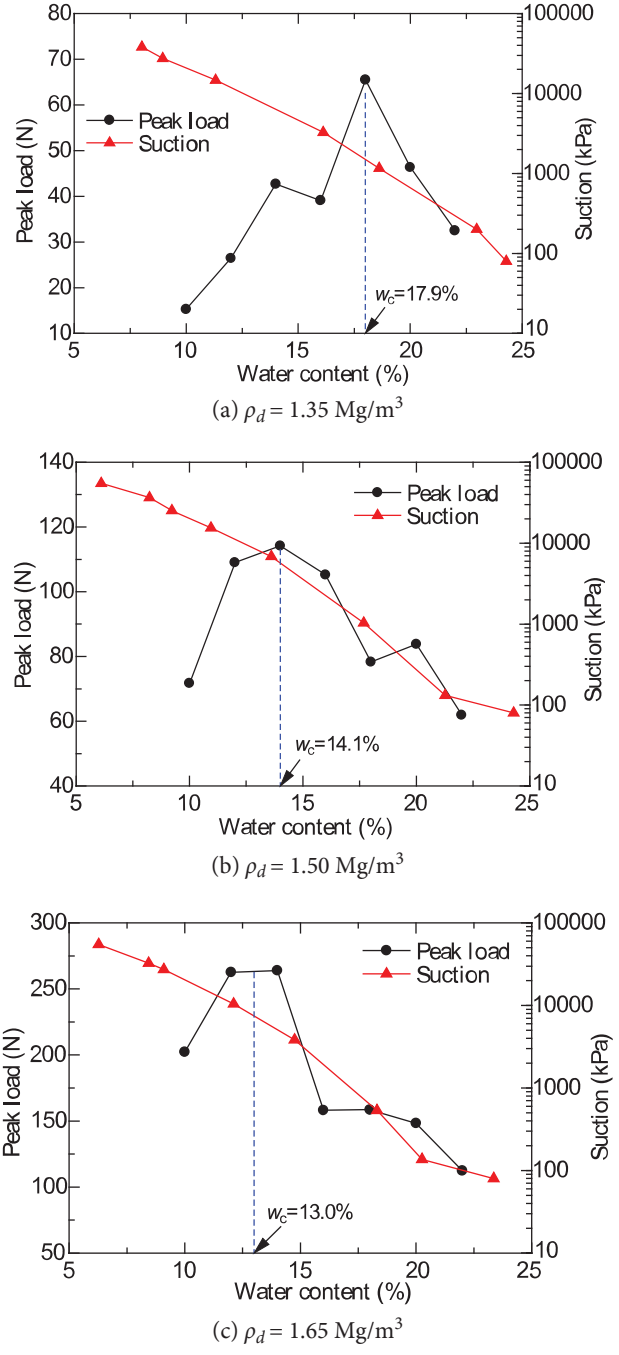

(a) ρ_d = 1.35 Mg/m^3

(b) ρ_d = 1.50 Mg/m^3

(c) ρ_d = 1.65 Mg/m^3

Figure 7. PLCCs and SWCCs at different initial dry densities.

Fig. 7 indicates that the PLCCs are unimodal curves and the PLCCs is influenced by the water content. Tang et al. [35] obtained similar results. The critical water content, w_c (~17.9 %, ~14.1 %, ~13 %), corresponding to the maximum peak load (65.5, 114.2, and 263.9 N) for different initial dry densities of 1.35, 1.50 and 1.65 Mg/m^3 are determined from Figure 7. When w is less than w_c, the peak load increases with an increase in the water content. However, when the water content is higher w_c, the peak load decrease with an increase in the water content. The reason is as follows.

The change of microstructure with water content should be considered [40]. Most of the water is stored inside the aggregate pores at low water contents and it is very difficult to form liquid bridges [10]. The soil's tensile strength depends mainly on the liquid bridges among the particles. When w is less than w_c, the liquid bridges form gradually with an increasing water content, and thus the peak load (tensile strength) increases with an increasing water content.

When the water content increases up to w_c, the liquid bridges appear at most contact points of particles. The liquid bridges among the particles will disappear gradually with a further increasing water content, resulting in a decrease in the tensile strength.

3.4 Effects of initial dry density and water content on the displacement vector field

Figs. 6 and 8 show that the water content has a very obvious effect on the tensile strength. The images taken during the tests were analyzed, with the initial image taken immediately prior to the load application. The PIV and DIC techniques allow characterization of the evolution of the deformation patterns. Typical results are presented in Fig. 9 and are related to specimens at low

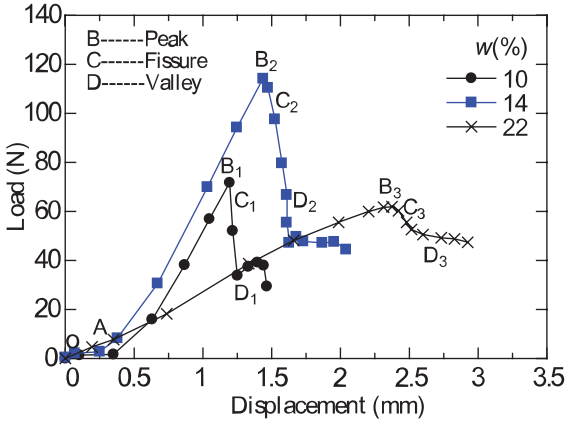

Figure 8. Typical relationship between load and displacement (ρ_d = 1.50 Mg/m^3)

water contents (i.e., $w = 10$ %), around w_c (i.e., $w = 14$ %), and a high water content (i.e., $w = 22$ %) and with an initial dry density of 1.50 Mg/m^3.

As shown in Fig. 8, the load-displacement curve of compacted, expansive soil with different water contents can be separated into four stages: a stress contact adjustment stage (I), for section OA, which is caused by the stress concentration of the upper and lower indenters on the contact parts of the specimens; stress approximately linearly increasing stage (II), for section AB, in which the load increases practically linearly with increasing displacement until reaching the peak (i.e., tensile strength); tensile failure stage (III), for section BC,

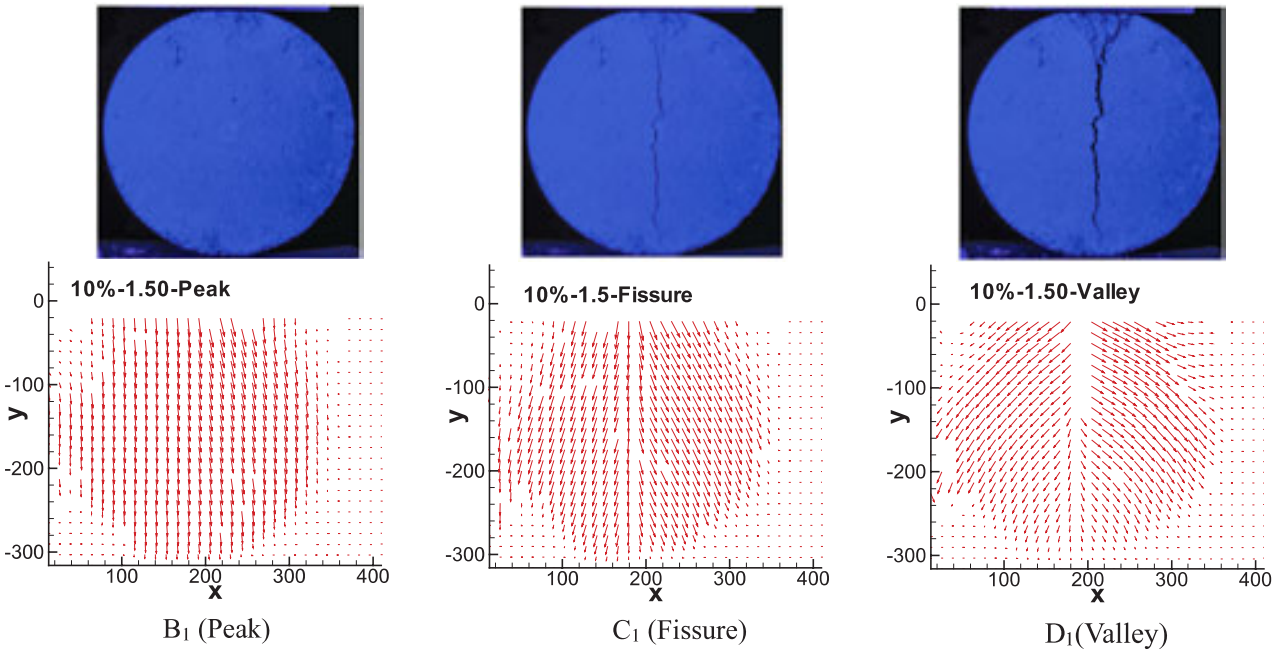

B_1 (Peak) C_1 (Fissure) D_1(Valley)

(a) $w = 10$ %

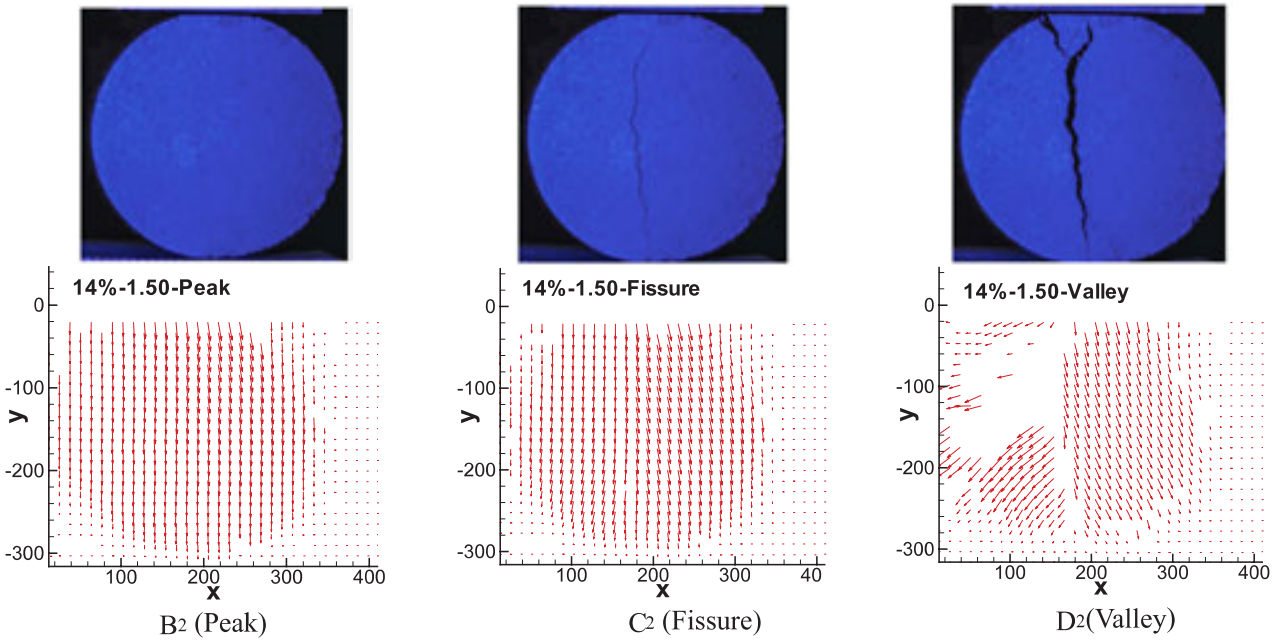

B_2 (Peak) C_2 (Fissure) D_2(Valley)

(b) $w = 14$ %

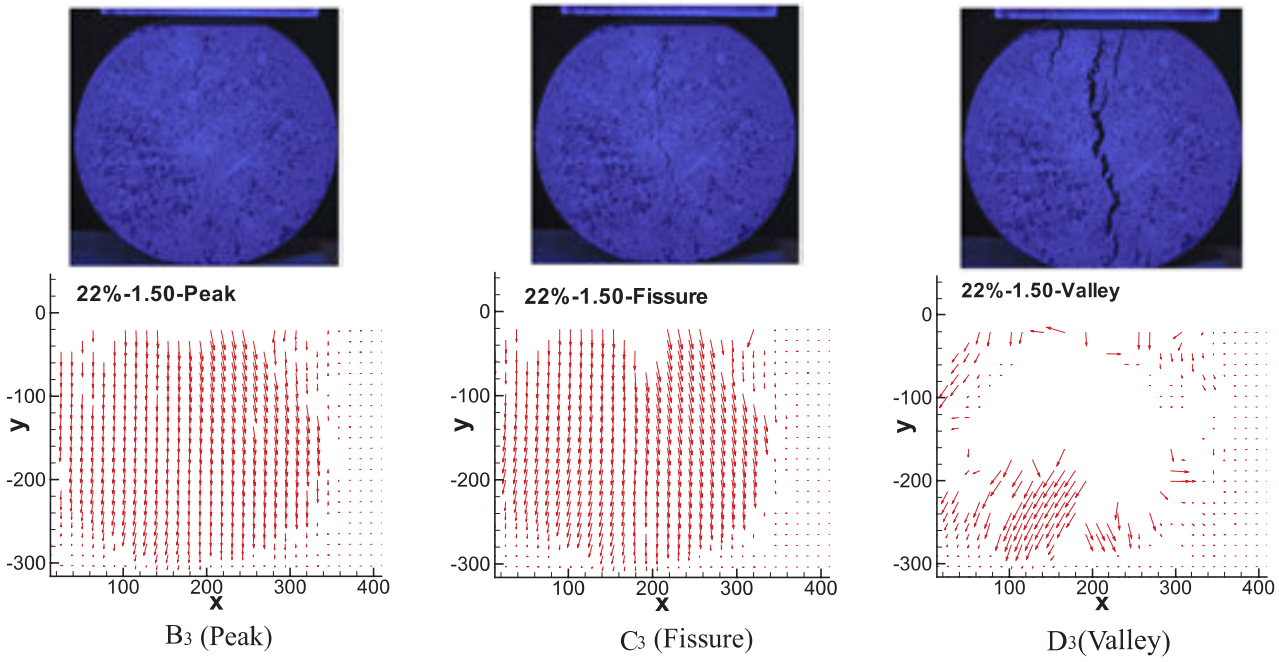

(c) $w = 22\ \%$

Figure 9. Failure process and displacement vector field for specimens with different water contents.

where the specimen begins to crack and the curve drops steeply after reaching the target value; and the residual stage (IV) for section CD, where the specimen shows clear splitting cracks, the curve decreases rapidly to zero and the specimen subsequently shows a certain residual strength. With increasing stress, the crack continues to expand until it is completely destroyed.

The fracture propagation of specimens with different water contents and their displacement vector fields are shown in Fig. 9. After the applied load experiences the AB segment, which is an approximately straight line, no obvious crack appears when the peak stress point B is reached. After the load drops to point C, a splitting crack appears on the splitting surface and the load drops sharply to point D. The fracture diagram and its displacement vector field of points B, C, and D are shown in Fig. 9a–9c, respectively. According to the displacement vector field in Fig. 9, the specimen at point B only underwent compression deformation without the formation of obvious cracks, owing to the plasticity of the soil mass. After the peak, cracks appear at point C and the displacement vector field is distributed symmetrically on both sides of the splitting surface. At point D, the load drops to the trough and the cracks connect. The failure part of the specimen is due to excessive displacement and the displacement vector field obtained by the PIV technique is a blank area. Moreover, the above phenomenon first increases and then decreases with increasing water content, which is most apparent at the optimal water content (i.e., $w = 14\ \%$), and the time required to complete the II–IV stages shows a similar trend with the increasing water content.

Figs. 5 and 10 show that the initial dry density has a very obvious effect on the tensile strength. The images taken during the tests were analyzed, with the initial image taken immediately prior to the application of the tensile load. The evolution of the deformation patterns is characterized using the PIV and DIC techniques. The typical results are presented in Fig. 11, and are related to specimens with different initial dry densities (1.35, 1.50, and

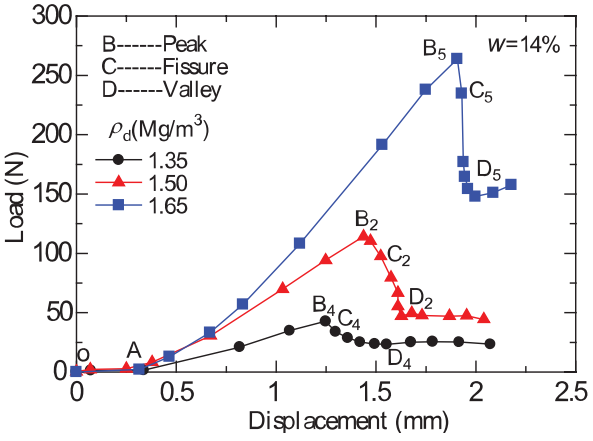

Figure 10. Typical relationship between load and displacement ($w = 14\ \%$).

1.65 Mg/m^3), and with a water content of 14 %. Under the same water content, the angle between the major direction of the displacement vector and the major crack decreases with increasing dry density, especially at point C, as two arrows show in middle figures of Fig. 11(a), (b) and (c). The above phenomenon might be caused by the specimens becoming increasingly hard as the dry density increases and the lateral displacement of the specimens decreases. Similar test results are observed for other specimens with different water contents (w = 10 %–22 %).

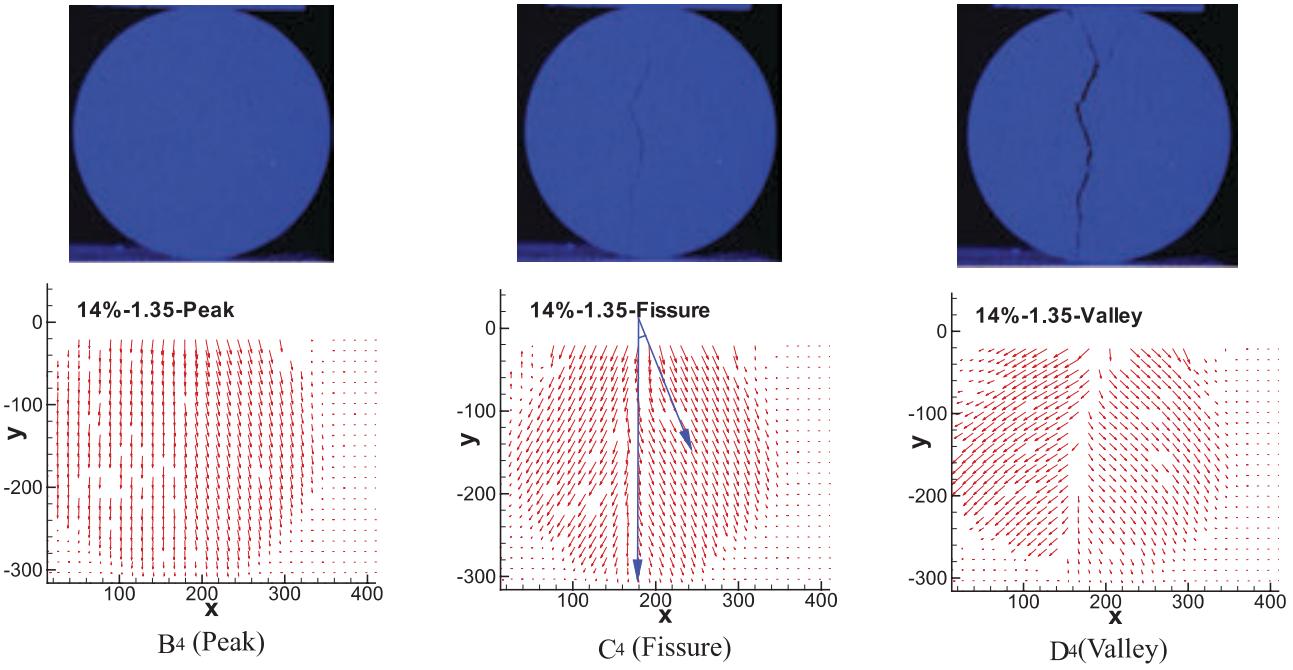

B4 (Peak) C4 (Fissure) D4(Valley)

(a) ρ_d = 1.35 Mg/m^3

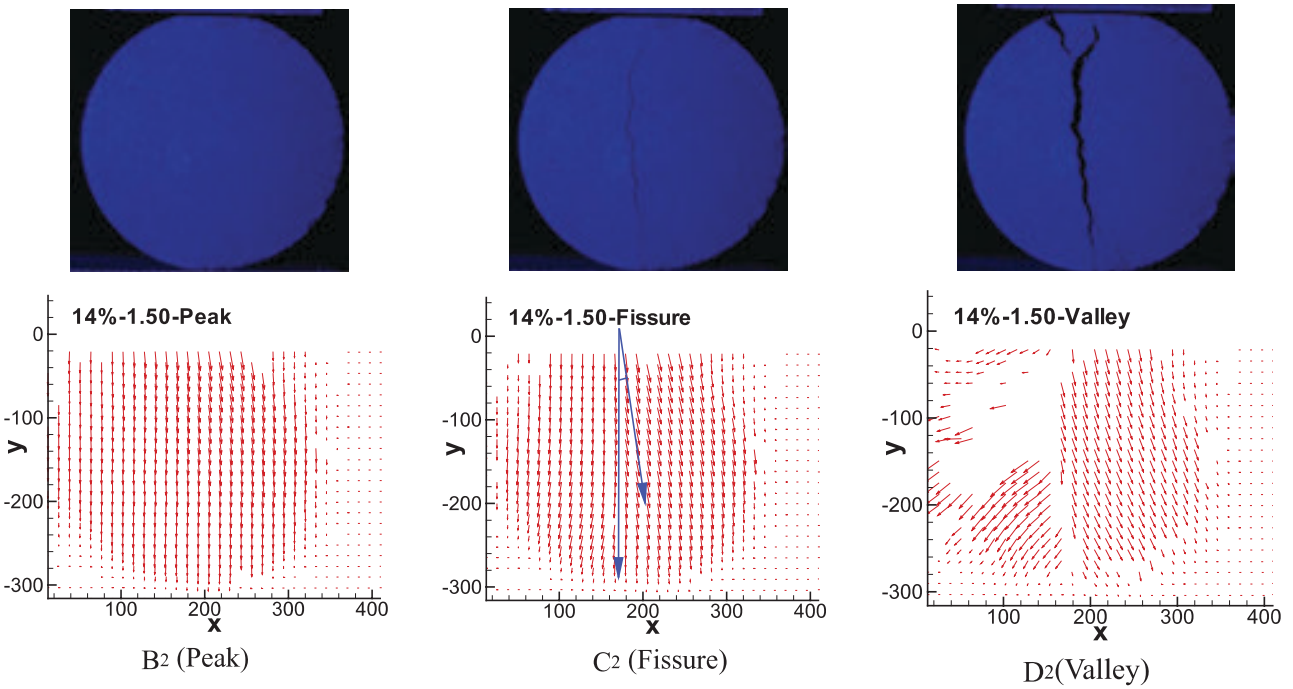

B2 (Peak) C2 (Fissure) D2(Valley)

(b) ρ_d = 1.50 Mg/m^3

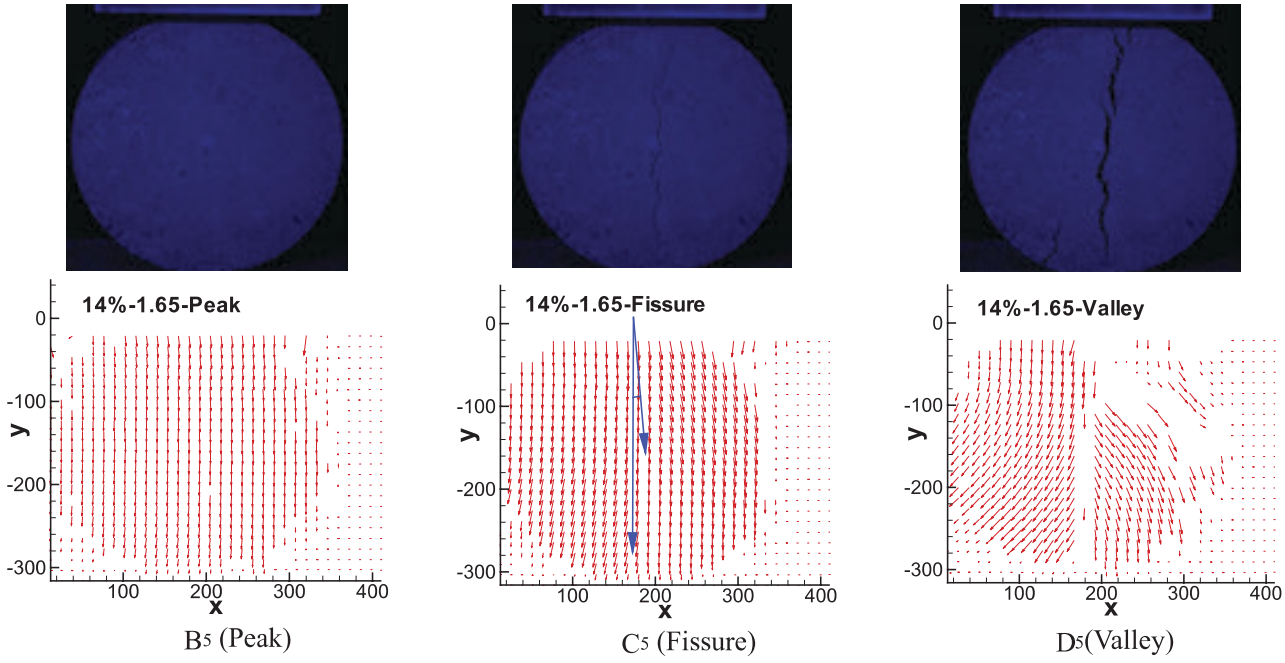

(c) ρ_d = 1.65 Mg/m^3

Figure 11. Failure process and displacement vector field for specimens with different initial dry densities.

4 CONCLUSIONS

A newly designed diametric splitting testing apparatus and particle-image-velocimetry (PIV) system were employed to study the tensile stress-strain in a full-failure process of expansive soil systematically. The main conclusions are as follows.

(1) The diametric splitting test process can be divided into four stages on the basis of the plotted peak load-displacement curves: stress contact adjustment stage (I); stress approximately linear increasing stage (II); tensile failure stage (III); and residual stage (IV).
(2) The water content and the initial dry density have obvious effects on the tensile behavior of the compacted expansive soil. The tensile strength increases first and then decreases with increasing water content, and there is a critical water content. The critical water contents are about of 17.9 %, 14.1 %, and 13 % for expansive soil specimens with initial dry densities of 1.35, 1.50, and 1.65 Mg/m^3, respectively. The peak load increases with increasing dry density, which is more obvious at a low water content.
(3) The PIV techniques can be applied to analyze the deformation during testing, which provides the displacement vector field at various stages. Under the same water content, the angle between the major direction of the displacement vector field and the major crack decreases with increasing dry density, especially when the fissure appears. The tensile fissures and the directions of the propagation of major displacement vector field can be determined, which reflects the tensile stress distribution characteristics in the soil.

Acknowledgments

This study was financially supported by the National Natural Science Foundation of China (Grant No. 41602295), the Foundation for University Key Teacher by the Ministry of Education of Henan Province (Grant No. 2020GGJS-094), and the Key Scientific Research Projects of Colleges and Universities in Henan Province (Grant No. 21A410002).

REFERENCES

[1] Adrian, R.J., 1999. Particle imaging techniques for experimental fluid mechanics. Annual Review of Fluid Mechanics. 23 (1), 261-304.
[2] Barzegar, A.R., Oades, J.M., Rengasamy, P., Murry, R.S., 1995. Tensile strength of dry, remoulded soils as affected by properties of the clay fraction. Geoderma, 65, 93-108.
[3] Blazejczak, D., Horn, R., and Pytka, J., 1995. Soil

tensile strength as affected by time. water content and bulk density. International Agrophysics, 9, 179-188.
[4] Beckett, C. T. S., Smith, C., Ciancio, D., and Augarde, C. E., 2015. Tensile strengths of flocculated compacted unsaturated soils. Géotechnique Letters, 5, 254-260.
[5] Divya, P.V., Viswanadham, B.V.S., Gourc, J.P., 2014. Evaluation of tensile strength-strain characteristics of fiber reinforced soil through laboratory tests. Journal of Materials in Civil Engineering, 26 (1), 14-23.
[6] Festugato, L., Da Silva, A.P., Diambra, A., Consoli, N.C. and Ibraim, E., 2018. Modelling tensile/compressive strength ratio of fibre reinforced cemented soils. Geotextiles and Geomembranes, 46 (2), 155-165.
[7] Frydman, S., 1964. The application of the Brazilian (indirect tension) test to soils. Australian Journal of Applied Science, 15, 335-343.
[8] Cai G.Q, Shi P.X, Kong X.A, Zhao C.G, Likos W.J., 2020. Experimental study on tensile strength of unsaturated fine sands. Acta Geotechnica, 15:1057-1065.
[9] Gao, Y., Sun, D.A., Zhu, Z., Xu, Y., 2019. Hydromechanical behavior of unsaturated soil with different initial densities over a wide suction range. Acta Geotechnica, 14 (2), 417-428.
[10] Gens, A. and Alonso, E.E., 1992. A framework for the behaviour of unsaturated expansive clays. Canadian Geotechnical Journal, 29 (6), 1013-1032.
[11] Hesselink, L., 1988. Digital Image Processing in Flow Visualization. Annual Review of Fluid Mechanics, 20 (1), 421-486.
[12] Kim, T.H., Kim, C.K., Jung, S.J., Lee, J.H., 2007. Tensile strength characteristics of contaminated and compacted sand-bentonite mixtures. Environmental Geology, 52 (4), 653-661.
[13] Lakshmikantha, M.R., Prat, P.C., Ledesma, A., 2012. Experimental evidence of size effect in soil cracking. Canadian Geotechnical Journal, 49(3), 264-284.
[14] Lakshmikantha, M.R., Prat, P.C., Ledesma, A., 2018. Boundary Effects in the Desiccation of Soil Layers with Controlled Environmental Conditions. Geotechnical Testing Journal, 41 (4), 675-697.
[15] Leong, E.C., He, L., Rahardjo, H., 2002. Factors affecting the filter paper method for total and matric suction measurements. Geotechnical Testing Journal, 25(3), 1-12.
[16] Li, H.D., Tang, C.S., Cheng, Q., Li, S.J., Gong, X.P., Shi, B., 2019. Tensile strength of clayey soil and the strain analysis based on image processing techniques.Engineering Geology, 253, 137-148.
[17] Li, Y., 2018. A review of shear and tensile strengths of the Malan Loess in China. Engineering Geology, 236, 4-10.
[18] Liang, Q., Wu, X., Li, C., Wang, L., 2014. Mechanical analysis using the unconfined penetration test on the tensile strength of Q3 loess around Lanzhou City, China. Engineering Geology, 183, 324-329.
[19] Liu, J.Y., Sui, W.H, Gao, Y., 2015. Visualization of Chemical Grout Permeation in Transparent Soil. Geotechnical Testing Journal, 38(5), 774-786.
[20] Lu, N., Wu, B., Tan, C.P., 2007. Tensile strength characteristics of unsaturated sands. Journal of Geotechnical and Geoenvironmental Engineering, 133 (2), 144-154.
[21] Lu, N., Kim, T.H., Sture, S., Likos, W.J., 2009. Tensile strength of unsaturated sand. Journal of Engineering Mechanics, 135 (12), 1410-1419.
[22] Maryam, Varsei., Gerald A. Miller, P.E., and ArashHassanikhah, S.M., 2016. Novel approach to measuring tensile strength of compacted clayey soil during desiccation. International Journal of Geomechanics, 16(6), D4016011.
[23] Nahlawi, H., Chakrabarti, S., Kodikara, J., 2004. A direct tensile strength testing method for unsaturated geomaterials. Geotechnical Testing Journal, 27 (4), 356-361.
[24] Narvaez, B., Aubertin, M., Saleh-Mbemba, F., 2015. Determination of the tensile strength of unsaturated tailings using bending tests. Canadian Geotechnical Journal, 52 (11), 1874-1885.
[25] Ng, C.W.W., Zhan, L.T., Bao, C.G., Fredlund, D.G., Gong, B.W., 2003. Performance of an unsaturated expansive soil slope subjected to artificial rainfall infiltration. Géotechnique, 53 (2): 143-157.
[26] Ranson, W.F., Peters, W.H., 1982. Digital image techniques in experimental stress analysis. Optical Engineering, 21 (3), 427-431.
[27] Romeroe, E., Vanat, J., 2000. Retention curve of deformable clays. In: Tarantino A, Mancuso C (eds) In experimental evidence and theoretical approaches in unsaturated soils. Balkema, Rotterdam, 91-106.
[28] Sun, D.A., Sheng, D.C., Sloan, S.W., 2007. Elastoplastic modeling of hydraulic and stress-strain behaviour of unsaturated compacted soils. Mechanics of Materials, 39 (3):212-221.
[29] Sun, D.A., Sun, W.J., Xiang, L., 2010. Effect of degree of saturation on mechanical behaviour of unsaturated soils and its elastoplastic simulation. Computer and Geotechnics, 37 (5), 678-688.
[30] Sun, W.J., Sun, D.A., 2012. Coupled modelling of hydro-mechanical behaviour of unsaturated compacted expansive soils. International Journal for Numerical and Analytical Methods in Geome-

chanics, 36 (8), 1002-1022.
[31] Stanier, S.A., Blaber, J., Take, W.A., White, D., 2015. Improved image-based deformation measurement for geotechnical applications. Canadian Geotechnical Journal, 53 (5), 727-739.
[32] Stirling, R.A., Hughes, P., Davie, C.T., Glendinning, S. 2015. Tensile behaviour of unsaturated compacted clay soils - A direct assessment method. Applied Clay Science, 112-113.
[33] Tang, C.S., Shi, B., Liu, C., Suo, W.B., Gao, L., 2011. Experimental characterization of shrinkage and desiccation cracking in thin clay layer. Applied Clay Science, 52 (1-2), 69-77.
[34] Tang, C.S., Shi, B., Liu, C., Zhao, L., Wang, B.J., 2008. Influencing factors of geometrical structure of surface shrinkage cracks in clayey soils. Engineering Geology, 101, 204-217.
[35] Tang, C.S., Pei, X.J., Wang, D.Y., Shi, B., Li, J., 2015. Tensile strength of compacted clayey soil. Journal of Geotechnical and Geoenvironmental Engineering, 141 (4), 1-8.
[36] Tang, C.S., Wang, D.Y., Cui, Y.J., Shi, B., Li, J., 2016. Tensile strength of fiber-reinforced soil. Journal of Materials in Civil Engineering, 28 (7), p.04016031.
[37] Thusyanthan, N.I., Tanke, W.A., Madabhushi, S.P.G., Bolton, M.D., 2007. Crack initiation in clay observed in beam bending. Géotechnique, 57 (7), 581-594.
[38] Tollenaar, R.N., van Paassen, L.A., Jommi, C., 2017. Observations on the desiccation and cracking of clay layers. Engineering Geology, 230, 23-31.
[39] Trabelsi, H., Jamei, M., Zenzri, H., Olivella, S., 2012. Crack patterns in clayey soils: experiments and modeling. International Journal for Numerical and Analytical Methods in Geomechanics, 36 (11), 1410-1433.
[40] Trabelsi, H., Romero, E., Jamei, M., 2018. Tensile strength during drying of remoulded and compacted clay: the role of fabric and water retention. Applied Clay Science, 162, 57-68.
[41] Venkataramana, K., Rao, B.H., Singh, D.N., 2009. A critical review of the methodologies employed for determination of tensile strength of fine-grained soils. Journal of Testing and Evaluation, 37 (2), 1-7.
[42] Wang, J.J., Zhu, J.G., Chiu, C.F., Zhang, H., 2007. Experimental study on fracture toughness and tensile strength of a clay. Engineering Geology, 94 (1-2), 65-75.
[43] Wang, L.L., Tang, C.S., Shi, B., Cui, Y.J., Zhang, G.Q. and Hilary, I., 2018. Nucleation and propagation mechanisms of soil desiccation cracks. Engineering Geology, 238, 27-35.
[44] Wang, L.L., Zhang, G.Q., Hallais, S., Tanguy, A., Yang, D.S., 2017. Swelling of shales: amultiscale experimental investigation. Energy Fuel, 31 (10), 10442-10451.
[45] White, D.J., Take, W.A., Bolton, M.D., 2003. Soil deformation measurement using particle image velocimetry (PIV) and photogrammetry. Géotechnique, 53 (7), 619-632.
[46] Yamaguchi, I., 1981. A laser-speckle strain gauge. Journal of Physics E Scientific Instruments, 20 (11), 1270-1273.
[47] Yin, P., Vanapalli, S.K., 2018. Model for predicting tensile strength of unsaturated cohesionless soils. Canadian Geotechnical Journal, 55 (9), 1313-1333.
[48] Zhang, J.R., Niu, G., Li, X.C., Sun, D., 2020. Hydro-mechanical behavior of expansive soils with different dry densities over a wide suction range. Acta Geotechnica, 15 (01): 265-278.
[49] Zhang, X., Liu, J., and Liu, M., 2019. Experimental Study on Uplift Behavior of Group Anchors in Sand. Geotechnical Testing Journal, 42 (3): 687-702.
[50] Zhou, A.N., Huang, R.Q., Sheng, D.C., 2016. Capillary water retention curve and shear strength of unsaturated soils. Canadian Geotechnical Journal, 53 (6): 974-987.

THRESHOLD SILT CONTENT DEPENDENCY ON PARTICLE MORPHOLOGY (SHAPE AND SIZE) OF GRANULAR MATERIALS: REVIEW WITH NEW EVIDENCE

ODVISNOST MEJNE VSEBNOSTI MELJA OD OBLIKE IN VELIKOSTI DELCEV ZA ZRNATE MATERIALE: PREGLED Z NOVIMI DOKAZI

Abdellah Cherif Taiba *(corresponding author)*
Hassiba Ben Bouali University of Chlef,
Laboratory of Material Sciences & Environment
B.P 78C, Ouled Fares Chlef 02180, Algéria
E-mail: a.cheriftaiba@univ-chlef.dz

Youcef Mahmoudi
Hassiba Ben Bouali University of Chlef,
Laboratory of Material Sciences & Environment
B.P 78C, Ouled Fares Chlef 02180, Algéria

Wiebke Baille
Bochum Ruhr University,
Laboratory of Soil Mechanics, Foundation
Engineering & Environmental Geotechnics
44801 Bochum, Germany

Torsten Wichtmann
Bochum Ruhr University,
Laboratory of Soil Mechanics, Foundation
Engineering & Environmental Geotechnics
44801 Bochum, Germany

Mostefa Belkhatir
Hassiba Ben Bouali University of Chlef,
Laboratory of Material Sciences & Environment
B.P 78C, Ouled Fares Chlef 02180, Algéria

Bochum Ruhr University,
Laboratory of Soil Mechanics, Foundation
Engineering & Environmental Geotechnics
44801 Bochum, Germany

DOI https://doi.org/10.18690/actageotechslov.18.1.28-40.2021

Keywords
threshold silt content, silty sand, particle shape and size, packing density

Ključne besede
mejna vsebnost melja (TSC), meljasti pesek, oblika in velikost delcev, gostota pakiranja delcev

Abstract

The threshold silt content is well known as a key parameter affecting the mechanical response of binary granular assemblies considering particle characteristics (size and shape). In this context, the threshold silt content (TSC) is determined from different laboratory tests based on packing density response (e_{max} and e_{min} versus silt content «S_c») and theoretical approaches proposed by several researchers in the specialized published literature using the characteristics of host sand and silt [$e_{max(sand)}$, $e_{min(sand)}$, $e_{max(silt)}$, $e_{min(silt)}$, G_s, G_f and x]. The analysis of the recorded data indicates that the TSC derived from the (e_{max}) curve appears more reliable than that obtained from the (e_{min}) one. Moreover, it is found that the proposed analytical methods are suitable to quantify the threshold silt content (TSC) than that determined

Izvleček

Mejna vsebnost melja (TSC) je dobro znana kot ključni parameter, ki vpliva na mehanski odziv dvojnih zrnatih sklopov glede značilnosti delcev, namreč velikosti in oblike. V tem okviru se TSC določi na podlagi različnih laboratorijskih preizkusov, ki temeljijo na odzivu gostote pakiranja delcev (e_{max} in e_{min} glede na vsebnost melja, S_c) in teoretičnih pristopov, ki jih je predlagalo več raziskovalcev v specializirani objavljeni literaturi z uporabo značilnosti vsebovanega peska in melja ($e_{max(sand)}$, $e_{min(sand)}$), $e_{max(silt)}$, $e_{min(silt)}$, G_s, G_f in x). Analiza zabeleženih podatkov kaže, da je TSC, izpeljan iz krivulje e_{max}, videti bolj zanesljiv kot tisti, dobljen iz krivulje e_{min}. Poleg tega je bilo ugotovljeno, da so predlagane analitične metode primernejše za kvantifikacijo TSC kot tiste, ki so bile eksperimentalno določene z uporabo gostote

experimentally using the packing density (e_{max} and e_{min}). In addition, the test results show that the new introduced ratios $[(D_{50s}\times A_s)/(D_{50f}\times A_f)]$ and $[(C_{us}\times A_s)/(C_{uf}\times A_f)]$ determined based on particle characteristics (shape and size) appear as appropriate parameters for predicting the threshold silt content (TSC) of sand-silt mixture of the compiled data from the published literature as well as that of the present research related to Chlef sand, Fontainebleau sand and Hostun sand mixed with Chlef silt.

pakiranja delcev (e_{max} in e_{min}). Razen tega rezultati preizkusov kažejo, da sta na novo uvedeni razmerji $(D_{50s}\times A_s)/(D_{50f}\times A_f)$ in $(C_{us}\times A_s)/(C_{uf}\times A_f)$, ki temeljita na značilnostih delcev oblike in velikosti, ustrezna parametra za napovedovanje TSC za mešanico peska in melja iz zbranih podatkov iz objavljene literature, kot tudi raziskave v zvezi s peskom Chlef, peskom Fontainebleau in peskom Hostun, pomešanim z meljem Chlef.

Abbreviations

A_s	=	Angularity of sand
A_f	=	Angularity of silt
C_{us}	=	Coefficient of uniformity of sand
C_{uf}	=	Coefficient of uniformity of silt
D_{10sand}	=	Effective diameter of sand (mm)
D_{50s}	=	Mean grain size of sand (mm)
D_{50f}	=	Mean grain size of silt (mm)
e_{max}	=	Maximum void ratio
e_{min}	=	Minimum void ratio
G_s	=	Specific gravity of sand
G_f	=	Specific gravity of silt
R^2	=	Coefficient of determination
S_c	=	Silt content
TSC	=	Threshold silt content
x	=	Disparity of size (D_{10sand}/d_{50silt})

1 INTRODUCTION

The contact level of soil inter-particles constitutes a fundamental index behind the evaluation of shear behavior sandy soils like the phenomenon of liquefaction while these particles participated in the forces chain created by monotonic and cyclic loading conditions [30]. They suggested that the relative density and consequently, the void ratio as key parameter in characterizing the contact between particles of sandy soils. However, the effectiveness of the global void ratio in sand-silt mixtures was questionable. In this context, they found that the silt particles filled up the void spaces between sand particles without supporting the coarse particles, while the silt content was less than the threshold silt content (*TSC*) and they gave a name of intergranular void ratio for this case (Figure 1a). In contrast, they reported when the silt content increased than (*TSC*), the silt particle might carry out the contact of the interparticle forces while the coarse particles acted as reinforced elements embedded with the matrix of silt particles and they proposed a new void ratio named as (interfine void ratio) (Figure 1b). Moreover, published studies reported contradictory findings on the influence of silt content on shear behaviour of sand-silt mixtures and several technical interpretations were addressed for analyzing the experimental results of the binary granular mixtures [2, 6, 7, 8, 9, 10, 11, 16, 17, 18, 19, 20, 21, 26 and 32].

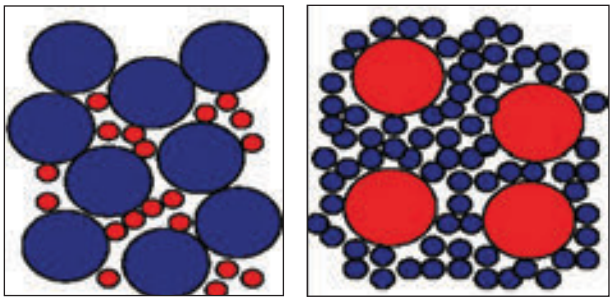

Figure 1. Intergranular binary granular classification system [28 and 30].

[22] studied the binary packing of spherical particles by mixing of coarse spheres with six different sizes of fine spheres. He found that for the lower diameter of the fine spheres, the greater packing density. Thus, he explained the obtained behaviour by the fact that the fine-grained soil particles filled up the void spaces of the coarse-grained material with vibrating until it reached a minimum volume. In the other hand, when the vibration of coarse particles stopped, and the fine particles were poured into the container and vibration continued until a minimum volume was again attained. He indicated also that the ultimate density of the packing process was independent of the formed rate which was related to the frequency and acceleration of mechanical vibration, density of materials, and number of particles per unit volume and evacuation of container during packing density (Figure 2).

In this context, [17] were the first researchers who defined the threshold silt content "*TSC*" characteristic as a relevant indicator in the change of the mechanical characterization of granular materials which was considered as the most important influent parameter to

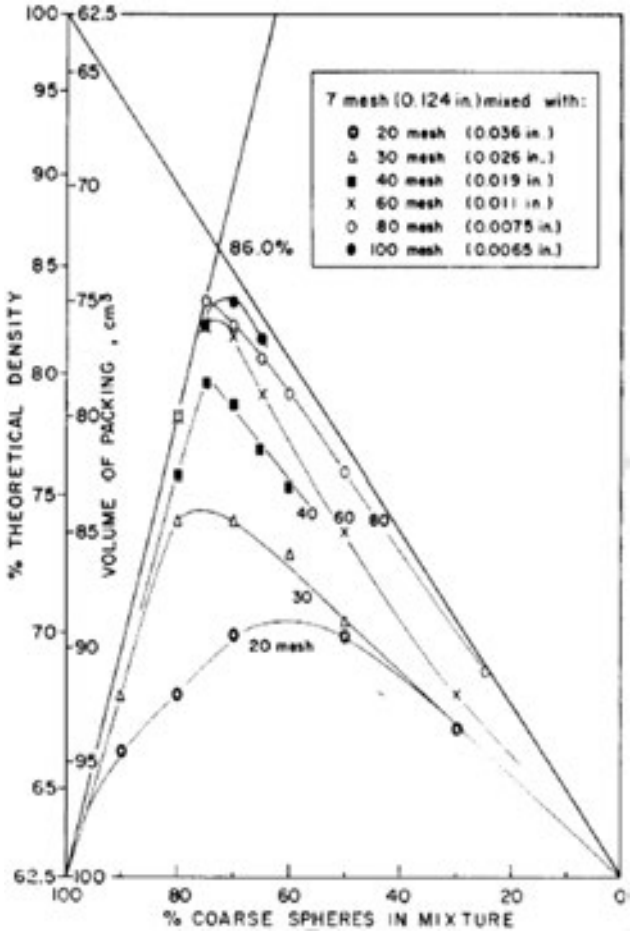

Figure 2. Binary mechanical packing of coarse steel shot with some other sizes [22].

predict the response of sand dominated and silt dominated in the binary granular systems. Based on their researches, they suggested that the threshold silt content has been related to the packing density (maximum void ratio "e_{max}" and minimum void ratio "e_{min}") of sand-sit mixtures (Figure 3 on the left side), where, they showed that the minimum void ratio was reached at the lowest point when the silt particles completely filled up the void spaces of coarse particles and the obtained silt content was termed as the threshold silt content (*TSC*) (point B on the right side of Figure 3).

[17] suggested an analytical method to determine the threshold silt content (*TSC*) based on the maximum void ratio of sand ($e_{max(sand)}$) and silt ($e_{max(silt)}$) according to following equation:

$$TSC = \left(\frac{e_{\max(sand)}}{1 + e_{\max(sand)} + e_{\max(silt)}} \right) \qquad (1)$$

Moreover, [14] considered the specific gravity difference of sand (G_s) and that of silt (G_f) and proposed an empirical relationship based on the maximum void ratio and specific gravity of the sand and silt under consideration (equation 2).

$$TSC = \left(\frac{G_f \cdot e_{\max(sand)}}{G_f \cdot e_{\max(sand)} + G_s \cdot (1 + e_{\max(silt)})} \right) \qquad (2)$$

In addition, [35] suggested another theoretical approach to evaluate the threshold silt content (*TSC*) based on

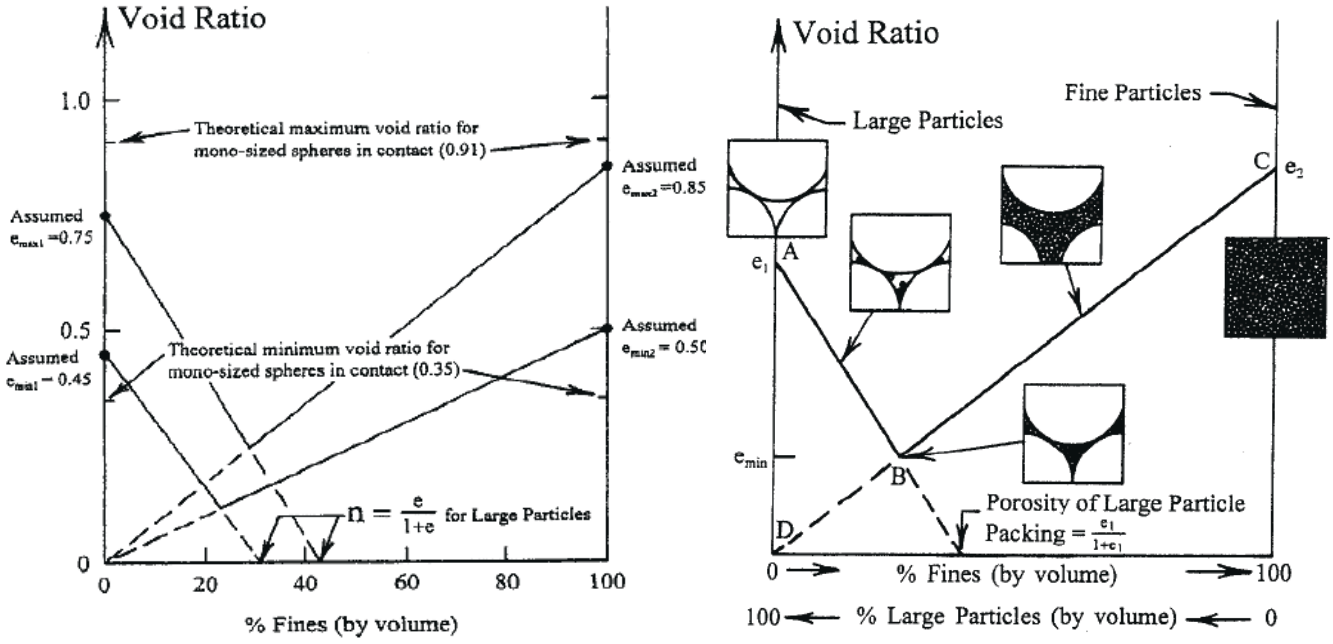

Figure 3. Variation of maximum and minimum void ratios with different silt content [17 and 32].

index properties of sand [minimum void ratio ($e_{min(sand)}$) and specific gravity (G_s)] and silt [minimum void ratio ($e_{min(silt)}$) and specific gravity (G_f)] (equation 3):

$$TSC = \left(\frac{G_f \cdot e_{\min(sand)}}{G_f \cdot e_{\min(sand)} + G_s \cdot (1 + e_{\min(silt)})} \right) \quad (3)$$

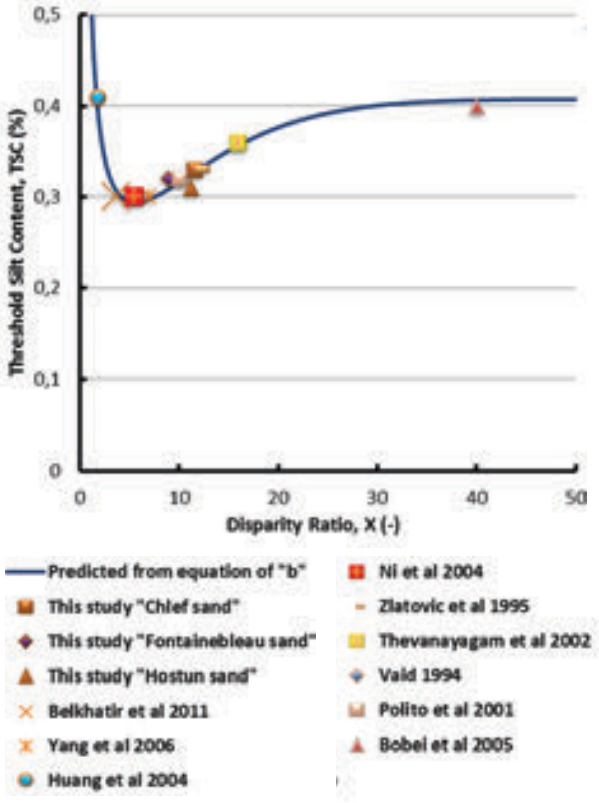

Figure 4. Variation of threshold silt content (*TSC*) with disparity ratio *x*.

However, [28] proposed a semi-analytical relationship between the threshold silt content (*TSC*) based on the disparity of size (x) defined as the ratio between the median size (D_{50f}) of fines and D_{10} which is the 10 % fractile of host sand according to the equation (4) and Figure (4).

$$TSC = 0.40\left(\frac{1}{1 + e^{0.5-0.13\chi}} + \frac{1}{\chi} \right) \quad (4)$$

On the other hand, [1, 8, 11, 12, 33] reported that sphericity (*S*) is quantified as the ratio of the diameter of the largest inscribed sphere relative to the diameter of the smallest circumscribed sphere, however, the roundness (*R*) as the ratio of the average radius of curvature of surface features relative to the radius of the maximum sphere that can be inscribed in the particle. Indeed, [27] subdivided the sphericity in two classes (higher sphericity and lower sphericity) and the angularity in six categories (very angular, angular, sub-angular, sub-rounded, rounded and well-rounded) according to Figure (5).

[3] performed a series of oedometer, triaxial and resonant column tests on saturated coarse rotund sand (i.e., Leighton Buzzard Sand) mixed with fines (i.e., mica) according to various mixture ratios. He found out the existence of close relationships between the transition fines content and mechanical properties of mixtures through the triaxial and resonant column tests. [23] conducted a series of undrained monotonic triaxial compression tests on thirty sands with varying fines contents, which were reconstituted by mixing three base sands (Sile Sands 20/30, 50/55, 80/100) with same geologic origin but with different gradations and three different non-plastic silts (*IZ*, *SI* and *TT* silts) with different gradations and shape properties. They showed that the influence of granulometric factors (C_{Usilt}, $d_{50\text{-}silt}$)

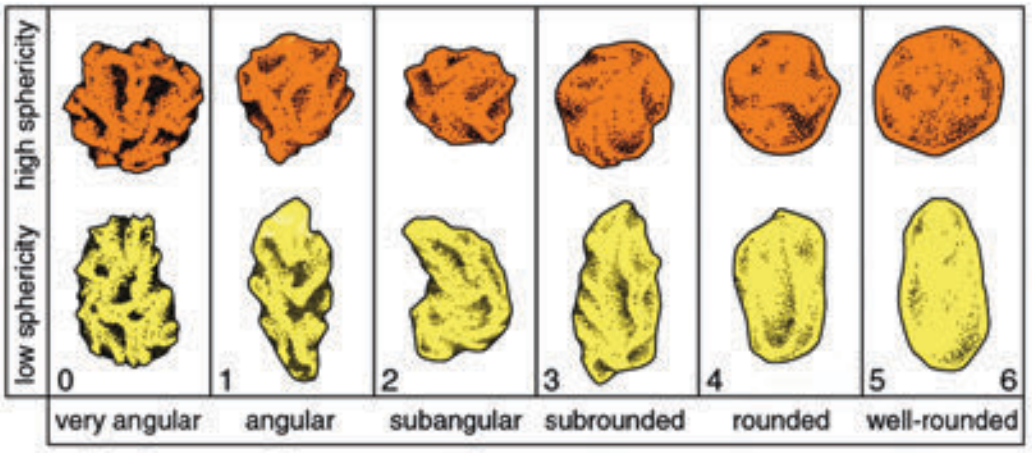

Figure 5. Classification of angularity and sphericity [27].

and shape characteristics (R, S) of silty grain matrix on undrained shear strength of Sile Sands was dependent on the value of fines content parameter. [4] conducted a series of fall cone tests on clay-sand mixtures to explore the variation of liquid limit with sand content and the link between the undrained shear strength and water content for various sand contents in the tested mixtures. They demonstrated clearly that an approximate linear relationship between the cone penetration and the water content for both clay-NS and clay-CSS mixtures in the range of mixtures proportions used. [29] performed a series of bender element and triaxial tests on the Ottawa sand-silt mixture considering the range of 5–20 % fines content. They observed that the addition of even small percentages of silt to clean sand considerably increased both the peak friction angle and the critical-state friction angle at a given initial relative density. [5] performed a series of hydraulic conductivity tests on coarse-grained soils with different particle sizes and shapes. They showed that the rounded sands exhibited lower hydraulic conductivity values than the angular sands. [9] proposed new empirical correlations relating the hydraulic conductivity with the packing density and particle shape of silty sand soils. They found that the saturated hydraulic conductivity decreased according to a polynomial function with the decrease of the predicted extreme void ratios (e_{max} and e_{min}) of the tested materials. Moreover, they indicated that the saturated hydraulic conductivity (K_s) decreased polynomially with the decrease of the roundness ratio ($R_r = R_{hs}/R_{mixture}$) and increase of the sphericity ratio ($S_r = S_{hs}/S_{mixture}$) for the ($F_c = 0\,\%$ - $30\,\%$) range of low plastic fines content of the used sand-silt mixtures. [12] demonstrated clearly that the size and shape of soil particles reflected the formation history of the grains. In addition, they found through a series of experimental tests and analysis of data from published literature that the particle shape characteristics of grains impacted significantly the

Table 1. Summary of the index properties of the sand-silt mixture from published literature and present study.

Sources	Materials	G_s	G_f	e_{max}	e_{min}	D_{50s}	D_{50f}	C_{us}	C_{uf}	A_s	A_f	A_s/A_f
This study	Chlef sand	2.652	-	0.795	0.632	0.596	-	2.634	-	0.439	-	0.70
This study	Fontainebleau sand	2.642	-	0.950	0.645	0.558	-	3.157	-	0.390	-	0.62
This study	Hostun sand	2.650	-	1.021	0.646	0.369	-	1.536	-	0.319	-	0.51
This study	Chlef silt	-	2.667	1.563	0.991	-	0.032	-	12.66	-	0.626	-
[2]	Chlef sand1	2.680	-	0.876	0.535	0.68	-	3.36	-	-	-	0.80
	Chlef silt1	-	2.700	1.137	0.720	-	-	-	-	-	-	
[32]	Hokksund sand	2.712	-	0.949	0.572	0.44	-	2.38	-	-	-	2.6
	Chengbei silt	-	2.739	1.413	0.731	-	0.032	-	1.95	-	-	
[31]	Sxinias-Marathon sand	2.69	-	1.04	0.66	0.12	-	-	-	-	-	-
	Sxinias-Marathon silt	-	2.69	1.77	0.66	-	0.02	-	-	-	-	
[16]	Mai Liao sand	2.69	-	1.125	0.646	0.123	-	1.75	-		-	1
	Mai Liao silt	-	2.71	-	-	-	0.044	-	2.79	-	-	
[24]	Alluvium sand	-	-	-	-	0.778	-	5.63	-	-	-	2.4
	Alluvium silt	-	-	-	-	-	0.038	-	5.43	-	-	
[34]	Toyoura sand	2.65	-	0.977	0.600	0.17	-	1.61	-	0.486	-	1
	Toyoura silt	-	-	1.754	0.500	-	0.01	-	6.08	-	0.486	
[30]	OS00 sand	-	-	0.800	0.608	0.25	-	1.69	-	-	-	2.8
	Silica silt	-	-	2.1	0.627	-	0.01	-	7.50	-	-	
[25]	M31 sand	2.65	-	0.841	0.582	0.30	-	-	-	-	-	3.4
	Assyros silt	-	2.66	1.663	0.658	-	0.02	-	-	-	-	
[28]	Sydney sand	2.63	-	0.855	0.565	0.27	-	1.26	-	-	-	1
	Majura silt	-	2.49	-	-	-	0.006	-	12.50	-	-	
[13]	Ahmedabad sand	2.65	-	0.68	0.42	0.375	-	3.58	-	-	-	-
	Quarry Dust silt	-	2.67	1.632	0.652	-	0.037	-	7.83	-	-	
[15]	Kaohsiung sand	2.70	-	0.696	0.238	-	-	7.92	-	-	-	-
	Kaohsiung silt	-	2.70	-	-	-	-	-	-	-	-	

packing density and small-to-large strain mechanical properties of sandy soils, where, they found out that the increase of the angularity or eccentricity produced an increase in the extreme void ratios (e_{max} and e_{min}) of soils. In this context, they proposed some empirical relationships between particle shape characteristics in terms of (roundness, sphericity and regularity) and packing density of compiled data from the published literature.

Finally, published literature accorded particular attention to the determination of the threshold silt content (*TSC*) based on the packing density in terms of extreme void ratios (e_{max} and e_{min}), index properties in terms of specific gravity (G_s and G_f) [14, 17, 35] and particle size in terms of disparity ratio (x) [28] of sand-silt mixtures. However, [35] emphasized the importance to evaluate the influence of shape of particles and packing density to harmonize the experimental and analytical prediction of the threshold silt content (*TSC*).

To achieve this goal, the present research intends to explore the relationships between the threshold silt content (*TSC*) and particle characteristics in terms of [particle size (mean grain size "D_{50}" and coefficient of uniformity "C_u") and particle shape (angularity "A")] through different methods reported in published literature as experimentally [packing density of sand and silt "extreme void ratios index, e_{max} and e_{min} versus silt content S_c"] and theoretically according to the approaches of [14, 17, 28] of the compiled data from the published sources as well as those of the present research related to three different sands [Chlef sand, Fontainebleau sand and Hostun sand with distinct shapes ["rounded shape", "sub-rounded shape" and "sub-angular shape"] respectively mixed with Chlef rounded shape silt.

2 EVALUATION OF THRESHOLD SILT CONTENT USING PACKING DENSITY CHARACTERISTICS FROM PUBLISHED STUDIES

Figure 6 reproduces the data from the published literature [2, 15 and 32] as well as those of the present study on three different sand-silt mixtures such as "Chlef rounded sand-silt mixtures, Fontainebleau sub-rounded sand-silt mixtures and Hostun sub-angular sand-silt mixtures" showing the relationship between the extreme void ratios indexes (e_{max} and e_{min}) with silt content ranging from ($S_c = 0$ % to $S_c = 100$ %). It is clear from Figure 6 that the overall extreme void ratios tendencies (e_{max} and e_{min}) exhibit a decrease with the increase of silt content of the range of $S_c = 0$ % to $S_c = 45$ %. Beyond that, they continue

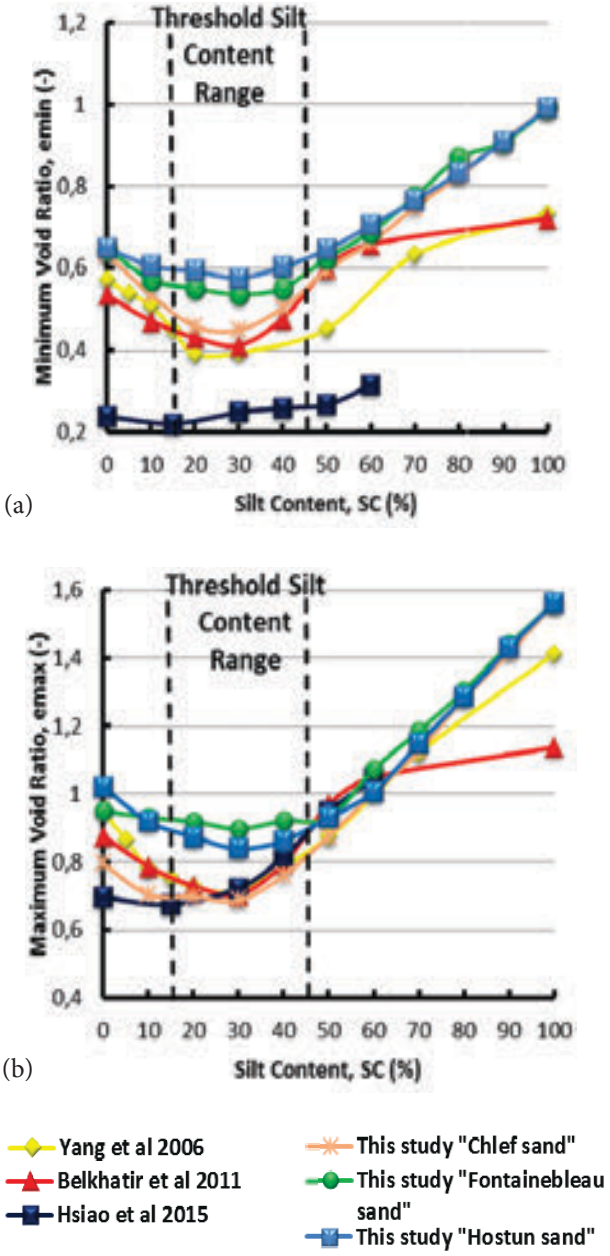

Figure 6. Void ratio index versus silt content of compiled data and those of the present study.
(a) Minimum void ratio (b) Maximum void ratio

to show a significant increasing with the increase of silt content from $S_c = 45$ % to $S_c = 100$ % for the collected data from the published literature [2, 15 and 32] as well as the data related to the present laboratory investigation on the different tested silty sand samples as "Chlef, Fontainebleau and Hostun sand-silt mixtures". Moreover, it appears that the threshold silt content of the compiled data and that of the present study ranges between $S_c = 15$ % and $S_c = 45$ % depending on the nature of the materials. In addition, Figure 6b demonstrates clearly that the

threshold silt content determined from the maximum void ratio (e_{max}) curves is more reliable than that derived from the minimum void ratio (e_{min}) curves, where it gives an indication of the possible range in which the threshold silt content (*TSC*) might occur. These findings are in good agreement with observations of [17].

3 EVALUATION OF THRESHOLD SILT CONTENT FROM EXPERIMENTAL AND ANALYTICAL METHODS OF DIFFERENT PUBLISHED STUDIES

In order to evlauate the threshold silt content (*TSC*) using the experimental method [extreme void ratios indexes "e_{max} and e_{min}" versus silt content "S_c"] based on packing density characteristics "e_{max} and e_{min}", the proposed analytical methods by [14, 17 and 35] and the suggested semi-analytical method by [28] for the different data compiled from the published literature [2, 13, 25, 30, 31 and 32] inculding those of the present study related to three distinct materials such as "Chlef rounded sand, Fontainebleau sub-rounded sand and Hostun sub-angular sand". The obtained data of the curent study indicate that the threshold silt content determined by

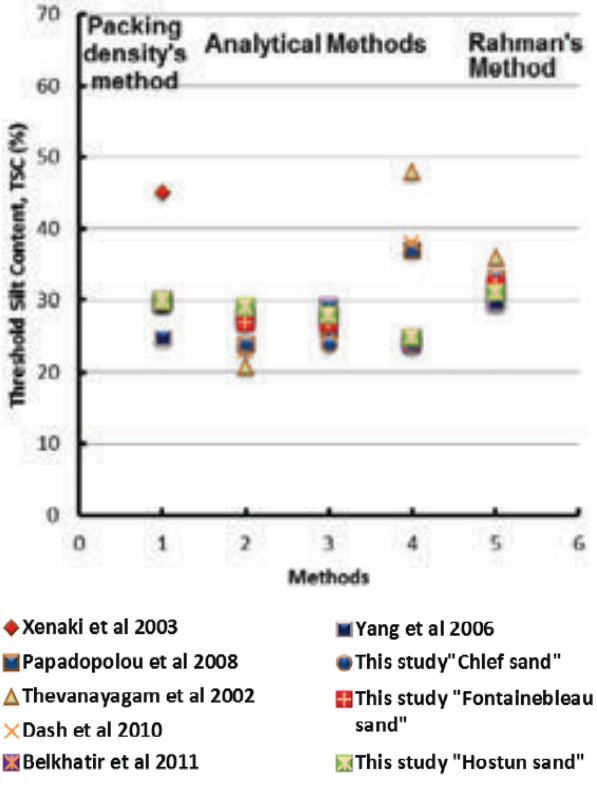

Figure 7. Comparison of different methods for evaluation of threshold silt content from data of published literature and those of current study.

packing density's method presents a larger range from *TSC* = 25 % to *TSC* = 45 %. Indeed, same findings were observed for the threshold silt content obtained by third analytical method proposed by [35] which is less scarttered than those deteremined by method 1 and 2, where the threshold silt content values range between *TSC* = 25 % and *TSC* = 48 %. Moreover, it could be seen from the analytical approaches proposed by [14 and 17] which were based on the index properties of sand and silt " maximum void ratio and specific gravity) showed a narrower range of threshold silt content (TSC) for all different silty sand soils under consideration. However, the determination of threshold silt content (*TSC*) from the semi-analytical approach proposed by [28] which was derived empirically from the experiemental published data and related to the sand-silt gradation (equation 4) is in good agreement with that obtained by the calculation methods 1 and 2. These findings confirm that the determination of the threshold silt content (*TSC*) from calculation approaches is better than those determined experimentally using the packing density of silty sand soils in terms of maximum void ratio (e_{max}) and mimimum void ratio (e_{min}). In addition, the evaluation of threshold silt content (*TSC*) from the analytical methods proposed by [14 and 17] (1 and 2) that was based on the maximum void ratio (e_{max}) and specific gravity of sand and silt (G_s and G_f) (equations 1 and 2) were more realistic than those determined by the third analytical approach proposed by [35] which was based on minimum void ratio (e_{min}) and specific gravity (G_s and G_f) of silty sand soils (equation 3). This confirms that the maximum void ratio (e_{max}) is a suitable index to evaluate experimentally and analytically the threshold silt content (*TSC*) of the different binary granular assemblies under consideration.

4 EVALUATION OF THRESHOLD SILT CONTENT BASED ON PARTICLE MORPHOLOGY FROM PUBLISHED LITERATURE

4.1 Particle angularity ratio (A_s/A_f)

Figure 8 illustrates the variation of threshold silt content (*TSC*) with angularity ratio [angularity of sand "A_s" and angularity of silt "A_f"] of compiled data from published literature [2, 16, 24, 28, 32 and 34] and those of the current study on three diffrent sands with dinstinct shapes [Chlef sand "rounded shape, $A_s = 0.439$", Fontainebleau sand "sub-rounded shape, $A_s = 0.390$" and Hostun sand "sub-angular shape, $A_s = 0.319$"] mixed with Chlef silt "rounded shape, $A_f = 0.626$"] using the different methods cited above for the determination of the threshold silt content (*TSC*) (equations 1, 2, 3 and

4) respectively. It seems that the threshold silt content (*TSC*) increases with the increase of angularity ratio (A_s/A_f) for all different data cited in this study. Moreover, the obtained results indicate that the threshold silt content presents a norrower range for the smallest angularity ratio values varying between $A_s/A_f = 0.5$ and $A_s/A_f = 1$ compared to the larger range of threshold silt content (*TSC*) for the highest angularity ratio values ranging between $A_s/A_f = 2.4$ and $A_s/A_f = 2.8$ for the the compiled points from published sources and those of the current study data for the experimental and analytical approaches used in this research to evaluate and determine the threshold silt content (*TSC*). In addition, for the case of $A_s/A_f = 2.8$ [30 and 35] reported that the particle shape has insignificant influence on the threshold silt content for the ratio beteween the larger sand particles and smaller silt particles (discussed in Figure 8). Theses observations indicate that the decreasing in angularity ratio (A_s/A_f) "increasing of silt angularity" has a significant effect on the threshold silt content comparing to the highest values of anuglarity ratio and this indicates the effect of particle shape of soil grains especially that of the silt particles playing a major role on the threshold silt content and consequently on the behaviour of binary granular soils under consideration.

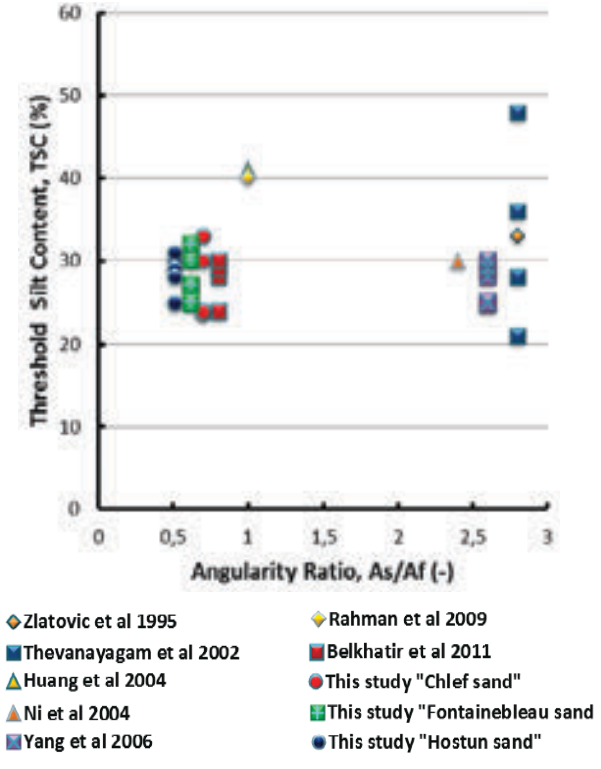

Figure 8. Threshold silt content versus angularity ratio of different studies from published literature and current study.

4.2 Mean grain size ratio (D_{50s}/D_{50f})

For the purpose of analyzing the relationship between the threshold silt content (*TSC*) and the ratio of the mean grain size of sand (D_{50s}) to the mean grain size of silt (D_{50f}) of some compiled studies from published sources and data of the present study on three sands having different mean grain sizes such as (Chlef sand, $D_{50} = 0.596$ mm, Fontainebleau sand, $D_{50} = 0.558$ mm, Hostun sand, $D_{50} = 0.369$ mm mixed with Chlef silt, $D_{50} = 0.032$ mm). The threshold silt content was determined using the analytical approaches proposed by [14, 17 28 and 35] which was based on the index properties of sand and silt (e_{max}, e_{min}, G_s, G_f) and grain size (D_{10} and D_{50}) of sand and silt respectively. It is clear from this plot that the threshold silt content increases with the increase of the mean grain size ratio (D_{50s}/D_{50f}) ranging from $D_{50s}/D_{50f} = 2.79$ for the study of [16] to $D_{50s}/D_{50f} = 25$ for the study of [30] for all distinct silty sand soils evaluated in this research. Moreover, the obtained data indicate that mean grain size ratio has a significant influence on the threshold silt content (*TSC*) for the intermediate value of (D_{50s}/D_{50f}) which varies between $D_{50s}/D_{50f} = 10$ to $D_{50s}/D_{50f} = 20$ concerning the studies of [24, 32 and 34] with the tested soils such as Chlef, Fontainebleau and Hostun sands respectively). This trend was explained by [35] in the way that the nature of fabric and type of packing including the grain size of mixtures participate in changing the threshold silt content and consquently

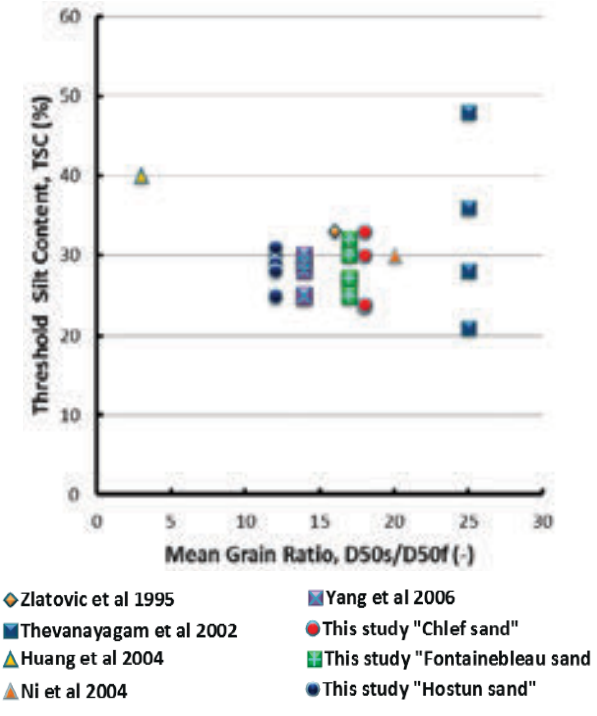

Figure 9. Threshold silt content versus mean grain ratio of different studies from published literature and current study.

changing the mechanical behaviour of silty sand soils. In addition, for the larger mean grain size ratio $D_{50s}/D_{50f} = 25$ (the silty sand soils tested by Thevanayagam et al. 2002), the threshold silt content (TSC) determined by analytical methods proposed by several researchers in literature ranges from $TSC = 20\,\%$ to $TSC = 48\,\%$ for the tested sand-silt mixtures. In this case, the mean grain size ratio between larger and smaller particles might be highlighted by packing density of mixtures rather than by the particle shape of silty sand soils [35].

4.3 Cofficient of uniformity ratio (C_{us}/C_{uf})

In the context of evaluating the variation of the threshold silt content (TSC) with the ratio of the coefficient of uniformity of sand (C_{us}) to the coefficient of uniformity of silt (C_{uf}) of nine different researches based on the compiled data from the pulished literature as [2, 16, 24, 28, 32 and 34] and those of the present study related to three sands with different coefficients of uniformity such as (Chlef sand "$C_u = 2.634$", Fontainebleau sand "$C_u = 3.157$" and Hostun sand "$C_u = 1.536$" mixed with Chlef silt with a coefficient of uniformity of "$C_u = 12.66$"). The obtained results indicate that the threshold silt content increases with the decrease of the coefficient of uniformity ratio (C_{us}/C_{uf}) for the plotted points compiled from different research sources using the analytical methods proposed by [14, 17, 28 and 35]. Moreover, it could be seen from this plot that the threshold silt content presents a norrower range for the coefficient of uniformity ratio (C_{us}/C_{uf}) varying between $C_{us}/C_{uf} = 0.1$ and ($C_{us}/C_{uf} = 0.3$ for (Hostun sand, Chlef sand, Fontainebleau sand and the studies of [2 and 30]). This confirms that the increase in the coefficient of uniformity of different silts used in the different studies leads to a significant decreasing in the coefficient of uniformity ratio (C_{us}/C_{uf}) inducing an important changing in the threshold silt content (TSC) and consequently affects in significant manner the mechanical response of sand-silt mixture samples under study. Therefore, the highest values of coefficient of uniformity ratio (C_{us}/C_{uf}) lead to more scatter between the granular assemblies with no appreciable trend for the studies of [16, 24 and 24]. In addition, the obtained results from Figures 8 and 9 show that the grain size of silt in terms of mean grain size (D_{50}) and coefficient of uniformity (C_u) appear as appropriate parameters to predict and determine the threshold silt content (TSC). Indeed, their increasing leads to a decrease of the mean grain size ratio (D_{50s}/D_{50f}) and coefficient of uniformity ratio(C_{us}/C_{uf}) of the silty sand inducing a significant effect on the threshold silt content and consequently on the behaviour of binary granular systems under consideration.

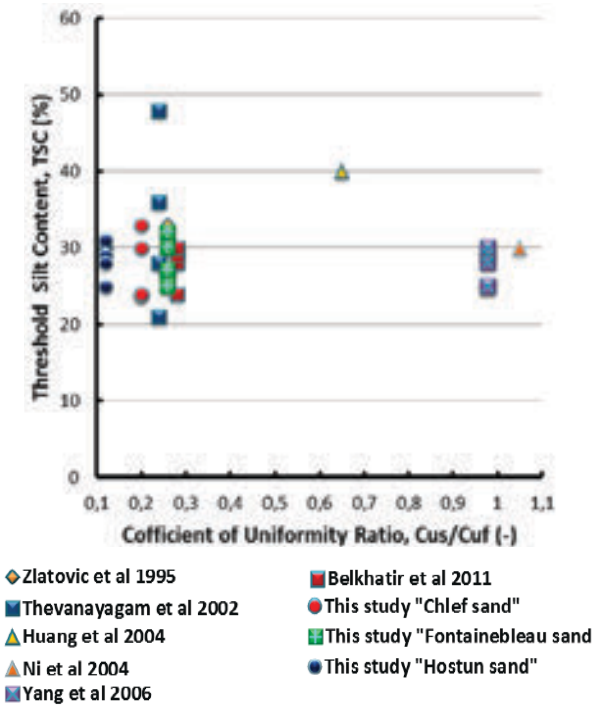

Figure 10. Threshold silt content versus coefficient of uniformity ratio of data from published literature and those of the present study.

5 EXPLORING THE RELATIONSHIP BETWEEN THRESHOLD SILT CONTENT WITH THE MEAN GRAIN SIZE AND PARTICLE ANGULARITY

For the purpose of suggesting suitable fittings and exploring eventual new correlations between the threshold silt content and particle characteristics in terms of [Coefficient of uniformity "C_u", mean grain size "D_{50}", Angularity "A"] of sand and silt based on the proposed analytical methods [17 "1", 14 "2", 35 "3" and 28 "4"] by several researchers to evaluate the threshold silt content, Figure 11 illustrates the variation of threshold silt content (TSC) with the ratio between the particle morphology index of sand ($D_{50s} \times A_s$) and that of silt ($D_{50f} \times A_f$) of different silty sand soils. As it could be seen in Figure 11, a polynomial relationship may express the variation of the threshold silt content (TSC) as a function of the ratio $[(D_{50s} \times A_s)/(D_{50f} \times A_f)]$ for all the considered analytical methods used in this study to determine the transitional point between sand dominated and silt dominated for the different granular assemblies. Moreover, the obtained results indicate that method 1 of [17] and method 2 of [35] present good polynomial correlations with higher coefficient of determination ($R^2 = 0.75$ and $R^2 = 0.99$ respectively) comapred to the anlaytical method proposed by [14] and

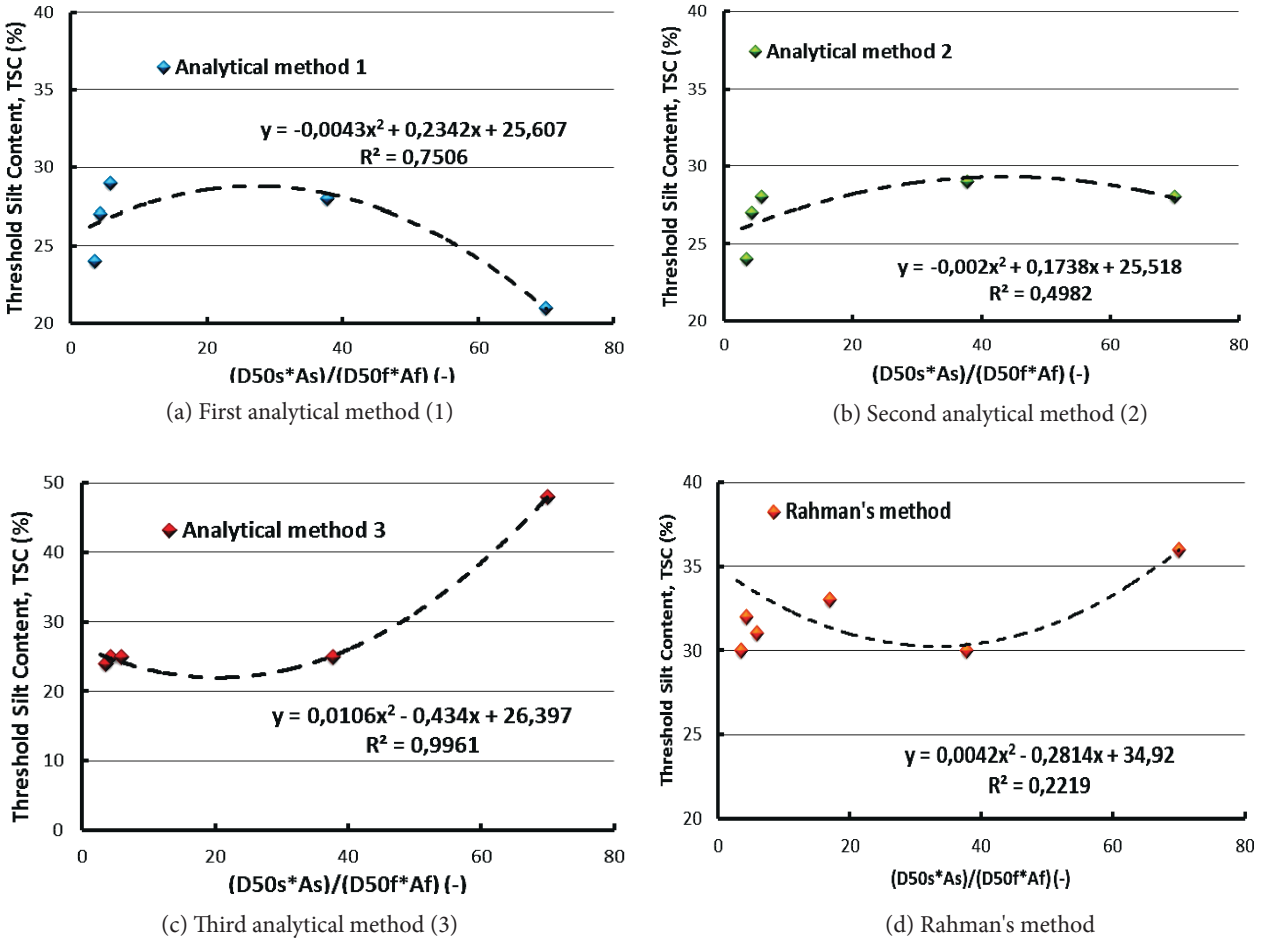

(a) First analytical method (1)

(b) Second analytical method (2)

(c) Third analytical method (3)

(d) Rahman's method

Figure 11. Variation of the threshold silt content as function of the ratio $(D_{50s}\times A_s)/(D_{50f}\times A_f)$ for different methods.

the semi-analytical approach proposed by [28] where the cofficient of determination were ($R^2 = 0.498$ and $R^2 = 0.221$) respectively. The obtained trend indicates that the new introduced ratio $[(D_{50s}\times A_s)/(D_{50f}\times A_f)]$ and consquently the particle size and shape characteristics of sand and silt impact significantly the packing denisty properties [emax in equation (1) and emin, G_f and G_s in equation (3)] for the considered binary granular mixtures. On the other hand, this finding confirms that the particle size (mean grain size of sand and silt) and particle shape parameter (angularity of sand and silt) and consequently the ratio $[(D_{50s}\times A_s)/(D_{50f}\times A_f)]$ appear as suitable parameter to pridect the threshold silt content (TSC) of binary granular systems according to the following expressions :

$$TSC = -0.043 \times [(D_{50s}\times A_s)/(D_{50f}\times A_f)]^2 + 0.23\times [(D_{50s}\times A_s)/(D_{50f}\times A_f)] + 25.607\ ;\ R^2 = 0.75 \quad (5)$$

$$TSC = 0.0106 \times [(D_{50s}\times A_s)/(D_{50f}\times A_f)]^2 - 0.434 \times [(D_{50s}\times A_s)/(D_{50f}\times A_f)] + 26.397\ ;\ R^2 = 0.99 \quad (6)$$

6 EXPLORING THE RELATIONSHIP BETWEEN THRESHOLD SILT CONTENT AND THE COEFFICIENT OF UNIFORMITY AND PARTICLE ANGULARITY

The data related to the correlation between the threshold silt content (TSC) and the ratio$[(C_{us}\times A_s)/ (C_{uf}\times A_f)]$ [ratio between coefficient of uniformity and particle angularity of sand with the cofficient of uniformity and particle angularity of silt] of different silty sand soils selected from the published sources as well as those of this study on (Chlef, Fontainebleau and Hostun sands) are discussed in this section. The analysis of the obtained data from Figure 12 confirm the existence of a power function relationship that may relate the threshold silt content (TSC) to the ratio $[(C_{us}\times A_s)/(C_{uf}\times A_f)]$ for the selected calculation methods used in this research as (Lade's method, Hazirbaba's method, Zuo's method and Rahman's method). As it can be seen, the Lade's method shows a good power function with a coefficient of deter-

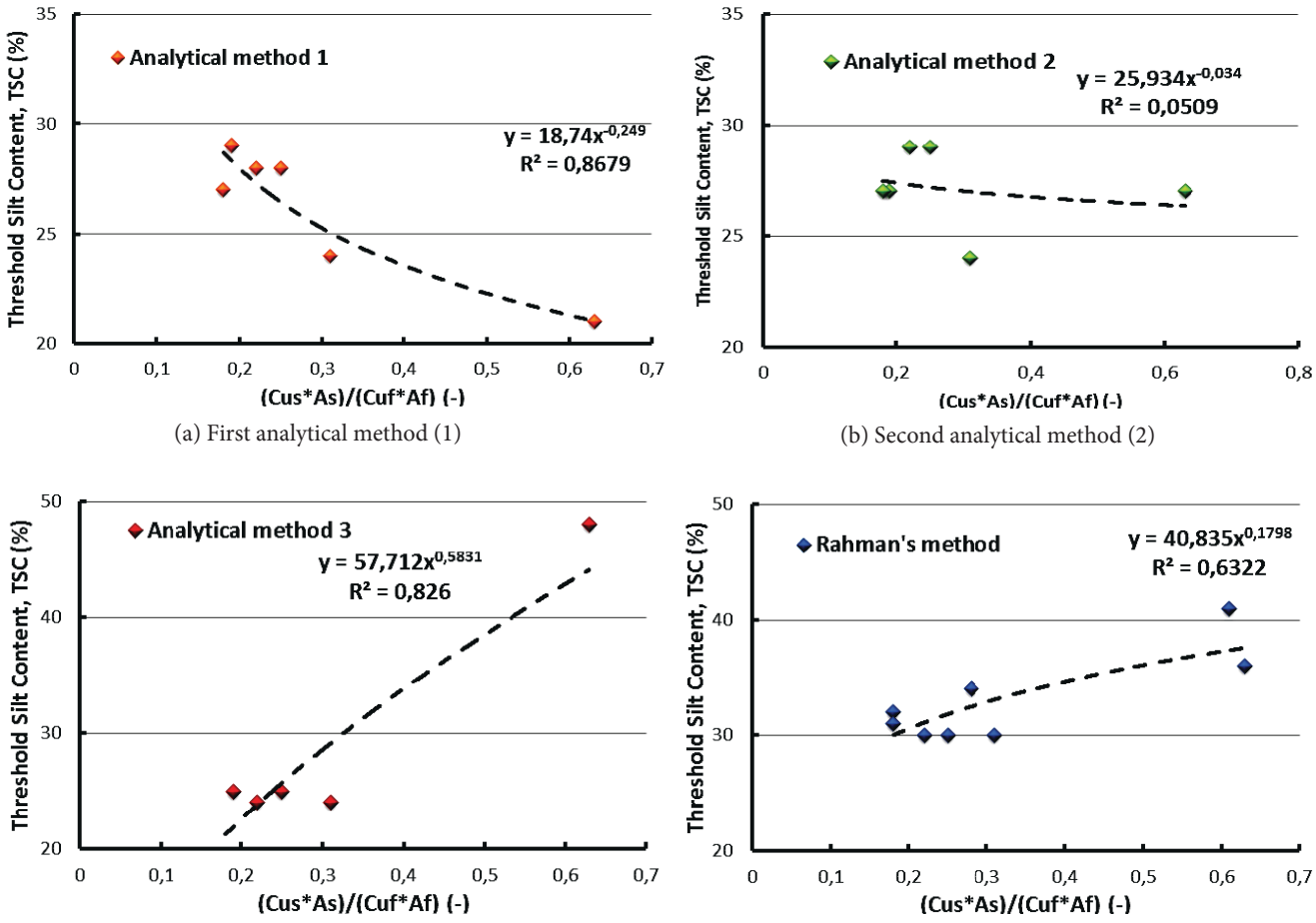

(a) First analytical method (1)

(b) Second analytical method (2)

(c) Third analytical method (3)

(d) Rahman's method

Figure 12. Evaluation of threshold silt content based on the ratio of $(C_{us}\times A_s)/(C_{uf}\times A_f)$ for different methods.

mination of ($R^2 = 0.87$) compared to the Hazirbaba's approach ($R^2 = 0.006$), Zuo's approach ($R^2 = 0.82$) and Rahman's method ($R^2 = 0.63$). This observation demonstrates clearly that the coefficient of uniformity and particle angularity of sand and silt and consquently the ratio $[(C_{us}\times A_s)/(C_{uf}\times A_f)]$ exhibits a consequent impact on the evolution of the threshold silt content (TSC) calculated through the packing density (emax) using the approach of [17] compared to the other proposed approaches suggested by several researchers in published literature. The obtained soil trend confirms that particle characteristics in terms of cofficient of uniformity and angularity may affect considerably the changing threshold silt content points between the sand dominated and silt dominated in the sand-silt matrix under study. the following equation is suggested to express the relationship between the threshold silt content (TSC) and the ratio $[(C_{us}\times A_s)/(C_{uf}\times A_f)]$ for the different binary granular assemblies under consideration.

$$TSC = 18.74^{*}[(C_{us}\times A_s)/(C_{uf}\times A_f)]^{-0.249};\ R^2 = 0.87 \qquad (7)$$

7. CONCLUSION

The threshold silt content (TSC) represents a key parameter in the physical identification and mechanical characterization of binary granular mixtures. It has been reported by many researchers that it is the boundary condition explaining the different properties of the sand dominated or silt dominated in the overall matrix sand-silt under consideration. This parameter was determined experimentally using laboratory tests (e_{max} and e_{min} versus S_c) curves and theoretically according to analytical and semi-analytical approaches that were proposed by several researchers in the published literature. In this context, the main results of this research are summarized as follows:

1. The analysis of the compiled data and those of the present study indicates that the theshold silt content may be established according to the variation of the extreme void ratios indexes (e_{max} and e_{min}) with silt content (S_c) for the tested silty sand soils. Indeed, the

threshold silt content determined from the (e_{max}) curve is more reliable than that derived from the (e_{min}) curve, where it represents an indicator characterizing the possible range in which the (*TSC*) might exist.

2. The recorded data from published literature and those of the present study show that the calculation methods used in the evaluation the threshold silt content give more clarification compared to the *TSC* calculated experimentally according to the packing density of binary granular assemblies. Moreover, the analysis of the collected data demonstrates clearly that the threshold silt content (*TSC*) increases with the increase of the ratio of [particle angularity of sand to that of silt "A_s/A_f"] and the ratio of [mean grain size of sand to that of silt "D_{50s}/D_{50f}"] of sand-silt mixtures. However, it exhibits an increase with the decrease of the ratio of the coefficient of uniformity of sand (C_{us}) to that of silt (C_{uf}) for the different silty sand soils under investigation.
3. The data collected from published literature and those of the present laboratory study confirm the existence of good correlations relating the threshold silt content (TSC) to the particle characteristics in terms of size and shape for the considered binary granular systems. Where, the new introduced ratios $[(D_{50s}\times A_s)/(D_{50f}\times A_f)]$ and $[(C_{us}\times A_s)/(C_{uf}\times A_f)]$ appear as pertinent parameters that could be used to predict the threshold silt content (TSC) derived from the compiled data from the published literature and those related to this study on (Chlef sand, Fontainebleau sand and Hostun sand mixed with Chlef silt).

Acknowledgments

This research work was performed in the context of mutual scientific cooperation between the Laboratory of Material Sciences & Environment, Hassiba Ben Bouali University of Chlef (Algeria) and the Laboratory of Soil Mechanics, Foundation Engineering & Environmental Geotechnics, Bochum Ruhr University (Germany). The authors are grateful for the financial support received from the Directorate General for Scientific Research and Technological Development, Algeria.

REFERENCES

[1] Barrett, P. J. 1980. The shape of rock particles, a critical review. Sedimentology. Vol. 27, pp. 291-303.

[2] Belkhatir, M., Arab, A., Missoum, H., Della, N., Schanz,T. 2011. Laboratory study on the liquefaction resistance of sand-siltmixtures: effect of grading characteristics. Granular Matter 13:599–609

[3] Cabalar , A,F 2010. Applications of the triaxial, resonant column and oedometer tests to the study of micaceous sands. Journal of Engineering Geology, 112, 21- 28

[4] Cabalar, A,F., Mustafa, W,S 2015. Fall cone tests on clay-sand mixtures. in Engineering Geology. 192, 154-165 DOI.org/10.1016/j.enggeo.2015.04.009

[5] Cabalar, A,F and Akbulut, N 2016. Effects of particle shape and size of sands on hydraulic conductivity. Acta Geotechnica Slovenica, 2016/2, 83-93

[6] Cherif Taiba, A., Mahmoudi, Y., Belkhatir, M., Kadri, A., Schanz, T., 2016. Insight into the effect of granulometric characteristics on static liquefation sucseptibility of silty sand soils. Geotech Geol Eng DOI 10.1007/s10706-015-9951-z

[7] Cherif Taiba,A,. Mahmoudi,Y,. Belkhatir,M,. Kadri,A,. and Tom Schanz,T 2017. Experimental Characterization of the Undrained Instability and Steady State of Silty Sand Soils under Monotonic Loading Conditions. International Journal of Geotechnical Engineering, DOI: 10.1080 /19386362.2017.1302643

[8] Cherif Taiba, A., Mahmoudi, Y., Belkhatir, M., and Schanz, T., 2018. Experimental Investigation into the Influence of Roundness and Sphericity on the Undrained Shear Response of Silty Sand Soils. Geotechnical Testing Journal, DOI.10.1520/ GTJ20170118.

[9] Cherif Taiba, A., Mahmoudi, Y., Hazout, L. Belkhatir, M., and Baille, W. 2019a. Evaluation of hydraulic conductivity through particle shape and packing density characteristics of sand–silt mixtures. Marine Georesources & Geotechnology, DOI: 10.1080/1064119X.2018.1539891

[10] Cherif Taiba, A., Mahmoudi, Y., Hazout, L. Belkhatir, M., and Baille, W. 2019b. Effects of Gradation on the mobilized Friction Angle for the Instability and Steady states of Sand-Silt Mixtures: Experimental Evidence. Acta Geotechnica Slovenica, DOI.org/10.18690/actageotechslov.16.1.79-95.2019

[11] Cherif Taiba, A., Mahmoudi, Y., Belkhatir, M., and Baille, W. 2019c. Assessment of the Correlation between Grain Angularity Parameter and Friction Index of Sand Containing Low Plastic Fines . Geomechanics and Geoengineering: An international journal. DOI.org/10.1080/17486025.2019.1648881

[12] Cho, G.-C., Dodds, J., Santamarina, J.C.,(2006. Particle shape effects on packing density, stiffness, and strength: natural and crushed sands.

J. Geotech. Geoenviron. Eng. ASCE 132 (5), 591–602.

[13] Dash, H.K.,Sitharam,T.G.,Baudet,B.A., 2010. Influence of non-plastic fines on the response of a silty sand to cyclic loading. Soils Found.50(5), 695–704.

[14] Hazirbaba, K., 2005. Pore Pressure Generation Characteristics of Sands and Silty Sands: A Strain Approach (Ph.D. Thesis). University of Texas, Austin, USA

[15] Hsiao D.H., Phan N.T.A., Hsieh Y.T, Kuo H.Y 2015. Engineering behavior and correlated parameters from obtained results of sand-silt mixtures. Soils dynamics and earthquake engineering 77, 137-151

[16] Huang YT, Huang AB, Kuo YC, Tsai MD 2004. A laboratory study on the undrained strength of a silty sand from Central Western Taiwan. Soil Dyn Earthq Eng 24:733–743

[17] Lade, P.V.,Liggio Jr.,C.D.,Yamamuro,J.A., 1998. Effects of non plastic fines on minimum and maximum void ratios of sand.Geotech.Test.J.,ASTM 21 (4),336–347.

[18] Mahmoudi, Y., Cherif Taiba, A., Belkhatir, M., Schanz, T., 2016a. Experimental Investigation on Undrained Shear Behavior of Overconsolidated Sand-Silt Mixtures: Effect of Sample Reconstitution. Geotechnical Testing J. DOI: 10.1520/GTJ20140183

[19] Mahmoudi, Y., Cherif Taiba, A., Belkhatir, M., Arab, A., and Schanz, T., 2016b. Laboratory study on undrained shear behaviour of overconsolidated sand–silt mixtures: effect of the fines content and stress state. International Journal of Geotechnical Engineering, DOI: 10.1080/19386362.2016.1252140

[20] Mahmoudi, Y., Cherif Taiba, A., Hazout, L., Wiebke, B. Belkhatir. 2018. Influence of Soil Fabrics and Stress State on the Undrained Instability of Overconsolidated Binary Granular Assemblies. Studia Geotechnica et Mechanica. 40(2): 96-116. doi.org/10.2478/sgem-2018-0011

[21] Mahmoudi, Y., Cherif Taiba, A., Hazout, L. Belkhatir, M., 2019. Experimental Evidence into the Impact of Sample Reconstitution on the Pore Water Pressure Generation of Overconsolidated Silty Sand Soils. Journal of Geo-engineering, DOI: 10.6310/jog.201912_14(4).3

[22] McGeary, R,K 1961. Mechanical packing of spherical particles. Journal of Am. Ceram. Soc. 44 (10), 513–522

[23] Monkul, M.M. Etminan E. Senol A. 2016. Influence of coefficient of uniformity and base sand gradation on static liquefaction of loose sand with silt. Soil Dynamics and Earthquake Engineering 89. 185-197.

[24] Ni, Q., Tan, T.S., Dasari, G.R., and Hight, D.W., 2004. Contribution of fines to the compressive strength of mixed soils. Geotechnique, 54 (9), 561--569.

[25] Papadopoulou, A. & Tika, T. 2008. The effect of fines on critical state and liquefaction resistance characteristics of non-plastic silty sands. Soils and Foundations 48, No. 5, 713-725.

[26] Polito, C.P., and Martin, J.R., 2001. Effects of non-plastic fines on the liquefaction resistance of solids. Journal of Geotechnical and Environmental Engineering, 127 (5), 408-415

[27] Powers, M. C. 1953. A new roundness scale for sedimentary particles. Journal of Sedimentary Petrology. Vol. 23, No. 2, pp. 117-119.

[28] Rahman MM 2009. Modelling the influence of fines on liquefaction behaviour. In: Department of Civil Engineering, University of New South Wales at Australian Defence Force Academy, PhD thesis, Canberra.

[29] Salgado, R, Bandini, P, Karim, A 2000. Shear strength and stiffness of silty sand. Journal of Geotechnical and Geoenviron Eng ASCE 126 (5), 451–462

[30] Thevanayagam, S., Shenthan, T., Mohan, S., and Liang, J., 2002. Undrained fragility of clean sands, silty sands, and sandy silts. Journal of Geotechnical and Geoenvironmental Engineering, 128 (10), 849-859.

[31] Xenaki, V.C., Athanasopoulos,G.A., 2003. Liquefaction resistance of sand–silt mixtures :an experimental investigation of the effect of fines. Soil Dyn. Earthquake Eng.23(3),1–12.

[32] Yang, S.L., Lacasse, S., and Sandven, R.F. 2006. Determination of the transitional fines content of mixtures of sand and non-plastic fines. Geotechnical Testing Journal, 29 (2), 102-107

[33] Yang. J and Wei L.M. 2012. Collapse of loose sand with the addition of fines: the role of particle shape. Geotechnique 62, No. 12, 1111–1125

[34] Zlatovic, S., and Ishihara, K., 1995. On the influence of nonplastic fines on residul strength. Proceedings of IS-TOKY0'95/ The First International Conference on Earthquake Geotechnical Engineering/ Tokyo/14--16 November 1995, Tokyo, Japan, 239-244.

[35] Zuo L, Baudet B A. 2015. Determination of the transitional fines content of sand-non plastic fines mixtures". Soils Found;55(1):213–9.

SMALL SCALE MODEL TEST ON LATERAL BEHAVIORS OF PILE GROUP IN LOOSE SILICA SAND

MODELNI PREIZKUS V MAJHNEM MERILU ZA BOČNO OBNAŠANJE SKUPINE PILOTOV V SILIKATNEM PESKU RAHLEGA GOSTOTNEGA STANJA

Amir Vakili
Islamic Azad university,
Dep. of civil engineering, Najafabad branch
Najafabad, Iran

Seyed Mohammad Ali Zomorodian
(corresponding author)
Islamic Azad university,
Dep. of civil engineering, Najafabad branch
Najafabad, Iran

Shiraz University,
Dep. of water engineering
Shiraz, Iran
E-mail: mzomorod@shirazu.ac.ir

Arash Totonchi
Islamic Azad university,
Dep. of civil engineering, Najafabad branch
Najafabad, Iran

Islamic Azad university,
Dep. of civil engineering, Marvdasht branch
Marvdasht, Iran

DOI https://doi.org/10.18690/actageotechslov.18.1.41-54.2021

Keywords

pile group, lateral load, p-y method, load angle, group reduction factor

Ključne besede

skupina pilotov, bočna obtežba, p-y metoda, naklon obtežbe, količnik redukcije skupine pilotov

Abstract

The accurate predictions of load- deflection response of the pile group are necessary for a safe and economical design. The behavior of piles under the lateral load embedded in soil, is typically analyzed using the Winkler nonlinear springs method. In this method, the soil-pile interaction is modeled by nonlinear p-y curves in a way that the single pile p-y curve is modified using a p-multiplier (P_m) for each row of piles in the group. The average P_m is called the group reduction factor. The P_m factor depends upon the configuration of pile group and the pile spacing (S). The present study was conducted to investigate the effects of various parameters, such as the pile spacing in the group, different layouts and the lateral load angle (Θ) change as a new parameter on the P_m factor and group efficiency based on the 1-g model test. The P_m factor is well comparable with the results of the full-scale test on pile group. However, based on the results, the calculated values of the P_m factor for 3×3 pile groups under 2.5-diameter spacing was estimated about 0.38 and under 3.5-diameter spacing was estimated

Izvleček

Za varno in ekonomično zasnovo skupine pilotov so potrebne natančne napovedi odziva obtežba-pomik. Obnašanje vpetih pilotov obremenjenih s prečno obtežbo, se običajno analizira z uporabo Winklerjeve metode nelinearnih vzmeti. S to metodo se interakcija zemljina-pilot modelira z uporabo nelinearnih krivulj p-y na način, da se krivulja p-y enega pilota spremeni s p-multiplikatorjem (P_m) za vsako vrsto pilotov v skupini. Povprečni P_m se imenuje količnik redukcije skupine pilotov. Faktor P_m je odvisen od konfiguracije skupine pilotov in razmika med piloti (S). V pričujoči študiji se raziskujejo učinki različnih parametrov, kot so razmik med piloti v skupini, različne postavitve pilotov in kot bočne obtežbe (Θ) kot novega parametra, ki vpliva na količnik P_m ter učinkovitost skupine pilotov na podlagi 1-g preizkusnega modela. Tako dobljen količnik P_m je zelo primerljiv z rezultati celovitega testa na skupini pilotov. Na podlagi rezultatov pa so bile izračunane vrednosti faktorja P_m za skupine pilotov 3×3 pri medsebojnem razmiku 2,5 premera ocenjene na približno 0,38, pri medsebojnem razmiku 3,5 premera

about 0.52, so the calculated values at S/D=3, obtained from interpolation the values of group reduction factor at S/D=2.5 and S/D=3.5, are close to the AASHTO recommendation.

pa približno 0,52. Zato so izračunane vrednosti količnika redukcije skupine pri S/D=3, dobljene z interpolacijo vrednosti količnika redukcije skupine pri S/D=2,5 in S/D=3,5, blizu priporočilu AASHTO.

1 INTRODUCTION

When the piles act in a group, the strength and lateral-bearing of the individual piles are reduced by soil-pile interaction. In general, the pile group will exhibit less lateral capacity than the sum of the lateral capacities of the individual piles. In the pile group, each pile pushes against the soil in front of it, creating a shear zone in the soil, which expand with increasing lateral loading. The overlap that occurs between the piles in the same row is called "edge effects", while the overlapping created between the different rows of piles in the group is called the "shadowing effect". These shadowing and edge effects are significant factors in the bearing capacity of pile groups, which may reduce the lateral resistance of each individual pile in the group [1, 2]. The overlapping of the shear zones created in the pile group is shown in Figure 1.

Several methods have been proposed to model lateral pile group response. For example, Ooi and Duncan (1994) developed a group amplification procedure.

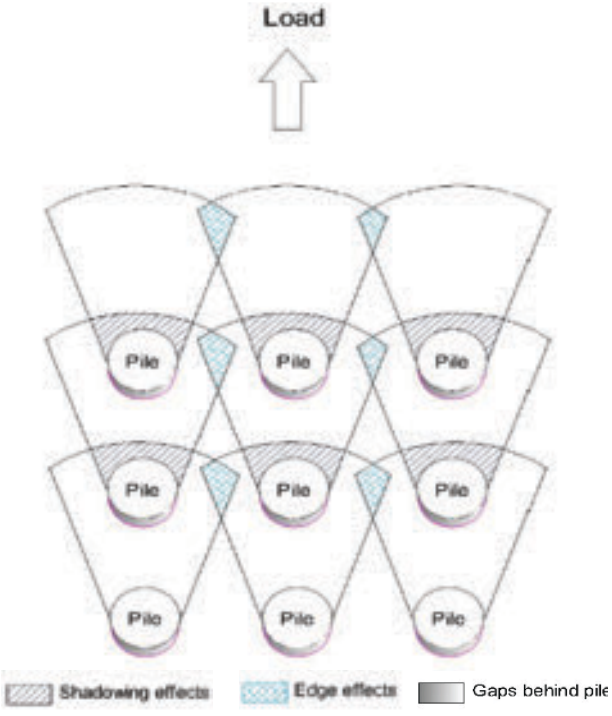

Figure 1. Overlapping of failure zones (shadowing) and gap formation behind piles [1].

However, they are neither able to estimate the distribution of loads among piles within a group nor take into account the pile group arrangement [3]. The group effects in pile groups are taken account of by reducing the subgrade modulus. Pise and Patra (2001) carried out lateral loading model 1-g tests on fixed head model piles and small pile groups in sand to investigate the ultimate lateral resistance of a pile group. Similar to Ooi and Duncan's procedure (1994), this method is not able to calculate the distribution of loads among piles in a group [4]. The lateral response of piles is typically analyzed using the beam on nonlinear Winkler springs model. The nonlinear springs are based on the *p-y* curves proposed by the American Petroleum Institute (API), where *p* indicates the soil resistance around the pile and *y* is the lateral deflection [5, 6]. One of the most common methods of accounting for the group effects in the Winkler model is to modify the single pile *p-y* curves using a P_m factor, as suggested by Brown et al. (1988). In this approach, the *p*-multiplier was determined by comparing with the *p-y* curves obtained in laterally loaded single pile tests as shown in figure 2. The value of the P_m coefficient for the leading row (the row which has the longest distance from the lateral load) is higher and for the trailing row is considered less because of the shadowing effects [7]. The leading and trailing rows interchange during the seismic and dynamic loading. Therefore, an average value of P_m is sometimes used for all the piles in the group. The average of the P_m coefficient is called "group reduction factor" (Brown et al., 2001) [8].

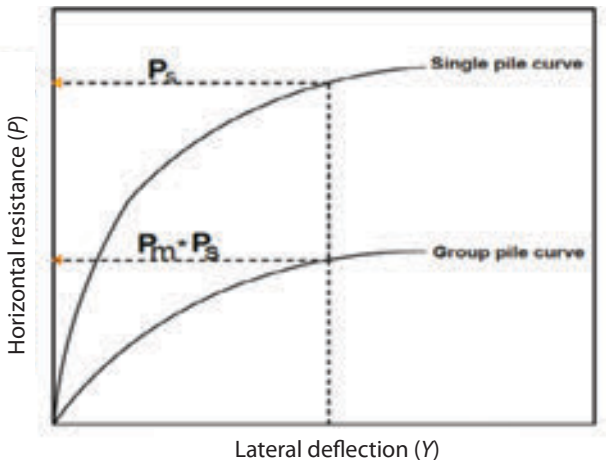

Figure 2. Definition of *p*-multiplier (P_m) and P_s horizontal resistance of soil for single pile [8].

Table 1. The group reduction factor from previous studies.

Reference	Soil type	Test type	Pile configuration	Pile type	D (cm)	S/D	Pile head condition	p-multiplier for row							Group reduction factor
								1	2	3	4	5	6	7	
Brown et al. (1988) [7]	medium dense sand	full scale	3×3	steel pipe	27.3	3	free	0.8	0.4	0.3	-	-	6	-	0.5
Morrison and Reese (1988) [14]	medium dense sand	full scale	3×3	steel pipe	27.3	3	free	0.8	0.4	0.3	-	-	-	-	0.5
McVay et al. (1995) [9]	medium loose sand	centrifuge	3×3	steel pipe	43	5	free	1	0.85	0.7	-	-	-	-	0.85
	medium dense sand	centrifuge	3×3	steel pipe	43	5	free	1	0.85	0.7	-	-	-	-	0.85
	medium loose sand	centrifuge	3×3	steel pipe	43	3	free	0.65	0.45	0.35	-	-	-	-	0.48
	medium dense sand	centrifuge	3×3	steel pipe	43	3	free	0.8	0.4	0.3	-	-	-	-	0.5
McVay et al. (1998) [10]	sand	centrifuge	3×3	square steel	42.9	3	fixed	0.8	0.4	0.3	-	-	-	-	0.5
	sand	centrifuge	3×4	square steel	42.9	3	fixed	0.8	0.4	0.3	0.3	-	-	-	0.45
	sand	centrifuge	3×5	square steel	42.9	3	fixed	0.8	0.4	0.3	0.2	0.3	-	-	0.4
	sand	centrifuge	3×6	square steel	42.9	3	fixed	0.8	0.4	0.3	0.2	0.2	0.3	-	0.37
	sand	centrifuge	3×7	square steel	42.9	3	fixed	0.8	0.4	0.3	0.2	0.2	0.2	0.3	0.34
Huang et al. (2001) [15]	silty clay	full scale	2×3	RC	150	3	fixed	0.93	0.7	0.74	-	-	-	-	0.79
Rollins and Sparks (2002) [16]	silty clay	full scale	3×3	steel pipe	32.4	3	fixed	0.6	0.38	0.43	-	-	-	-	0.47
Rollins et al. (2005) [17]	sand	full scale	3×3	steel pipe	32.4	3.3	free	0.8	0.4	0.4	-	-	-	-	0.53
Walsh (2005) [18]	sand	full scale	3×5	steel pipe	32.4	3.92	free	1	0.5	0.35	0.3	0.4	-	-	0.51
Christensen (2006) [19]	sand	full scale	3×3	steel pipe	32.4	5.65	free	1	0.7	0.65	-	-	-	-	0.78
Rollins et al. (2006) [20, 21]	stiff clay	full scale	3×3	steel pipe	32.4	5.65	free	0.95	0.88	0.77	-	-	-	-	0.87
Kim and Yoon (2011) [11]	sand	small scale	3×3	steel pipe	1.2	3	fixed	0.69	0.35	0.3	-	-	-	-	0.5

The group reduction factor can be obtained using laboratory studies or full-scale tests. Full-scale tests are the best means for investigating the behavior of laterally loaded piles. It is, however, very expensive and difficult to perform a full-scale test on a pile group. The capacity of the loading equipment also limits the size of the pile group that can be tested. Therefore, full-scale tests are often performed on small models of pile groups at close distance between piles. Centrifuge test is considered as a useful alternative to full-scale test, which can be used to study the "group reduction factor" (McVay et al., 1995 and 1998) [9, 10]. Kim and Yoon (2011) proposed the response assessment of a laterally loaded pile group in 3, 4 and 6-diameter pile spacing based on laboratory modeling and suggested that pile spacing of more than six times the pile diameter in group seemed to be large enough to eliminate the group effects of the pile [11]. Soomro et al. (2018), presented lateral responses of an existing 2×2 pile group for advancing side-by-side twin tunnels at various depths in dry sand. [12]. Al-Shamary

et al. (2018) used three-dimensional finite-element approach to assess the responses of lateral pile and pile group subjected to pure lateral load. Based on the results, the behavior of the pile group 2×2 was close, but not the same as the behavior of pile group 2×1. Regarding the group 3×2, the lateral pile displacement and lateral soil resistance had similar values for the first and second trailing rows. The values of the *p*-multiplier (p_m) for leading pile are always greater than those obtained for first and second trailing pile [13]. Table 1 indicates a list of full-scale, small-scale, and centrifuge experimental studies. Most experiments have been conducted on pile groups with 3×3 arrangement, with free head conditions, center to center spacing of 3 pile diameters ($S/D = 3$).

A review of past researches reveals that few studies are available on the behavior of the pile group under lateral loads on a small-scale model in the laboratory. In addition, small-scale models, compared to full-scales studies, are easier and have lower cost. In small-scale modeling, group pile can also be created with small spaces for investigating the soil-pile interaction on ultimate lateral resistance, group efficiency and group reduction factor based on the 1-g model test. Finally, since the arrangement of piles with small spaces in full-scale models is very difficult, the results are generalized to full-scale studies and used to control their results. Due to the possibility of changing the lateral load direction during the lifetime of the pile structure, the effect of lateral load angle change as a new parameter on the group efficiency and group reduction factor is investigated. Since the group reduction factor is directly affected by the stress zone overlapping, evaluation of this parameter is expected to yield new results.

2 MATERIALS AND METHODS

2.1 Soil

The type of soil is dry silica sand, which was passed through a sieve size of 100. In addition, the Standard soil tests were carried out on the soil to determine the soil properties and the results are shown in Table 2.

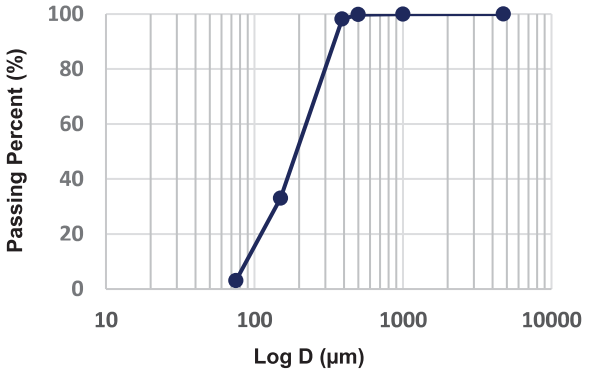

Figure 3. Grain size distribution curve for the silica sand.

Table 2. Physical properties of used silica sand.

Parameters	Quantity	ASTM Standard	Comments
G_s	2.67	D854	Pycnometer Test
φ (deg)	31.5	D3080-90	Direct Shear Test
$\gamma_{d,min}$ (kN/m^3)	15.4	D4254	Dry Pour Test
$\gamma_{d,max}$ (kN/m^3)	17.6	D4253	Dynamic Cyclic Loading
γ_d (kN/m^3)	16.2	D7263	In-situ Density
D_r [%]	39.5	-	-
D_{10} , D_{30} , D_{50} & D_{60}	0.09, 0.15, 0.19 & 0.23	-	-
C_c & C_u	1.09 & 2.56	-	-

The grading test was performed according to the ASTM D421-87 standard [22]. The used sand was classified as poorly graded sand (SP) based on the unified soil classification system (USCS). The grain size distribution for the silica sand is shown in Figure 3.

2.2 Pile

The model pile used for the lateral loading tests was 20 mm and 16 mm in external and internal diameter respectively and 200 mm in length. Pile rigidity can be evaluated based on the criteria presented in the Elhakim et al.'s (2014) study, where the piles are considered as rigid when ($L/T < 2$) and flexible when ($L/T > 4$), where L indicates the pile length and T shows the elastic length calculated by using Equation 1 [2]:

$$T = \sqrt[5]{\frac{E_p I_p}{n_h}} \qquad (1)$$

Where, E_p indicates the elastic modulus of the pile material, I_p shows the moment of inertia of the pile ($E_p I_p$ is 966 Nm^2), and n_h is considered the empirical value which depends on the sand relative density. The n_h value for loose sand was considered as 1900 kN/m^3, (Terzaghi, 1955) [23]. The estimated values of T and (L/T) are 0.22m and 0.91, respectively, for piles embedded in loose sand. Broms (1964) suggested that for a pile, the embedded length of the pile to be considered as a short rigid pile, must be smaller than $2T$ and for considering as a long flexible pile, the value must be greater than $4T$ [24]. Since the tests were carried out on the piles with the length of 0.2 m and this length is less than $2T$, so the pile categorized as short rigid pile. The characteristics of model piles is shown in Table 3.

Table 3. The characteristics of model piles.

embedded length (mm)	pile thickness (mm)	external diameter (mm)	free length (mm)	spacing/diameter (*S/D*)
20	4	150	50	1.5, 2.5, 3.5

The pile arrangement of the group pile used in the model tests is shown in figure 4. The piles were placed in a layer of sand in single position and in five group arrangements with center to center spacing of 1.5, 2.5, and 3.5 diameters of the piles.

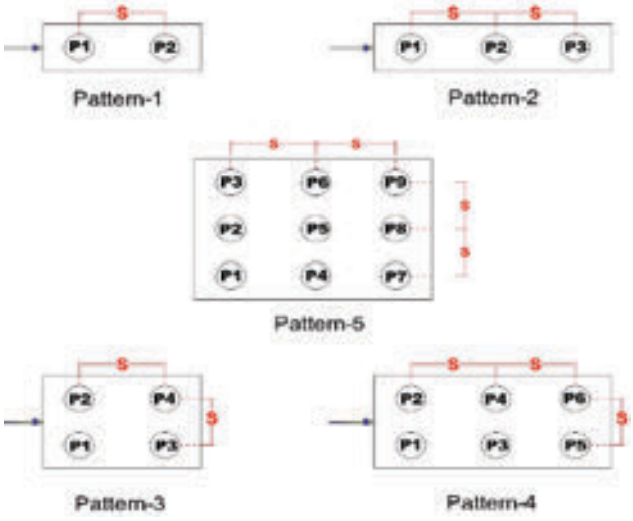

Figure 4. Pile array type for model group pile test.

2.3 Model pile group test

A side view of the model pile group test during the static fixed-head testing and the dimensions of test box and pile cap plan for 3×3 pile group are shown in Figure 5 a, and b. Based on the studies conducted on the lateral loading of piles, it was shown that the size of the model box must be sufficiently large enough to minimize side effects. Dong et al. (2018) studied the boundary condition effects on laterally loaded pile behavior both numerically and experimentally and suggested that the ratio of dimensions of the model box in the plan to the pile diameter must be more than 15 in order to ignore the boundary condition effects [25]. Based on some other studies, when pile groups are under lateral loading, the effect of the stress zone extends up to 8-12*D* and 3-4*D* in the directions of lateral loading and perpendicular to the loadings, respectively (Poulos and Davis, 1980; Zomorodian and Dehghan, 2011; Memar et al., 2019) [26, 27, 28].

However, in order to validate the dimensions which were chosen for test box, a numerical analysis was executed using a commercially available finite-element program Abaqus3D. The geometry of a typical finite-element model verified for the analysis is shown in figure 6. According to the numerical modeling performed with the mentioned software, it was determined that the area under the effective stress of the soil mass did not reach the boundary of the model and no changes developed at the model boundary. Therefore the test box was made of steel cubes with the length of 1m and the width and height of 0.8 m with a special frame with a thickness of 3 mm. A place on the test box was considered for installing the pneumatic jack which was used for loading in a horizontal direction.

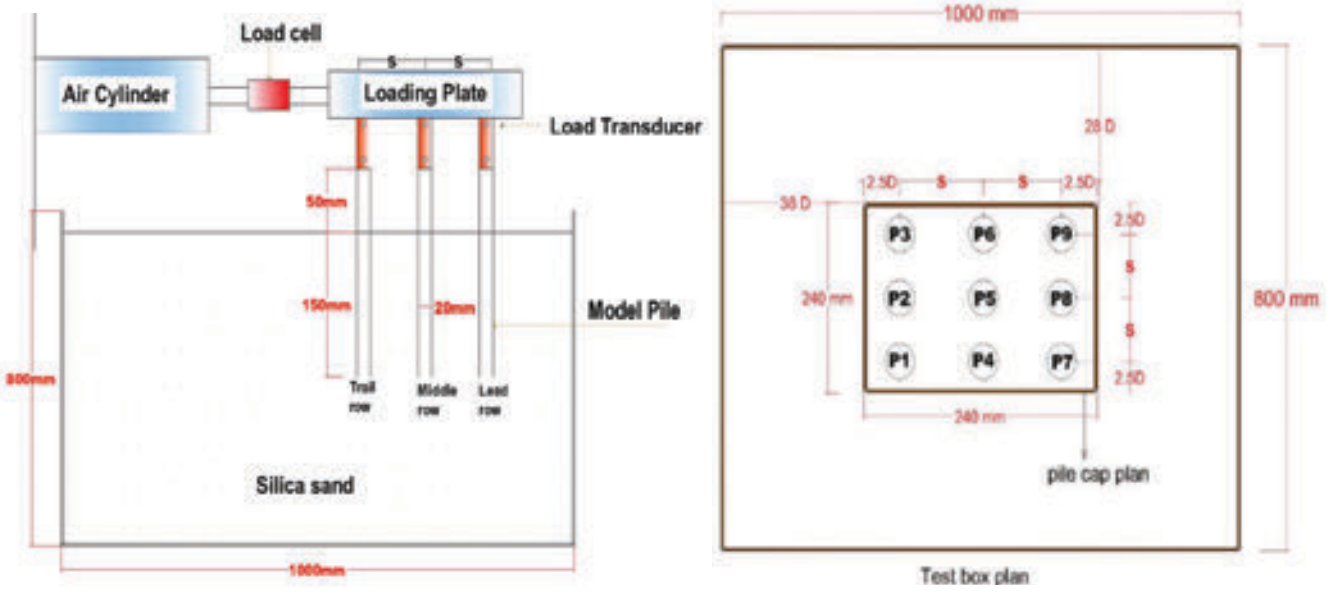

Figure 5. (a) Side view of reservoir and loading system and (b) Dimensions of test box and pile cap plan for 3×3 pile group in *S/D* = 3.5.

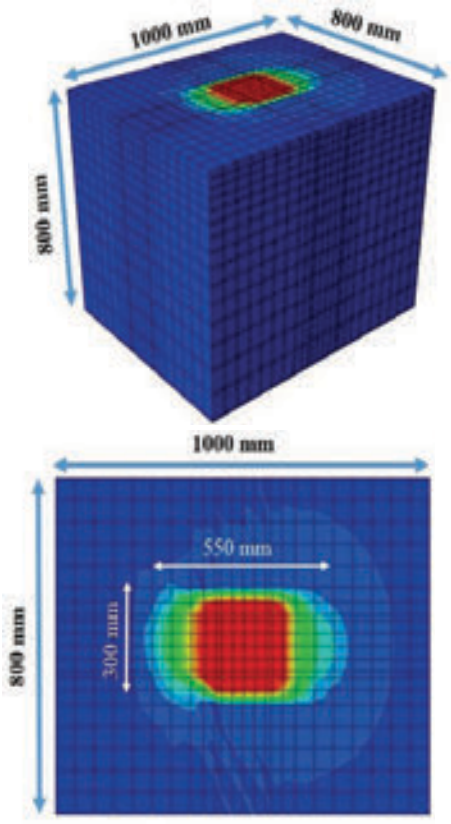

Figure 6. The geometry of a typical finite-element model.

2.4 Testing procedure and equipment

The loading system should provide lateral force by hydraulic, pneumatic (air pressure) or electrical loading to apply the lateral load on the pile group. In this test, a pneumatic pressure control panel and an air compressor connected which were used to apply the controlled force via the jack. In this panel, a regulator was used to adjust the output pressure and a pair of automatic valves to apply force on two opposite directions. In addition, a load cell with a maximum load capacity of 1000 (N) was used to measure the total loads applied to the loading plate. Further, the loading plate consisted of rectangular plate and a pile cap that was essentially rigid compared with the lateral pile stiffness. Since obtaining the rate of stress and tolerable force by each pile of the group was considered as the main objective, appropriate measurements should be made regarding the total lateral load and distribution of loads among piles in a group. In addition, the measurement was performed through load transducers in the laboratory model. Load transducers were made of steel, which were connected to the pile cap from one side and the piles from the other side to form the system rigidity and the transducer resolution is classified in class A with ±0.05 relative error (Figure 5). The displacement of the pile group during the test was measured using a linear variable differential transducer (LVDT), which were attached to the centerline of the loading plate. The measured total load applied to the loading plate transferred lateral load to each pile, and the displacement data from the load cell, load transducer, and LVDT were simultaneously stored on a computer data acquisition system. The advantage of this method is that the load share of each pile could be obtained from the total group load and the *p-y* curve of each pile could be easily drawn.

The test box was filled using a sand precipitation method through a mechanized device. The sand precipitation was conducted through a series of netted plates connected to the bottom of the calibrated precipitation funnel which could move up and down through a reel and frame and holder arm. The system provides the possibility of adjusting the precipitation heights and the horizontal motion of the precipitation funnel along the length of the test box easily. Before starting the main experiments, the precipitation of the sand was determined using a series of trial and error tests, with a specified outflow and from a certain height, in order to reach the intended relative density. The use of sand precipitation method created a very homogeneous sand mass so that the relative density changes in the test box were determined to be less than 1 %. During the testing process, the relative density of the soil inside the box was checked to determine whether it is constant and uniform by placing small cans with specific dimensions in different places of the test box. In this way, after the sand falls from a certain height (30 cm), the amount of weight and volume of the soil inside the cans are obtained and finally, the amount of soil dry unit-weight and relative density are obtained and controlled.

3 LABORATORY RESULTS

A series of 34 model pile group tests were performed to determine the effects of pile spacing, type of pile group arrangement and lateral load angle change on the average lateral resistance of the group pile. Table 4 indicates the experimental and numerical model plan. In addition, the effect of the case study parameters on the load-displacement response of the loaded piles were evaluated, along with the load distribution within pile groups with fixed head condition.

The load on a single pile and pile group was increasingly applied to obtain a horizontal deflection versus nonlinear load diagram. A large number of data were obtained based on the lateral load and displacement of the piles cap. It is worth noting that the tests were conducted on a single pile, as well as on pile groups up to the lateral deflection of about 4 mm (the ratio of lateral deflection to diameter is 0.2). The result of the lateral load-normalized deflection curve of the single pile embedded

Table 4. Experimental model plan.

Variable	Number of pile	Pile spacing	Lateral load angle	Type of modeling
Pile arrangement	1, 2, 3, 4, 6 & 9	1.5*D*, 2.5*D* & 3.5*D*	$\Theta = 0^\circ$	small scale
Pile spacing	4, 6 & 9	1.5*D*, 2.5*D* & 3.5*D*	$\Theta = 30^\circ$	small scale
Lateral load angle	4, 6 & 9	1.5*D*, 2.5*D* & 3.5*D*	$\Theta = 45^\circ$	small scale

in loose sand is shown in Figure 7. The results indicated that when (*Y*/*D*) is less than 0.1 the *Q* - (*Y*/*D*) slope is increased rapidly comparing to (*Y*/*D*) more than 0.1.

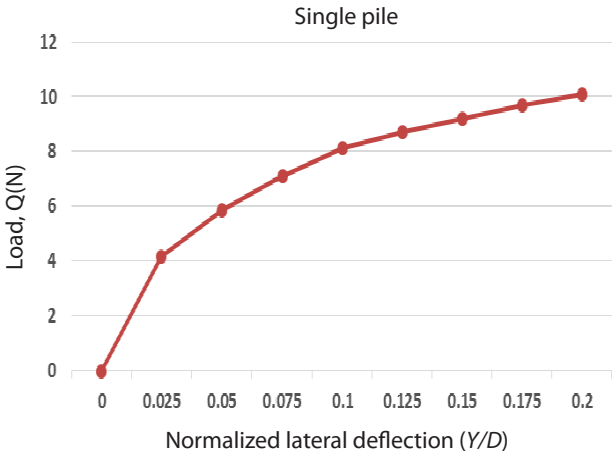

Figure 7. Lateral load-normalized deflection response for single pile test

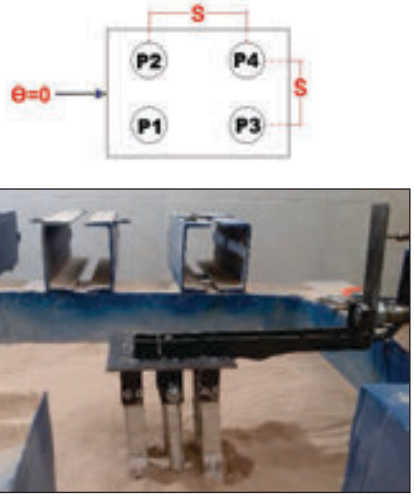

(a)

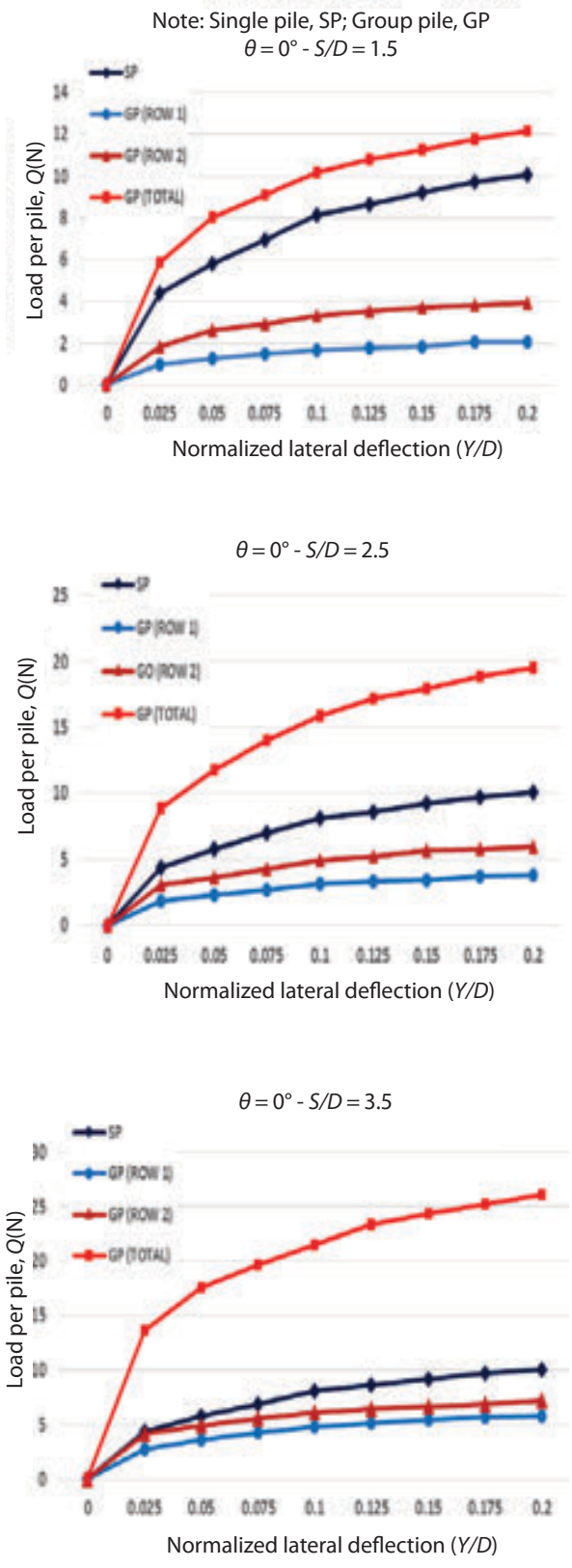

(b)

Figure 8. (a) Schematic view of lateral load applied to the pile group and (b) Lateral load–normalized deflection response for the 2×2 pile group in different ratio of *S*/*D*.

3.1 Lateral load – deflection response of pile groups

Figure 8 (a, and b) displays a schematic view of lateral load applied to the pile groups and the piles spacing effect on lateral load-normalized deflection response for the 2×2 pile group with square arrangement. Based on the results, the measured average lateral resistance increases with an increase in pile spacing. Figure 9 shows the response of the variations of the lateral deflection to diameter ratio versus the average lateral load for the pile group in two square and parallel modes (at $S/D = 3.5$) and also single pile. For a constant ratio of lateral deflection to diameter (about 0.2), the average lateral resistance levels for each pile in the 2×2 and 3×2 pile groups were about 34 % and 39 % less than the single pile, respectively.

The ratio between the average lateral load carried by a pile in each row and the total loads carried by a pile group (pile groups 2×2, 3×2 and 3×3) is shown in Figure 10. Based on the results, the front and rear piles carry 56 % and 44 % of the total pile group loads (at pile group 2×2) and the front, middle and rear piles carry 44 %, 32 % and 24 % (at pile group 3×2) and 46 %, 31 % and 23 % (at pile group 3×3) of the total pile group loads,

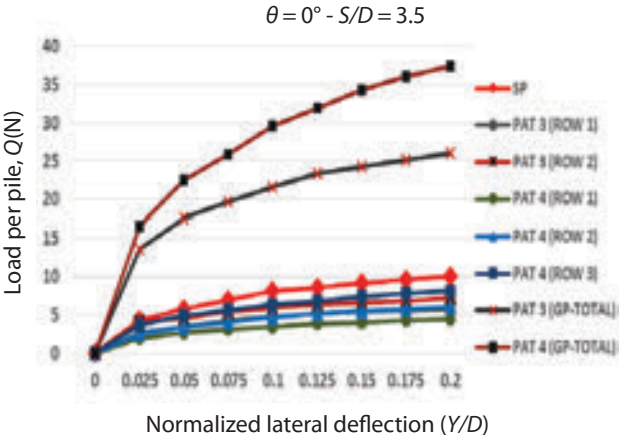

Figure 9. Lateral load– normalized deflection response for the pile groups (pile models 2×2 and 3×2).

respectively. The ratio of each row load to group lateral load for a leading row is higher than this ratio for a trailing row because of the shadowing effect.

Due to the possibility of changing the lateral load direction, the effect of load angle change on ultimate lateral resistance is investigated. Figure 11 (a, and b) displays a schematic view of angular lateral loads applied to the pile groups and the different load angles effect on the lateral load-normalized deflection response for the 2×2 pile group with square arrangement. Based on the

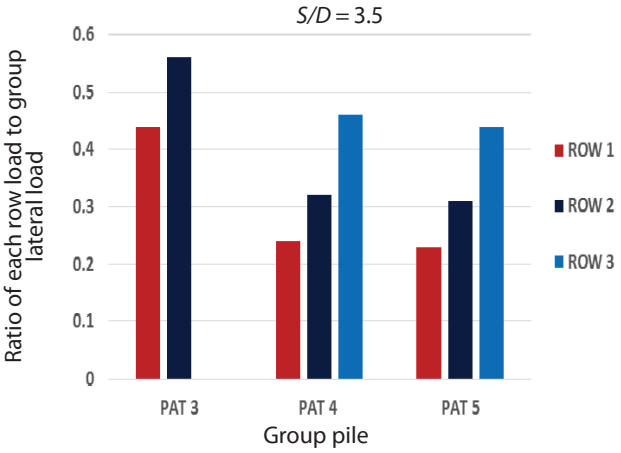

Figure 10. Variations ratio of each row load to group lateral load for the different pile groups.

results, the measured average lateral resistance increases with changing lateral load angles from 0˚ to 45˚. Regarding a constant ratio of lateral deflection to diameter (about 0.2), the average lateral resistance levels for each pile in the group at $S/D = 3.5$ under angular lateral loads in $\Theta = 0$ ˚, $\Theta = 30$ ˚, and $\Theta = 45$ ˚ were about 34 %, 24 %, and 20 % less than the single pile, respectively.

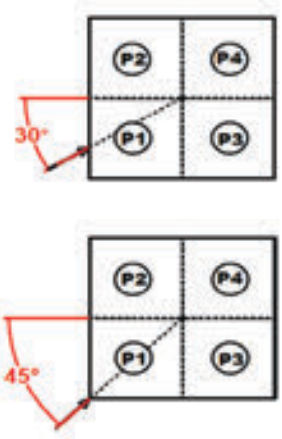

(a)

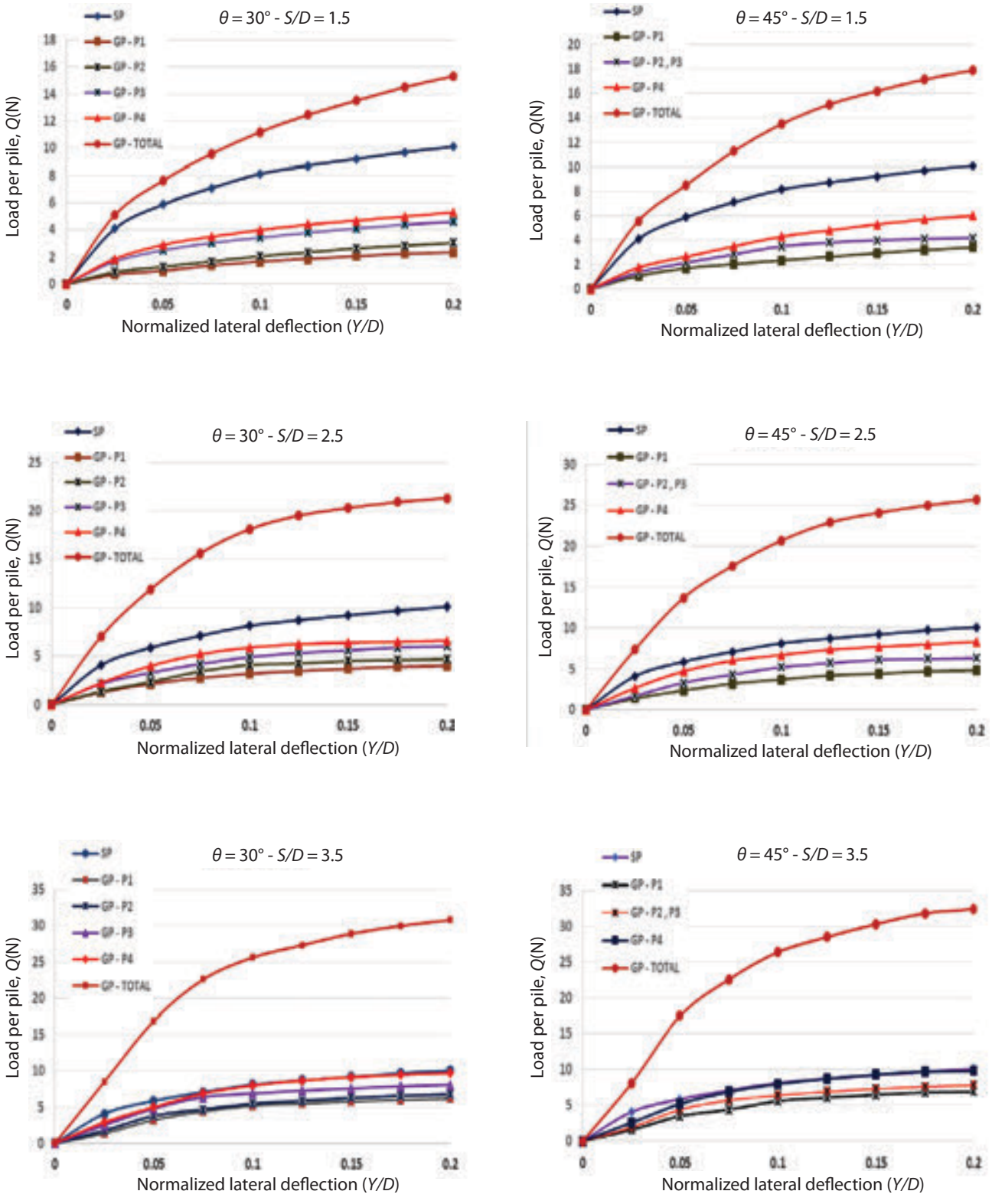

(b)

Figure 11. (a) Schematic view of angular lateral load applied to the pile groups and (b) Lateral load–normalized deflection response in different load angles for the 2×2 pile group.

3.2 Group efficiency

The efficiency of the group is important to estimate the resistance of the pile group from the result of the single pile resistance. The efficiency of the group η, in a specific deflection here, in terms of ultimate lateral resistance of the pile group to that of the single pile is expressed as:

$$\eta = \frac{Q_{LG}}{n_1 n_2 Q_{LS}} \qquad (2)$$

Where, Q_{LG} is the lateral resistance of the pile group, Q_{LS} is the lateral resistance of the single pile, n_1 is the number of rows in the pile group, and n_2 is the number of columns in the pile group. Wakai et al. (1999) conducted the 1-g model test on pile group under lateral load (3×3 piles group at $S/D = 2.5$) and reported a group efficiency of about 0.7 (when the deflection reached $0.1D$) [29]. Figure 12 shows the relationship between the efficiency of the group versus the spacing to diameter ratio of the piles in the group at different arrangements. Based on the results, the measured group efficiency increases with an increase in pile spacing to diameter ratio. For the case of a 2×2 pile group, the efficiency of the group varied from about 0.3 to 0.65 by increasing the pile spacing to diameter ratio from 1.5 to 3.5. As expected in Figure 13, the group reduction factor decreases with an increase in the number of piles in the group, and the trend is dependent on the pile spacing and number of piles in the group.

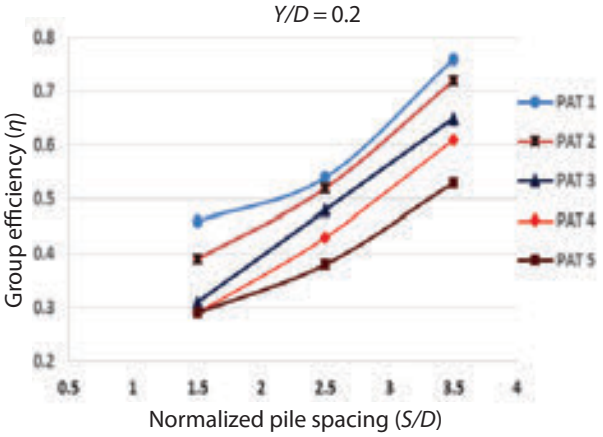

Figure 12. Group efficiency - normalized pile spacing relationship in pile groups.

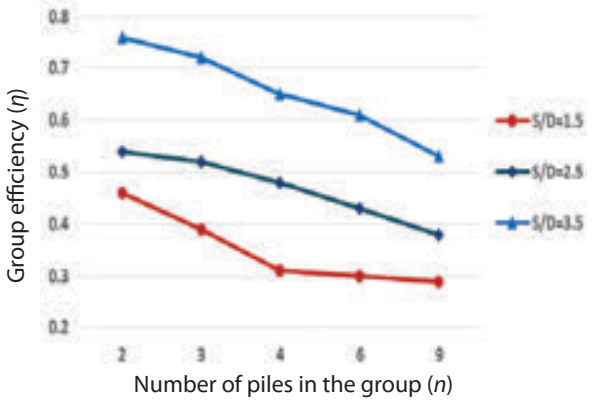

Figure 12. Effects of the number of pile (n) on group efficiency (η)

Figure 14 shows the effect of the lateral load angles on the group efficiency for the 2×2 and 3×3 pile groups. Also, the results showed that the effects of overlapping stress zones (shadowing effect) decrease and the group efficiency increases by changing the angle of lateral load from 0˚ to 45˚ due to the change in the trajectory of stress.

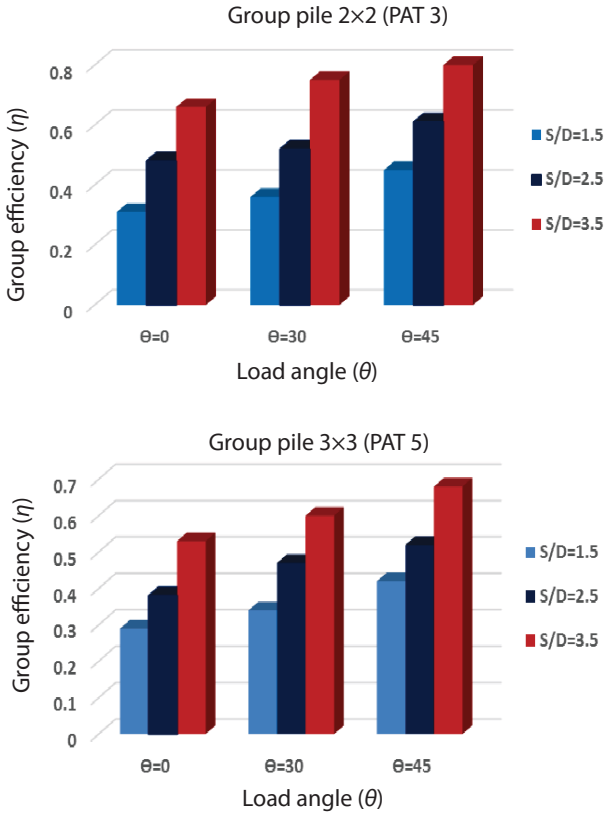

Figure 14. The effect of the lateral load angles on the group efficiency.

3.3 Calculation of the group reduction factor from model test

As previously mentioned, modifying the single pile p-y curves by using a group reduction factor (P_m) for each row of piles in the group is considered as one of the most common and useful methods to evaluate the interac-

Table 5. *p*-multiplier factors for laterally loaded pile groups with different arrangements in Θ=0˚.

Y/D	*S/D*	Group layout	Average P_m	*p*-multiplier factors								
				P_1	P_2	P_3	P_4	P_5	P_6	P_7	P_8	P_9
0.2	1.5	2×1	0.46	0.38	0.54	-	-	-	-	-	-	-
0.2	2.5	2×1	0.54	0.46	0.62	-	-	-	-	-	-	-
0.2	3.5	2×1	0.81	0.74	0.87	-	-	-	-	-	-	-
0.2	1.5	3×1	0.39	0.24	0.33	0.59	-	-	-	-	-	-
0.2	2.5	3×1	0.52	0.37	0.50	0.71	-	-	-	-	-	-
0.2	3.5	3×1	0.71	0.53	0.69	0.93	-	-	-	-	-	-
0.2	1.5	2×2	0.31	0.20	0.20	0.41	0.41	-	-	-	-	-
0.2	2.5	2×2	0.48	0.37	0.37	0.59	0.59	-	-	-	-	-
0.2	3.5	2×2	0.66	0.59	0.59	0.74	0.74	-	-	-	-	-
0.2	1.5	3×2	0.29	0.18	0.18	0.25	0.25	0.45	0.45	-	-	-
0.2	2.5	3×2	0.42	0.27	0.27	0.42	0.42	0.57	0.57	-	-	-
0.2	3.5	3×2	0.60	0.44	0.44	0.58	0.58	0.80	0.80	-	-	-
0.2	1.5	3×3	0.28	0.17	0.17	0.17	0.29	0.29	0.29	0.40	0.40	0.40
0.2	2.5	3×3	0.38	0.24	0.24	0.24	0.38	0.38	0.38	0.52	0.52	0.52
0.2	3.5	3×3	0.52	0.36	0.36	0.36	0.50	0.50	0.50	0.71	0.71	0.71

tion effects in pile groups. Based on the results of the experimental modeling, Tables 5 and 6 indicate the sets of average *p*-multiplier factors for the pile groups with different arrangements, different spacing to diameter ratio, and different lateral load angles. The values of the P_m factors given in the Table are actually the average of multiplier factors of each pile located in the group. These factors for the lead row are independent of the type of pile group arrangement and pile spacing, but for the middle and trail rows of the pile groups are, however, highly dependent on the type of arrangement and pile spacing. As shown in Table 5, the factor of P_m obtained for the lead row is higher, while it is lower for the trail rows. In the pile group, each pile pushes against the soil in front of it, creating a shear zone in the soil. These shear zones begin to enlarge and overlap as the lateral load increases and more overlapping occurs if the piles are closely spaced to each other. The overlap in the shear areas are significant factors in the bearing capacity of pile groups, which may reduce the lateral resistance of pile groups. As shown in Table 6, the factor of P_m increases by changing the angle of lateral load from 0˚ to 45˚, due to more diameter distances between the piles.

The effect of spacing piles in the group, the number and layout of piles on the average value of the group

Table 6. Average *p*-multiplier for different lateral load angles in pile groups with different arrangements.

Y/D	*S/D*	Group layout	Average *p*-multiplier (P_m)		
			$\Theta = 45^\circ$	$\Theta = 30^\circ$	$\Theta = 0^\circ$
0.2	1.5	2×2	0.31	0.37	0.43
0.2	2.5	2×2	0.48	0.51	0.62
0.2	3.5	2×2	0.66	0.77	0.81
0.2	1.5	3×2	0.29	0.36	0.43
0.2	2.5	3×2	0.42	0.49	0.59
0.2	3.5	3×2	0.60	0.64	0.74
0.2	1.5	3×3	0.28	0.35	0.40
0.2	2.5	3×3	0.38	0.48	0.55
0.2	3.5	3×3	0.52	0.61	0.69

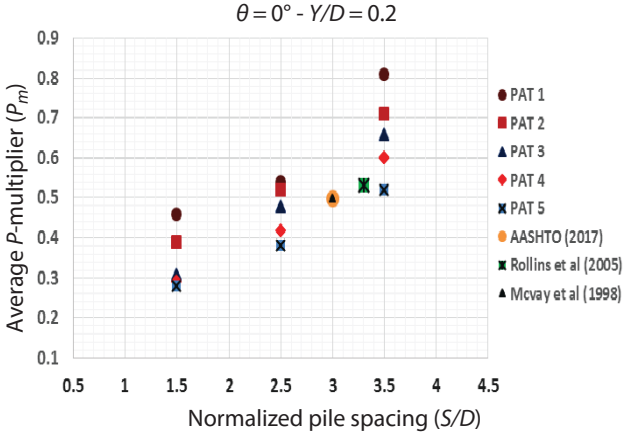

Figure 15. Average *p*-multiplier (P_m) - normalized spacing relationship for pile groups.

reduction factors (P_m) in $\Theta = 0^\circ$ is shown in Figure15. Based on the results, the value of the P_m factor increases significantly by increasing pile spacing from 1.5 to 3.5 diameter. Also the value of the P_m factor for pile groups for different layouts were estimated from 0.38 (3×3 pile group) to 0.54 (2×1 pile group) in 2.5-diameter spacing and were estimated from 0.52 (3×3 pile group) to 0.81 (2×1 pile group) in 3.5-diameter spacing, respectively.

These results are very close to the average P_m factor values of about 0.5 and 0.53, conducted by Mcvay et al. (1998), for 3×3 pile group at $S/D = 3$ on a centrifuge experiment and Rollins et al. (2005), for 3×3 pile group at $S/D = 3.3$ on a full-scale experiment based on the results in Table1 respectively [10, 17]. Table 7 indicates the evaluation of the group reduction factors and comparison of the results against those recommended in different design guidelines such as AASHTO (2017). The calculated values of the P_m factor for lateral load (in $\Theta = 0^\circ$) at $S/D = 3$, obtained from the interpolation of the values of group reduction factor at $S/D = 2.5$ and $S/D = 3.5$, are close to the ones recommended by AASHTO [30]. However, regarding angular lateral load (in $\Theta = 30^\circ, 45^\circ$), the results indicated that AASHTO underestimates the group reduction factors and the lateral resistance, especially for the fixed pile head condition. The AASHTO recommendations for choosing *p*-multipliers are based on data from free head pile group tests. Fixed head group reduction factors are close and slightly lower than free head factors at $S/D = 3$. This means that group effects in fixed pile head groups are more pronounced than in free head pile groups.

Table 7. Comparison between p-multiplier suggested in AASHTO (2017) and Modeling results.

Reference	Test type	Load angle Θ (°)	Group pile	S/D	P_m
AASHTO (2017)	Full scale	0	3×3	3	0.5
Modeling results	Small scale	0	3×3	3	0.45
Modeling results	Small scale	30	3×3	3	0.55
Modeling results	Small scale	45	3×3	3	0.62

4 EFFECTS OF SCALE AND LIMITATIONS

Since a lot of time and cost are spent on full-scale models in situ testing, laboratory tests on small-scale models were used as a method herein. In the experiments, the model piles were made smaller by specific scale, while the sand used in the small-scale of the laboratory model was the same as in the real models. Therefore, it is possible for both the pile and the sand, in a small scale, to have a different behavior in reality, and this might influence the experimental results, referred to as scale effects. The diameter of the pile (D) used in the experiments was more than 100 times bigger than the average diameter of aggregates (D_{50}). Ovesen (1979) proposed that the ratio of pile diameter (D) to the average diameter of aggregates (D_{50}) is required to be greater than 40 [31]. Based on the experimental results on small-scale models, it is impossible to predict the real in situ behavior. However, the present study showed comparable results of the small-scale tests (laboratory models), which could be generalized to the results of full-scale tests.

5 CONCLUSION

The group reduction factor is considered as a parameter which is commonly used in spring models of pile groups to account for the group effects in soil-pile interaction analysis. There are various guidelines to determine the average of group reduction factors. These guidelines are derived from several available experiments that are often conducted on full-scale pile group with limited spaces, and mostly under free head conditions [30, 32]. The group reduction factors can be obtained using laboratory (small-scale) and in-situ (full-scale) tests. However, creating and performing a full-scale test on pile groups is very difficult and costly. Therefore, small-scale criteria were used to study the pile groups under the lateral load in fixed head conditions. For this purpose, several different models of pile groups were prepared in different arrangements and were studied by changing the spaces between the piles and lateral load angles in the group in each case. Based on the results, the following conclusions are made:

- Load–deflection behavior of piles in a group was more flexible than single-pile behavior. This difference in behavior was reduced due to the reduction of shadow overlap effects, when the spaces between the piles increased in the groups.
- By increasing the ratio of spacing to diameter piles in the group, the efficiency coefficient of the group as well as the group reduction factors (P_m) increased. For a 2×2 pile group, the group efficiency varied from about 0.3 to 0.65 by increasing the ratio of spacing to diameter piles from 1.5 to 3.5.
- By changing the angle of lateral load from 0° to 45°, the group efficiency increases, due to the change of trajectory of stress and decreasing the effects of overlapping stress zones (shadowing effect).

- For fixed head pile groups, the leading row of the group tolerated the highest load, while the middle and trailing rows tolerated less load for the certain deflection value. The group reduction factors in 3×2 pile group arrangement, and in $S/D = 2.5$, were estimated to be 0.57, 0.42 and 0.27, respectively, for the leading, middle, and trailing rows.
- The results of small-scale tests in laboratory were comparable and verified with the results of full-scale experiments on pile group under lateral load. Therefore, the experimental results of the pile group under the lateral load on a small-scale can be useable.
- The calculated values of the P_m factor for the lateral load ($\Theta = 0^\circ$) at $S/D = 3$, were close to the ones recommended by AASHTO. However, regarding the angular lateral load ($\Theta = 30^\circ, 45^\circ$), the results indicated that AASHTO underestimated the group reduction factors, hence the lateral resistance and their reports were conservative due to unknown direction of lateral loads.

REFERENCES

[1] Mokwa, R.L., 1999, "Investigation of the resistance of pile caps to lateral loading", Doctoral dissertation, Virginia Polytechnic Institute and State University, Virginia.

[2] Elhakim, A.F., El khouly, M. and Awad, R., 2014, "Three dimensional modeling of laterally loaded pile groups resting in sand", HBRC Journal.

[3] Ooi, P.S.K., and Duncan, J.M., 1994, "Lateral load analysis of groups of piles and drilled shafts", Journal of Geotechnical and Geoenvironmental Engineering, ASCE, Vol. 120, No. 6, PP. 1034-1050.

[4] Pise, P.J., and Patra, N.R., 2001, "Ultimate lateral resistance of pile groups in sand", Journal of Geotechnical and Geoenvironmental Engineering, ASCE, Vol. 127, No. 6, PP. 481-487.

[5] API, 1984, "Recommended practice for planning, designing and constructing fixed offshore platforms", 15th ed., API RP2A, American Petroleum Institute, 115 PP.

[6] API, 2007, "Recommended practice for planning, designing, and constructing fixed offshore platforms", API Recommended Practice 2A-WSD, 21st ed. American petroleum Institute, Washington, D. C.

[7] Brown, D.A., Morrison, C., and Reese, L.C., 1988, "Lateral load behavior of pile group in sand", Journal of Geotechnical Engineering, 114(11), PP. 1261-1276.

[8] Brown, D.A., O'Neill, M.W., Hoit, M., Mcvay, M., E1-Naggar, M.H., and Chakraborty, S., 2001, "Static and dynamic lateral loading of pile groups". Technical Report NCHRP, Report No. 461. National Cooperative Highway Research Program, Washington, D.C.

[9] McVay, M., Casper, R., and Shang, T., 1995, " Lateral response of three-row groups in loose to dense sands at 3D and 5D pile spacing", Journal of Geotechnical Engineering, 121(5), PP. 436-441.

[10] McVay, M., Zhang, L., Molnit, T., and Lai, P., 1998, "Centrifuge testing of large laterally loaded Pile groups in sands", Journal of Geotechnical and Geoenvironmental Engineering, 124(10), PP. 1016-1026.

[11] Kim, B.T. and Yoon, G. L., 2011, "Laboratory modeling of laterally loaded pile groups in sand", KSCE Journal of Civil Engineering, 15(1), PP. 65-75.

[12] Soomro, M. A., Ng, C. W. W., Memon, N. A., and Bhanbhro, R., 2018, "Lateral behaviour of a pile group due to side-by-side twin tunnelling in dry sand: 3D centrifuge tests and numerical modelling", Computers and Geotechnics, 101, PP. 48-64.

[13] Al-Shamary, J. M. A., Chik, Z., and Taha, M. R., 2018, "Modeling the lateral response of pile groups in cohesionless and cohesive soils", International Journal of Geo-Engineering, 9(1), 1.

[14] Morrison, C., and Reese, L.C., 1988, "Lateral load test of a full-scale pile group in sand", Technical Report. Geotechnical Engineering Report CR86-1. U.S. Army Engineer Waterway Experiment Station, Vicksburg, Miss.

[15] Huang, A., Hsueh, C., ONeill, M. W., Chen, S., and Chen, C., 2001, "Effects of construction on laterally loaded pile groups", Journal of Geotechnical and Geoenvironmental Engineering, 127(5), PP. 385-397.

[16] Rollins, K. M. and Sparks, A., 2002, "Lateral resistance of full-scale pile cap with gravel backfill", Journal of Geotechnical and Geoenvironmental Engineering, 128(9), PP. 711-723.

[17] Rollins, K.M., Lane, J.D., and Gerber, T.M., 2005, "Measured and computed lateral response of a pile group in sand", Journal of Geotechnical and Geoenvironmental Engineering, 131(1), PP. 103-114.

[18] Walsh, J. M., 2005, "Full-scale lateral load tests of a 3×5 pile group in sand", Master's thesis, Brigham Young University.

[19] Christensen, D. S., 2006, "Full scale static lateral load test of a 9 pile group in sand", Masters Thesis, Brigham Young University.

[20] Rollins, K. M., Olsen, R. J., Egbert, J. J., Jensen, D. H., Olsen, K. G., and Garrett, B. H., 2006, "Pile spacing effect on lateral pile group behavior: Load tests", Journal of Geotechnical and Geoenviron-

mental Engineering, 132(10), PP. 1262-1271.
[21] Rollins, K. M., Olsen, R. J., Egbert, J. J., Jensen, D. H., Olsen, K. G., and Garrett, B. H., 2006, "Pile spacing effect on lateral pile group behavior: Analysis", Journal of Geotechnical and Geoenvironmental Engineering, 132(10), PP. 1272-1283.
[22] ASTM D-4253 & 4254, 2002, "Annual book of ASTM standards 2002", Baltimore, USA.
[23] Terzaghi, K., 1955, "Evaluation of coefficients of subgrade reaction", Geotechnique, (5). PP. 297-326.
[24] Broms, B. B, 1964, "Lateral resistance of piles in cohesionless soils", Journal of the soil Mechanics and Foundations Division, 90(3), PP.123-156.
[25] Dong, J., Chen, F., Zhou, M. and Zhou, X., 2018, "Numerical analysis of the boundary effect in model tests for single pile under lateral load", Bulletin of Engineering Geology and the Environment, 77(3), PP.1057-1068.
[26] Poulos, H.G., and Davis E.H., 1980, "Pile foundation analysis and design", John Wiley & Sons Inc., New York.
[27] Zomorodian, M.A. and Dehghan, M., 2011, "Lateral resistance of a pile installed near a reinforced slope", International Journal of Physical Modelling in Geotechnics, 11(4), PP. 156-165.
[28] Memar, M., Zomorodian, M.A. and Vakili, A.H., 2019, "Effect of pile cross-section shape on pile group behaviour under lateral loading in sand", International Journal of Physical Modelling in Geotechnics.
[29] Wakai, A., Gose, S., and Ugai, K., 1999, "3-D elasto-plastic finite element analysis of pile foundations subjected to lateral loading", Soil and Foundation, Tokyo, Vol. 39, No. 1, PP. 97-111.
[30] AASHTO, 2017, "AASHTO LRFD bridge design specification". 6th ed. American Association of State Highway and Transportation Officials (AASHTO), Washington, D.C.
[31] Ovesen, N.K., 1979, "The use of physical models in design: The scaling law relationship", Proc., 7th European Conf. on Soil Mechanics and Foundation Engineering, 4, PP. 318-323.
[32] FEMA, 2012, "Foundation analysis and design", FEMA p-751. In NEHRP recommended provisions: design examples. Federal Emergency Management Agency. National Institute of Building Sciences, Building Seismic safety Council, Washington, D.C., chapter 5.

IMPROVED GENERAL SLICE METHOD OF LIMIT EQUILIBRIUM FOR SLOPE STABILITY ANALYSIS

IZBOLJŠANA SPLOŠNA LAMELNA METODA MEJNEGA RAVNOVESJA ZA STABILNOSTNE ANALIZE POBOČIJ

Shiguo Xiao *(corresponding author)*
Southwest Jiaotong university,
Ministry of education, Key laboratory of high-speed railway engineering
Chengdu 610031, China

Southwest Jiaotong University,
Department of Geological Engineering
Chengdu 610031, China
E-mail: xiaoshiguo@swjtu.cn

Tingjun Chen
Southwest Jiaotong University,
Department of Geological Engineering
Chengdu 610031, China

DOI https://doi.org/10.18690/actageotechslov.18.1.55-64.2021

Keywords

slope stability, limit equilibrium, slice method, non-linear programming; interslice force

Ključne besede

stabilnost pobočja, mejno ravnovesje, lamelna metoda, nelinearno programiranje, medlamelna sila

Abstract

For traditional slice methods of limit equilibrium used to analyze slope stability, some hypothetical conditions on interslice force are generally introduced to solve the problem. In order to reduce the defect theoretically due to the related hypothesis, more rigorous constraints of interslice force are completely considered in light of static equilibrium conditions and energy dissipation principle of the interface between two adjacent slices. Without hypothesis of interslice force, the slope stability analysis is transformed consistently into a non-linear programming problem to be solved. So, a generally improved solution of slice method of limit equilibrium to slope stability is put forward. In particular, influence of the dilation angle of soil on slope stability can be involved in the method. The proposed method can be utilized for any slopes with arbitrary slip surfaces.

Izvleček

Za tradicionalne lamelne metode mejnega ravnovesja, ki se uporabljajo za analizo stabilnosti pobočij, so za rešitev problema glede medlamelne sile na splošno uvedene nekatere predpostavke. Da bi teoretično zmanjšali napake zaradi teh predpostavk, se glede na statična ravnovesna stanja in načelo disipiranja energije na kontaktu med dvema sosednjima lamelama upoštevajo strožje omejitve za medlamelne sile. Brez predpostavke o medlamelni sili se analiza stabilnosti pobočij dosledno spremeni v reševanje problema nelinearnega programiranja. Predlagana je torej splošno izboljšana rešitev lamelne metode mejnega ravnovesja stabilnosti pobočij. Pri tej metodi je mogoče zlasti vključiti vpliv kota dilatacije zemljine na stabilnost pobočij. Predlagano metodo lahko uporabimo za vsa pobočja s poljubnimi drsnimi površinami.

1 INTRODUCTION

Limit equilibrium methods of slope stability analysis are easily operated and widely used in practical slope engineering [1]. In 1916, Petterson and Hultin proposed circle sliding surfaces for stability analysis of undrained soil slopes [2], which is later called the Swedish circle method and marks the beginning of the application of limit equilibrium method for slope stability. In 1926, Fellenius introduced both cohesive and frictional strength of soil into slope stability analysis using the circular sliding surface. Thus, the Fellenius method

is regarded as one of the significant limit equilibrium methods with fully considering soil strength for slope stability analysis [3]. Later, Lorimer once used Euler spiral or clothoid instead of circular slip surface to explain failure mode of soil slope by referring to experiments and investigations. In these methods, potential slide mass is divided vertically into finite slices with small width. And interslice forces on the two sides of a slice are assumed to be a pair of balance forces. Bishop (1955) [4] improved further the assumption of interslice force with neglecting the difference between their vertical components and proposed the simplified Bishop method for the soil slope with circular slip surface. Janbu (1954) [5] also neglected the tangent component of interslice force but provided the simplified Janbu method used for the soil slope with arbitrary slip surface. In order to reduce the disadvantage of the previous methods without considering the tangent component of interslice force, Lowe and Karafiath (1960) [6] assumed that the dip angle of the interslice force is equal to the average of the dip angle of the top and bottom of the slice. The US Army Corps of Engineers (1967) [7] recommended that the dip of interslice force is equal to the average of the dip angles of all slices (Corps of Engineers #1) or the dip of the top of the slice (Corps of Engineers #2). However, for the Imbalanced Thrust Force Method (ITFM) [8], the dip angle of the interslice force is assumed to be consistent with the dip of the bottom of the previous slice. Since these methods mentioned above cannot include all equilibrium equations of force and moment of a slice, analysis results of slope stability by them sometimes are not possibly certainly reasonable [9].

Morgenstern and Price (1965) [10] proposed a general slice method which satisfies both force and moment equilibrium by assuming that the ratio of tangential over normal component of interslice force is a specified function. Spencer (1967) [11] presumed that the ratio is an unknown constant. In fact, it is a special case of the Morgenstern-Price method (MPM). Janbu (1973) [12] obtained the solution of slice method by considering all static equilibrium conditions and assuming the location of action point of the interslice force. Fredlund and Krahn (1977) [13] provided an alternative derivation for the Morgenstern-Price method and fully exhibited the relationship between factor of safety and the scaling parameter defined in the MPM. Sarma (1979) [14] proposed a method of non-vertical slicing with considering interfaces between adjacent slices to be in the limit state, which is widely used for stability analysis of rock slope. Chen and Morgenstern (1983) [15] improved the MPM and promoted the function of interslice force further to approximate practical condition. Correia (1988) [16] assumed the shear force on the slice sides to be a function characterizing the shape of the shear force across the slide mass multiplied by a scaling parameter with the unit of force. Zhu (2001) [17] presented a new concise formulation of force and moment equilibrium equations within the framework of the MPM. Although these methods involved completely in both force and moment equilibrium conditions of slices, they all stemmed from assumptions of the direction or magnitude of interslice force.

Therefore, rationality of slice methods of limit equilibrium depends to great extent on whether interslice force is reasonably coped with. Rigorously speaking, although some investigations [9,15] indicate assumptions of interslice force tend to have possibly small effects on the results of the slice method, the minimum value of the factor of safety of slope stability by the slice method in theory has not been completely demonstrated.

From the perspective of rigorous theory, in spite of various assumptions of interslice force adopted in the previous studies, acceptable hypotheses of interslice force based on the practically physical sense are that: (1) The shear forces on the sides of slices should not exceed the related shear resistances; (2) There is no tensile stress between adjacent slices [9]. On the basis of the two elementary constrain conditions, this paper provided a more rigorous derivation for the slice method satisfying all static equilibrium conditions of slices and boundary conditions of the slope without introducing any prescribed relationship between the tangential and normal force on the slice sides. As far as the calculation procedure in mathematics is concerned, the slope stability analysis is transformed rigorously into a non-linear programming problem to ensure the solution of the minimum factor of safety.

2 BASIC PROCEDURE

A typical analysis model of slope stability by slice method is shown in Fig. 1. The key points of slope stability analysis can be regarded essentially as solving the unknown forces on potential sliding surfaces and sides of slices under various factors of safety. Based on the general slice method [10], each slice must satisfy the static equilibrium conditions. Namely, there are two force equilibrium and one moment equilibrium equations for each slice.

Therefore, for the ith slice the three static equilibrium equations can be expressed as (the meaning of all symbols are explained in the Notation)

$$E_i + N_i \cdot \sin\alpha_i = E_{i+1} + T_i \cdot \cos\alpha_i \qquad (1)$$

$$W_i + X_i = X_{i+1} + N_i \cdot \cos\alpha_i + T_i \cdot \sin\alpha_i \qquad (2)$$

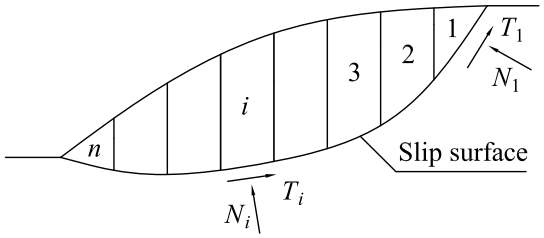

(a) Potential slide mass and its slices.

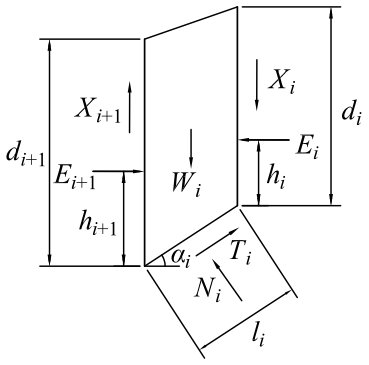

(b) Forces on the i^{th} slice.

Figure 1. Analysis model of a general slope.

$$(X_i + X_{i+1}) \cdot \frac{l_i \cos\alpha_i}{2} + E_{i+1} \cdot (h_{i+1} - \frac{l_i \sin\alpha_i}{2}) = E_i \cdot (h_i + \frac{l_i \sin\alpha_i}{2}) \quad (3)$$

Besides, the bottom of each slice is in the limit state. So according to the Mohr-Coulomb strength criterion and shear strength reduction strategy [18] for the factor of safety, there is

$$T_i = (N_i \cdot \tan\varphi_i + c_i \cdot l_i) / F_s \quad (4)$$

In fact, vertical interfaces subjectively divided between slices of potential slide soil mass are not certainly in the limit state, which is different from the hypothesis assumed by Sarma (1979) [14]. In other words, shear force on the sides of the slice is not over the related shear resistance. Namely,

$$X_i \le (E_i \cdot \tan\varphi_i + c_i \cdot d_i) / F_s \quad (5)$$

Introducing a non-negative coefficient K_i no more than 1, Eq. (5) can be rewritten as

$$X_i = K_i \cdot (E_i \cdot \tan\varphi_i + c_i \cdot d_i) / F_s \quad (6)$$

where E_i is not less than zero due to the fact that there is no tension between slices.

We can suppose that there is a thin transition layer with a small thickness of δ between two adjacent slices (see Fig. 2). And there are average tangential and normal stress on the layer. Thus, general energy dissipation rate in the transition layer can be expressed as [19]

$$D = \tau \frac{\partial \eta}{\partial t} - \sigma \frac{\partial \varepsilon}{\partial t} \quad (7)$$

According to the geometric relationships, one can get

$$\begin{cases} \dfrac{\partial \eta}{\partial t} = \dfrac{\Delta v_s}{\delta} \\ \dfrac{\partial \varepsilon}{\partial t} = \dfrac{\Delta v_n}{\delta} \end{cases} \quad (8)$$

Further, based on the conception of the average stresses on the layer, there is

$$\begin{cases} \tau = \dfrac{X_i}{d_i} \\ \sigma = \dfrac{E_i}{d_i} \end{cases} \quad (9)$$

Substituting Eqs. (8) and (9) into Eq. (7), one can obtain

$$D = \frac{X_i \Delta v_s - E_i \Delta v_n}{d_i \delta} \quad (10)$$

Then, taking into account that the energy dissipation rate in the transition layer should not be negative ($D \ge 0$), one can further get

$$\frac{X_i}{E_i} \ge \frac{\Delta v_n}{\Delta v_s} \quad (11)$$

Since the transition layer is not necessarily in the limit state, the shear stress on it is not beyond the related shear strength. Further, the corresponding actual shear strain is not more than the ultimate shear strain. So, one can get

$$\Delta v_s \le (\Delta v_s)_{\text{limit}} \quad (12)$$

According to the admissible failure mechanism of kinematical system of soil mass which can be reasonably used in slope stability analysis [19], the ratio of normal velocity over tangential velocity in the transition layer is the tangent value of dilation angle ψ of the soil. Thus, Substituting Eq. (12) into Eq. (11) one can obtain

$$\frac{X_i}{E_i} \ge \frac{\Delta v_n}{\Delta v_s} \ge \frac{\Delta v_n}{(\Delta v_s)_{\text{limit}}} = \tan\psi \quad (13)$$

Therefore, Eq. (13) exhibits that the dip angle of the resultant interslice force should be not less than the dilation angle of the soil.

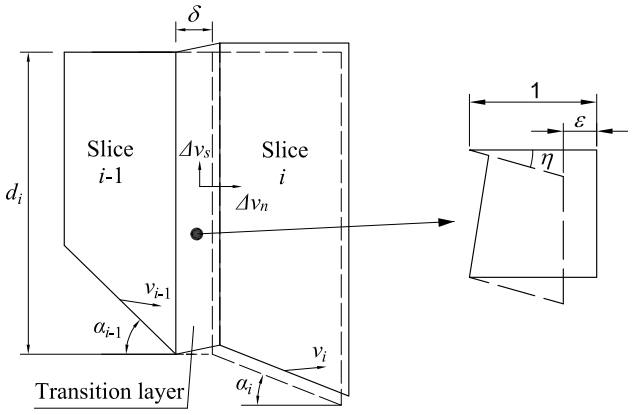

Figure 2. Diagram of thin transition layer between adjacent soil slices.

Then, the problem of slope stability analysis is equivalent to solving the minimum value of the factor of safety under the control conditions of Eqs. (1) to (4) and restraint conditions of Eqs. (6) and (13). A potential slide mass is divided into n slices, and for the last slice, there are $E_{n+1} = 0$, $X_{n+1} = 0$ and $h_{n+1} = 0$. So for each slice there are five unknowns: N_i, T_i, E_i, X_i, and h_i. In addition, the factor of safety of slope stability F_s is another unknown. Consequently, there are totally $5n+1$ unknowns. Based on Eqs. (1) to (4), one can obtain $4n$ independent equations. And for the first slice, there are $E_1 = 0$, $X_1 = 0$ and $h_1 = 0$. Thus, solving the factor of safety of a slope with potential slide mass divided into n (≥3) slices can be actually regarded as an n-2 dimensional non-linear programming problem to find the minimum factor of safety. As long as the factor of safety is sought out, the other variables including the tangential and normal force on the sides of all slices can be also obtained simultaneously. As for the specifically operating procedure, Sequential Quadratic Programming (SQP) method in MATLAB software can be used to solve this programming problem [20]. There is a locally optimal solution to the problem with constrained variables, and it can be carried out via the inserted fmincon function (*Constrained nonlinear minimization*) of the optimization tool in MATLAB [20].

3 VERIFICATION EXAMPLES AND DISCUSSION

In order to verify the proposed method, five examples are taken next. Since experiments show that the dilation angle of soil is smaller than the internal friction angle [21], the dilation angle is adopted as φ, $3\varphi/4$, $\varphi/2$, $\varphi/4$, and 0, respectively to sufficiently reflect the influence of dilation angle on the analysis results of slope stability.

3.1 Example 1: a homogeneous clay slope with circular slip surface and $F_s > 1$

Fig. 3 shows an example of a soil slope with a circular slip surface and 10 m height [10]. Point O_c is the rotation center of a potential slip surface, and the potential slide mass of the slope is divided into 9 slices. Point O is the top point of the slip surface. The factors of safety figured out by SQP are exhibited in Table 1, where the symbols of MPM-I, MPM-II, MPM-III, and MPM-IV represent correspondingly four cases that the function $f(x)$ of interslice force is assumed as constant, custom unimodal curve, custom unimodal curve with two valleys, and straight line, respectively. Besides the results by the non-circular analysis method, circular analysis result (Slip circle analysis) is also listed after Morgenstern and Price (1965) [15]. The results show the maximum relative error between the proposed method and MPM is 5 %. Moreover, the factors of safety obtained by the proposed method are not more than those by the non-circular MPM and circular analysis method. The reason is that the proposed method is actually able to obtain the optimal solution of the factor of safety using the optimization search procedure with considering all constraint equations of slices, rather than introducing the assumption of interslice force function as does the MPM. Therefore, the proposed method is more general and rigorous than existing methods and can theoretically find the minimum value of the factor of safety.

Also, Table 1 shows the factor of safety obtained using the proposed method increases very slightly with the increase of the dilation angle. If the dilation angle varies from 0 to φ, the factor of safety increases only about 0.2 %. So it means the dilation angle has little effect on the analysis results of slope stability. In fact, a numerical simulation model of the example via FLAC3D (see Fig. 4) is established to reflect further the influence of the dilation angle on the factor of safety. The numerical model consists of 11632 quadrangle elements and 23780 nodes. Perfectly elastoplastic constitutive model and Mohr-Coulomb strength principle are assumed to simulate the slope soil. As shown in Fig. 5, the factor of safety by FLAC3D is marginally increasing with the dilation angle and has only 0.8 % growth if $\psi = \varphi$. The tendency of F_s varied with ψ/φ by the proposed method is in good agreement with that by FLAC3D, which also indicates the proposed method is acceptable.

In order to indicate the directions of interslice force or interslice thrust line obtained by various methods, $\lambda f(x)$ [10] is still cited here to express the ratio of tangential over normal force on the side of slice.

$$\lambda f(x) = \frac{X_i}{E_i} \qquad (14)$$

As shown in Fig. 6, there are remarkable differences of the dip angles of interslice forces among the various methods including classical Lowe and Karafiath method (LKM) [6], Corps of Engineers #1 method (CEM1) [7], Corps of Engineers #2 method (CEM2) [7], ITFM [8], and MPM-I [10]. However, the results obtained by the ITFM are relatively close to those calculated using the proposed method. Fig. 7 indicates further that there are distinct alterations of the interslice thrust lines between

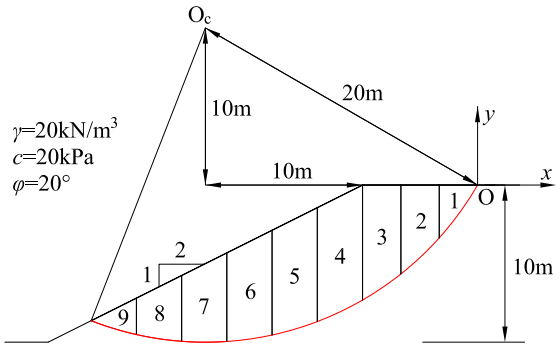

Figure 3. Sketch map of the slope example 1.

Table 1. Analysis results of example 1.

Methods	F_s
Proposed method ($\psi = \varphi$)	2.044
Proposed method ($\psi = 0.75\varphi$)	2.042
Proposed method ($\psi = 0.5\varphi$)	2.041
Proposed method ($\psi = 0.25\varphi$)	2.041
Proposed method ($\psi = 0$)	2.04
Slip circle analysis	2.098
MPM-I	2.045
MPM-II	2.136
MPM-III	2.134
MPM-IV	2.044

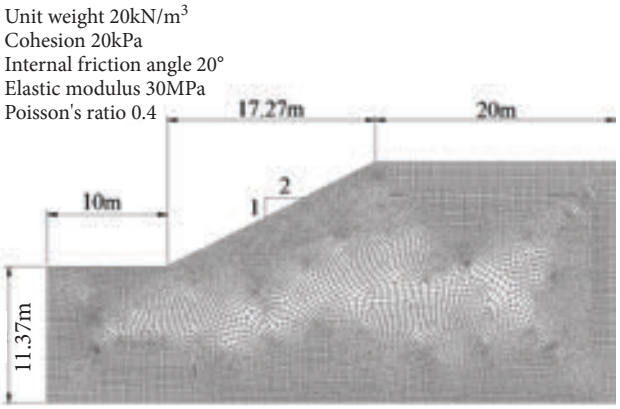

Figure 4. Numerical simulation model of example 1 via FLAC3D.

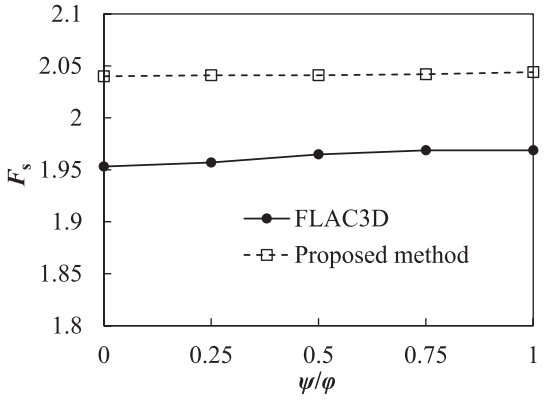

Figure 5. Relationship between factor of safety and soil dilation angle in example 1.

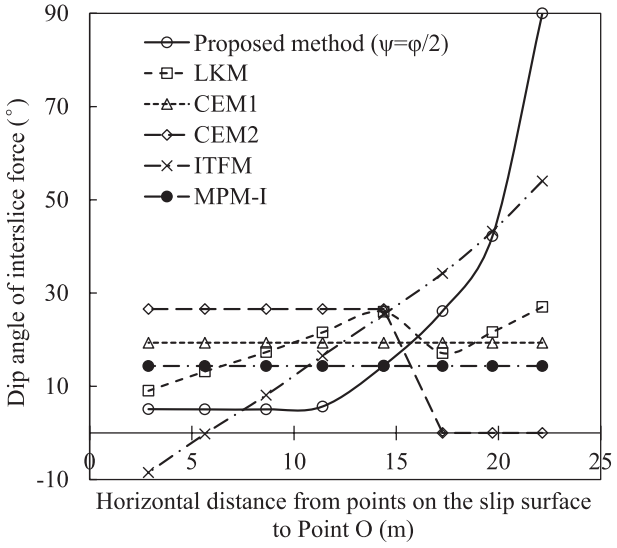

Figure 6. Variation of dip angle of interslice forces in example 1.

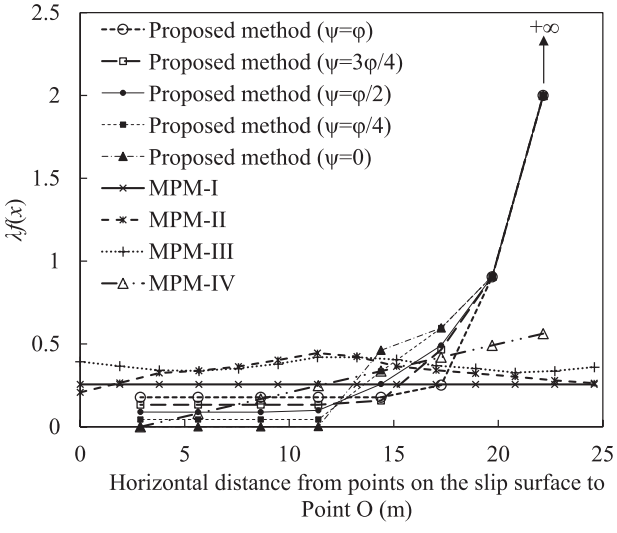

Figure 7. Variation of ratio of tangential force over normal force on the sides of slices in example 1.

the proposed method and the MPM. It can be comprehensively seen from Table 1 and Fig. 7 that the more approximate the interslice force function selected in the MPM is to that by the proposed method, the closer the factor of safety by the MPM is to the minimum value or that obtained by the proposed method. In this regard, the proposed method is fairly helpful to conducting the selection of the interslice force function in the MPM.

3.2 Example 2: a homogeneous clay slope with circular slip surface and F_s close to 1

Fig. 8 shows a soil slope with a circular slip surface and 10m height [22], which is one of the examinations of slope stability by Australia Computer Aided Design Society (ACADS). A potential slide mass of the slope is divided into 10 slices. The results of the ratio of tangential force over normal force on the sides of slices are shown in Fig. 9, where MPM-V represents the case that the function of interslice force is semi-sinusoidal curve. It can be seen that the ratios obtained by the proposed method under various dilation angles are almost consistent in trend. For the slices with the higher ratio, the dilation angle has no effect on the ratio; but for the slices with the lower ratio, the dilation angle has only small effect on the ratio. The factor of safety by the proposed method increases only about 0.05 % with the increase of dilation angle, and they are very close to the results by the MPM. But the factor of safety under $\psi = 0$ is not more than that by the MPM. Fig. 10 shows the variations of dip angle of interslice forces by several classical slice methods such as the LKM, CEM1, CEM2, ITFM, and MPM-I. The results also indicate that the dip angles assumed by the ITFM are rather closer to those computed by the proposed method.

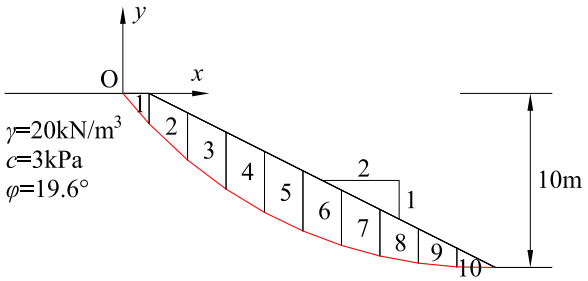

Figure 8. Sketch map of the slope example 2.

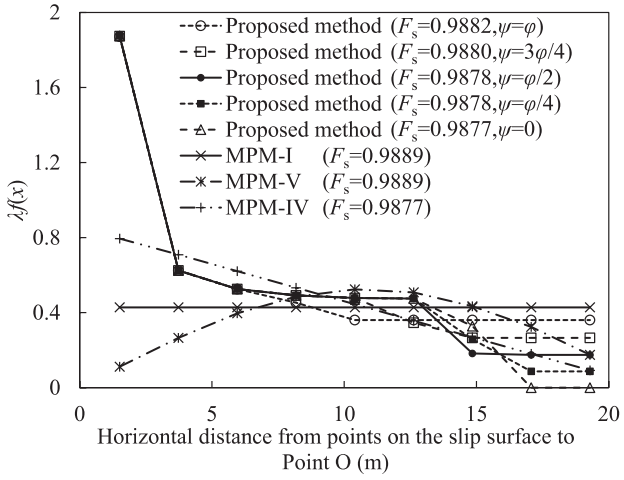

Figure 9. Variation of ratio of tangential force over normal force on the sides of slices in example 2.

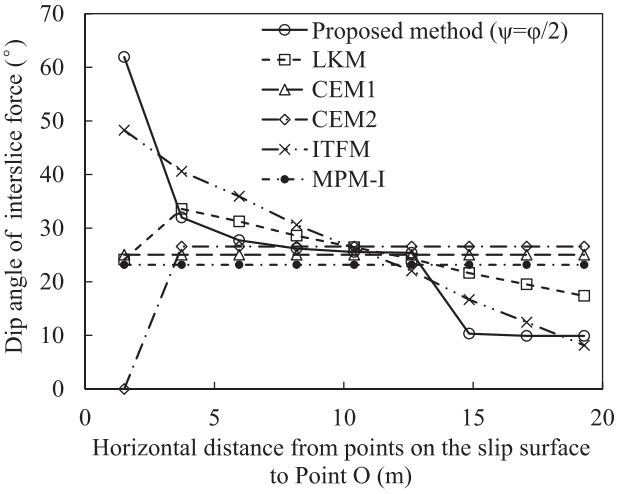

Figure 10. Variation of dip angle of interslice forces in example 2.

3.3 Example 3: a nonhomogeneous soil slope with circular slip surface

Fig. 11 shows an example of a nonhomogeneous soil slope with two layers [23]. The potential slide mass of the slope is divided into 9 slices. As shown in Fig. 12, the ratios of tangential force over normal force on the sides of slices obtained by the proposed method are clearly different from those computed by the MPM. Similar to the analysis results of the examples mentioned above, the factor of safety obtained by the proposed method under $\psi = 0$ is the minimum. And it is about 0.1 % less than that by the MPM. Also, there are obvious differences of

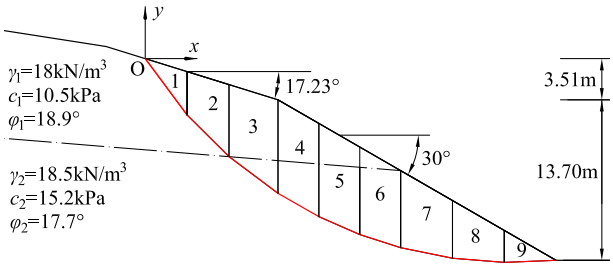

Figure 11. Sketch map of the slope example 3.

the dip angles of interslice forces between the proposed method and the classical slice methods, but the dip angles assumed by the ITFM are relatively closer to those obtained using the proposed method (see Fig. 13).

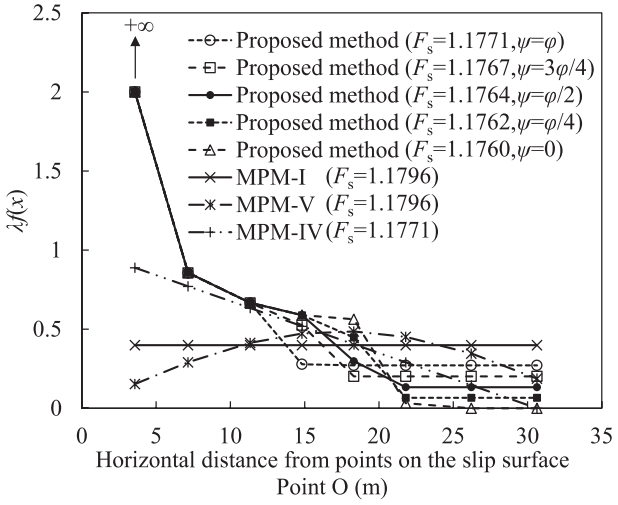

Figure 12. Variation of ratio of tangential force over normal force on the sides of slices in example 3.

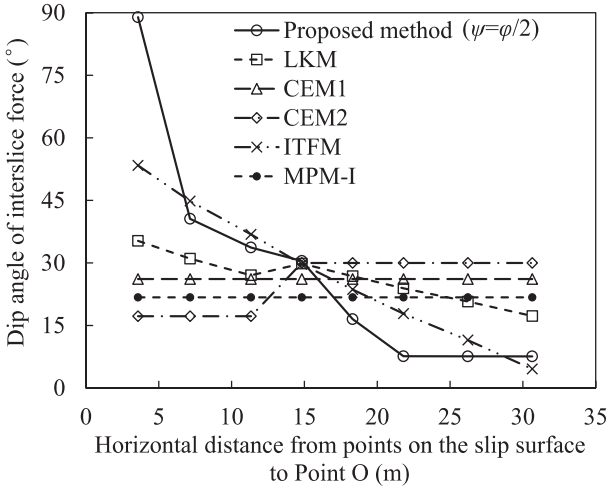

Figure 13. Variation of dip angle of interslice forces in example 3.

3.4 Example 4: a nonhomogeneous cohesionless slope with non-circular slip surface

As shown in Fig. 14, potential slide mass of a nonhomogeneous cohesionless slope with non-circular slip surface is divided into 5 slices. It can be seen from Fig. 15 the values of $\lambda f(x)$ obtained by the proposed method are close to those by MPM-I and MPM-III, but apparently different from those by MPM-II. The proposed factor of safety is almost identical with that by MPM. Moreover, there are observable differences of the dip angles of interslice forces between the proposed method and ITFM as well as CEM2, but the proposed dip angles are fairly closer to those by CEM1 and LKM (see Fig. 16). In particular, the dip angles using the proposed method are between 16° and 20°. Therefore, the calculation results show further the dip angles are between ψ and φ as demonstrated theoretically above.

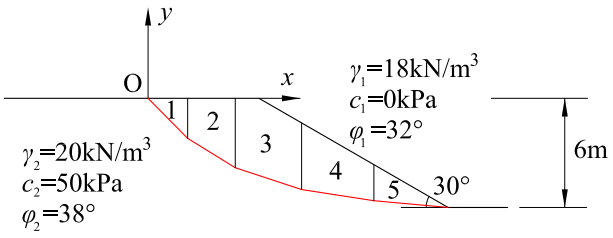

Figure 14. Sketch map of the slope example 4.

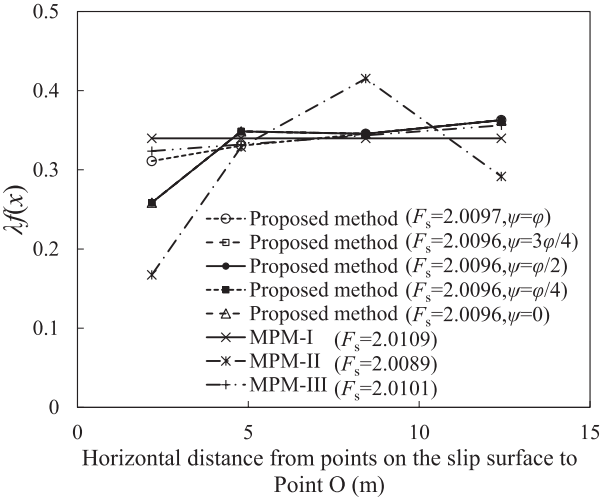

Figure 15. Variation of ratio of tangential force over normal force on the sides of slices in example 4.

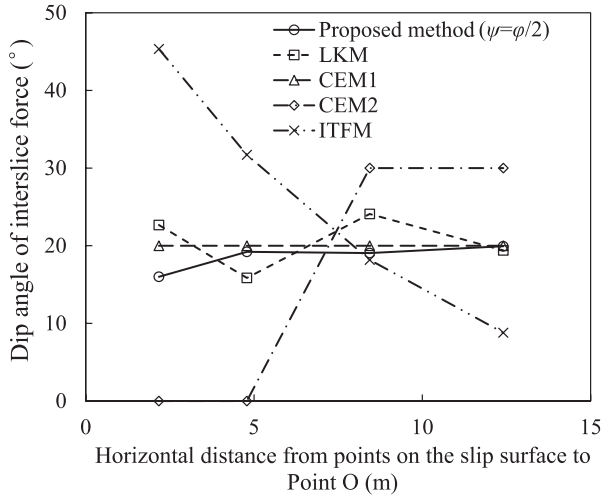

Figure 16. Variation of dip angle of interslice forces in example 4.

3.5 Example 5: a nonhomogeneous clay slope with non-circular slip surface

Fig. 17 shows a nonhomogeneous clay slope with non-circular slip surface and potential slide mass divided into 4 slices. As shown in Fig. 18, $\lambda f(x)$ by the proposed method are evidently different from those computed by MPM-I, but relatively closer to those by MPM-II and MPM-III. The proposed values are observably influenced by ψ in the example. Similarly, the factor of safety obtained by the proposed method is very close to that by MPM. Besides, there are still noticeable differences of the dip angles of interslice forces between the proposed method and the classical slice methods (see Fig. 19).

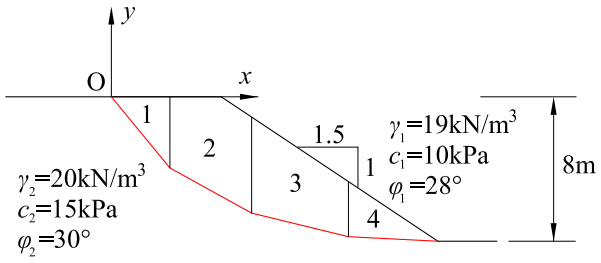

Figure 17. Sketch map of the slope example 5.

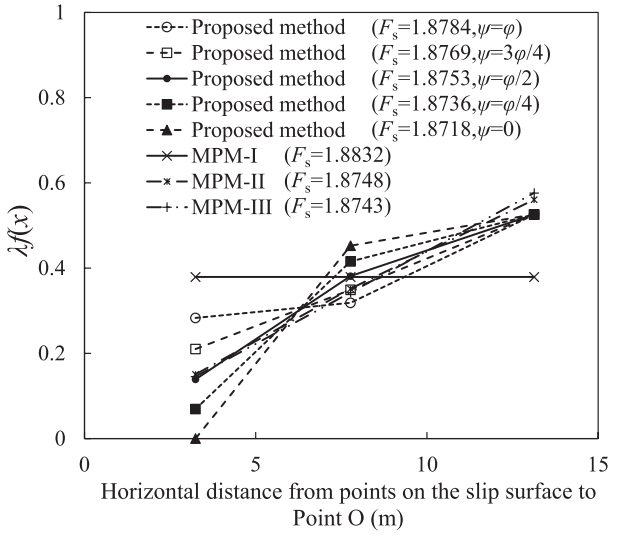

Figure 18. Variation of ratio of tangential force over normal force on the sides of slices in example 5.

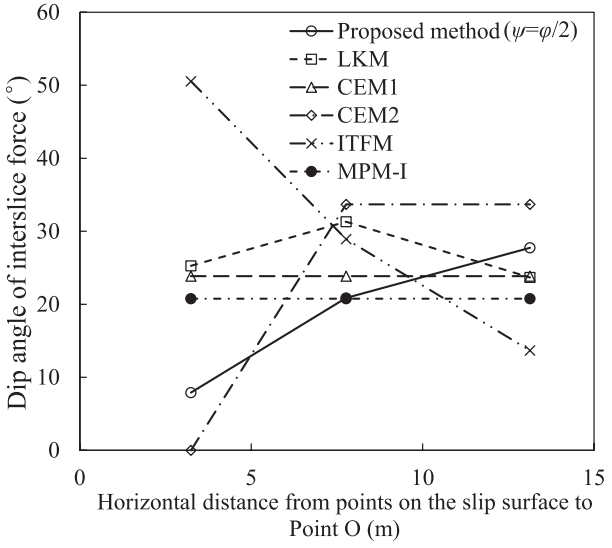

Figure 19. Variation of dip angle of interslice forces in example 5.

4 CONCLUDING SUMMARY

The general slice method with satisfying all equilibrium conditions of slices for slope stability analysis can be improved further without assuming the direction or magnitude of interslice forces. Based on the admissible failure mechanism of kinematical system of soil mass which can be used in slope stability analysis, it is demonstrated that the dip angles of interslice forces should not be less than the dilation angle of the slope soil. Therefore, the slope stability analysis can be transformed equivalently into a non-linear programming problem to be solved with clear ranges of the directions of interslice forces. Moreover, the closed-form solution of the slice method for slope stability analysis is obtained.

The proposed method is applicable to both homogeneous and nonhomogeneous soil slopes without any limitation of potential slip surfaces. Compared to classical slice methods of limit equilibrium, the proposed method can more rigorously find the minimum value of the factor of safety of slope stability. The effect of the dilation angle of slope soil on the factor of safety is involved in the proposed method, but analysis results of some examples show the dilation angle has little effect on the slope stability. In addition, among the classical slice methods with different assumption of the dip angle of interslice force for stability analysis of slopes with circular slip surfaces, the directions of interslice forces obtained by the ITFM are fairly closer to those computed using the proposed method. However, for slopes with non-circular slip surfaces, there are obvious differences of the interslice force directions between the proposed method and ITFM.

Acknowledgments

The research was supported by the National Natural Science Foundation of China (Grant Nos. 51578466 and 51278430) and the Program for New Century Excellent Talents in University (NCET-13-0976).

Notation

c	=	Cohesion of the slope soil
d_i	=	Height of the interface between slice i and slice i-1
D	=	Internal energy dissipation rate of the thin transition layer between adjacent slices
E_i	=	Normal force on the interface between slice i and slice i-1
F_s	=	Factor of safety of slope stability
h_i	=	Height of action point of the interslice force between slice i and slice i-1
i	=	Number of the i^{th} slice
K_i	=	Development coefficient of shear limit resistance on the interface between slice i and slice i-1
l_i	=	Length of the bottom of slice i
n	=	Total number of slices of the potential slide mass of a soil slope vertically divided
N_i	=	Normal force on the bottom of slice i
t	=	Minimal time
T_i	=	Tangential force on the bottom of slice i
W_i	=	Weight of slice i
x	=	Horizontal coordinate with respect to the origin O
X_i	=	Tangential force on the interface between slice i and slice i-1
y	=	Vertical coordinate with respect to the origin O
α_i	=	Dip angle of the bottom of slice i
γ	=	Unit weight of slope soil
δ	=	Thickness of the thin transition layer between adjacent slices
ε	=	Normal strain in the thin transition layer
φ	=	Internal friction angle of the slope soil
η	=	Shear strain in the thin transition layer
$\lambda f(x)$	=	Assumed function of the ratio of tangential force X_i over normal force E_i of slices, where λ is a dimensionless coefficient
σ		Average normal stress on the thin transition layer
τ		Average shear stress on the thin transition layer
τ_s		Shear stress on the thin transition layer in the plastic limit state
ψ		Dilation angle of the slope soil
v		Resultant velocity of a rigid slice, where subscript i and i-1 denote slice i and i-1, respectively
Δv_s		Tangential velocity of slice i relative to slice i-1
Δv_n		Normal velocity of slice i relative to slice i-1
$(\Delta v_s)_{limit}$		Tangential velocity of slice i relative to slice i-1 in the plastic limit state

REFERENCES

[1] Huang, Y.H. 2014. Slope Stability Analysis by the Limit Equilibrium Method: Fundamentals and Methods. American Society of Civil Engineers (ASCE), Reston, USA. http://doi:10.1061/9780784412886.

[2] Petterson, K.E. 1955. The early history of circular sliding surfaces. Geotechnique 5(4), 275–296. http://doi:10.1680/geot.1955.5.4.275.

[3] Fellenius, W. 1936. Calculation of the stability of earth dams. In Proceedings of the 2nd Congress on Large Dams, Washington, D.C. Vol. 4, pp. 445–462.

[4] Bishop, A.W. 1955. The use of the slip circle in the stability analysis of slopes. Géotechnique 5(1), 7–17. http://doi:10.1680/geot.1955.5.1.7.

[5] Junbu, N. 1954. Application of composite slip surface for stability analysis. In Proceedings of European conference on stability of earth slopes, Stockholm, vol. 3, pp. 43–49.

[6] Lowe, J., Karafiath, L. 1960. Stability of earth dams upon drawdown. In Proceedings of the1st Pan-American Conferenceon Soil Mechanics and Foundation Engineering, Mexico City. Vol. 2, pp. 537–552.

[7] U.S. Army, Corps of Engineers 1967. Stability of slopes and foundations, Engineering Manual, Visckburg, Miss.

[8] China Norm 2013. GB50330-2013: Technical code for building slope engineering. China Architecture & Building Press, Beijing.

[9] Duncan, J.M. 1996. State of the art: limit equilibrium and finite-element analysis of slopes. Journal of Geotechnical Engineering, ASCE 122(7), 577–596. http://doi:10.1061/ (ASCE)0733-9410(1996)122:7(577).

[10] Morgenstern, N.R., Price, V. 1965. The analysis of the stability of general slip surface. Géotechnique 15(1), 79–93. http://doi:10.1680/geot.1965.15.1.79.

[11] Spencer, E. 1967. A method of analysis of the stability of embankments assuming parallel interslice forces. Géotechnique 17(1), 11-26. http://doi:10.1680/geot.1967.17.1.11.

[12] Janbu, N. 1973. Slope stability computations. In Embankment Dam Engineering, Casagrande Memorial Volume. Edited by E. Hirschfield and S. Poulos, Wiley, New York, pp. 47–86.

[13] Fredlund, D.G., Krahn, J. 1977. Comparison of slope stability methods of analysis. Canadian Geotechnical Journal 14(3), 429-439. http://doi:10.1139/t77-045.

[14] Sarma, S.K. 1979. Stability analysis of embankments and slopes. ASCE Journal of the Geotechnical Engineering Division 105(GT12), 1511-1524.

[15] Chen, Z., Morgenstern, N.R. 1983. Extensions to the generalized method of slices for stability analysis. Canadian Geotechnical Journal 20(1), 104–119. http://doi:10.1139/t83-010.
[16] Correia, R.M. 1988. A limit equilibrium method of slope stability analysis. In Proc. 5th Int. Symp. Landslides, Lausanne, 595–598.
[17] Zhu, D. 2001. A method for locating critical slip surfaces in slope stability analysis. Canadian Geotechnical Journal 38(2), 328–337. http://doi:10.1139/t00-118.
[18] Zienkiewicz, O.C., Humpheson, C., Lewis, R.W. 1975. Associated and non-associated visco-plasticity and plasticity in soil mechanics. Géotechnique 25(4), 671-689. http://doi:10.1680/geot.1975.25.4.671.
[19] Chen, W.F. 1975. Limit analysis and soil plasticity. Elsevier Scientific Publishing Company, Amsterdam, the Netherlands.
[20] The MathWorks Inc. 2018. Global Optimization Toolbox: User's Guide (R2018b). Retrieved September 2018, available from: http://www.mathworks.com/help/pdf doc/gads/gads tb.pdf (cited November 10, 2018).
[21] Giampa, J.R., Bradshaw, A.S., Schneider, J.A. 2016. Influence of dilation angle on drained shallow circular anchor uplift capacity. International Journal of Geomechanics 17(2), 04016056. http://doi:10.1061/(ASCE)GM.1943-5622.0000725.
[22] Donald, I., Giam, P. 1992. The ACADS slope stability programs review. In Proceedings of the 6th International Symposium on Landslides, Christchurch, New Zealand, February 10-14, Vol. 3, pp. 1665–1670.
[23] Xiao, S.G., Guo, W.D., Zeng, J.X. 2018. Factor of safety of slope stability from deformation energy. Canadian Geotechnical Journal 55(1), 296-302. http://doi: 10.1139/cgj-2016-0527.

DYNAMIC ANALYSIS OF EARTH DAM USING NUMERICAL METHOD – A CASE STUDY: DOYRAJ EARTH DAM

DINAMIČNA ANALIZA ZEMELJSKE PREGRADE Z UPORABO NUMERIČNE METODE: ŠTUDIJA PRIMERA ZEMELJSKE PREGRADE DOYRAJ

Ahmad R. Mazaheri *(corresponding author)*
Ayatollah Borujerdi University, Engineering Faculty,
Department of Civil Engineering
Borujerd, Iran
E-mail: a.mazaheri@abru.ac.ir

Mehdi Komasi
Ayatollah Borujerdi University, Engineering Faculty,
Department of Civil Engineering
Borujerd, Iran

Majid Veisi
Ayatollah Borujerdi University, Engineering Faculty,
Department of Civil Engineering
Borujerd, Iran

Masoud Nasiri
Razi University, Engineering Faculty,
Department of Civil Engineering
Kermanshah, Iran

DOI https://doi.org/10.18690/actageotechslov.18.1.65-78.2021

Keywords
case study, dynamic analysis, earth dam

Ključne besede
študija praktičnega primera, dinamična analiza, 2D metoda končnih razlik zemeljska, pregrada

Abstract

The precise study of the response of earth dams to earthquakes is one of the most complex issues in the field of soil structures. In this research, dynamic analysis of earth dam structures (a case study: Doyraj dam in the west of Iran) have been performed using 2D Finite Difference Method (2D F.D.M.). The aim of this study is to investigate accelerations, lateral (horizontal) and vertical displacements (i.e. settlements) due to earthquake occurrence. The results of dynamic analysis indicate that the performance of the dam is satisfactory for each one of the seismic scenarios considered in this investigation. The maximum settlements at the dam crest is considerably smaller than that of the dam freeboard, with maximum value of 540 mm, which is comparable to recommendation of the Department of Safety of Dams (DSOD). Depth of sliding surfaces is better shown in the Finn model, and the settlements based on the Finn model is about 2.5 times higher than that of Mohr model. In contrast to what is commonly accepted

Izvleček

Eno najbolj zapletenih vprašanj na področju zemljinskih konstrukcij predstavlja natančna študija odziva zemeljskih pregrad na potres. V tej raziskavi je bila izvedena dinamična analiza konstrukcije zemeljske pregrade (študija primera: jez Doyraj na zahodu Irana) z uporabo 2D metode končnih razlik (2D FDM). Cilj te študije je raziskati pospeške, bočne (vodoravne) in navpične premike (tj. posedke) zaradi pojava potresa. Rezultati dinamične analize kažejo, da je zmogljivost pregrade zadovoljiva za vsakega od potresnih scenarijev, obravnavanih v tej preiskavi. Največje posedanje na grebenu jezu je bistveno manjše kot pri prosti višini jezu, z največjo vrednostjo 540 mm, kar je primerljivo s priporočilom Ministrstva za varnost jezov (DSOD). Globina drsnih površin je bolje prikazana v Finnovem modelu, posedki, ki temeljijo na Finnovem modelu, pa so približno 2,5-krat večji kot pri Mohrovem modelu. V nasprotju s splošno sprejetimi vrednostmi potresnih pospeškov (povečanje

about earthquake acceleration (the increase in earthquake acceleration from the base to the top of the dam), it cannot generalize to all cases, and it can be limited to very strong dams or can be related to poor earthquakes.

potresnega pospeška od dna do vrha jezu), ugotavljamo, da se ne more posploševati na vse primere in je lahko omejeno na zelo močne jezove ali pa potrese majhnih intenzitet.

1 INTRODUCTION

Damage and loss of life caused by earthquakes are immense. This is amplified when accompanied by the collapse of essential infrastructures, such as a dam or a power plant, which have the potential of destroying the entire cities. The water and power supplied by dams are essential for the survival of a community. However, when a dam fails, the destruction is often deadly, causing irreparable damage to the land, the people, and to the economy [1]. In fact, the deformations resulting from the earthquake may cause overtopping of water from the dam, leading to severe damages [2]. Earth dams are widely used throughout the world due to the availability of suitable materials and their flexibility. There are numerous earth dams in each country, including Iran. Dams are used for irrigation, flood mitigation, and hydroelectric power generation purposes.

Due to soil nature and its flexibility, the earth dams have better seismic performances in comparison to concrete dams. However, many earth dams were damaged during strong earthquake, and even collapsed in some serious cases [3]. It is essential to carry out post-earthquake investigation and analysis on the earth dams; however, researches have been focused in this field [4-7]. As Iran lies in one of the world's most seismically active areas, the main issue in dam management and construction is seismic safety. Therefore, to assure dam safety, proper evaluation of dynamic analysis is crucial.

In general, the assessment of the seismic stability of new or existing dams can be performed via (a) pseudo-static analysis [8], (b) displacement-based (Newmark or sliding block) methods [9-11], and (c) dynamic stress-deformation numerical analysis [12]. These above-mentioned analyses provide insight into the seismic response of zoned earth dams and homogeneous embankments and ascertain the relative significance of various parameters. Such parameters included excitation characteristics (intensity and frequency content), dam geometry (height and existence of stabilizing berms), foundation soil conditions, and the dam's operation phase ("*end of construction*" and "*steady-state seepage*" conditions). Note that in addition to the excitation characteristics, the other parameters under study are crucial to the static stability of earth dams, but their significance in terms of seismic loading is unknown [13].

Although dam failures are rare, studies have been conducted based on such events to understand the causes of those failures. One example is the failure of the Teton dam, an earth dam located in Idaho, the United States. The dam failed on June 5th in 1976, as it was being filled for the first time, owing to internal erosion known as "piping". The failure caused a huge flood that damaged the city downstream, which cost about 2 billion US$ [14]. The Lower San Fernando dam, which was a 40-meter-high hydraulic-fill earth dam located in San Fernando, California, failed on February 9th in 1971 [3]. In Japan, the Aratozawa dam is a rock-fill impervious-core dam with the height of 74.4 m, located in Kurihara. The Iwate–Miyagi Nairiku earthquake in 2008 caused huge landslides occurred in the left bank of the reservoir from the dam. This caused settlement of the core zone about 20 cm. There was no evidence of severe damage to the dam structure, but it was taken out of operation because of safety concerns [15]. Tschuschke, et al. [16] investigated quality control for construction of tailings dam, they also examine the effects of the applied technology on the condition of the natural environment.

Other researchers have also evaluated the safety of earth dams. For example, Soralump, et al. [17] conducted a dynamic response analysis on the Srinagarind dam by using 213 records of 35 earthquake events and the equivalent linear method for the nonlinear behavior of dam materials. Similarly, Fallah and Wieland [18] conducted an evaluation on earthquake effects and the safety of the Koman concrete-faced rock-fill dam in Albania, by using a 2D F.E. models for the maximum cross section. Their study was undertaken using the equivalent linear method. The dam was checked for the safety evaluation against earthquake with a peak ground acceleration of the horizontal component of 0.45g.

This study aims to gain insight into the behavior of the Doyraj dam (a case study in Iran) in case of the earthquake by using the 2D F.D.M. numerical modeling. In order to select the input motion, seismic hazard analysis was performed by deterministic and probabilistic methods of probable horizontal and vertical acceleration in the dam area. Then, the nearest earthquake record for the region has been selected from the earthquakes that occurred in all around the world as a baseline earthquake. By completing modeling and performing dynamic analyzes, the results have been discussed. The

importance of such research is not only to examine the behavior of a dam or the level of damage it can sustain, but also to preserve it against future earthquakes.

2 NUMERICAL MODELLING

2.1. Analysis Approach

During a seismic event, stress waves propagate through soils and attenuate with distance. Energy dissipation, volume changes, and stiffness degradation of the materials are the factors, which affect this attenuation. During shaking, soils exhibit continuous hysteresis modulus degradation resulting in increasing levels of damping, which in turn decrease the amplitudes of the stress waves. The representation of this material behavior is important in seismic analysis of embankment dams. Two approaches are conventionally used in simulation of inelastic characteristics of soils subjected to cyclic loading: Equivalent Linear Methods (E.L.M.) and nonlinear numerical methods [19]. In the E.L.M. nonlinear behavior of soil is simulated by adjusting the shear modulus and damping ratio as functions of maximum shear strain in the soil. On the other hand, nonlinear methods use nonlinear constitutive models to represent the nonlinear behavior during cyclic loading. Constitutive equations used in predicting inelastic cyclic behavior of soils can become quite complex and may require various material parameters. Alternatively, simple elastic–plastic constitutive models may be used with additional damping added, to represent inelastic damping behavior [19]. The latter method has been adopted in the present study.

Damping in soils is primarily hysteretic, since energy dissipation occurs when grains slide over one another [20]. During dynamic analysis, as effective stresses decrease with increase in pore pressure, the soil begin to yield and increments of permanent deformation are accumulated. Simultaneous coupling of pore pressure generation with non-linear, plasticity based, stress analysis produces a more realistic dynamic response than that can be achieved with the equivalent linear method [20]. The above-described approach has been verified in the literature through analysis of well-documented case histories [21] and was adopted herein for the dynamic analysis of embankment dams with a center core.

In the present study, a bilinear elastic-perfectly plastic stress–strain relationship with a Mohr–Coulomb failure criterion has been used in the dynamic analyses. In this model, energy dissipation is achieved by plastic flow when shear stresses reach the yield strength. For cycles generating shear stress levels remaining in the elastic range, energy dissipation is achieved by viscous damping. Rayleigh damping consisting of two viscous elements is generally used in the numerical analyses. The two elements of Rayleigh damping are both frequency dependent; one increases linearly with frequency (stiffness damping as a function of strain rate) and the other decreases exponentially with increase in frequency i.e. mass damping as a function of particle velocity [20]. The finite difference grid dimensions were selected taking into account the maximum frequency, *f*, of the shear wave that the model could respond to during earthquake loading [22].

2.2. Doyraj Earth Dam

Doyraj Reservoir Dam is located on the river Doyraj at about 13 km north of Moosian and southwest of Ilam province, in Iran. The main purpose of Doyraj dam construction was irrigation of about 10,000 acres of agricultural land in Moosian Plain. The normal level of operation in this dam is 226.5 meters and the level of the river bed is 176 meters above sea level. Seismic monitoring equipment has been located in different parts of the Doyraj dam. The location of the project, and Doyraj dam layout is shown in Figure 1. The maximum height of the Doyraj dam is 58 meters and the operational reservoir

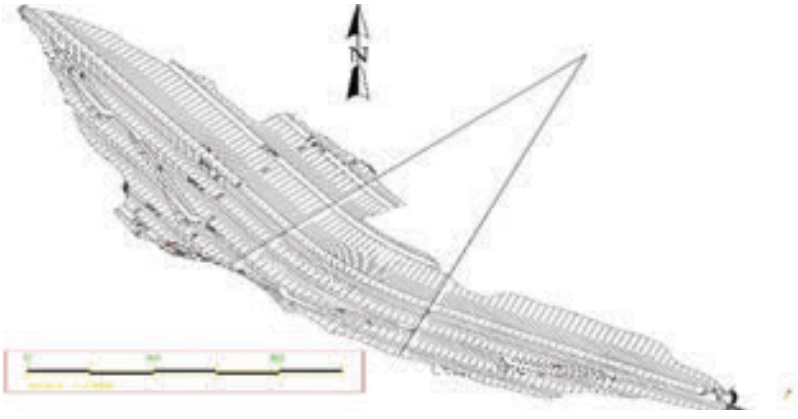

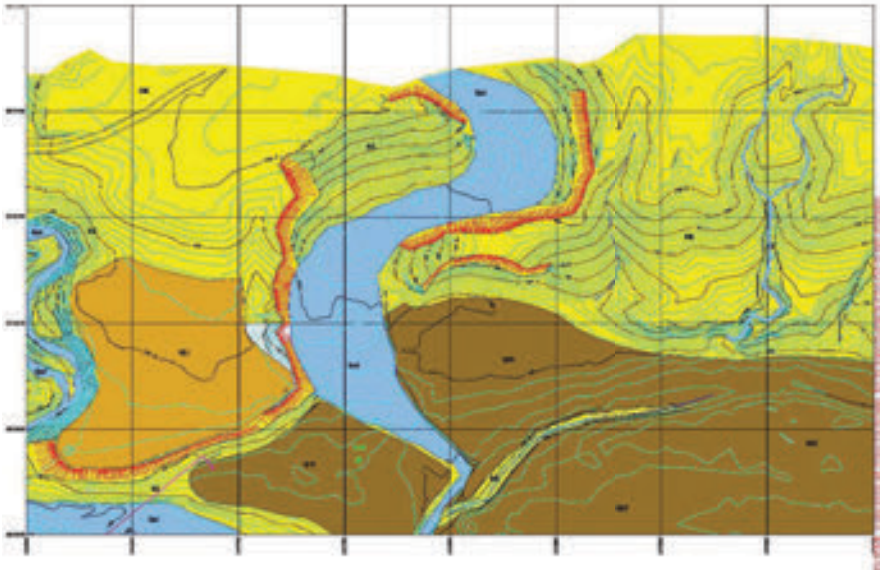

Figure 1. Doyraj earth dam location.

surface is 50 meters. The length of the dam is 1160 m and the crest width is 10 m. In numerical modelling, the dam body was modeled in 8 layers of the same thickness, so that the conditions for the construction of the dam can be simulated.

2.3 Geometry and properties of Doyraj dam

Two-dimensional plane strain models of the embankment were considered in the parametric analyses of this study. The geometry of the model is shown in Figure 2. Doyraj Dam is mainly composed of silty soil and sand. The filter and drainage layers are composed of fine-grained sand for drainage of water leakage and variable deformations between the core and the crater embankment. Suitable materials were used for the core

Table 1. Properties of materials used in 2D F.D.M. analysis.

Materials	γ_{dry} (kN/m^3)	k_x (m^2/s)	E (MPa)	v	c (kPa)	ϕ (°)
Foundation Rock Layer	22.0	1.0×10^{-9}	300.0	0.3	0.0	32
Foundation Clay Layer	20.0	3.9×10^{-5}	200.0	0.25	0.0	28
Gravel Shell	21.0	1.0×10^{-7}	100.0	0.33	0.0	38
Gravel Drainage	19.5	1.0×10^{-3}	90.0	0.25	0.0	39
Clay Core	20.5	1.0×10^{-9}	75.0	0.25	50.0	13
Filter	19.5	1.0×10^{-5}	35.0	0.3	0.0	35

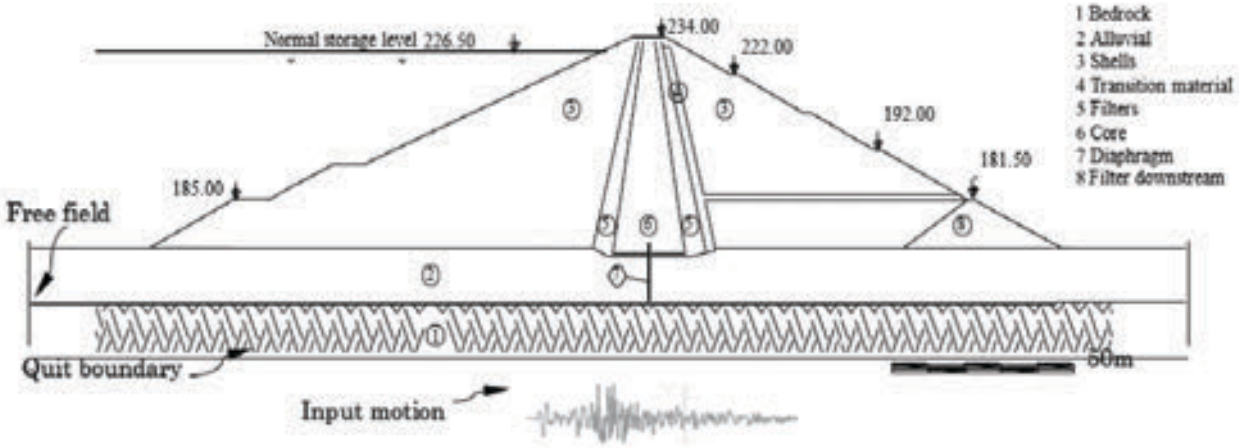

Figure 2. Cross section of Doyraj earth dam.

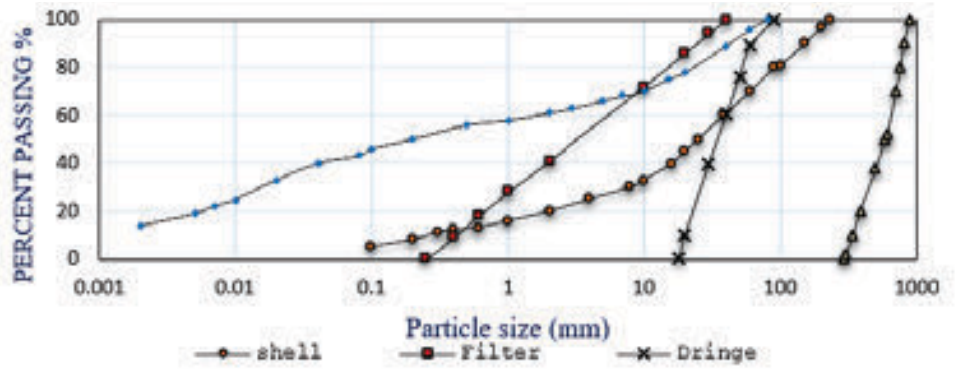

Figure 3. Grain size distribution of Doyraj dam materials.

and cutting off the clay and concrete. In fact, the area of gravel levee and embankment were constructed with the excavated materials near site of the project. The particle size distribution for different materials of the Doyraj dam is shown in Figure 3. Physical and mechanical properties of the embankment and foundation soils used in the numerical models, are presented in table 1.

2.4. Finite difference modelling

The technique of layered construction was employed in the static stress analyses. Since pore pressure generation during construction was a concern, the following procedures were used to model the static effective stress conditions:

(a) Embankment materials were divided into eight layers and placed sequentially. Following the placement of each layer, other layers were added to the layer and the model was set to run for a time period equal to the estimated time required for actual construction of the layer under field conditions. The time needed was calculated by assuming an embankment construction with rate of 1000 m^3/day and multiplying this by the total fill volume of each layer.
(b) The water level was then raised to full the pool. Boundary water pressures were applied along the interior dam surface and the reservoir bed to account for water pressures.
(c) Seepage analysis was performed to achieve steady state conditions within the embankment and the foundation.
(d) Mechanical adjustment of stresses was allowed by performing mechanical calculations in which, flow calculations turned off, and forcing the model to reach equilibrium.

Once initial stresses for the steady state condition were achieved, the following steps were taken to prepare the model for dynamic analyses:

(a) Apply dynamic boundary conditions. In order to enforce free field conditions in the numerical boundaries of the discretized half space foundation, free field boundary conditions available in the code were adopted for the lateral boundaries. For the horizontal boundary, the simulation of outward propagating waves in the foundation was achieved by employing the absorbing boundary conditions which are also available in the finite difference code. Absorbing boundaries have been shown to be effective in absorbing outward propagating waves, and hence simulating half space conditions. The viscous boundaries developed by Lysmer and Kuhlemeyer [23] are adopted in the finite difference code, and were employed in the analyses herein. One restriction in applying absorbing boundaries in numerical modeling for dynamic analysis is that such boundary conditions cannot be simultaneously applied to a model, where acceleration or velocity input is applied; since prescribing acceleration or velocities to a boundary would nullify the effect of the absorbing boundary. In such situations it is necessary to convert acceleration or velocity inputs into stress waves, as described below.
(b) Prepare input motion and apply seismic loading to the numerical model. Horizontal component of the acceleration record from Loma Preita earthquake was applied to the base of the model. Since quiet boundaries were already attributed to the horizontal boundary, the acceleration time history of the input motion was converted to shear stress waves, as described above. A nearly perfect match between the input acceleration time history and the time history recorded after applying the shear wave time history, confirmed the validation of the process employed in this paper. After preparing the input motion by filtering the acceleration time history and converting it to a shear stress time history, the resulting shear stress time history was prescribed to each of the

grid points at the horizontal boundary in which, absorbent boundary conditions were previously prescribed.

(c) Rayleigh damping was assigned to each element of the model in the mid-range between the natural frequency of the model and the predominant frequency of the input motion. The value of Rayleigh damping was chosen based on shear strains recorded from undamped analysis, by taking 65 % of the peak recorded strain. The damping ratios obtained by this procedure ranged from 3 % to 7 %.

(d) Dynamic analysis was performed for the duration of the earthquake, and results were extracted for interpretation and further assessment.

It should be mentioned that for simplification purposes, the hydrodynamic interaction effects of the dam reservoir were neglected. Furthermore, the vertical components of the seismic input were not considered in the seismic loading, since the present study aims to provide qualitative results of the behaviour of a dam under seismic loading conditions. The maximum shear modulus of materials used in the dam body, derived from empirical relationships. In these relationships, the shear modulus can be determined by the porosity of the materials. The relationships to determine the G_{max} for materials of different areas of the dam body used in this research, are presented in table 2.

In order to determine the most probable horizontal and vertical acceleration due to the earthquake in the study area, two approaches of determination of the earthquake magnitude have been considered. 1) Definitive determination and 2) probabilistic determination. In the definitive determination of the earthquake magnitude based on seismic studies and earthquake studies, the most important seismic spring relative to the site of the Doyraj Dam is the hidden fault of the Black Sea Anticline "SZ4". This fault has the maximum seismicity ($Ms = 7.0$) at 42 km north of the dam site and approximately 13.6 km of the earth surface; with the maximum horizontal and vertical acceleration of 0.3 and 0.19 g, respectively. As compared to other seismic springs, that is the highest one.

Table 2. Shear Modulus of dam materials.

Materials	G_{max}
Foundation Rock Layer	1.62 GPa
Foundation Clay Layer	1.62 GPa
Gravel Shell [24]	$G_{\max} = 13000\frac{(2.17-e)^2}{(1+e)}(\sigma)$ Kokusho & Esachi (1981)
Gravel Drainage [24]	$G_{\max} = 8400\frac{(2.17-e)^2}{(1+e)}(\bar{\sigma})^{0.55}$ Kokusho & Esachi (1981)
Clay Core [25]	$G_{\max} = 3270\frac{(2.973-e)^2}{(1+e)}(\bar{\sigma}_0)^{0.5}$ Hardin & Black (1968)
Filter [26]	$G_{\max} = 220K_{2\max}(\bar{\sigma}_0)^{0.6}$, $K_{2\max} = 59$ Seed & Idriss (1970)

In the probabilistic method for determining the earthquake magnitude, a large return period has been estimated for the radial range of 100, 150 and 200 kilometers around the Doyraj Dam site using Gothenburg-Richter preparatory method, the final fit method, and the maximum likelihood estimator or probable maximum (KIKO) method. By comparing the various methods presented for determining the maximum return magnitude, it is concluded that the method of estimating the maximum exponential (KIKO method) is closer to reality because this approach has been used besides the use of the Guthenberg-Richter cumulative distribution function of historical earthquakes. Figure 4 shows the graphs of the return periods of surface magnitudes in the studied areas. Finally, the results of calculations based on a range of 100 km with a conservative view and appropriately fitted to seismic springs for earthquake hazard analysis are attributed. In this regard, an earthquake event with a magnitude of $Ms = 5.5$ has a return period of about 100 years, an earthquake with magnitude given af $Ms = 6.1$ has a return period of about 500 years, an earthquake with $Ms = 6.3$ has a return period of about 1000 years, and an earthquake with $Ms = 6.6$ will have a return period of about 2000 years. However, seismicity exceeding $Ms = 6.6$ corresponds to a return period over 2000 years.

By studying maximum acceleration of probabilistic method for the 1000-year return period, the maximum horizontal and vertical acceleration were projected to be 0.24 and 0.16 g, respectively. In order to study the seismic behavior of earth dams in this study, the time history of Loma Prieta earthquake acceleration was selected as the input movement in the dam foundation section. Horizontal time histories of the desired earthquake were considered as a two-way input to the dam base for a period of 40 seconds in the dynamic analysis. In the Loma Prieta earthquake, the maximum horizontal and vertical acceleration at high level of the MCL design for this acceleration is 0.367 and 0.28 g, respectively. This historical history has the closest horizontal and vertical acceleration to the most probable predictable earthquake in that area. Record of the earthquake input is shown in Figure 5.

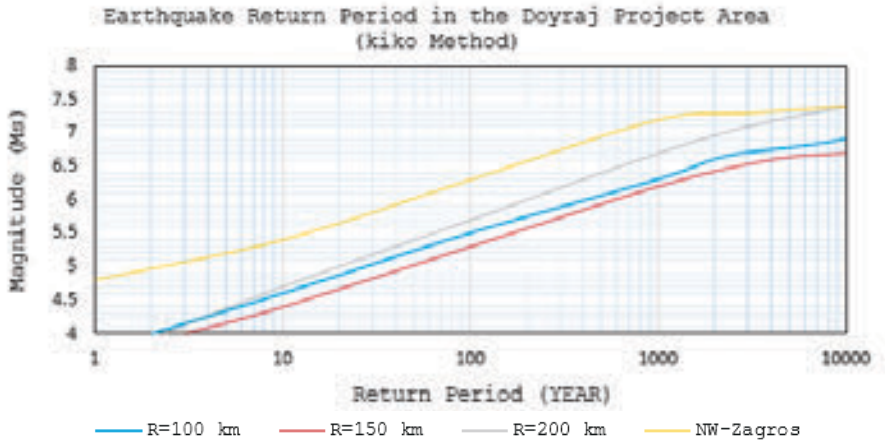

Figure 4. Return period of earthquakes according to surface magnitude in the radial ranges of 100, 150 and 200 km.

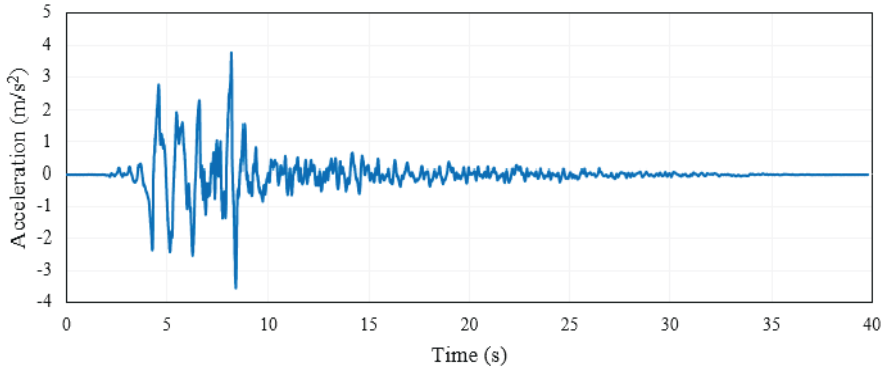

Figure 5. The recorded of horizontal acceleration time history for the Loma Prieta earthquake at the base of the Doyraj dam.

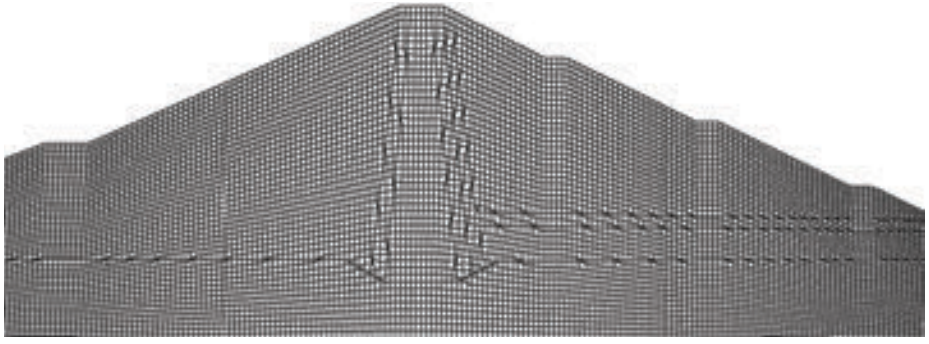

Figure 6. The model of Doyraj dam in F.D.M. analysis.

The Meshing of the Doyraj dam contained 15360 quadrangular and triangular elements. For investigating of the displacements in the static and dynamic analyses, a nonlinear model with Mohr-Coulomb failure criterion has been used to simulate the elasto-plastic behavior of the foundation material and the embankment body of the dam. For the pore water pressure analysis, the fine model is used. Figure 6 shows the model built in the F.D. environment.

3 RESULTS AND DISCUSSION

3.1 Static Analysis of Doyraj Dam

Prior to studying the dam response to earthquake loading, the construction of the earth dam was simulated to reproduce the initial state of effective stress. Actually, static analysis has been performed with the aim of

reviewing and controlling the static behavior of the Doyraj dam. The horizontal and vertical displacement of the Doyraj dam at the time of completion (10/02/2013; and before impounding) and at the first impounding is shown in Figure 7. The horizontal displacement changes of the dam is presented in Figure 7.a and after impounding is shown in Figure 7.b. The results of vertical deformations of the dam at the time of construction and after impounding are shown in Figures 7.c and 7.d, respec-

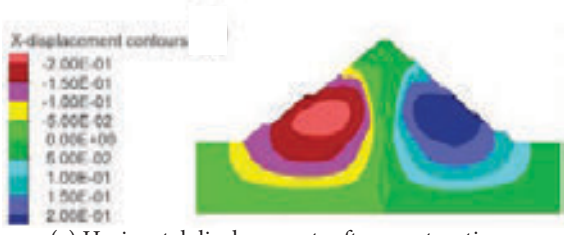

(a) Horizontal displacements after construction.

(b) Horizontal displacement after impounding.

(c) Settlement pattern before dewatering.

(d) Settlement pattern after impounding.

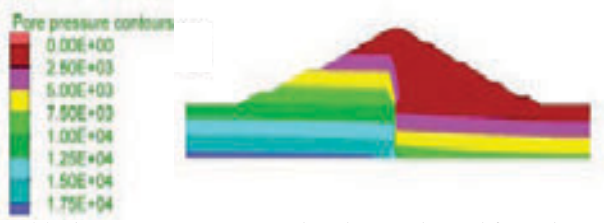

(e) The pore water pressure distribution derived from the seepage analysis; height of retained water is 51 m.

Figure 7. The amount of settlements, pore water pressure and horizontal displacements in the Doyraj dam.

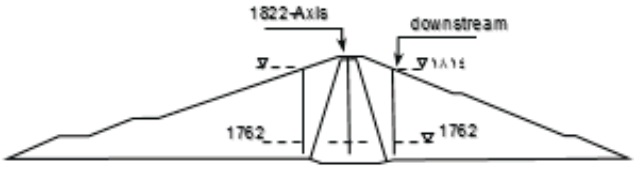

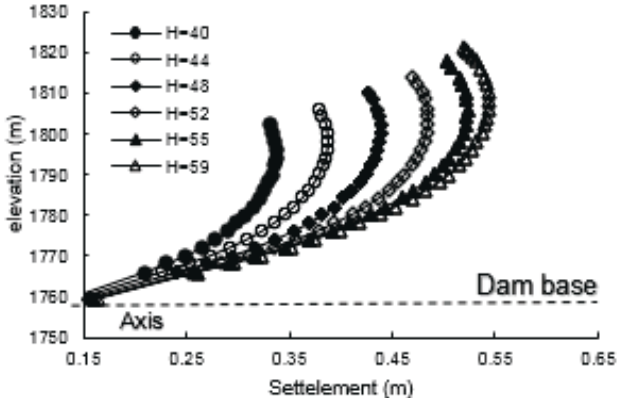

(a) Settlements of the core.

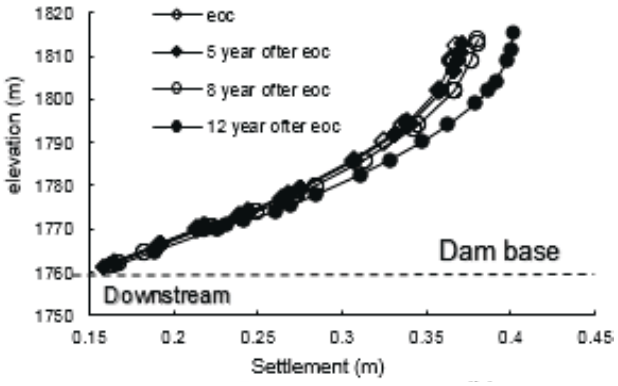

(b) Settlements of Doryaj dam over the time.

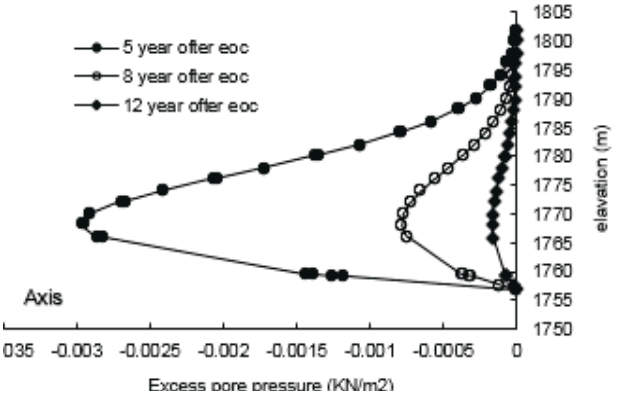

(c) Excess pore pressure pattern over time.

Figure 8. Excess pore pressures and computed settlement profiles.

tively. In Figure 7.e, the pore water pressure is shown in which, the dam located at the impounding stage.

Due to the construction process of the embankment, the clay core has vertical settlements about 530 mm. With reference to Figure 8.a, it is observed that with the different heights of the embankment in the central axis of the core, which has not yet been completed, the most settlements are located at about one third of the center of the clay core, which is approximately 540 mm. However, there is not much change in the amount of settlements after impounding and before impounding in the clay core. In Figure 7.b, it is clear that the amount of horizontal displacement variations has doubled compared to before impounding, increasing from 60 mm to 120 mm. In fact, the increase in horizontal displacements in the dams is due to increased reservoir pressure. In the case of a reservoir drop stage, the elastic deformation of the dam material because of impounding can be improved due to discharge of the reservoir. Figure 8.b shows the consolidation process at different times in the downstream vertical axis. As it can be seen, the amount of change in the consolidation settlements with the increase in time is not much noticeable and the validity of this issue can be seen in Figure 8.c, so there is not much excess pore pressure in the dam. Furthermore, as shown in this figure, the excess pore water pressure is reduced over time.

In the analysis stage of the permanent leakage of the dam, it is assumed that the reservoir water height has its maximum value (approximately 51 meters). Therefore, an analysis of the steady state seepage was performed for the water level of 51 m. Steady state seepage analysis was performed separately from the mechanical analysis. Therefore, according to the patterns, the maximum sum of the settlements is located at one third of the dam height from the foundation, with maximum value of 540 mm. The maximum pore water pressure is also obtained at around 700 kPa.

3.2 Dynamic Analysis of Doyraj Dam

Dynamic analysis performed to investigate the probable behavior of the dam during an earthquake. Using the initial stress state obtained from the previous static analysis, the dam has been analyzed using the Loma Prieta earthquake history as an input quake. The earthquake time incoming on the dam was about 40 seconds.

3.2.1 Acceleration Distribution Inside the Dam Body

Acceleration contours showed that the maximum acceleration at the end of the earthquake was about 2 m/s^2. But the history of acceleration at the dam crest and the maximum acceleration at the crest of the analysis in 8 seconds step, was calculated about 5.3 m/s^2.

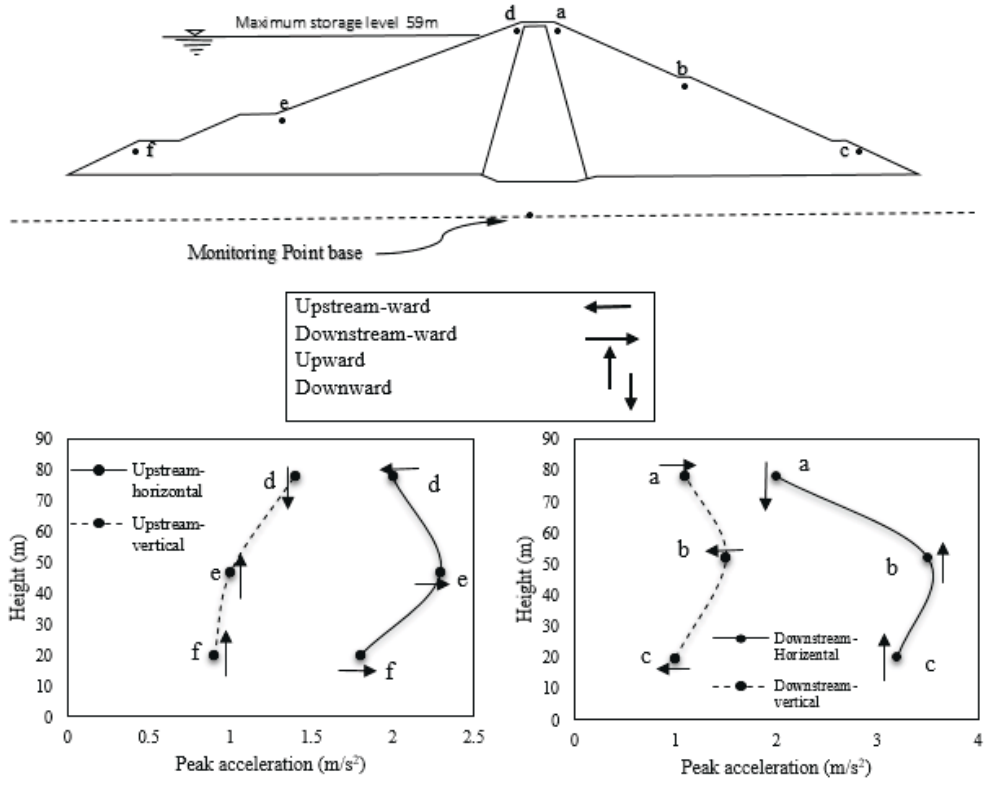

Figure 9. Horizontal and vertical acceleration changes on upstream and downstream slopes.

History of acceleration time for 6 points from the upstream slope and downstream slope of the dynamic finite difference analysis indicated in Fig. 9 (Point d-f and a-c). Peak acceleration at 6 points in front of its height is depicted in Figure 9, showing that from the base of the dam to its crest, it first increased and then slightly decreased. As it can be seen, the amount of horizontal and vertical acceleration changes is higher than the rest of the points in the middle third part of the upstream and downstream shells; this is also indicative of the possibility of slipping wedges in these areas. In addition, the horizontal acceleration is higher than the vertical acceleration peak in the dam. Given that the motion of the bed is stronger in the vertical direction, it is clear that the dam is substantially strengthened in the direction of the horizontal motion of the earth. Peak acceleration direction at 6 points is also shown in Figure 9. Peak acceleration in the upstream of slope is mainly downward to upstream, while in the downstream of slope, is often upward. Finally, at the same elevation, the peak acceleration in the upstream of slope is larger than the downward of slope indicating that there is more seismic deformation on the upstream side of the dam. Another matter that can be stated is that, the acceleration at the point H located at the bed of the foundation is slightly higher than the rest of the points, and the cause can be attributed to the effect of the shear force caused by the earthquake on the base of the foundation and where the earthquake force it enters. So, with respect to this, we can say that Finn model is not very successful in acceleration analysis in the model based on performance of this model which proves the opposite belief about this model. As shown in Figure 10, in relation to the acceleration on the crown and the base of the foundation, the two Finn and Mohr models have been the opposite of each other.

3.2.2 Deformations

Deformations can be used to assess the safety of the dam due to the loss of free height. After dynamic analysis, the calculated changes for comparing the damping behavior presented in Figure 11, which show horizontal and vertical contours, respectively. Deformations contour indicate that the maximum settlement at the dam was 61 cm. It is obvious that the settlements in the clay core have continued to the crest. However, horizontal deformations in the clay core are less than the upstream and downstream shells. Patterns show that the maximum horizontal displacements occur in the downstream shell,

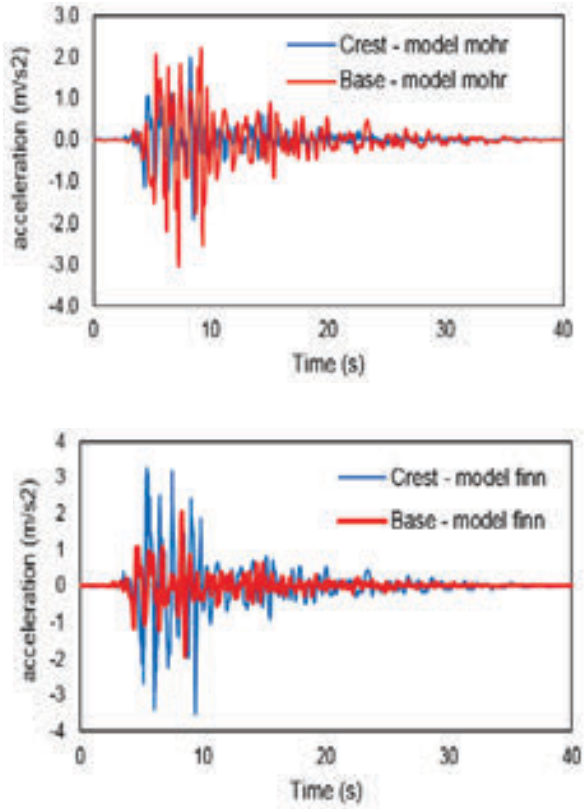

Figure 10. Horizontal acceleration changes on crest and base of the Doyraj dam.

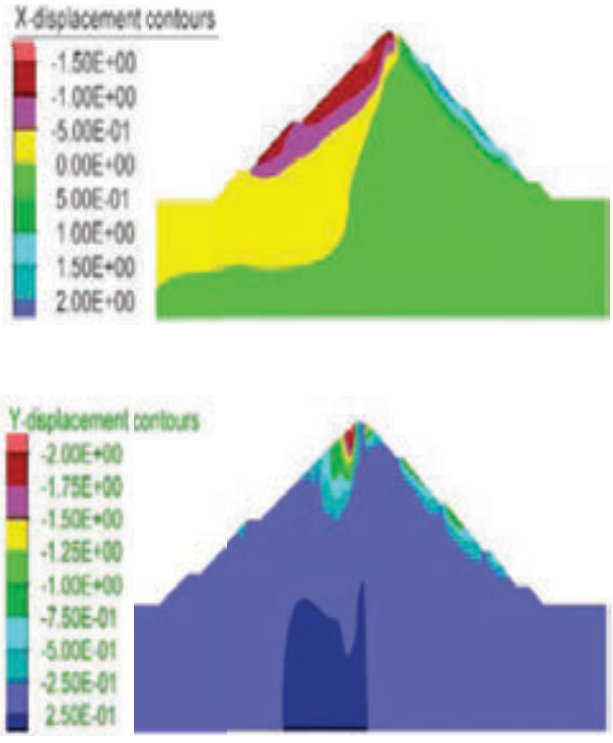

Figure 11. Horizontal and vertical displacement contours of the Doyraj Dam after the earthquake.

which is approximately 60 cm in size. Of course, the depth of horizontal displacements is not much on the downstream slope. The results of this section are based on Mohr model.

Figure 12 show the location of the monitoring points. As shown in this figure, these points have experienced the modest changes in horizontal displacements. Figure 12.a shows the history of horizontal displacement during dynamic loading based on the Mohr model in the monitoring point. Figure 12.c also shows the history of horizontal displacement during dynamic loading based on the Finn model in the monitoring point. It is observed that the most horizontal displacement in the Mohr model occurred about 38 cm at the point "*f*". However, in the Finn model, the maximum horizontal displacement of about 46 cm occurred at the same point. Figure 12.b and 12.d show the history of the vertical displacements at the monitoring points based on the Mohr and Finn models, respectively. It is observed that the maximum settlements at the point "*f*" occurred on both models. But the difference between the amounts of settlements in two models is considerable. The settlement based on the Finn model is about 2.5 times higher than that of Mohr model. This proves that the Finn model shows the displacements more than the predicted value. In general, according to the obtained results, the lasting displacement in the side of the crest of the dam has its highest value.

3.2.3 Strains

Shear strain provide information for understanding the locations inside the dam that may have been damaged during severe earthquake stimulations. Shear contours

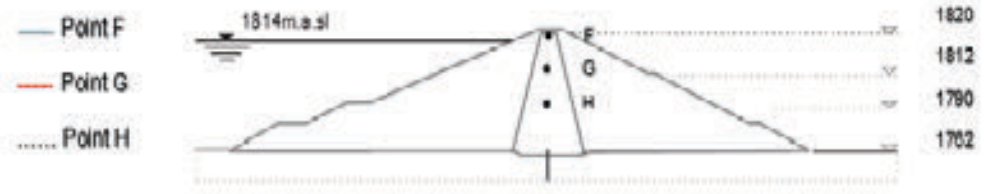

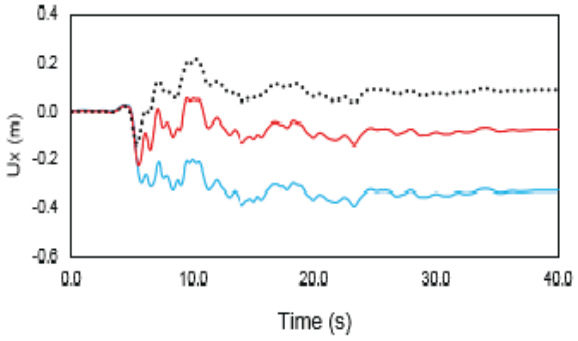

(a) Horizontal displacements based on Mohr model.

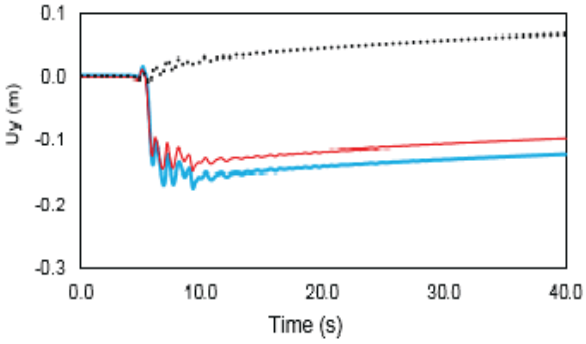

(b) Vertical displacements based on Mohr model.

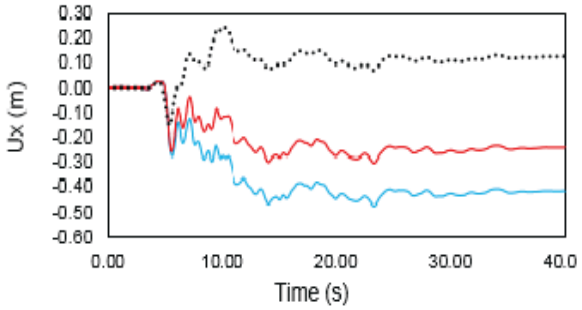

(c) Horizontal displacements based on Finn model.

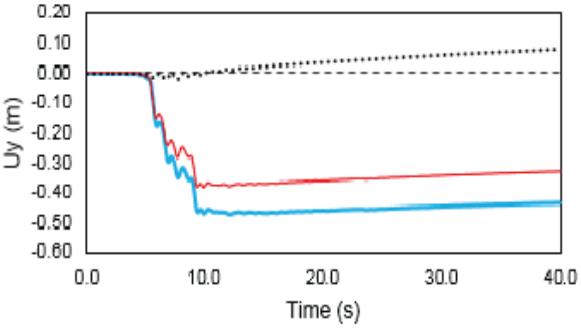

(d) Vertical displacements based on Finn model.

Figure 12. History of horizontal displacement and settlements of Doyraj dam in the monitoring points.

of dynamic analysis for different models are shown in Figure 13. Most parts of the dam body have experienced a small amount of shear strain. Shear strains can be seen in the upper part and close to the crest. In fact, at 6 seconds from the occurrence of the earthquake, the shear strain had more penetration in the dam body. Thereafter, the occurrences of large shear strain can be observed clearly on both sides of the dam in the middle and bottom portions of the slope downstream. As seen in Figure 13.a, in Mohr model, all the shear strains have occurred on a slope downstream, but in the Finn model (Figure 13.b.), all shear strains happened in the upper slope of the dam. This shows that the Finn model considers saturated areas more critical. It is even observed that the depth of shear strain penetration in the Finn model is more than that of Mohr model.

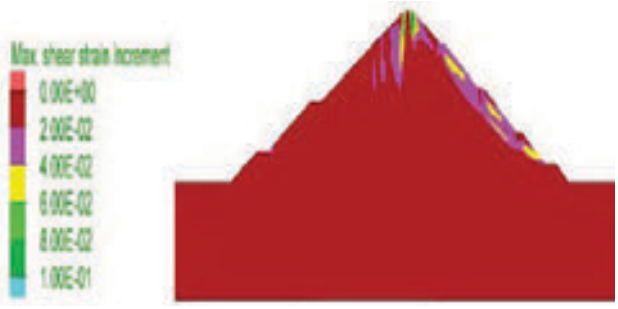

(a) Shear strain based on Mohr model.

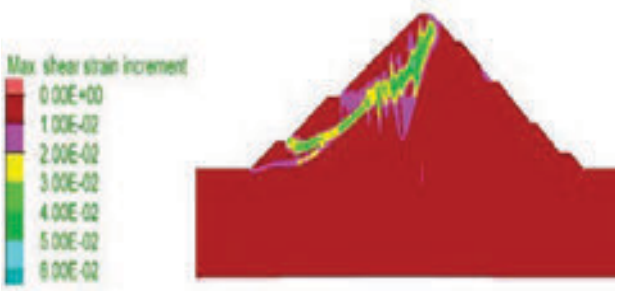

(b) Shear strain based on Finn model.

Figure 13. Counter of shear strains at different times of dynamic analysis.

3.2.4 Stability of Doyraj Dam

Changes in the coefficient of slope stability of an earth dam can occur during different periods from construction to operation time; therefore, stability analysis of the upstream and downstream slopes of the earth dams in different conditions, the operation of the reservoir of dams, execution of the body at the end of construction are important. Significant parts in this matter are the design, implementation and operation of the dam body at various stages. Therefore, in the present study, static and seismic properties of the Doyraj earth dam located in Ilam province, which is in operation at the moment, have been investigated. For this purpose, F.D.M. and Newmark methods have been used. The results show that the dam has a fixed stability in the static and seismic states. FOS for upstream and downstream in F.D.M. analysis was 1.57 and 1.49, whilst for Newmark method the values were 1.44 and 1.55, respectively.

The results of deformation analysis for the Loma Prieta earthquake are shown in Figure 14. The amount of permanent deformation obtained by this analytical method is about 470 mm, which is close to the results of F.D.M. analysis. Although the Newark Slip Block Method cannot fully model the mechanism of settlements occurrence in an earth dam in the case of an earthquake, the previous studies have shown that if the appropriate assumptions were considered in the analysis, the displacement values could be in good agreement with both elasto-plastic dynamic analysis and the method used in this research (Newmark Slip Block).

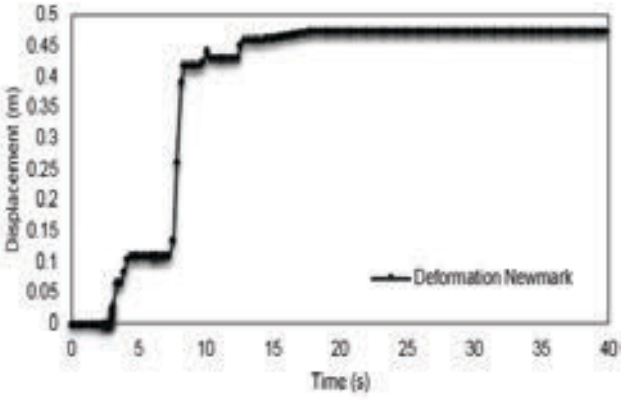

Figure 14. Permanent deformation of the Doyraj earth dam using Newmark's analytical method.

4 CONCLUSION

Based on 2D F.D. analysis of a case study earth dam located in the west of Iran (Doyjay earth dam) the following results obtained:

In the static state, major settlements occur at the center of the core. The maximum settlement of the dam body is 530 mm at the end condition which occurs in the middle of the core. The maximum horizontal displacement at the end of the construction is about 6 cm. In fact, the

increase in horizontal displacements in the dams is due to increased reservoir pressure, since the amount of horizontal displacement variations has doubled compared to before impounding. The impounding does not change the amount of settlements, but the horizontal displacement of the dam reaches 120 mm. In this investigation for the ssettlements of the crest dam, the assumption of a sliding circles runway from the middle section of the upstream and downstream slopes (Middle Dam), are more critical. The maximum amount of sustained settlements by the Newmark sliding block method is 47 cm which is far less than the Free Board, accelerated magnification values at the crest of the dam in the seismic analysis for accelerated mapping used between 2 and 5, indicating significant acceleration in the dam body. Nonlinear analysis showed that the amount of cyclic shear strains inside the core are very small compared to other parts of the dam. Deformations contour indicate that the settlements in the clay core have continued to the crest. However, horizontal deformations in the clay core are less than the upstream and downstream shells. The static stability coefficients of the downstream slope are close, in all cases. This demonstrates that in a static state, the safety of embankment is not affected by changes in water level in the reservoir. The maximum shear strains distribution in the dam body, especially on the upstream and downhill slopes, are obtained by the accelerograms, which can represent a lower coefficient of certainty against the failure of susceptible levels of slippage. Sliding surfaces is shown deeper in the Finn model. Contrary to what is commonly accepted (the increase in earthquake acceleration from the base to the dam is always expected), this is not a general phenomenon and it can be limited to very strong dam (whose behavior remains earthquake-resistant, i.e. elastic) or related to poor earthquakes. Conversely, due to strong earthquakes, some parts of the dam may reach plasticity. Earthquake acceleration does not increase along the altitude. However, at the same time, the body of the dam gradually surrenders and may collapse.

REFERENCES

[1] Charatpangoon, B., Kiyono, J., Furukawa, A., and Hansapinyo, C. (2014). "Dynamic analysis of earth dam damaged by the 2011 Off the Pacific Coast of Tohoku Earthquake". Soil Dynamics and Earthquake Engineering, 64, pp 50–62.

[2] Rampello, S., Cascone, E., and Grosso, N. (2009). "Evaluation of the seismic response of a homogeneous earth dam". Soil Dynamics and Earthquake Engineering, 29(5), pp 782–798.

[3] Seed, H. B., Idriss, I. M., Lee, K. L., and Makadisi, F. I. (1975). "Dynamic analysis of the slide in the Lower SanFernando dam during the earthquake of February 9, 1971". Journal of Geotechnical Engineering, ASCE 9, pp 889–911.

[4] Bardet, J. P., and Davis, C. A. (1996). "Performance of San Fernando dams during Northridge earthquake". Journal of Geotechnical Engineering, ASCE, 122(7), pp 554–564.

[5] Tani, S., and Ozkan, (2000). "Behavior of large fill dams during earthquake and earthquake damage". Soil Dynamics and Earthquake Engineering, 20(1), pp 223–229.

[6] Jin, L. P., Chen, G. X., Li, Y. Q., and Tang, H. (2009). "Investigation on earthquake-induced dam damage during Wenchuan earthquake". Journal of Earthquake Engineering and Vibration, 29, pp 14–23.

[7] Yoshikazu, Y., Masafumi, K., and Toshihide, K. (2012). "Safety inspections and seismic behavior of embankment dams during the 2011 off the Pacific Coast of Tohoku earthquake". Soils and Foundations, 52(5), pp 945–955.

[8] Terzaghi, K. (1950). "Mechanisms of landslides." Engineering geology (Berkey), Geological Society of America.

[9] Newmark, N. (1965). "Effects of earthquakes on dams and embankments". Geotechnique, 15(2), pp 139–60.

[10] Franklin, A. G., and Chang, F. K. (1977). "Permanent displacements of earth embankments by Newmark sliding block analysis." Report 5, Miscellaneous paper S-71-17, US Army Corps of Engineers, Waterways Experiment Station, Vicksburg, Mississippi.

[11] Yegian, M. K., Marciano, E. A., and Gharaman, V. G. (1991). "Earthquake-induced permanent deformations: probabilistic approach". Journal of Geotechnical Engineering, ASCE, 117(1), pp 35–50.

[12] Seed, H. B., Lee, K. L., Idriss, I. M., and Makdisi, R. (1973). "Analysis of the slides in the San Fernando dams during the earthquake of Feb. 9 1971". Report No. EERC 73–2, Earthquake Engineering Research Center, University of California, Berkeley, p. 150.

[13] Andrianopoulos, K. I., Papadimitriou, A. G., Bouckovalas, G. D., and Karamitros, D. K. (2015). "Insight into the seismic response of earth dams with an emphasis on seismic coefficient estimation". Computers and Geotechnics, 55, pp 195-210.

[14] Randall, M. J., and Knopoff, L. (1970). "The mechanism at the focus of deep earthquakes". Journal of Geophysical Research, 75(26), pp 4965-4976.

[15] Yamaguchi, Y., Iwashita, T., and Mitsuishi, S.

(2008). "Preliminary investigation of dams stricken by the Iwate–Miyagi Nairiku Earthquake in 2008". In Proceedings of the 5th East Asian regional dam conference international symposium on co-existence of environment and dams.

[16] Tschuschke, W., Wróżyńska, M., and Wierzbicki, J. (2017). "Quality control for the construction of a tailings dam" ACTA GEOTECHNICA SLOVENICA, 2017/1. Pp. 3-9.

[17] Soralump, S., and Tansupo, K. (2009). "Safety analyses of Srinagarind dam induced by Earthquakes using dynamic response an analysis method". In Proceedings of the international conference on performance-based design in earthquake geotechnical engineering, IS-Tokyo, pp 987–994.

[18] Fallah, H., and Wieland, M. (2010). "Evaluation of earthquake safety of Koman Concrete Face Rock fill Dam in Albania". In Proceedings of the 3rd Asian conference on the Earthquake engineering, ACEE, Bangkok, Thailand.

[19] Han, Y., and Hart, R. (2006). "Application of a simple hysteretic damping formulation in dynamic continuum simulations". In Varona P, Hart R, editors. In Proceedings of the 4th international FLAC symposium on numerical modeling in geomechanics, Madrid, Spain.

[20] Zhai, E., Roth, W., Dawson, E., and Davis, C. (2004). "Seismic deformation analysis of an earth dam a comparison study between equivalent-linear and nonlinear effective-stress approaches". In Proceedings of the 13th world conference on earthquake engineering, Vancouver, BC, Canada.

[21] Roth, W.H., Dawson, E., Somerville, P., Davis, C., and Plumb, C. C. (2004). "Evaluating the seismic performance of Stone Canyon Dam with 2-D and 3-D analyses". In Proceedings of the 13th world conference on earthquake engineering, Vancouver, BC, Canada.

[22] Kuhlemeyer, R. L., and Lysmer, J. (1973). "Finite element method accuracy for wave propagation problems" Journal of Soil Mechanics and Foundation Engineering Division, ASCE, 99 (SM5). pp. 421–427.

[23] Lysmer, J., and Kuhlemeyer, R. L. (1969). "Finite dynamic model for infinite media". Journal of Engineering Mechanics; 95 (EM4), pp 859–877.

[24] Kokusho, T., and Esachi, Y. (1981). "Cyclic triaxial test on sands and coarse materials, In Proceedings of the Xth International Conference on Soil Mechanics and Foundation Engineering, Stockholm, Vol. 1.

[25] Hardin, B. O., and Black, W. L. (1968). "Vibration Modulus of Normally Consolidated Clay," Journal of the Soil Mechanics and Foundations, ASCE. 94 (SM2), pp 353–369.

[26] Seed, H. B., and Idriss, I. M. (1970). "Soil Module and Damping factors for dynamic response analyses". Report EERC 70-10, earthquake engineering Research center, University of California, Berkeley.

INVESTIGATION OF THE END BEARING LOAD IN PILE GROUP MODEL IN DRY SOIL UNDER HORIZONTAL EXCITATION

PREISKAVA NOSILNOSTI KONICE V MODELU SKUPINE PILOTOV V SUHIH TLEH OB VODORAVNEM VZBUJANJU

Mohammed Y. Fattah
University of Technology,
Civil Engineering Department
Baghdad, Iraq
E-mail: myf_1968@yahoo.com

Hussein H. Karim
University of Technology,
Civil Engineering Department
Baghdad, Iraq
E-mail: Hussein_karim@yahoo.com

Makki K. M. Al-Recaby
University of Technology,
Civil Engineering Department
Baghdad, Iraq
E-mail: Makki_Recaby@yahoo.com

DOI https://doi.org/10.18690/actageotechslov.18.1.79-106.2021

Keywords

pile group, horizontal shaking, dry sand, end bearing

Ključne besede

skupina pilotov, horizontalno tresenje, suha zemljina, nosilnost konice

Abstract

A series of 94 laboratory tests were conducted to measure the response of pile foundation when subjected to dynamic loads. Eight tests were conducted on single pile in dry soil at relative density 30 % (loose) and 50 % (medium); 66 tests on group of piles with different spacings and patterns. All tests were carried out under operating frequencies 0.5, 1 and 2 Hz under horizontal shaking. All tests were achieved with one embedment ratio (L/d = 30). These tests were grouped in three different numbers of piles; 2 piles in row and line patterns, 3 piles and 4 piles; and three pile spacing ratios (s/d = 3, 4 and 5).

The results of dry soil indicating the mechanism of dynamic response of piles and soil subjected to dynamic horizontal shaking include the variation and distribution of acceleration with time in different states of soil in addition to the vertical and horizontal displacements, end-bearing load, peak acceleration and the peak velocity of foundation.

It was concluded that for a dry soil bed, the acceleration amplitudes increase with frequency for both soil relative densities (loose and medium) and different pile patterns (number; single or group and different spacing ratios s/d). The maximum acceleration in the foundation is lower than in the soil bed for all operating shaking frequencies, pile spacing ratios and soil states. The decreasing of the maximum acceleration recorded in the foundation as

Izvleček

Izveden je bil niz 94 laboratorijskih preizkusov za merjenje odziva temeljenja na pilotih, ki so bili izpostavljeni dinamičnim obtežbam. Osem preizkusov je bilo izvedenih na posamičnem pilotu v suhi zemljini z relativno gostoto 30 % (rahlo gostotno stanje) in 50 % (srednje gostotno stanje); 66 testov na skupini pilotov z različnimi razmiki in vzorci. Vsi preizkusi so bili izvedeni pri delovnih frekvencah 0,5, 1 in 2 Hz pri horizontalnem tresenju. Vsi preizkusi so bili izvedeni z enim razmerjem vpetosti (L/d = 30). Ti preizkusi so bili združeni v tri skupine z različnimi števili pilotov; 2 pilota v vrsti in linijskem vzorcu, 3 piloti in 4 piloti; ter tri razmerja razmika med piloti (s/d = 3, 4 in 5).

Rezultati za suho zemljino kažejo mehanizem dinamičnega odziva pilotov in zemljine, izpostavljenih dinamičnemu vodoravnemu tresenju, dodatno k vertikalnim in vodoravnim premikom, nosilnostim na konici, največjemu pospešku in največji hitrosti temeljenja vključujejo še spreminjanje in porazdelitev pospeška s časom v različnih stanjih zemljine.

Ugotovljeno je bilo, da se za suho zemljinsko osnovno plast amplitude pospeševanja s frekvenco povečujejo tako za relativni gostoti zemljine (rahlo in srednjo gosto gostotno stanje) kot za različne vzorce pilotov (število; posamični pilot ali skupina pilotov in različna razmerja razmika s/d). Pri vseh delovnih frekvencah tresenja, razmerjih razmikov med piloti in stanji zemljine je največji pospešek v temelju nižji kot v zemljinski osnovni plasti. Zmanjšanje največjega pospeška,

compared to that in the soil bed is between 10-100 % for loose and medium state of soil, and the decrease in loose state is more than in medium state. This means that there is damping effect or attenuation of vibration waves. The amplitudes of recorded acceleration in the pile cap are much higher than in the soil bed for single pile and pile group with different pile spacing ratios, also these amplitudes are increasing with increase of shaking frequency and relative density of the soil.

zabeleženega v temelju, v primerjavi s pospeškom v zemljinski osnovni plasti znaša med 10 % in 100 % za zemljine v rahlem in srednje gostem gostotnem stanju, zmanjšanje za rahlo gostotno stanje pa je večje kot za srednje gostotno stanje. To pomeni, da pride do dušenja ali oslabitve vibracijskih valov. Amplitude zabeleženih pospeškov v blazini pilotov so veliko večje kot v zemljinski osnovni plasti za en pilot in skupino pilotov z različnimi razmerji razmikov med piloti, prav tako pa se te amplitude povečujejo s povečanjem frekvence tresenja in relativne gostote zemljine.

1 INTRODUCTION

The pile foundations response under dynamic loading is comparatively more complicated than that for static loading. Unfortunately till now, the piled foundation system performance subjected to cyclic loads or during earthquakes is not completely understood [22]. The soil-pile-foundation interaction is one of the main vital issues in the dynamic analysis which needs more understanding. However, a very little information is available on observed dynamic behavior of pile foundations which is due to difficulties in performing such tests involving the several variables related to both soils and piles.

Numerous shaking table tests have been conducted on sand soils, with and without the pile models. These practical examinations include tests to study ground responses and behavior of the sand, and model pile tests to evaluate the pile behaviors and soil-pile interactions under shakings. Further tests and analyses of the shaking test data are required for a better understanding of behaviors of soil, soil-pile interaction, and combining between the generated movement and pile responses under earthquake shakings. The shaking table test data may be used for verification of analysis methods and numerical modeling for ground responses and soil-pile interactions during earthquake shakings.

Full-scale tests are generally assessed to submit the most reasonable results but, are limited because of their high costs. The limitations highlight the two main difficulties of carrying out field full-scale tests on piles subjected to earthquake excitation, essentially the difficulty in modeling bedrock excitation and providing enough energy to excite large pile groups in addition to their significant cost, time and effort. However, a number of studies dealt with centrifuge and shaking table model testing. The most common previous studies on dynamic testing of piles have been achieved with full scale piles are; Maxwell et al. [19], Novak and Grigg [20], Gui [17]; on small scale tests; Fattah et al. [14][15].

Brown [12] studied dynamic and static lateral loading on pile groups using different full-scale field tests carried out on groups of piles of six to 12 piles, both driven and bored, in relatively cohesionless and soft cohesive soils. All the pile groups were loaded laterally statically reaching large deflections, and instrumented pipe pile groups were also tested under dynamic loads reaching large deflections, equivalent to those that might the pile be subjected to due to major impact of ships and earthquakes. Dynamic loading was exerted by a number of impulses of increasing magnitude adopting a horizontally mounted Statnamic device. While this loading did not cover the characteristics of lateral loading and ground motion that may cause development of high pore water pressures, it did cover the damping that occurs at high levels of pile deflections and the inertial effects of the structure.

Banerjee [9] presented the behavior of pile foundations under earthquake loading. The study investigated the interaction between soil behavior, pile stiffness and superstructure inertial loading on pile response during earthquake. It was noted that the soil around the piles does not just support the piles, it also exerts inertial loading on the piles. Pile head loading cannot replicate this effect. Experimental data have been deduced from a centrifuge modeling, which then used as a basis for validating and calibrating numerical analyses. The research involved four major components: (1) characterization of the dynamic properties of kaolin clay through element testing using the cyclic triaxial and resonant column apparatus; (2) dynamic centrifuge testing on pure kaolin clay beds (without structure) followed by 3-D finite element back-analyses; (3) dynamic centrifuge testing on clay-pile-raft systems and the corresponding 3-D finite element back-analyses and (4) parametric studies leading to the derivation of a semi-analytical closed-form solution for the maximum bending moment in a pile under seismic excitation.

Boominathan et al. [11] carried out a study by full-scale lateral dynamic pile load testing to determine the dynamic characteristics of soil-pile system. The results of

two full-scale field dynamic lateral pile load tests carried out at two different sites in India (Chennai and Hazira) and the results of a nonlinear three-dimensional finite element analysis of piles under dynamic lateral loads using the program ABAQUS were presented. The non-destructive technique known as Multichannel Analysis of Surface Waves (MASW) was used for determination of the shear wave velocities of different layers up to a depth of 12.5 m below the ground level based on the average SPT-N value and for evaluation the stiffness (maximum dynamic shear modulus) of the subsurface required finite element analysis. A steady state sinusoidal force was generated with a 5-tonne capacity mechanical oscillator. The forced vibration response of the piles was measured using two acceleration transducers fixed at the mid height of the pile cap, and at the pile cut off level. After every steady state lateral vibration test, the eccentricity of the oscillator was increased to raise the dynamic force and the test was repeated to cover a wide range of lateral displacements expected during a typical dynamic loading of the pile.

Janalizadeh and Zahmatkesh [18] applied a pseudo-static method for estimation of the response of pile during dynamic loading. The geometry and the soil modeling parameters have been defined, and then the numerical model was verified by means of the centrifuge test. Next, the behaviors of piles were studied with the effects of various parameters such as soil layering, kinematic and inertial forces, boundary condition of pile head and ground slope. A method for analysis of piles in liquefiable soil under seismic loads has been presented. Three cases were considered to evaluate the effects of variations in stiffness and lateral resistance of the p-y curves on the testing results.

The dynamic response of pile foundation in dry sandy soil excited by two opposite rotary machines was considered experimentally by Fattah et al. [15]. A small scale physical model was manufactured to accomplish the experimental work in the laboratory. The physical model consists of two small motors supplied with eccentric mass (0.012 kg) and eccentric distance (20 mm) representing the two opposite rotary machines, an aluminum shaft as the pile, and a steel plate a pile cap. The experimental work was achieved taking the following parameters into considerations: pile embedment depth ratio (L/d, where L is the pile length and d is its diameter) and operating frequency of the rotary machines. All tests were conducted in medium dense fine sandy soil with 60 % relative density. To predict precisely the dynamic load that will be induced from the rotary machines, a mini load cell with a capacity of 100 kg was mounted between the aluminum plate (the machine base) and the steel plate (pile cap). The results revealed that, before machine operation, the pile tip load was approximately equal to the static load (machine and pile cap), whereas during machines' operation, the pile tip load decreased for all embedment depth ratios and operating frequencies. This reduction was caused by the action of skin friction that was mobilized along the pile during operation, and as a result the factor of safety against pile bearing failure increases. For all operating frequencies and pile lengths, the factor of safety against bearing failure increased during machines' operation, where the pile tip load became less than its value before starting operation. During operation, the skin friction resistance mobilized along pile length led to decrease the bearing load.

The objectives of the present study are determination of the frequency independent dynamic response of both single pile and group of piles to lateral vibration for different patterns and spacings, calculation of a velocity and acceleration- time history in addition to displacement - time history of pile groups subjected to earthquake excitation, and investigating the effect of soil confinement due to pile spacing on the load transfer in pile groups.

2 TESTING APPARATUS AND METHODOLOGY

The testing device (the manufactured model) is a metal structure, which consists of three main interrelated parts. All these parts have the ability to slide (slip) one against the other by means of ball bearings, which can work together giving a relative horizontal motion between them as shown in Figure 1a. The two parts have been linked by a piece of metal connected by steel screws to fix these movable sliding parts.

In the second part (slide II), a metal holder (with dimensions 800 mm wide and 400 mm long) is mounted which is also being slided by ball bearings along the longitudinal axis with a distance more than 600 mm in the two directions (sides). But in this work, this distance was limited to only 50 and 60 mm.

A steel piece (plate) of L-shape (with dimensions of 900 mm wide, 1000 mm long and 300 mm high) is mounted while strengthening its edge and base by three triangular stiffeners to avoid any rush or slippage of interior or exterior parts as shown in Figure 1b. Another two ball bearings with internal diameters of 45 mm are mounted within the bracket base in which a connectivity and installation screw (PIN) enters to get a reciprocating motion as shown in Figure 1c. A decentralized source motion must be generated and connected via an arm to the L-shaped base plate which is installed on the

(a) (b) (c) (d)

Figure 1. Slides and base bracket system during manufacturing of shake box.

(a) (b) (c) (d)

Figure 2. CAMA and pin connected during manufacturing of the shaking box.

metal holder. Then, a linear reciprocating movement must be determined at distances of 50 mm and 60 mm that means a drift from the center by 25 mm or 30 mm radius from every direction as illustrated in Figure 1d. Two decentralized Cama which is a rotating pin for translation of movement (with diameter of 95 mm) have been manufactured with downward drift distance of 25 mm or 30 mm from the center as shown in Figure 2c. They were mounted on three-phase engine, with capacity of 3 horsepower. A rotation speed of 1450 rpm was used as an incentive for the rotational motion as shown in Figure 2.

This decentralized Cama rotates inside the bearing ball (needle bearing) which is linked by a 400 mm long connecting arm (or connecting rod) to the eccentricity installed by a pin as shown in Figure 2. As the test in this research requires obtaining the reciprocating motion at different speeds and frequencies, so an electric current controller (AC Inverter from Hyundai Company) for different rotational speeds of the engine was chosen. The inverter is used to determine the type and speed of rotation. To get the required velocities in this research, the inverter has been linked to a gear box (Configuration Gear Box through the shaft) to reduce the speed by around 3 folds.

3 STEEL BOX

The other part of the manufactured device is the steel box, which is used for model tests. Its dimensions are (800 × 800) mm for its base and 1000 mm height, it is connected with the L-shaped steel plate by four screws M12 for installation and to prevent any movement as shown in Figure 3. A side slot 400 mm wide and 700 mm high of the steel box has been made to facilitate the process of discharging sand or soil as shown in Figure 3. A steel angle has been installed at the top of the steel box to make a platform for the devices and sensors used in the test as shown in Figure 3.

During tests different velocities are used from slow to rapid motion (1 up to 14) Hz, the motion is slow without any strong vibrations. But, with increasing the rotational velocity, the motion is converted to be a linear speed accompanied with the appearance of a direction change after the cycle end for outgoing and return giving unacceptable vibrations due to the great moving mass, which generates a high momentum and high inertia (I).

A little change of soil mass for different model tests has a limited effect on (I) but the speed is of greatest value in increasing the value of (I), so when the velocity is incre-

Figure 3. Steel box.

ased, the linear mass starts to move quickly making it difficult to change the direction smoothly, therefore this problem has been solved by adding operating dampers to absorb the surging mass momentum at the end of the half, then give the initial speed in the opposite direction of the movement after the arrival of the CAMA to the tipping point as shown in Figure 4.

It is worthy to mention that in order to make the damping value variable in correspondence to the change (increase or decrease) in the linear speed; the dampers have been connected with source of pneumatic pressure from the compressor tank added to the system. The compressor contains a regulator valve for air pressure to provide air to the dampers at different pressures according to the selected speeds as shown in Figure 4.

4 RAINING TECHNIQUE

To obtain a homogeneous fill of sand with specific relative densities inside the steel box, a sand raining technique device had been manufactured with dimensions (700×700×200) mm^3. The device is supplied with perforated cone holes distributed in an adequate way in correspondence to the speed of the sand falling, height of fall and the required relative density. This technique regulates the mechanism of sand fall, filling method, and the homogeneity of distribution, Figure 5. This box is fitted from its four corners by hooks and steel chain

Figure 5. Sand raining box and meshes.

Figure 4. Pneumatic dampers system.

through a mechanism allowing its vertically upward and downward movement for the required distances of sand fall. The sand box is supplied in its bottom by mechanical gates. Wherever the height reached, the gates are opened simultaneously. The main job of this gate is to open the holes and allowing sand fall and vice versa.

The "raining technique" is used to deposit the soil in the testing tank at a known and uniform density, and in preparing the tested soil. The device consists of a steel tank, with dimensions of 700 mm length, 700 mm width and 200 mm height.

5 DATA ACQUISITION SYSTEMS

The system of data acquisition was utilized so that all data could be scanned and recorded automatically, this system consists of the following:

1. Strain gauge data logger
2. Pile's tip load data system
3. LVDT data system
4. Accelerometer Data System
5. Vibration data system

6 MODEL PILES

The model pile used has a diameter of 18 mm. The size of pile's model was chosen after reviewing the literature about the suitable pile size that could be considered representative. Although, Vesic [23] stated that " scale effects will be complex for model of piles smaller than 35 mm in diameter", many researchers used smaller diameters in their tests: Al-Mhaidib [1] used steel piles with 30 mm in diameter, Boominathan and Lakshmi [10] used aluminum pile with a diameter of 19 mm and Al-Mhaidib [2] used steel piles with (25 mm) in diameter. The dimensions of the pile model that will be used in this study were also selected to minimize the boundary effects of the soil container in the experimental setup.

The ratio between the equivalent ground plane diameter of tank and the structural plane size of the test object (pile) was taken equal to 44. This equivalent diameter is large enough, so as the circumferential circle radius exceeds the extent far beyond the zone of primary compaction around the pile in sand; therefore, the effect of lateral boundaries of container is minor and could be ignored.

7 SOIL

In this work, poorly grained fine to medium dry sand taken from one of the sites middle of Baghdad city at a depth of 10 to 15 m was used to study the responses of piles subjected to dynamic actions. The soil properties are given in Table 1.

Table 1. Physical properties of sandy soil used for testing.

Standard of the test	Value	Property
Grain size analysis		
Effective size, D_{10} (mm)	0.14	ASTM D 422 and ASTM D 2487 (2007)
Mean size, D_{50} (mm)	0.22	ASTM D 422 and ASTM D 2487 (2007)
Coefficient of uniformity, C_u	1.70	ASTM D 422 and ASTM D 2487 (2007)
Coefficient of curvature, C_c	0.96	ASTM D 422 and ASTM D 2487 (2007)
Classification (USCS)*	SP	ASTM D 422 and ASTM D 2487 (2007)
Specific gravity, G_s	2.69	ASTM D 854 (2006)
Dry unit weights		
Maximum, $\gamma_{d(\max.)}$ kN/m^3	15.2	ASTM D 4253 - (2000)
Minimum, $\gamma_{d(\min.)}$ kN/m^3	13.2	ASTM D 4254 - (2000)
Maximum void ratio, e_{max}	0.99	----------
Minimum void ratio, e_{min}	0.74	----------
Initial dry unit weight, $\gamma_{d(\text{test})}$	13.74 ,14.13	----------

8 PILES

The pile's model used in the present study is made of smooth aluminum tube having outer diameter of 18 mm and inner diameter of 15 mm covered with plastic sleeve to protect strain gauges. Pile-embedment ratio (depth-to diameter) (*L/d*) used in testing single and group piles was (30). four different arrangements of the pile groups (2×1,1×2, triangle and 2×2) with different spacing ratios (*S/d*) (3, 4 and 5) are used for testing a group of piles. The mechanical properties of pile used are shown in Table 2.

Table 2. Mechanical properties of aluminum pile used.

Embedded length (mm)	Outer diameter (mm)	Wall thickness (mm)	Bending stiffness , E_PI_P (kNmm^2)
540	18	1.5	0.18×10^6

The piles were instrumented with 8 pairs of strain gauges on each pile attached along the shaft to measure bending

strain by pasting (8) electrical- resistance-half bridge type strain gauges at distances of (0 *L*, l/4 *L*, l/2 *L*, and 3/4 L) from the top of the pile for single and group of piles tested in dry soil.

Each strain gauge has a length of 5 mm, gauge factor of 2.10, and resistance of (350 Ω), and was fixed with its axis corresponding to the pile axis. The wires of strain gauges were passed on a longitudinal pile covered with waterproof past to avoid damage.

9 LOAD CELLS

Mini load cell with a diameter of 20 mm and a capacity of 100 kg was mounted at the tip of the pile, in a way to prevent the load cell from splitting from the pile and to predict the end-bearing load as shown in Figure 6.

10 PILE CAP AND PAYLOAD

Two steel plates with dimensions of (100 × 100 × 10) mm^3 and (150 × 150 × 10) mm^3 were used to simulate the pile caps, Figure 7. The purpose of using steel plate rather than aluminum plate is to ensure the rigidity of the pile cap with respect to the piles. Also another steel plates were used as payloads on the pile foundation.

A set of measurements have been performed after applying different loads which were induced by static payload which represent the vertical allowable load carried by pile.

11 MODELS PREPARATION

Preliminarily experiments were conducted to determine the uniformity of the process and how sand density changes with raining from different heights. Results from raining the sand from different elevations over known volume molds placed on the model floor demonstrated that uniform sand density could be achieved across the width of the model. By adjusting the pluvation height, different sand densities were obtained. The trial results suggested that the distance between the raining box and top of the sand should be 550 mm and 850 mm in order to produce uniform loose sand of relative density 30-50 %.

In order to attain the selected relative densities of (30 %) and (50 %), the heights of the free fall were found to be 55 mm and 85 mm, respectively. While the sand tank parts were placed together, sand layers were prepared so that the sand layers were not disturbed and consequently any change to the required density of the sand did not happen. After filling the raining box (tank) with sand and choosing the proper height of drop, the sand was poured into the test tank by moving the box

Figure 6. Mini load cell fixed at the pile's tip.

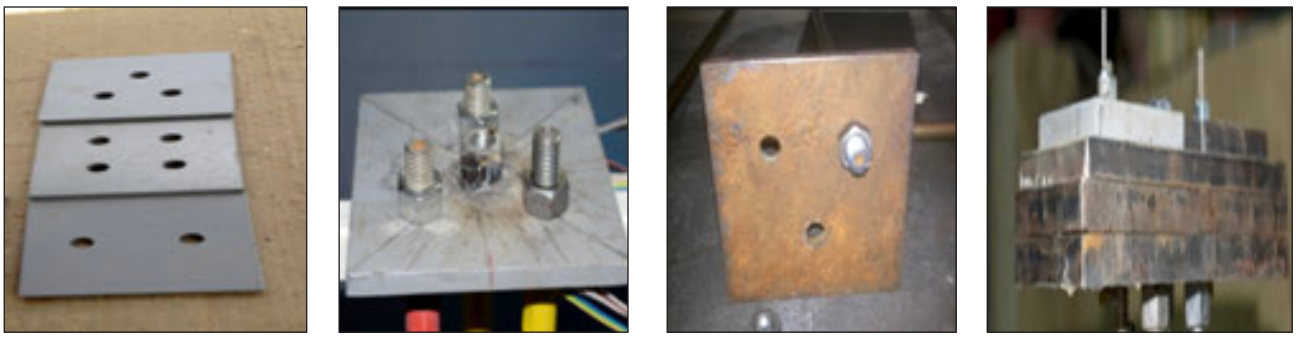

Figure 7. Steel plate used as pile cap and payloads.

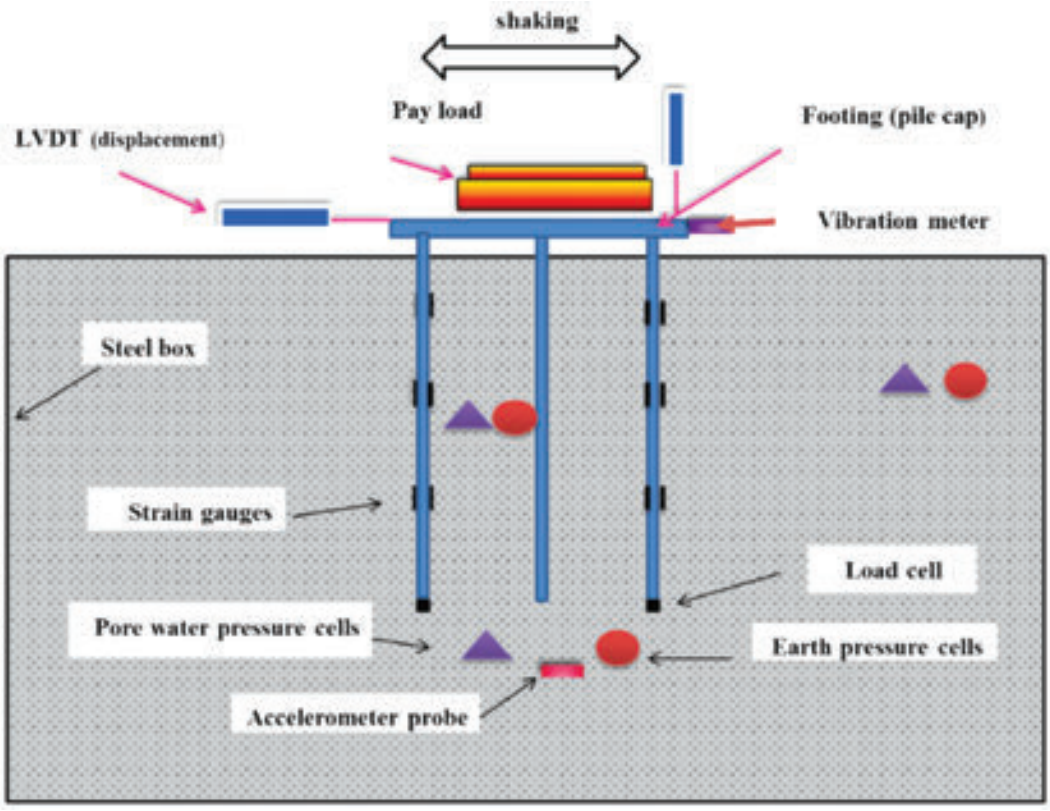

Figure 8. Steel plate used as pile cap and payloads.

forth and rear. The soil layer was prepared in 10 layers with 100 mm constant height for each one to attain the last elevation of 1000 mm from the bottom of container.

To minimize the influence of buried instruments on the soil deformation, miniature earth pressure cells (EPCs) and miniature accelerometers were used. The active EPCs diameter to grain size ratio (D/d_{50}) is 12, which is twice the recommended minimum to ensure a continuum response between the soil and the EPC active face [24]. Details of the instrumentation used in this work are shown in Figure 8. The EPCs were used to measure the total pressure on the soil at the target locations and for estimating the total stresses. Instrumentation records were acquired and recorded by multi data acquisition systems model.

12 RESULTS AND DISCUSSION

12.1 Variation of the vertical displacement of foundation with time

Figures 9 to 11 illustrate the variation of vertical displacement and settlement (permanent displacement when shaking is stopped) with time of the single pile and group of piles with $s/d = 3$ ratio, different number of piles and different frequencies and soil states.

Generally, it can be observed that the vertical displacement increased with frequency for all cases regardless the soil type and pile number and spacing. The rate of settlement increase in loose sandy soil is greater than that in dense sandy soil. From the results, it can be seen that the vertical displacements slightly increased with time with short shaking period then stayed constant to the end of the test, then the settlements increased significantly. After that, the values are increasing gradually and slightly with time in all cases.

For all cases and at different frequencies, the records of the first period (around 50-100 sec.) show sharp increase in the vertical displacement with time. While, gradual increase (or slight increase to steady) is observed in the rest times. The reason for these cases may be due to that the soil gradually densified during shaking which provided low settlement and more response.

It is also observed that some records particularly under 2 Hz frequency using pile group (triangle and 2×2) show sharp increase with time (more than 25 mm). In comparison of single pile with pile group, the vertical displacement values are lower in group with respect to single pile foundation and decrease with the increase of pile spacing in groups. Also, the values decreased with increasing the soil relative density.

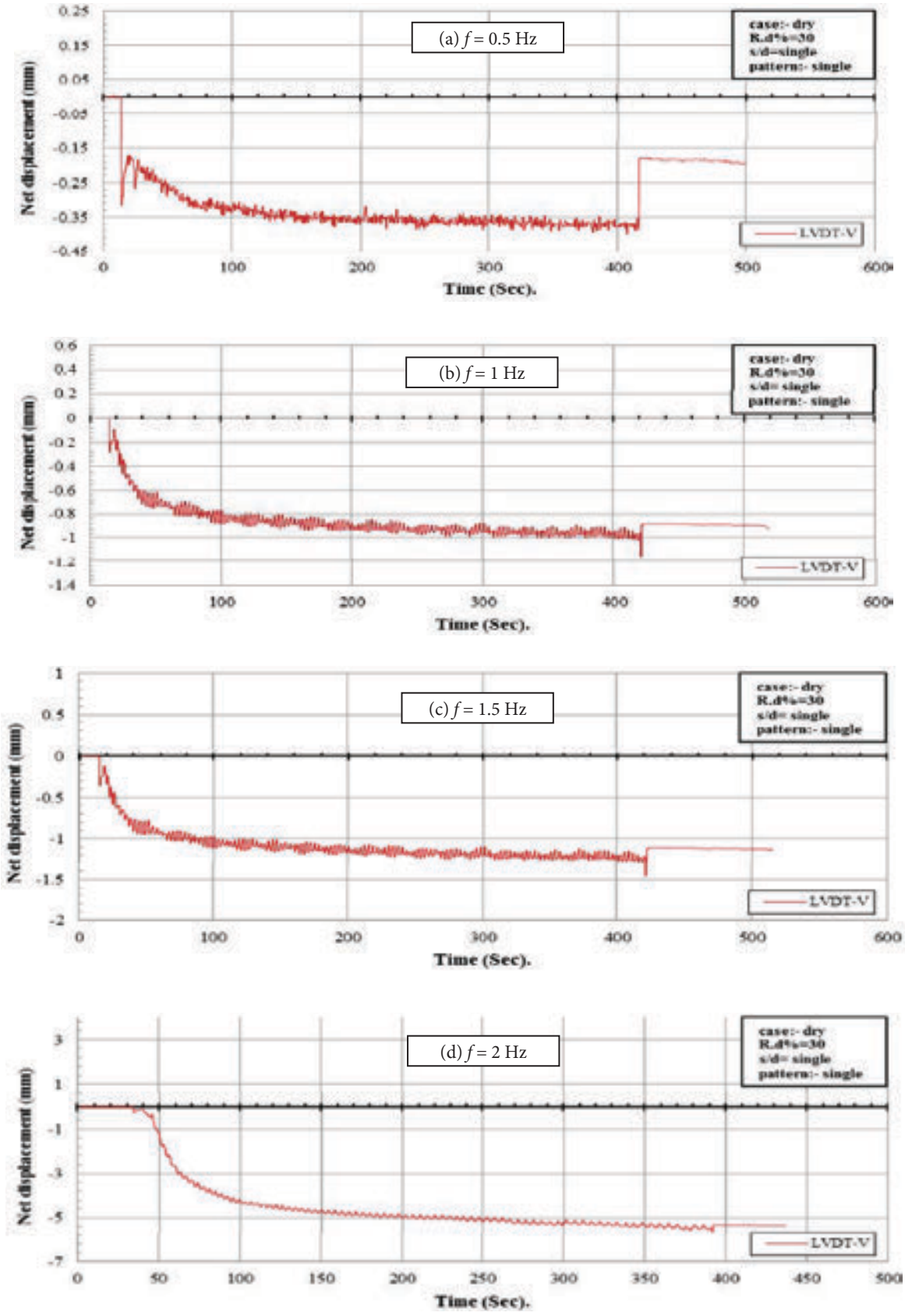

Figure 9. Variation of vertical displacement of foundation with time of (single) pile in loose dry sand under different frequencies.

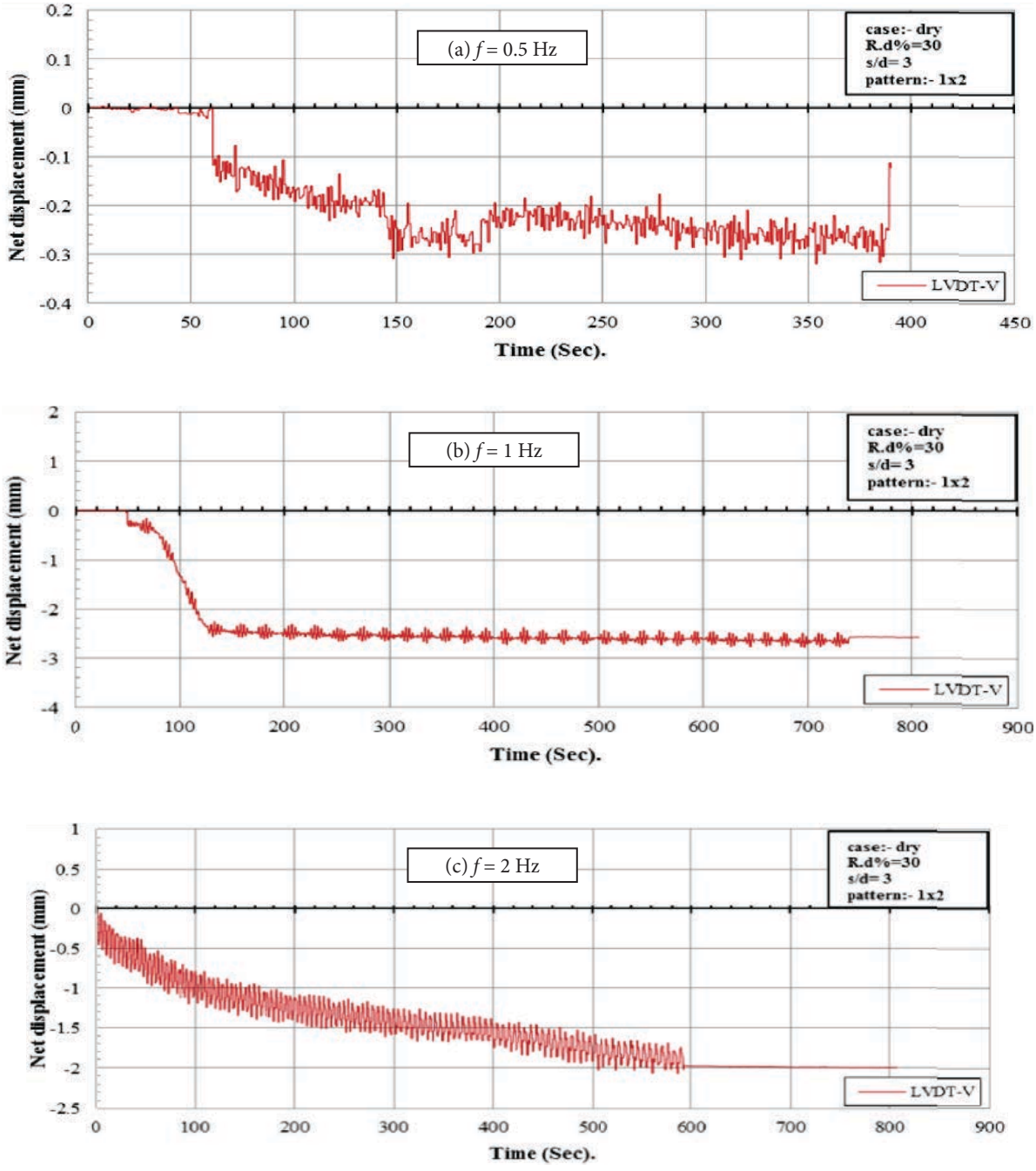

Figure 10. Variation of vertical displacement of foundation with time of pile group (1×2) for pile (1) in loose dry sand under different frequencies.

During the shearing, a granular material will typically have a net gain or loss of volume. If it had been originally in a dense state, then it typically, gains volume, a characteristic known as a Reynolds dilatancy. If it had originally been in a very loose state, then compaction may occur before the shearing begins or in conjunction with the shearing. It was observed that the increasing of shaking frequency leads to reduction in the oscillation of wave propagation values recorded due to densification of soil during shaking.

In general, it was noticed that the sandy soil rebound represents small part of settlement as the device shut down. Therefore, it is important to mention that the plotted values of total settlement represent the settlement taken simultaneously as the shaking stops. Thus, the residual or rebound displacements represent

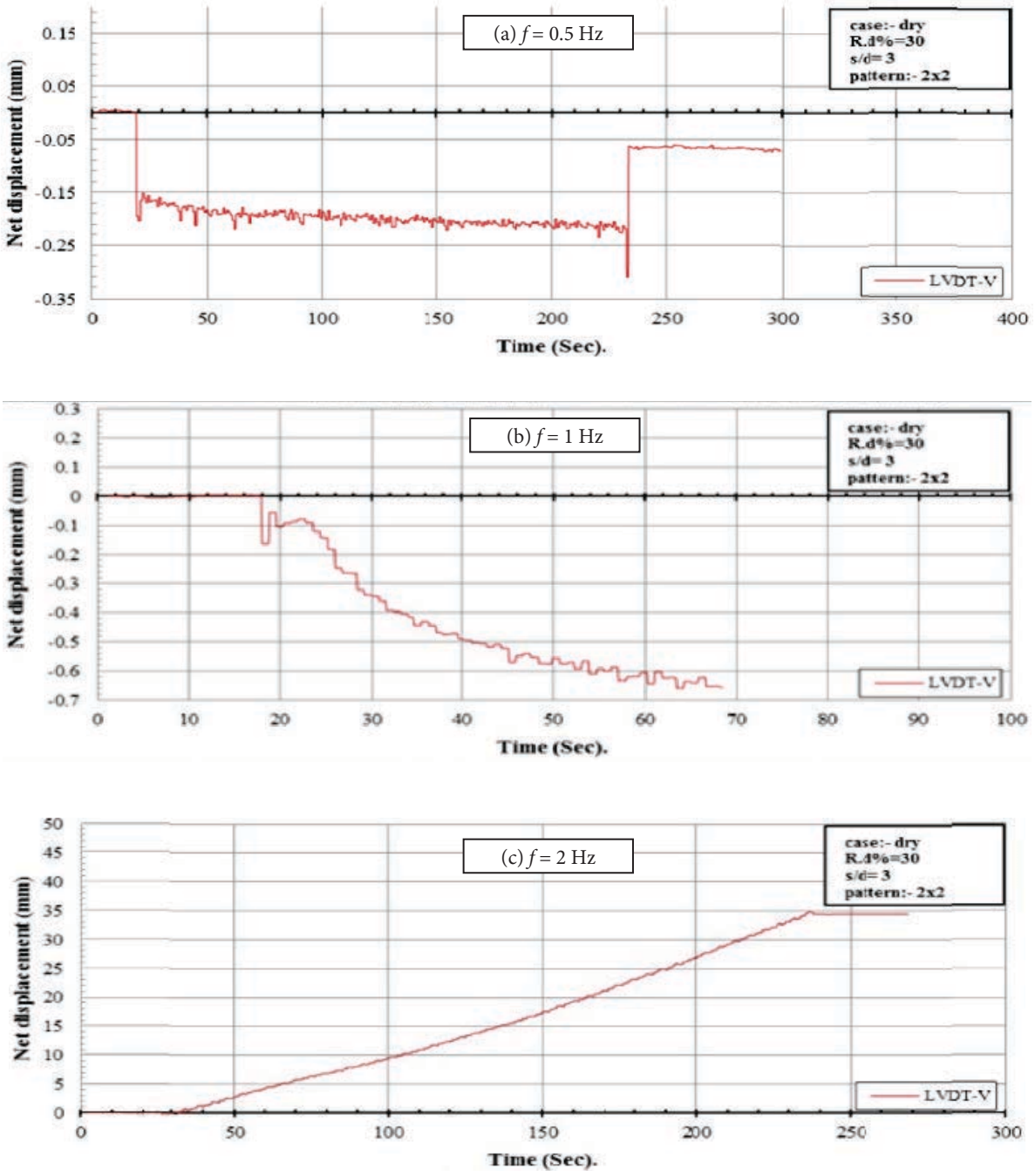

Figure 11. Variation of vertical displacement of foundation with time of pile group (2×2) for pile (1) in loose dry sand under different frequencies.

the settlement of the foundation. As well as, the rate of settlement increase in loose sandy soil is greater than that of dense sandy soil.

It is worth mentioning that the (+) sign means that the displacement into the left and upward for the horizontal and vertical moving, respectively and vice versa, also the net displacement means the displacement for dynamic shaking to the end of test (without initial static case).

12.2 Variation of the end-bearing load of the piles with time

The net (due to the dynamic effect only) bearing loads of piles were measured and recorded using miniature load cells with diameter 20 mm placed at tip of piles. The variations of the end bearing load in single pile and some groups of piles with time for $s/d = 3$ ratio and different number of piles and different

frequencies and states of soil are illustrated in Figures 12 to 17.

After careful examination of these figures, it can be seen that at the end of shaking, some piles maintain their values while others reset to zero load. The end bearing load values increase with frequency for both loose and medium soil states. Also, the end bearing load values increase with increasing number of piles for both states of soil.

In general, the end bearing load values increase when s/d ratio increases from 3 to 4 while they decrease with $s/d = 5$. For triangle group, an increase in end bearing load is observed with increasing the pile spacing.

When the spacing ratio is below $s/d = 5$, the pile group behaves as one mass, therefore, the inertia load becomes high which reflects the high percent of load transferred to the pile ends.

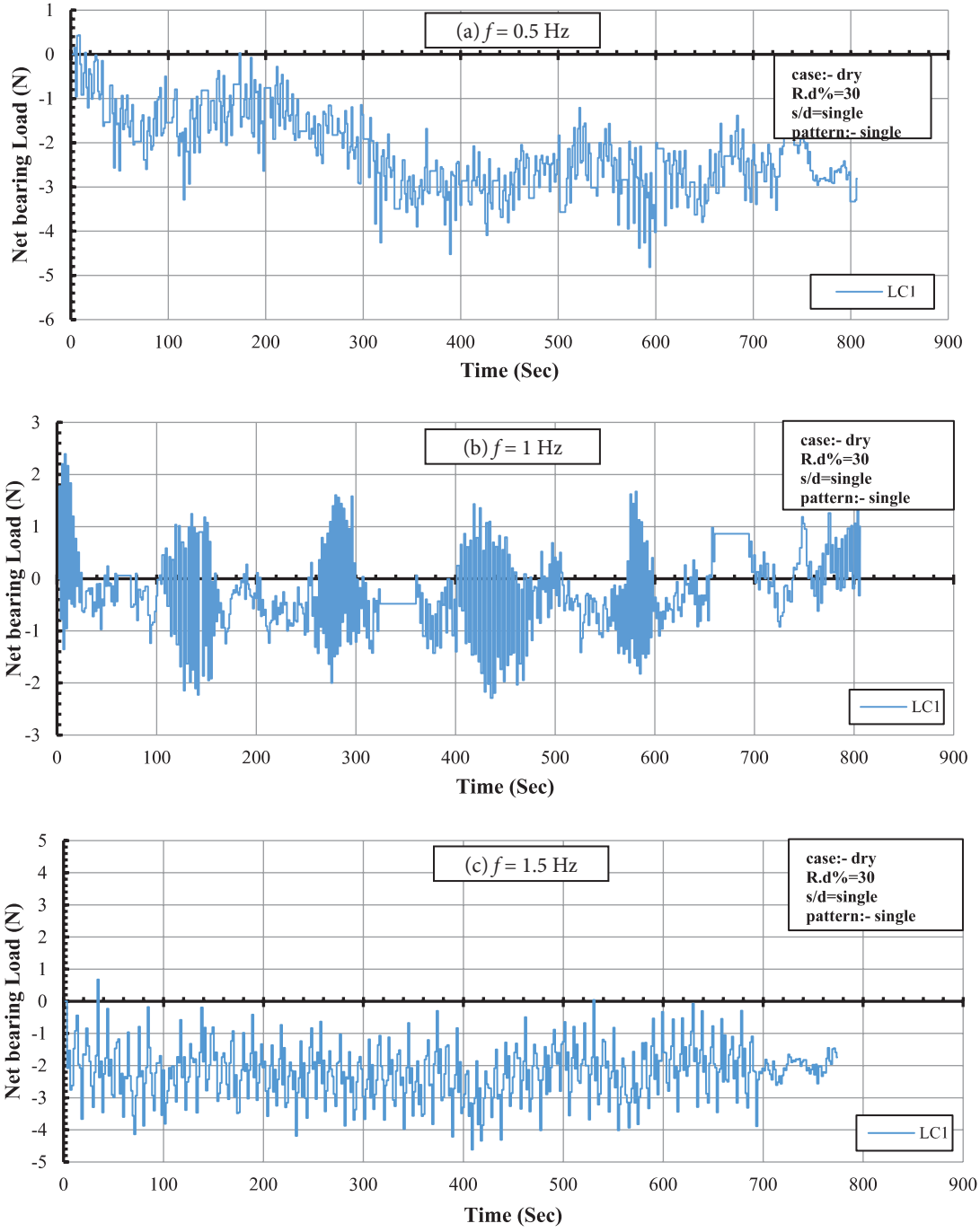

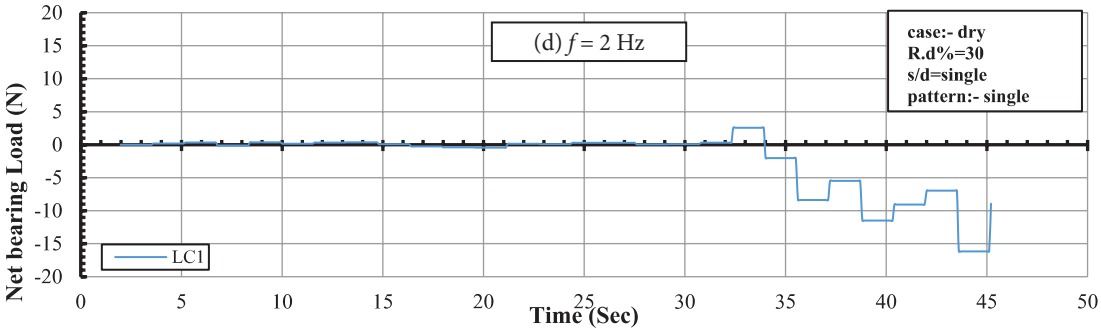

Figure 12. Variation of end bearing load of foundation with time of (single) pile in loose dry sand under different frequencies.

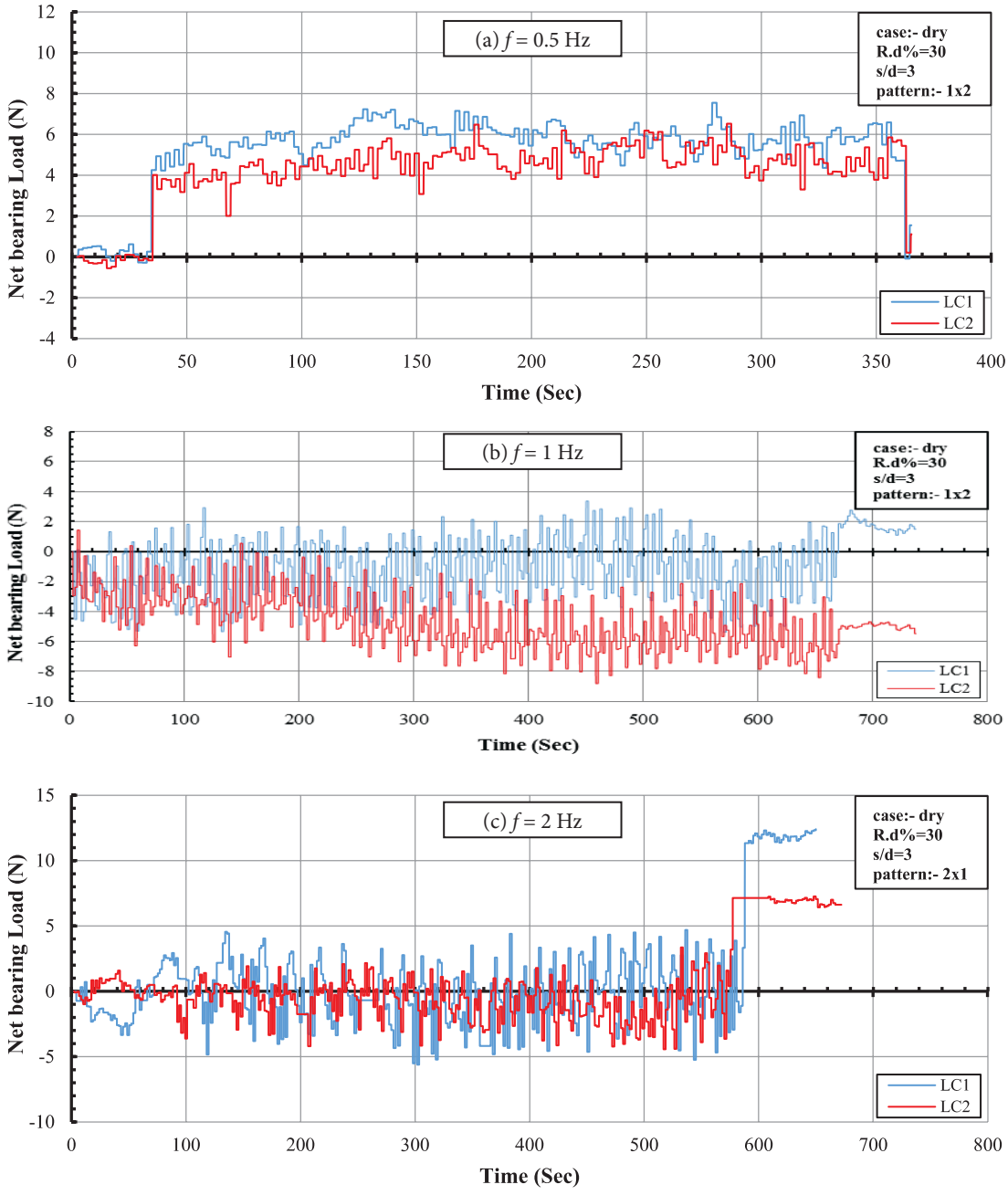

Figure 13. Variation of end bearing load of foundation with time of pile group (1×2) in loose dry sand under different frequencies.

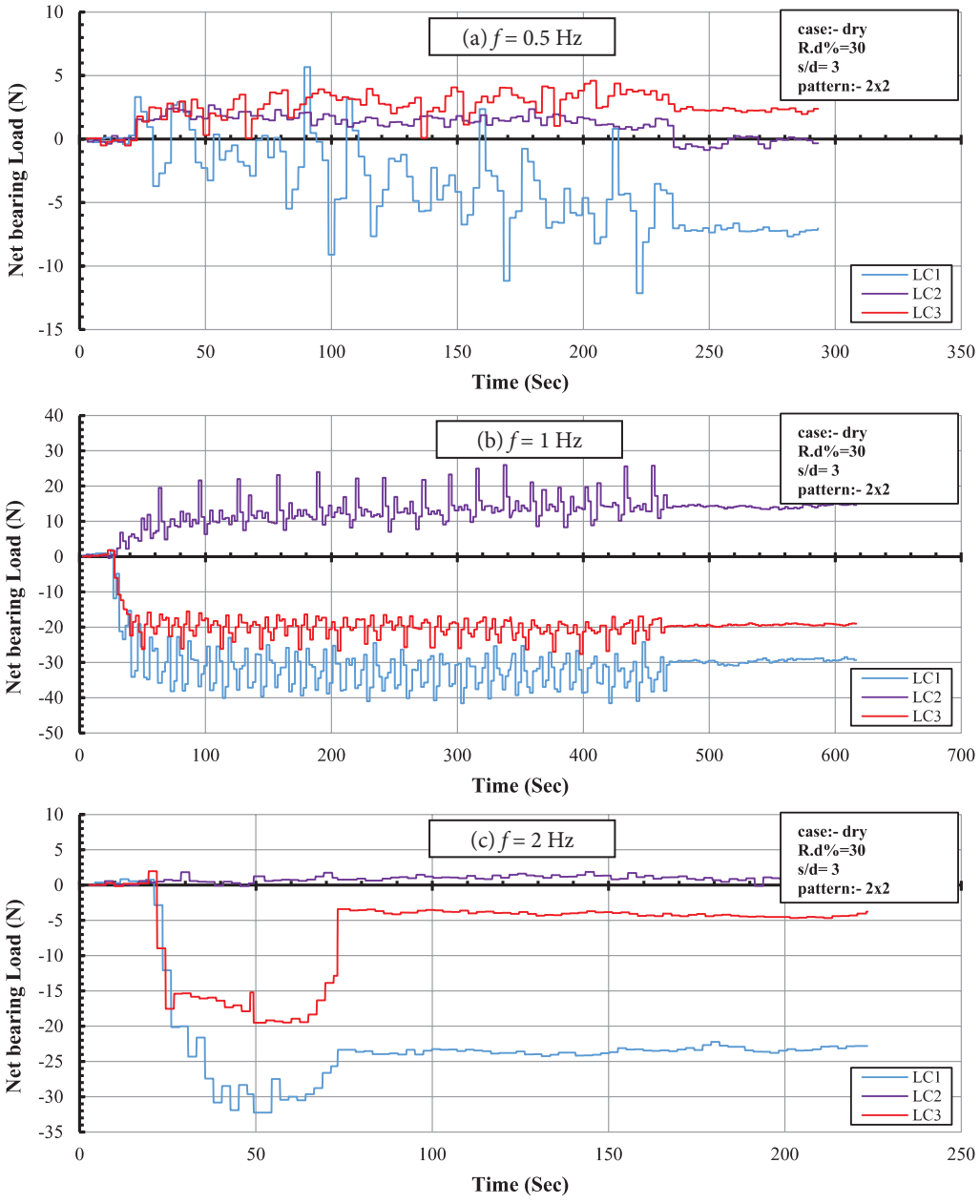

Figure 14. Variation of end bearing load of foundation with time of pile group (2×2) in loose dry sand under different frequencies.

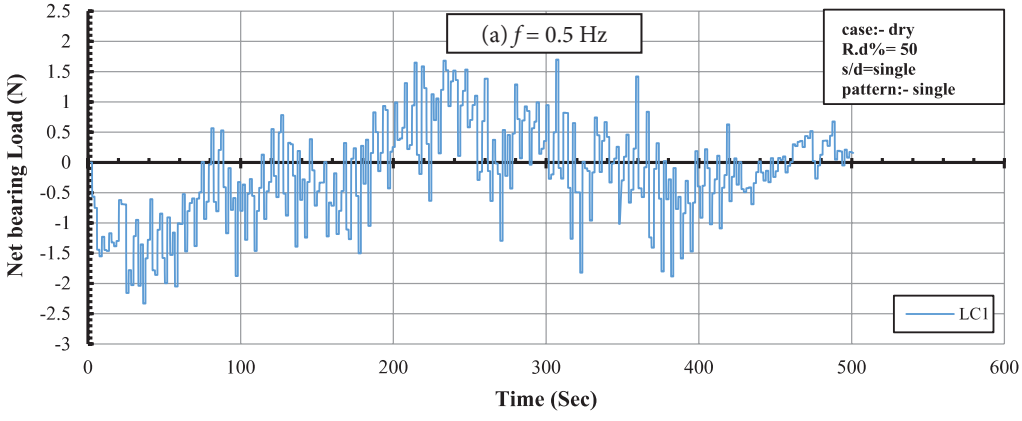

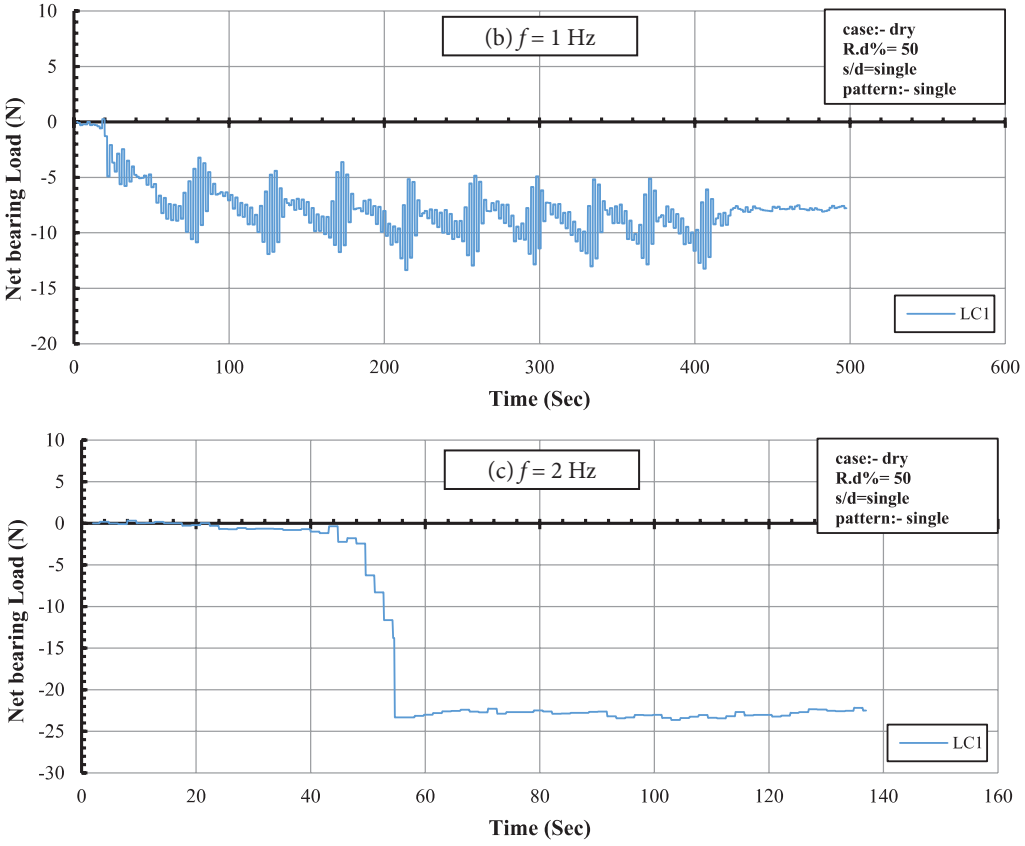

Figure 15. Variation of end bearing load of foundation with time of pile group (single) in medium dry sand under different frequencies.

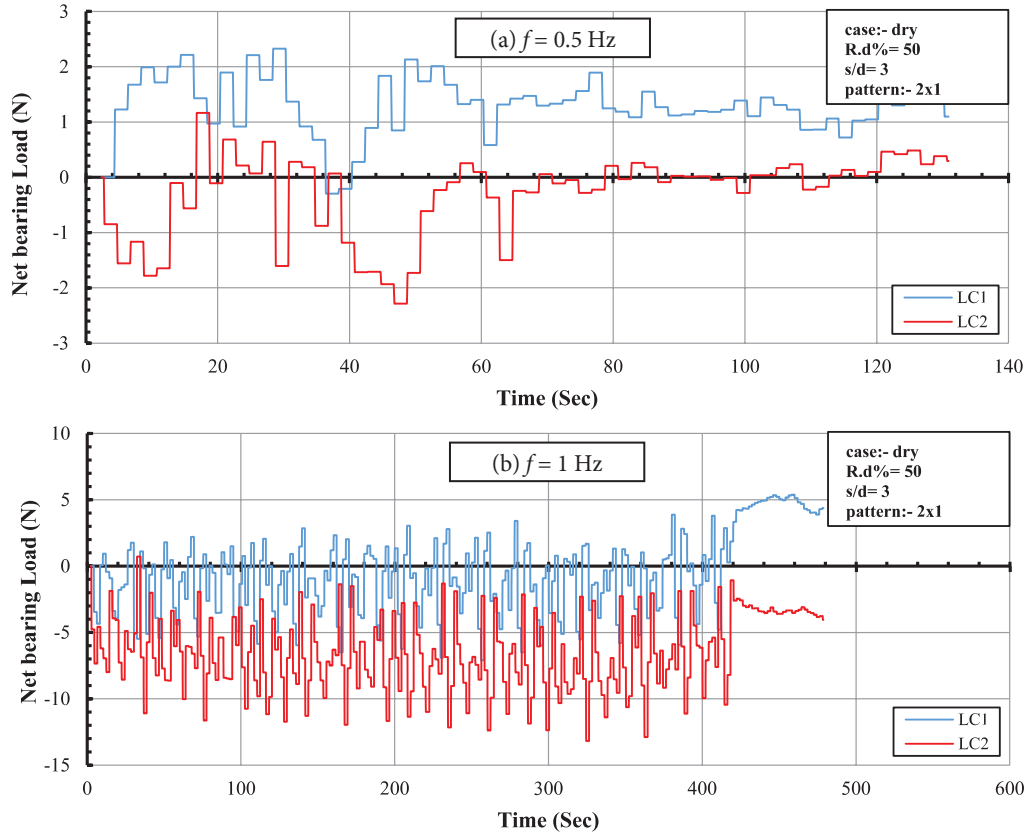

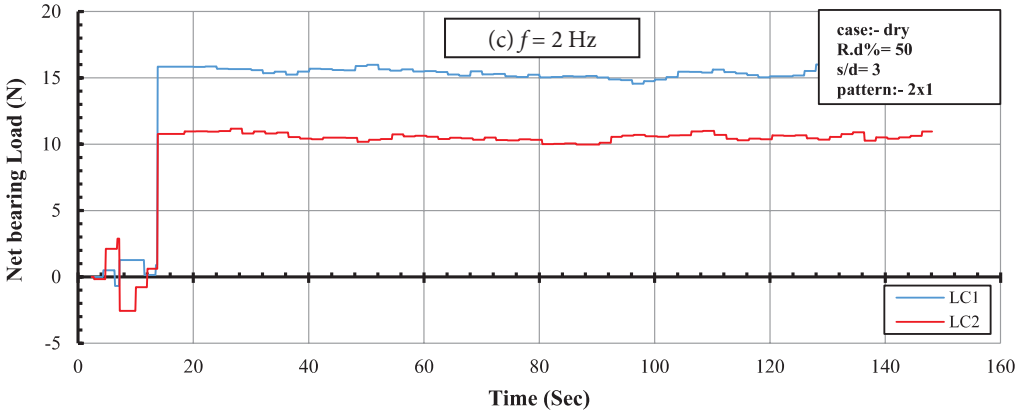

Figure 16. Variation of end bearing load of foundation with time of pile group (1×2) in medium dry sand under different frequencies.

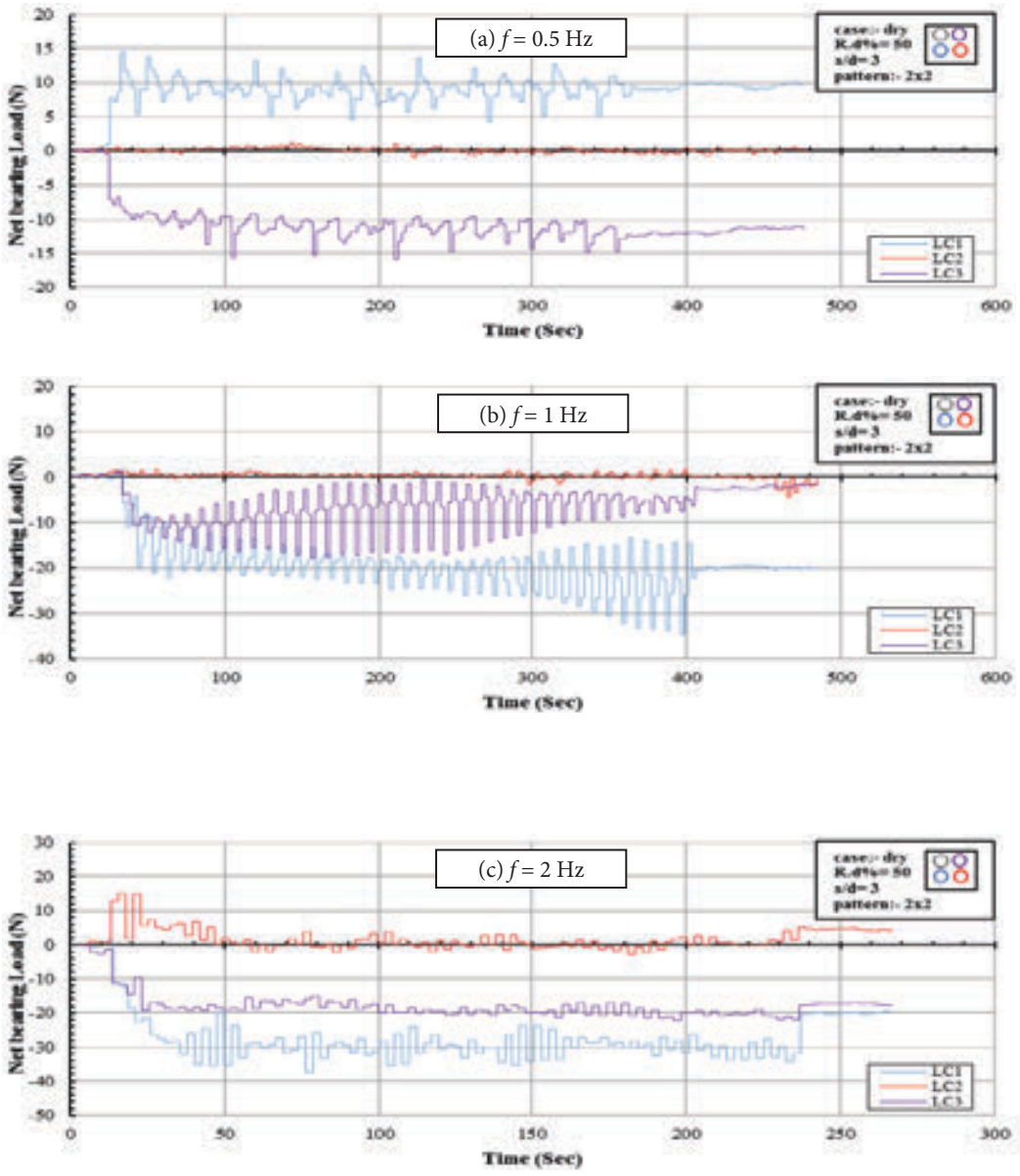

Figure 17. Variation of end bearing load of foundation with time of pile group (2×2) in medium dry sand under different frequencies.

The figures show that the behavior of the net bearing load at the tip of piles seems to be constant for a long period of test. On the other hand, the values of the net bearing load are 0.25 to 3.5 N in single pile for models in loose and medium sand, respectively.

At the start of vibration, there will be a rapid mobilization of skin friction along piles, then after a short period of time, the skin friction and end bearing reach a plateau and no noticeable change in the components was recorded.

The most important result is that, the pile tip load (net end bearing load) during shaking operation increased or decreased depending on many factors: number of piles, pile spacing, operating frequency, as well as, the state of soil.

From all figures, it is noted that, the oscillation of the frequented values decreases with increasing the shaking frequency.

When the frequency of vibration is high, there will be no enough time for sand particles to move over each other, so that the oscillation in the measured displacements and end bearing load decreases.

Fattah et al. [16] found that the final settlement of the foundation increases with increasing the amplitude of dynamic force, operating frequency and degree of saturation. Meanwhile, it is reduced with increasing the relative density of sand, modulus of elasticity, and embedding inside soils.

During operation, the skin friction resistance mobilized along the pile length due to increasing in settlement and densification (increase in pile soil interaction effect of soil) led to increase in the bearing load. This increase becomes clear as the spacing between piles increases.

A small settlement occurs due to low operating frequency, which means a small skin friction resistance along the pile mobilizes, which reduces more due to the interaction effect of piles, and that mobilized resistant is less than the induced dynamic load. As a result, the pile's tip load increases. When increasing the operating frequency, the settlement increased, which means that increasing the mobilized resistance, and the increasing in pile's tip load became less. In general, the increasing in pile tip load is not more than the applied dynamic load divided by the number of piles.

During shaking, when the end bearing load reaches a steady condition, the pile group behaves in a manner similar to the system under static loads; the load applied on the pile group is divided between the skin resistance and end bearing and no contribution is observed to the inertia effects.

Ercan [13] concluded that load developed in outer piles is about 1.25 times the load developed in inner piles. On the other hand, lateral deflection increased considerably as pile spacing decreased from 5D to 2D. However, this behavior was seen more clearly in the first two row piles. Pile spacing affects load distribution in pile groups significantly. As pile spacing increases, pile load decreases. As pile spacing increases, maximum bending moment occurred decreases under the same load applied.

12.3 Variation of the peak acceleration of the foundation with time

The variation of peak acceleration of the foundation in the axis of shaking was measured using a vibration meter (vibrometer) in addition to the previous measurements of acceleration of the foundation and soil bed using accelerometer. Figures 18 to 23 display the variation of the acceleration of the single pile and some groups of

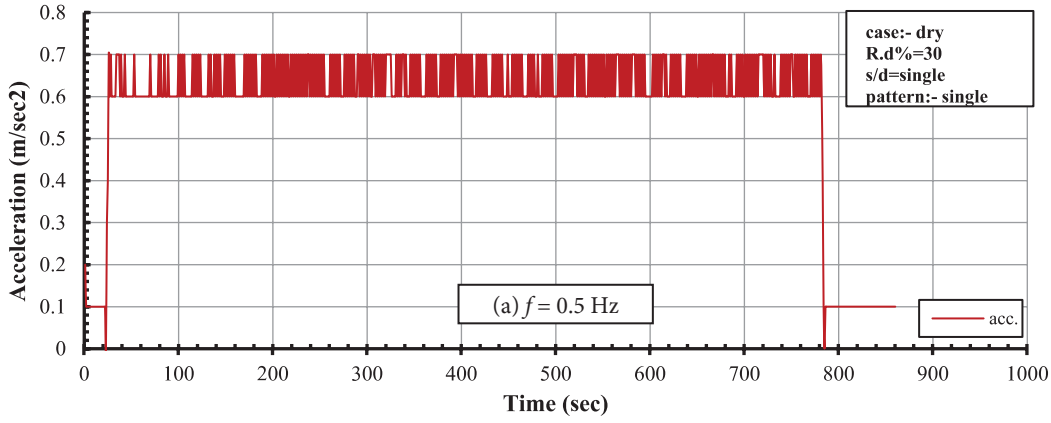

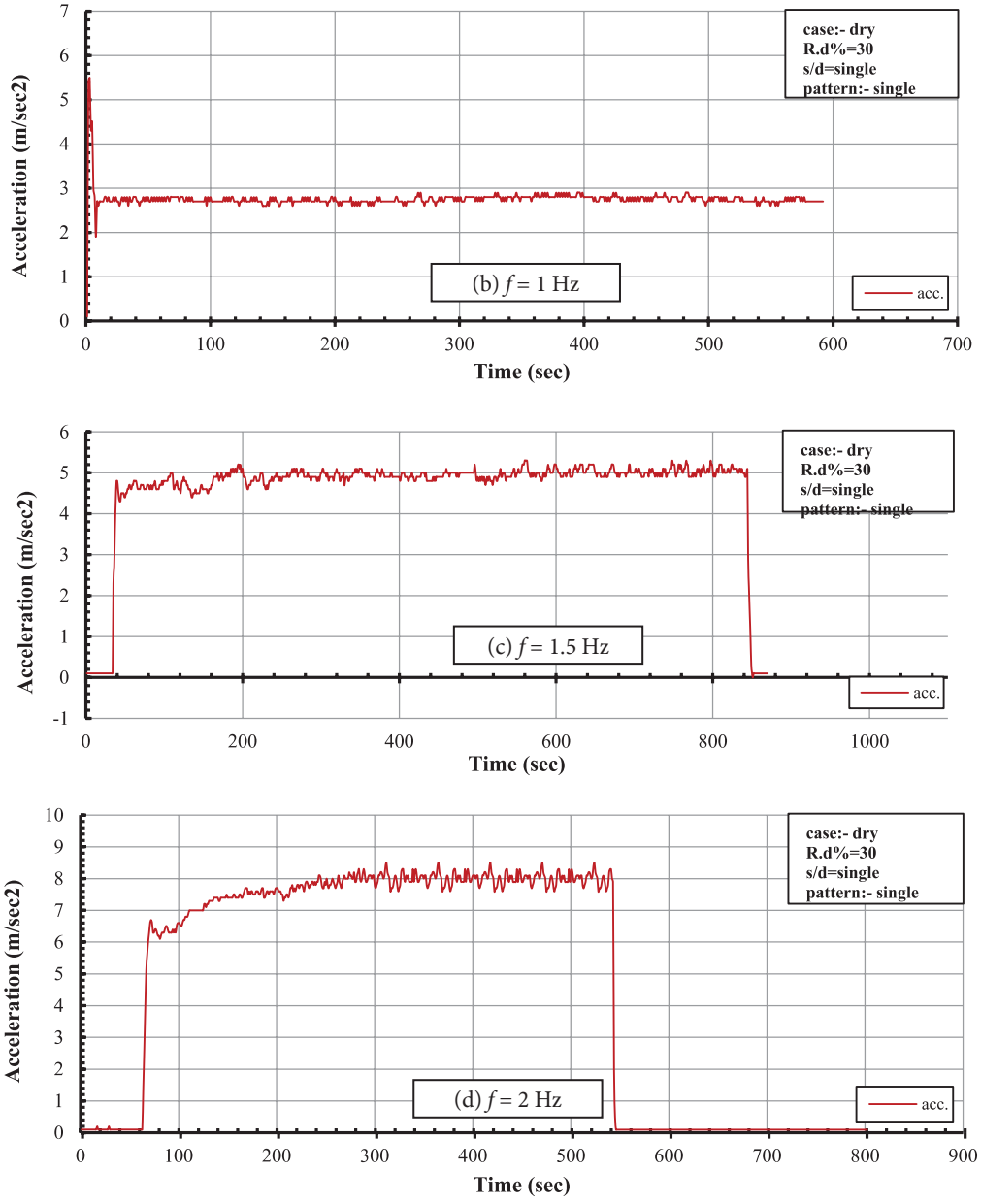

Figure 18. Variation of peak acceleration of foundation with time of (single) pile in loose dry sand under different frequencies.

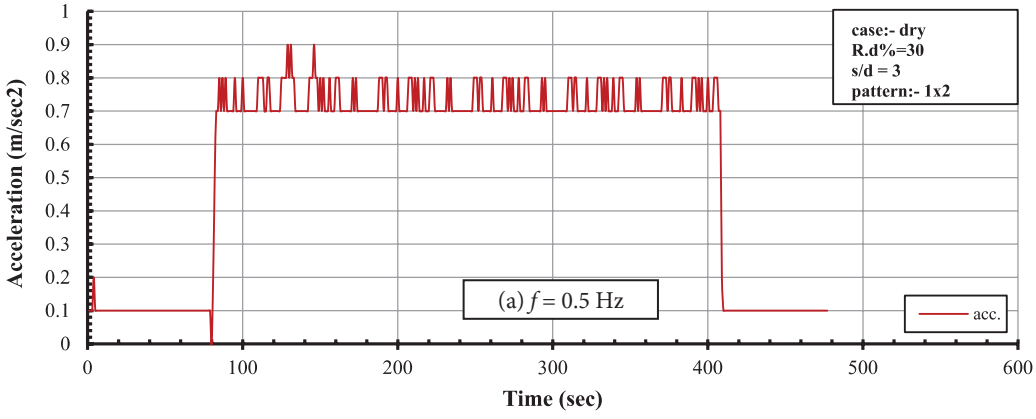

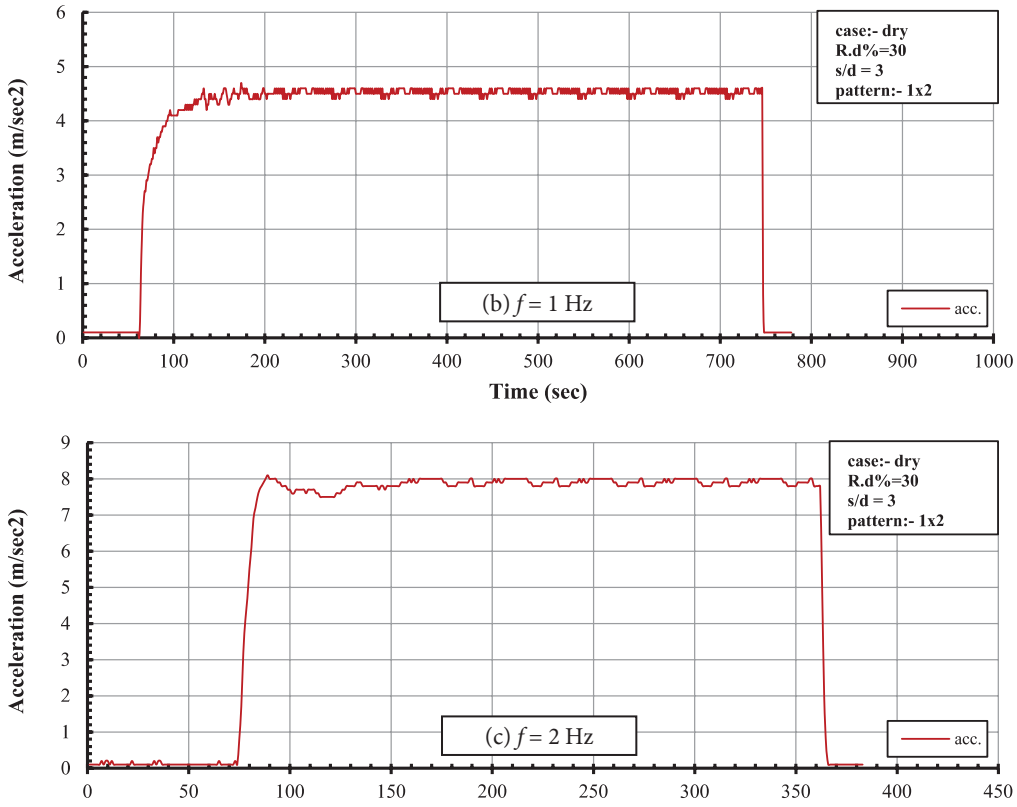

Figure 19. Variation of peak acceleration of foundation with time of pile group (1×2) in loose dry and under different frequencies.

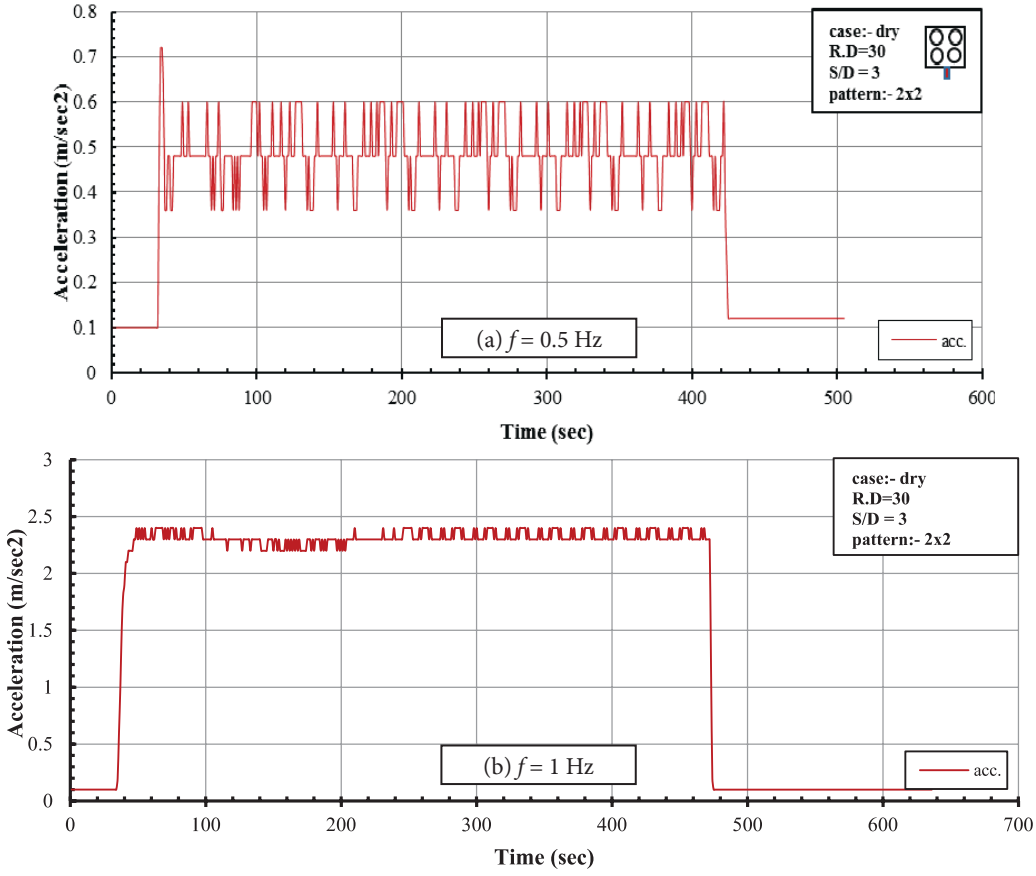

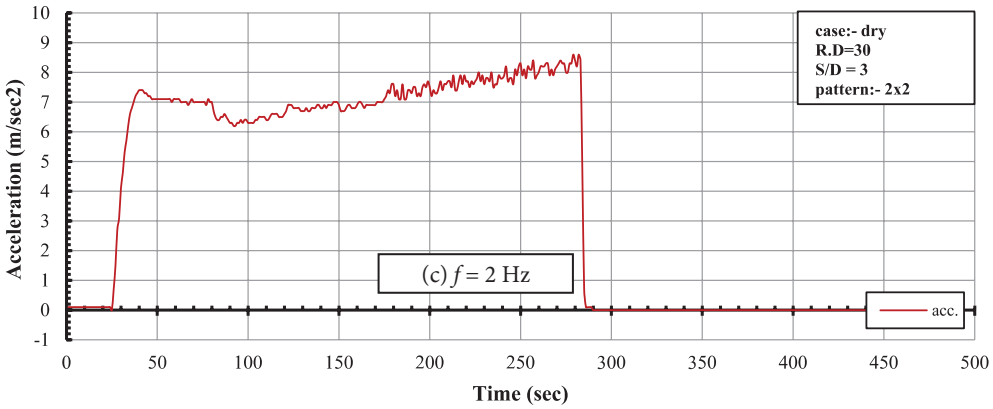

Figure 20. Variation of peak acceleration of foundation with time of pile group (2×2) in loose dry sand under different frequencies.

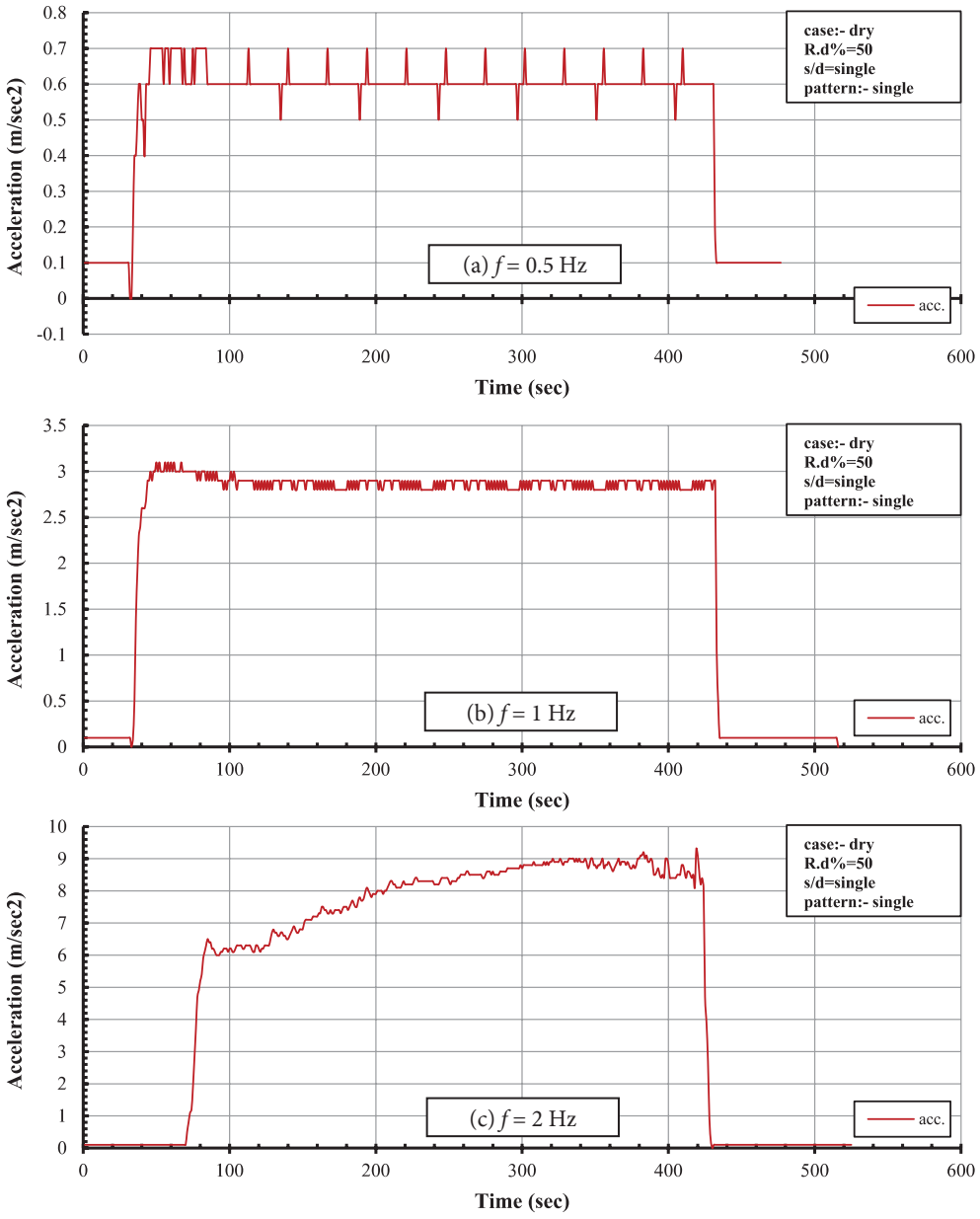

Figure 21. Variation of peak acceleration of foundation with time of pile group (single) in medium dry sand under different frequencies.

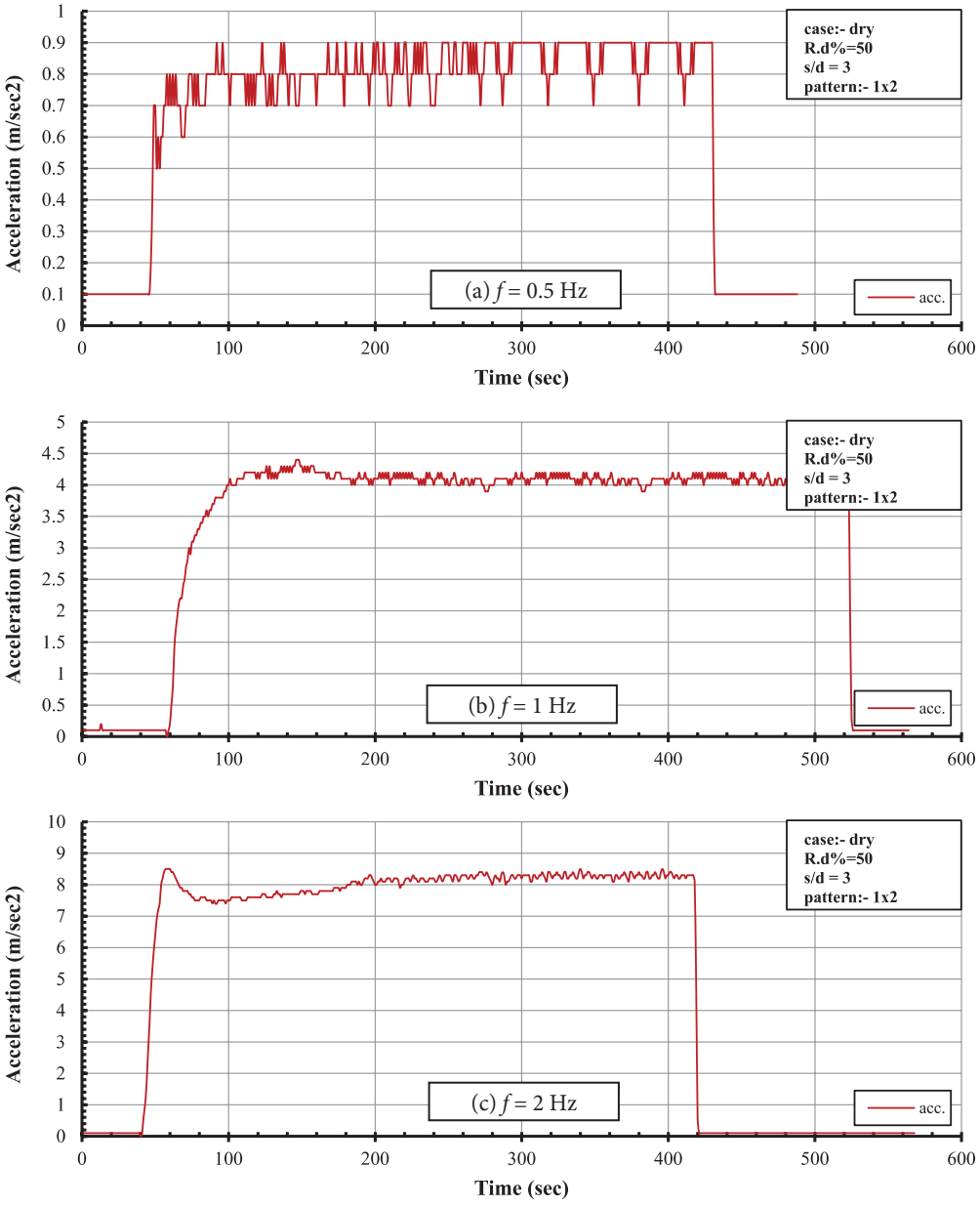

Figure 22. Variation of peak acceleration of foundation with time of pile group (1×2) in medium dry sand under different frequencies.

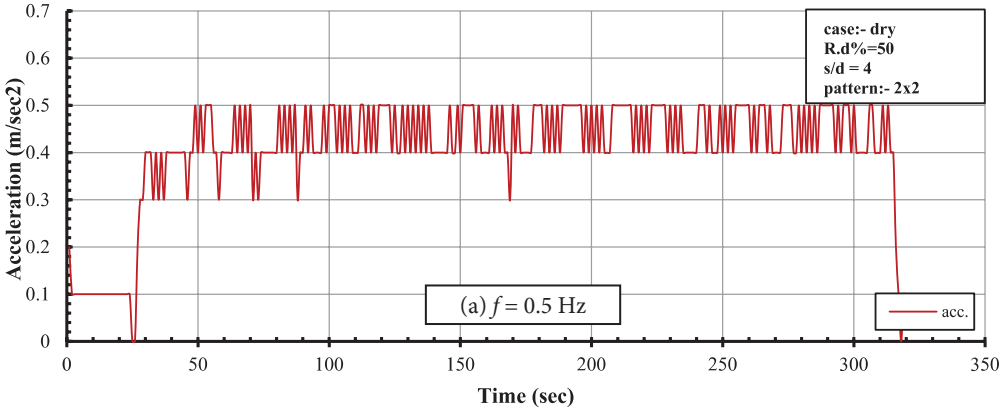

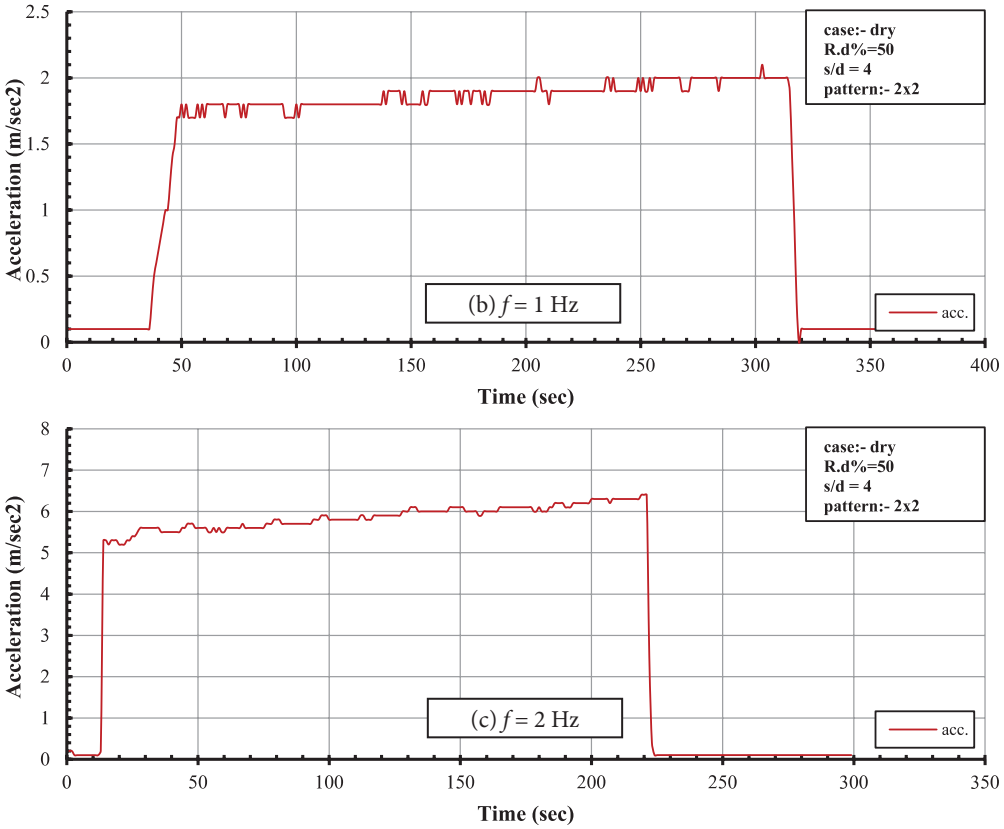

Figure 23. Variation of peak acceleration of foundation with time of pile group (2×2) in medium dry sand under different frequencies.

piles with time for s/d = 3 and 4 and different number of piles and operating frequencies for both states of soil.

From these figures, in general it can be seen the increase in acceleration measured by vibration meter with time and frequency for both states of soil and for different number of piles in the group and different spacings. The figures also show the slight decrease in the rate of vibration with increasing s/d ratio of the pile group. Concerning the effect of type of soil, the rate of vibration, in general, or the acceleration decreases when the soil is of higher relative density (medium).

The horizontal acceleration of foundation (pile cap) ranges between (0.65-8) m/sec^2 and (0.65-9) m/sec^2 for single pile in loose and medium sand, respectively for shaking frequency (0.5-2) Hz. For group of piles, the acceleration ranges from (0.45-7.5) m/sec^2 and (0.45-7.5) m/sec^2 for loose and medium sand respectively for the same shaking frequency. This means that there is a small attenuation of vibration due confinement offered by pile groups.

The above observation indicates that there is a small attenuation of vibration due confinement offered by pile groups.

12.4 Variation of the peak velocity of the foundation with time

The variation of velocity of the foundation measured using a vibration meter was also detected and recorded. Figures 24 to 29 display the variation of the velocity of some groups of piles with time for s/d = 3 and 4, different number of piles, operating frequencies and states of soil. It can be shown from these figures that the peak velocity measured using the vibration meter increases with time and frequency for both soil and different number of piles and pile spacing. The figures also show a decrease in the rate of vibration with increasing s/d ratio and relative density.

13 CONCLUSIONS

In the light of experimental tests on model piles in sand and analysis of the results and other observations during the experimental approach, the following major conclusions drawn from the test are summarized as follows:

1. For a soil bed in dry state, the acceleration amplitudes increase with frequency for both soil relative

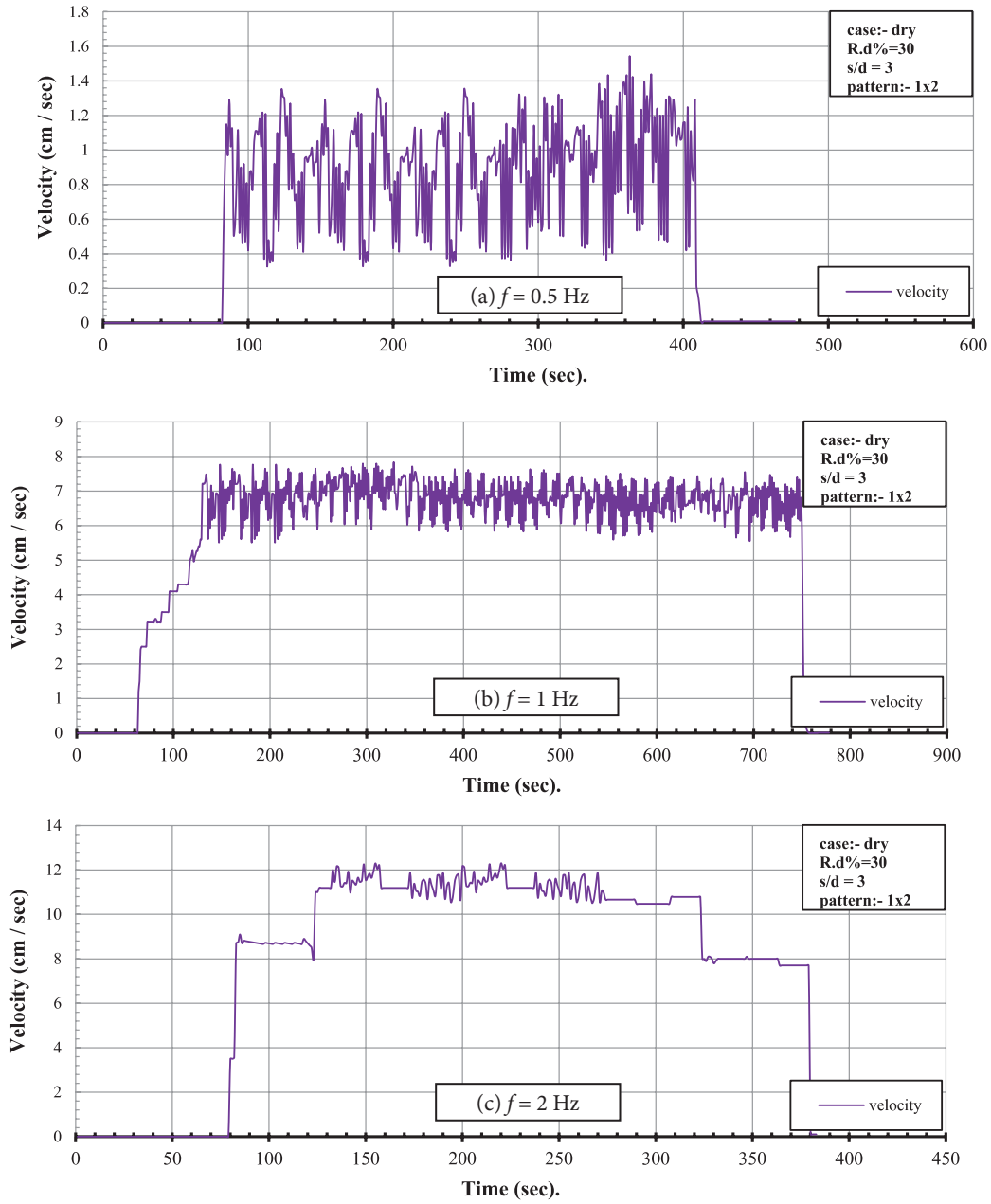

Figure 24. Variation of peak velocity of foundation with time of pile group (1x2) in loose dry sand under different frequencies.

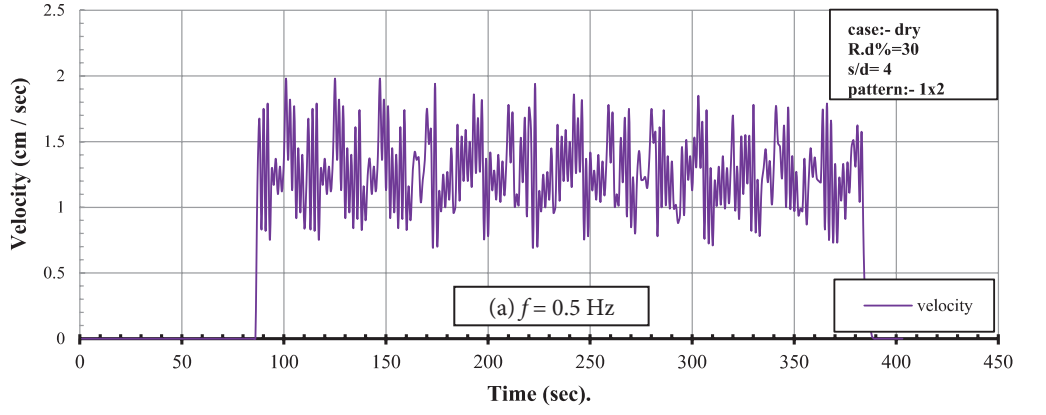

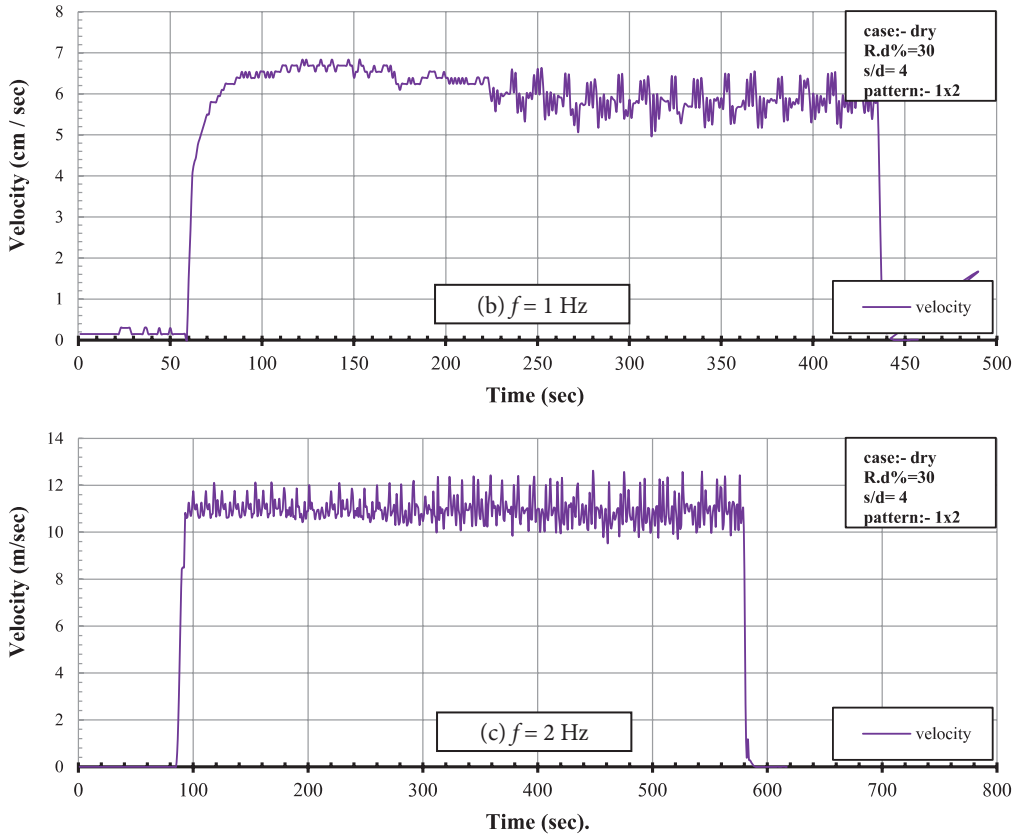

Figure 25. Variation of peak velocity of foundation with time of pile group (1×2) in loose dry sand under different frequencies.

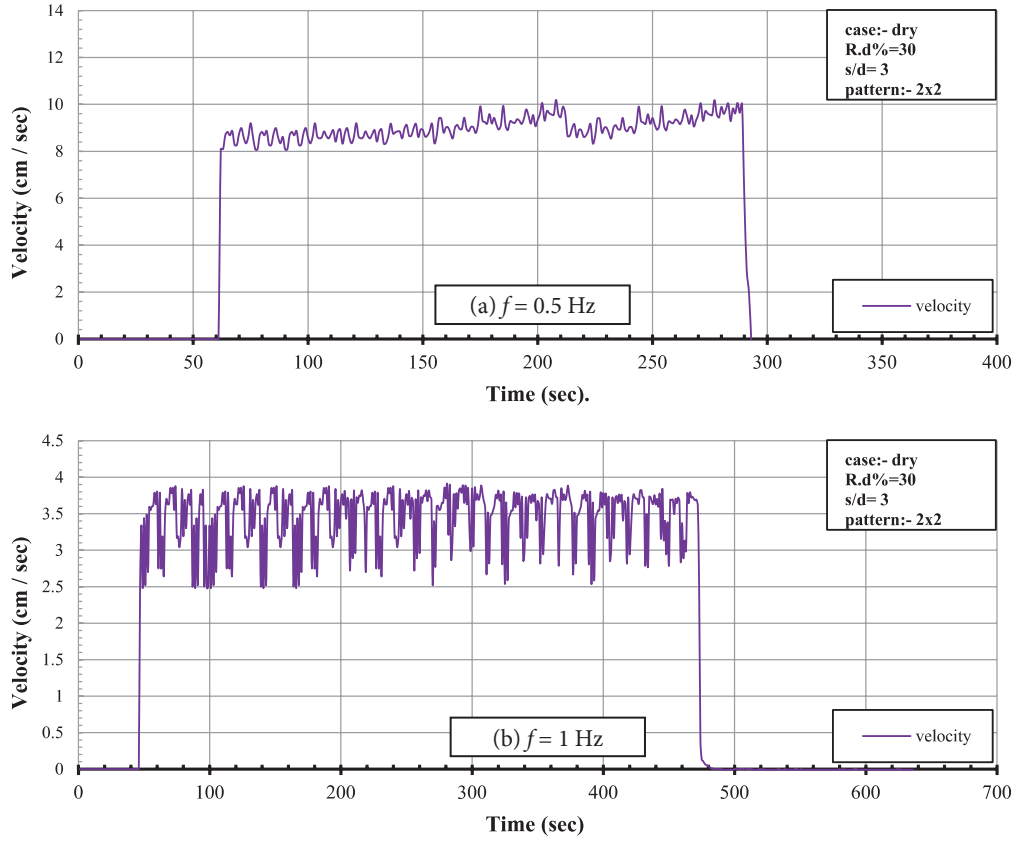

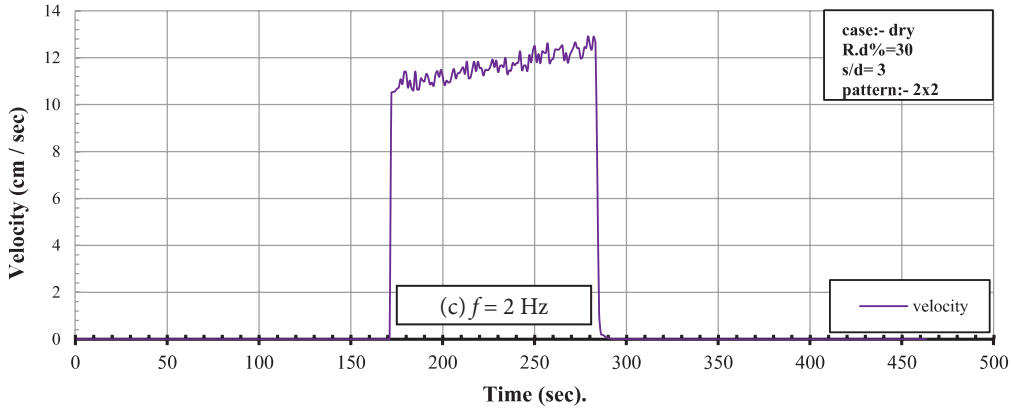

Figure 26. Variation of peak velocity of foundation with time of pile group (2×2) in loose dry sand under different frequencies.

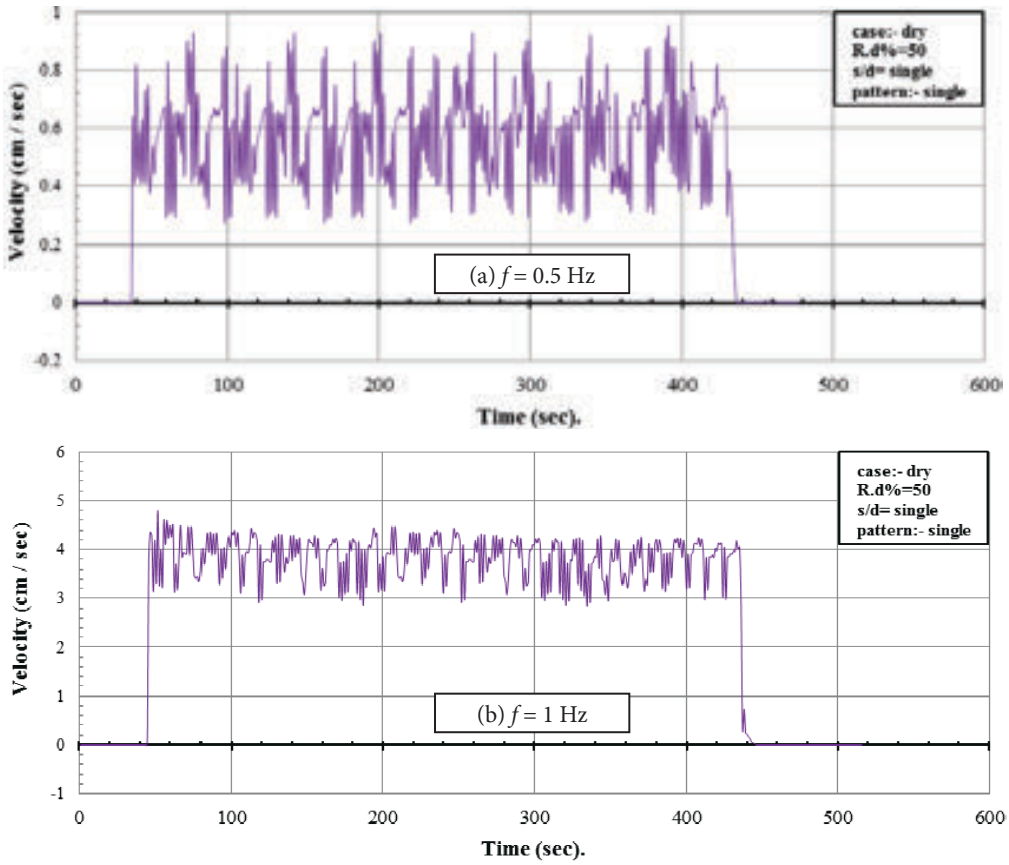

Figure 27. Variation of peak velocity of foundation with time of (single) pile in medium dry sand under different frequencies.

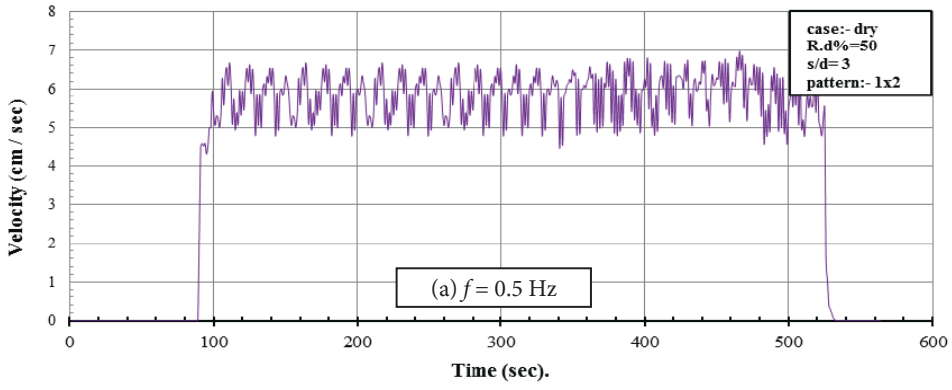

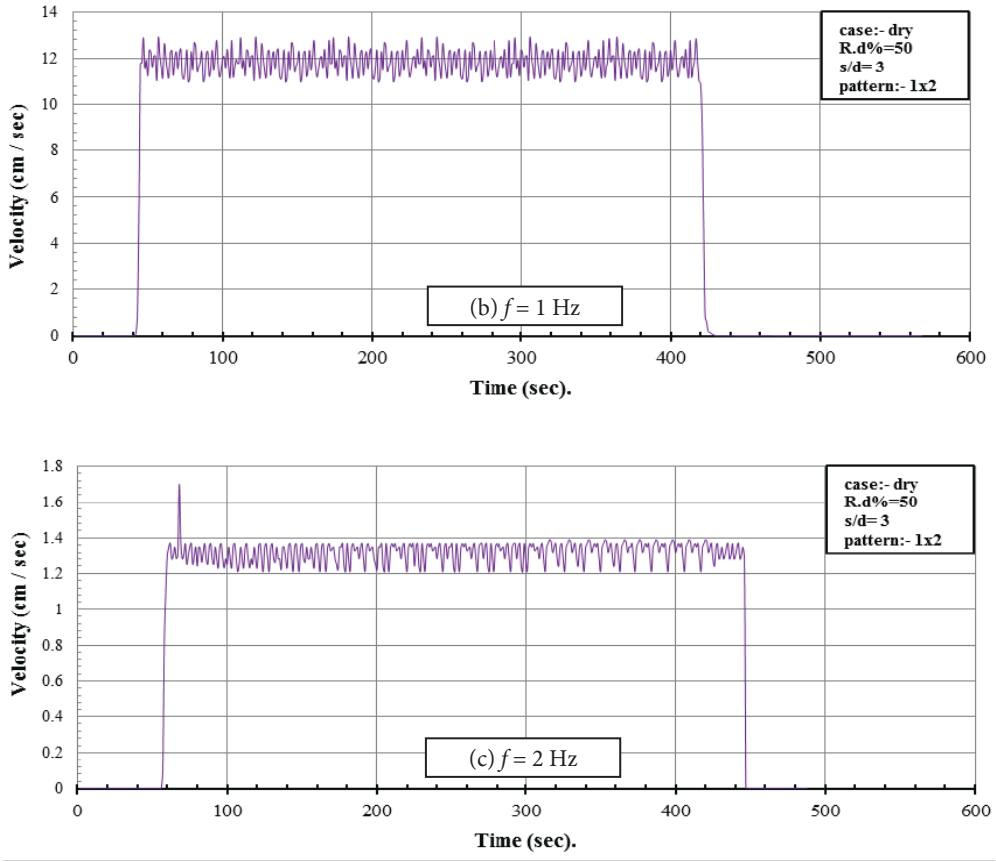

Figure 28. Variation of peak velocity of foundation with time of pile group (1×2) in medium dry sand under different frequencies.

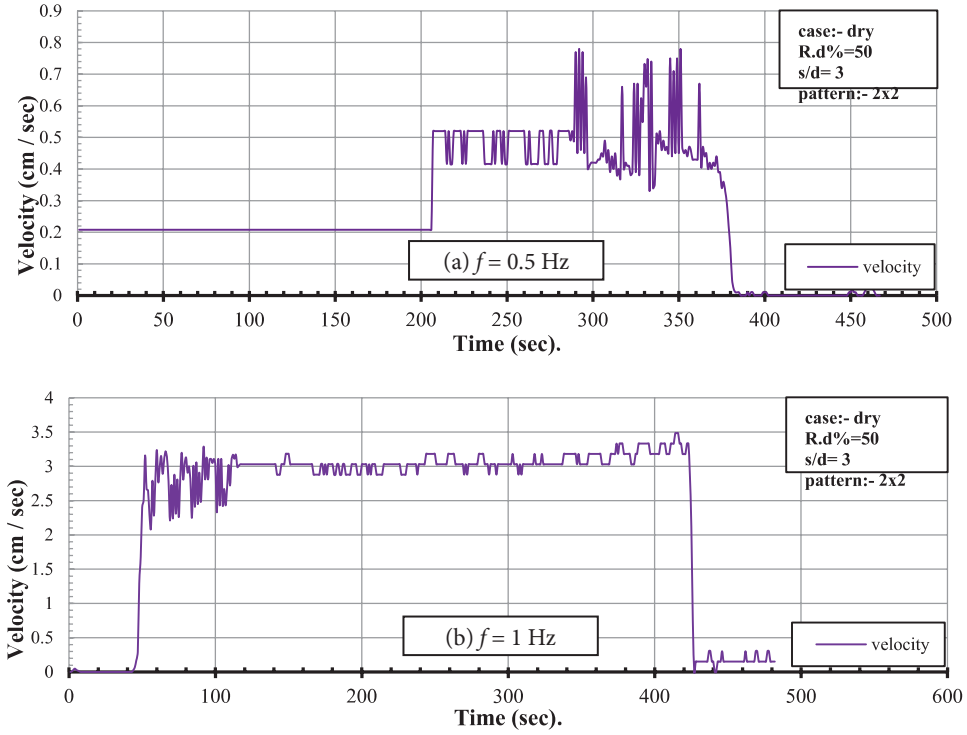

Figure 29. Variation of peak velocity of foundation with time of pile group (2×2) in medium dry sand under different frequencies.

densities (loose and medium) and different pile patterns (number; single or group and different spacing ratios *s/d*). The maximum acceleration in the foundation is lower than in the soil bed for all operating shaking frequencies, pile spacing ratios and soil states. The decreasing of the maximum acceleration recorded in the foundation as compared to that in the soil bed is between 10-100 % for loose and medium state of soil, and the decrease in loose state is more than in medium state. This means that there is damping effect or attenuation of vibration waves. The amplitudes of recorded acceleration in the pile cap are much higher than in the soil bed for single pile and pile group with different pile spacing ratios, also these amplitudes are increasing with increase of shaking frequency and relative density of the soil.

2. The increase in shaking frequency leads to reduce the oscillation of wave propagation values recorded due to densification of soil during shaking.
3. The pile tip load (net end bearing load) during shaking operation increases or decreases depending on number of piles, pile spacing, operating frequency and the soil state. During operation, the skin friction resistance mobilized along the pile length due to increasing in settlement and densification (increase in pile soil interaction effect of soil) led to increase the bearing load.
4. There is increase in acceleration and peak velocity of the foundation measured by vibration meter with time and frequency for both states of soil and for different pile numbers and spacings.
5. The most important result is that, the pile tip load (net end bearing load) during shaking operation increased or decreased depending on many factors: number of piles, pile spacing, operating frequency, as well as, the state of soil. The oscillation of the frequented values decreases with increasing the shaking frequency.
6. The pile group deflects significantly more than the isolated single pile when loaded to similar average load per pile. Moreover, the row position had an effect on the efficiency of the individual piles. The front row (leading row) piles exhibited stiffer responses than the trailing rows (second and third row). The pile spacing is an important indicator that affects the acceleration and time frequency characteristics of the displacement at pile top. With the increasing of *S/D*, the internal forces are slightly reduced.

REFERENCES

[1] Al-Mhaidib A. I., (1999), "Bearing capacity of a model pile in sand under different loading rates", Proceedings of the (9th) International offshore and Polar Engineering Conference, Brest, France, Vol. 1, pp. 724-730.

[2] Al-Mhaidib A. I., (2006), "Experimental investigation of the behavior of pile groups in sand under different loading rates", Journal of Geotechnical and Geological Engineering, Vol. 24, pp. 889-902.

[3] American Society of Testing and Materials (ASTM) (2006), "Standard test method for particle size-analysis of soils" ASTM D422-63 (2002), West Conshohocken, Pennsylvania, USA.

[4] American Society of Testing and Materials (ASTM) (2006), "Standard test method for specific gravity of soil solids by water pycnometer" ASTM D854, West Conshohocken, Pennsylvania, USA.

[5] American Society of Testing and Materials (ASTM) (2006), "Standard test method for maximum index density and unit weight of soils using a vibratory table " ASTM D4253-00 (2006), West Conshohocken, Pennsylvania, USA.

[6] American Society of Testing and Materials (ASTM) (2006), "Standard test method for minimum index density and unit weight of soils and calculation of relative density " ASTM D4254-00 (2006), West Conshohocken, Pennsylvania, USA.

[7] American Society of Testing and Materials (ASTM) (2006), "Standard test method for permeability of granular soils (constant head)" ASTM D2434-68, West Conshohocken, Pennsylvania, USA

[8] American Society of Testing and Materials (ASTM) (2006), "Standard test method for classification of soils for engineering purposes (unified soil classification system)" ASTM D2487-06, West Conshohocken, Pennsylvania, USA.

[9] Banerjee S., (2009), "Centrifuge and numerical modelling of soft clay-pile-raft foundations subjected to seismic shaking", Ph.D. Thesis, Department of Civil Engineering National University of Singapore.

[10] Boominathan A. and Lakshmi T., (2000), "Dynamic characteristics of pile group under vertical vibration ", The 12th world conference on Earthquake Engineering, Auckland, New Zealand, pp. 1-8.

[11] Boominathan A., Subramanian. R. M., Krishna Kumar S., (2015), "Lateral dynamic response and effect of weak zone on the stiffness of full scale single piles". Indian Geotechnical Journal, J 45(1): 43–50, DOI 10.1007/s40098-014-0106-6.

[12] Brown D. A. (2001), "Static and dynamic lateral loading of pile groups", National Academy press Washington, D.C. 2001.

[13] Ercan A., (2010), "Behavior of pile groups under lateral loads", M.Sc. thesis. The Graduate School

of Natural and Applied Sciences of Middle East Technical University, Turkey.
[14] Fattah, M. Y., Karim, H. H., Al- Recaby, M. K. M., (2016), "Dynamic Behavior of Pile Group Model in Two – Layer Sandy Soil Subjected to Lateral Earthquake Excitation", Global Journal of Engineering Science and Research Management, Vol. 3, No. 8, pp. 57-80.
[15] Fattah, M. Y., Zabar, B. S., Mustafa, F. S., (2017a), "Vertical Vibration Capacity of a Single Pile in Dry Sand", Marine Georesources & Geotechnology, doi.org/10.1080/1064119X.2017.1294219, Vol. 35, No. 8, pp. 1111-1120, Taylor & Francis.
[16] Fattah, M. Y., Al-Mosawi, M. J., Al-Ameri, A. F. I., (2017b), "Dynamic Response of Saturated Soil – Foundation System Acted upon by Vibration", Journal of Earthquake Engineering, Vol. 21, No. 7, pp. 1158-1188, Taylor & Francis Group, LLC, DOI: 10.1080/13632469.2016.1210060.
[17] Gui M. W., (1995), "Centrifuge and numerical modeling of pile and penetrometer in sand ", Ph.D. Dissertation, University of Cambridge.
[18] Janalizadeh A, Zahmatkesh A. (2015), "Lateral response of pile foundations in liquefiable soils", Journal of Rock Mechanics and Geotechnical Engineering, Vol. 7, pp. 532-539.
[19] Maxwell A. A., Fry Z. B., and Poplin J.K., (1969), "Vibratory loading of pile foundation" Special Technical Publication, ASTM, STP 444, pp. 338-361.
[20] Novak M. and Grigg R. F., (1976), "Dynamic experiments with small pile foundation", Canadian Geotechnical Journal, Vol. 13, p.p. 372-395.
[21] Pathak S.R. and Dalvi R.S., (2011), "Effect of sample preparation method on liquefaction of sandy soil", Electronic Journal of Geotechnical Engineering, Vol.16, pp. 1411-1426.
[22] Prusty S. K., (2010), "Dynamic response of pile foundations under coupled vibration", Final year project submitted to National Institute of Technology, Rourkela for the award of the degree of Bachelor of Technology.
[23] Vesic A. S., (1977), "Design of pile foundation, national cooperative highway research program", Synthesis of Highway Practice, No. 42, Transportation Research Board, Washington, D.C.
[24] Weiler W. A. and Kulhawy F. H. (1982), "Factors affecting stress cell measurements in soil", Journal of Geotechnical Engineering, ASCE, 108(12), 1529-1548.

NAVODILA AVTORJEM

Vsebina članka

Članek naj bo napisan v naslednji obliki:

- Naslov, ki primerno opisuje vsebino članka in ne presega 80 znakov.
- Izvleček, ki naj bo skrajšana oblika članka in naj ne presega 250 besed. Izvleček mora vsebovati osnove, jedro in cilje raziskave, uporabljeno metodologijo dela, povzetek izidov in osnovne sklepe.
- Največ 6 ključnih besed, ki bi morale biti napisane takoj po izvlečku.
- Uvod, v katerem naj bo pregled novejšega stanja in zadostne informacije za razumevanje ter pregled izidov dela, predstavljenih v članku.
- Teorija.
- Eksperimentalni del, ki naj vsebuje podatke o postavitvi preiskusa in metode, uporabljene pri pridobitvi izidov.
- Izidi, ki naj bodo jasno prikazani, po potrebi v obliki slik in preglednic.
- Razprava, v kateri naj bodo prikazane povezave in posplošitve, uporabljene za pridobitev izidov. Prikazana naj bo tudi pomembnost izidov in primerjava s poprej objavljenimi deli.
- Sklepi, v katerih naj bo prikazan en ali več sklepov, ki izhajajo iz izidov in razprave.
- Vse navedbe v besedilu morajo biti na koncu zbrane v seznamu literature, in obratno.

Dodatne zahteve

- Vrstice morajo biti zaporedno oštevilčene.
- Predložen članek ne sme imeti več kot 18 strani (brez tabel, legend in literature); velikost črk 12, dvojni razmik med vrsticami. V članek je lahko vključenih največ 10 slik. Isti rezultati so lahko prikazani v tabelah ali na slikah, ne pa na oba načina.
- Potrebno je priložiti imena, naslove in elektronske naslove štirih potencialnih recenzentov članka. Urednik ima izključno pravico do odločitve, ali bo te predloge upošteval.

Enote in okrajšave

V besedilu, preglednicah in slikah uporabljajte le standardne označbe in okrajšave SI. Simbole fizikalnih veličin v besedilu pišite poševno (npr. *v*, *T* itn.). Simbole enot, ki so sestavljene iz črk, pa pokončno (npr. Pa, m itn.). Vse okrajšave naj bodo, ko se prvič pojavijo, izpisane v celoti.

Slike

Slike morajo biti zaporedno oštevilčene in označene, v besedilu in podnaslovu, kot sl. 1, sl. 2 itn. Posnete naj bodo v katerem koli od razširjenih formatov, npr. BMP, JPG, GIF. Za pripravo diagramov in risb priporočamo CDR format (CorelDraw), saj so slike v njem vektorske in jih lahko pri končni obdelavi preprosto povečujemo ali pomanjšujemo.

Pri označevanju osi v diagramih, kadar je le mogoče, uporabite označbe veličin (npr. *v*, *T* itn.). V diagramih z več krivuljami mora biti vsaka krivulja označena. Pomen oznake mora biti razložen v podnapisu slike.

Za vse slike po fotografskih posnetkih je treba priložiti izvirne fotografije ali kakovostno narejen posnetek.

Preglednice

Preglednice morajo biti zaporedno oštevilčene in označene, v besedilu in podnaslovu, kot preglednica 1, preglednica 2 itn. V preglednicah ne uporabljajte izpisanih imen veličin, ampak samo ustrezne simbole. K fizikalnim količinam, npr. *t* (pisano poševno), pripišite enote (pisano pokončno) v novo vrsto brez oklepajev. Vse opombe naj bodo označene z uporabo dvignjene številke[1].

Seznam literature

Navedba v besedilu

Vsaka navedba, na katero se sklicujete v besedilu, mora biti v seznamu literature (in obratno). Neobjavljeni rezultati in osebne komunikacije se ne priporočajo v seznamu literature, navedejo pa se lahko v besedilu, če je nujno potrebno.

Oblika navajanja literature

V besedilu: Navedite reference zaporedno po številkah v oglatih oklepajih v skladu z besedilom. Dejanski avtorji so lahko navedeni, vendar mora obvezno biti podana referenčna številka.

Primer: »..... kot je razvidno [1,2]. Brandl and Blovsky [4], sta pridobila drugačen rezultat…«

V seznamu: Literaturni viri so oštevilčeni po vrstnem redu, kakor se pojavijo v članku. Označimo jih s številkami v oglatih oklepajih.

Sklicevanje na objave v revijah:

[1] Jelušič, P., Žlender, B. 2013. Soil-nail wall stability analysis using ANFIS. Acta Geotechnica Slovenica 10(1), 61-73.

Sklicevanje na knjigo:
[2] Šuklje, L. 1969. Rheological aspects of soil mechanics. Wiley-Interscience, London
Sklicevanje na poglavje v monografiji:
[3] Mitchel, J.K. 1992. Characteristics and mechanisms of clay creep and creep rupture, in N. Guven, R.M. Pollastro (eds.), Clay-Water Interface and Its Rheological Implications, CMS Workshop Lectures, Vol. 4, The clay minerals Society, USA, pp. 212-244..
Sklicevanje na objave v zbornikih konferenc:
[4] Brandl, H., Blovsky, S. 2005. Slope stabilization with socket walls using the observational method. Proc. Int. conf. on Soil Mechanics and Geotechnical Engineering, Bratislava, pp. 2485-2488.
Sklicevanje na spletne objave:
[5] Kot najmanj, je potrebno podati celoten URL. Če so poznani drugi podatki (DOI, imena avtorjev, datumi, sklicevanje na izvorno literaturo), se naj prav tako dodajo.

Podatki o avtorjih

Članku priložite tudi podatke o avtorjih: imena, nazive, popolne poštne naslove, številke telefona in faksa, naslove elektronske pošte. Navedite kontaktno osebo.

Sprejem člankov in avtorske pravlce

Uredništvo si pridržuje pravico do odločanja o sprejemu članka za objavo, strokovno oceno mednarodnih recenzentov in morebitnem predlogu za krajšanje ali izpopolnitev ter terminološke in jezikovne korekture. Z objavo preidejo avtorske pravice na revijo ACTA GEOTECHNICA SLOVENICA. Pri morebitnih kasnejših objavah mora biti AGS navedena kot vir.

Vsa nadaljnja pojasnila daje:

Uredništvo
ACTA GEOTECHNICA SLOVENICA
Univerza v Mariboru,
Fakulteta za gradbeništvo, prometno inženirstvo in arhitekturo
Smetanova ulica 17, 2000 Maribor, Slovenija
E-pošta: ags@um.si

INSTRUCTIONS FOR AUTHORS

Format of the paper

The paper should have the following structure:

- A Title, which adequately describes the content of the paper and should not exceed 80 characters;
- An Abstract, which should be viewed as a mini version of the paper and should not exceed 250 words. The Abstract should state the principal objectives and the scope of the investigation and the methodology employed; it should also summarise the results and state the principal conclusions;
- Immediately after the abstract, provide a maximum of 6 keywords;
- An Introduction, which should provide a review of recent literature and sufficient background information to allow the results of the paper to be understood and evaluated;
- A Theoretical section;
- An Experimental section, which should provide details of the experimental set-up and the methods used to obtain the results;
- A Results section, which should clearly and concisely present the data, using figures and tables where appropriate;
- A Discussion section, which should describe the relationships shown and the generalisations made possible by the results and discuss the significance of the results, making comparisons with previously published work;
- Conclusions, which should present one or more conclusions that have been drawn from the results and subsequent discussion;
- A list of References, which comprises all the references cited in the text, and vice versa.

Additional Requirements for Manuscripts

- Use double line-spacing.
- Insert continuous line numbering.
- The submitted text of Research Papers should cover no more than 18 pages (without Tables, Legends, and References, style: font size 12, double line spacing). The number of illustrations should not exceed 10. Results may be shown in tables or figures, but not in both of them.
- Please submit, with the manuscript, the names, addresses and e-mail addresses of four potential referees. Note that the editor retains the sole right to decide whether or not the suggested reviewers are used.

Units and abbreviations

Only standard SI symbols and abbreviations should be used in the text, tables and figures. Symbols for physical quantities in the text should be written in Italics (e.g. *v*, *T*, etc.). Symbols for units that consist of letters should

be in plain text (e.g. Pa, m, etc.).
All abbreviations should be spelt out in full on first appearance.

Figures

Figures must be cited in consecutive numerical order in the text and referred to in both the text and the caption as Fig. 1, Fig. 2, etc. Figures may be saved in any common format, e.g. BMP, JPG, GIF. However, the use of CDR format (CorelDraw) is recommended for graphs and line drawings, since vector images can be easily reduced or enlarged during final processing of the paper.

When labelling axes, physical quantities (e.g. *v*, *T*, etc.) should be used whenever possible. Multi-curve graphs should have individual curves marked with a symbol; the meaning of the symbol should be explained in the figure caption. Good quality black-and-white photographs or scanned images should be supplied for the illustrations.

Tables

Tables must be cited in consecutive numerical order in the text and referred to in both the text and the caption as Table 1, Table 2, etc. The use of names for quantities in tables should be avoided if possible: corresponding symbols are preferred. In addition to the physical quantity, e.g. *t* (in Italics), units (normal text), should be added on a new line without brackets.
Any footnotes should be indicated by the use of the superscript[1].

LIST OF references

Citation in text

Please ensure that every reference cited in the text is also present in the reference list (and vice versa). Any references cited in the abstract must be given in full. Unpublished results and personal communications are not recommended in the reference list, but may be mentioned in the text, if necessary.

Reference style

Text: Indicate references by number(s) in square brackets consecutively in line with the text. The actual authors can be referred to, but the reference number(s) must always be given:

Example: "... as demonstrated [1,2]. Brandl and Blovsky [4] obtained a different result ..."

List: Number the references (numbers in square brackets) in the list in the order in which they appear in the text.

Reference to a journal publication:
[1] Jelušič, P., Žlender, B. 2013. Soil-nail wall stability analysis using ANFIS. Acta Geotechnica Slovenica 10(1), 61-73.

Reference to a book:
[2] Šuklje, L. 1969. Rheological aspects of soil mechanics. Wiley-Interscience, London

Reference to a chapter in an edited book:
[3] Mitchel, J.K. 1992. Characteristics and mechanisms of clay creep and creep rupture, in N. Guven, R.M. Pollastro (eds.), Clay-Water Interface and Its Rheological Implications, CMS Workshop Lectures, Vol. 4, The clay minerals Society, USA, pp. 212-244.

Conference proceedings:
[4] Brandl, H., Blovsky, S. 2005. Slope stabilization with socket walls using the observational method. Proc. Int. conf. on Soil Mechanics and Geotechnical Engineering, Bratislava, pp. 2485-2488.

Web references:
[5] As a minimum, the full URL should be given and the date when the reference was last accessed. Any further information, if known (DOI, author names, dates, reference to a source publication, etc.), should also be given.

Author information

The following information about the authors should be enclosed with the paper: names, complete postal addresses, telephone and fax numbers and E-mail addresses. Indicate the name of the corresponding author.

Acceptance of papers and copyright

The Editorial Committee of the Slovenian Geotechnical Review reserves the right to decide whether a paper is acceptable for publication, to obtain peer reviews for the submitted papers, and if necessary, to require changes in the content, length or language.
On publication, copyright for the paper shall pass to the ACTA GEOTECHNICA SLOVENICA. The AGS must be stated as a source in all later publication.

For further information contact:

Editorial Board
ACTA GEOTECHNICA SLOVENICA
University of Maribor,
Faculty of Civil Engineering, Transportation Engineering and Architecture
Smetanova ulica 17, 2000 Maribor, Slovenia
E-mail: ags@um.si

NAMEN REVIJE

Namen revije ACTA GEOTECHNICA SLOVENICA je objavljanje kakovostnih teoretičnih člankov z novih pomembnih področij geomehanike in geotehnike, ki bodo dolgoročno vplivali na temeljne in praktične vidike teh področij.

ACTA GEOTECHNICA SLOVENICA objavlja članke s področij: mehanika zemljin in kamnin, inženirska geologija, okoljska geotehnika, geosintetika, geotehnične konstrukcije, numerične in analitične metode, računalniško modeliranje, optimizacija geotehničnih konstrukcij, terenske in laboratorijske preiskave.

Revija redno izhaja dvakrat letno.

AIMS AND SCOPE

ACTA GEOTECHNICA SLOVENICA aims to play an important role in publishing high-quality, theoretical papers from important and emerging areas that will have a lasting impact on fundamental and practical aspects of geomechanics and geotechnical engineering.

ACTA GEOTECHNICA SLOVENICA publishes papers from the following areas: soil and rock mechanics, engineering geology, environmental geotechnics, geosynthetic, geotechnical structures, numerical and analytical methods, computer modelling, optimization of geotechnical structures, field and laboratory testing.

The journal is published twice a year.

AVTORSKE PRAVICE

Ko uredništvo prejme članek v objavo, prosi avtorja(je), da prenese(jo) avtorske pravice za članek na izdajatelja, da bi zagotovili kar se da obsežno razširjanje informacij. Naša revija in posamezni prispevki so zaščiteni z avtorskimi pravicami izdajatelja in zanje veljajo naslednji pogoji:

Fotokopiranje

V skladu z našimi zakoni o zaščiti avtorskih pravic je dovoljeno narediti eno kopijo posameznega članka za osebno uporabo. Za naslednje fotokopije, vključno z večkratnim fotokopiranjem, sistematičnim fotokopiranjem, kopiranjem za reklamne ali predstavitvene namene, nadaljnjo prodajo in vsemi oblikami nedobičkonosne uporabe je treba pridobiti dovoljenje izdajatelja in plačati določen znesek.

Naročniki revije smejo kopirati kazalo z vsebino revije ali pripraviti seznam člankov z izvlečki za rabo v svojih ustanovah.

Elektronsko shranjevanje

Za elektronsko shranjevanje vsakršnega gradiva iz revije, vključno z vsemi članki ali deli članka, je potrebno dovoljenje izdajatelja.

COPYRIGHT

Upon acceptance of an article by the Editorial Board, the author(s) will be asked to transfer copyright for the article to the publisher. This transfer will ensure the widest possible dissemination of information. This review and the individual contributions contained in it are protected by publisher's copyright, and the following terms and conditions apply to their use:

Photocopying

Single photocopies of single articles may be made for personal use, as allowed by national copyright laws. Permission of the publisher and payment of a fee are required for all other photocopying, including multiple or systematic copying, copying for advertising or promotional purposes, resale, and all forms of document delivery.

Subscribers may reproduce tables of contents or prepare lists of papers, including abstracts for internal circulation, within their institutions.

Electronic Storage

Permission of the publisher is required to store electronically any material contained in this review, including any paper or part of the paper.

ODGOVORNOST

Revija ne prevzame nobene odgovornosti za poškodbe in/ali škodo na osebah in na lastnini na podlagi odgovornosti za izdelke, zaradi malomarnosti ali drugače, ali zaradi uporabe kakršnekoli metode, izdelka, navodil ali zamisli, ki so opisani v njej.

RESPONSIBILITY

No responsibility is assumed by the publisher for any injury and/or damage to persons or property as a matter of product liability, negligence or otherwise, or from any use or operation of any methods, products, instructions or ideas contained in the material herein.

www.fgpa.um.si

www.sloged.si

University of Ljubljana

Faculty of Civil and Geodetic Engineering

Faculty of Natural Sciences and Engineering

www.fgg.uni-lj.si
www.ntf.uni-lj.si

www.ita-slovenia.si